WADC TECHNICAL REPORT 54-113
PART II
ASTIA DOCUMENT NO. AD 110593

(UNCLASSIFIED TITLE)

THREE-DIMENSIONAL SUPERSONIC FLUTTER MODEL TESTS NEAR MACH NUMBER 1.5

Part II. Experimental and Theoretical Data For Bare Wings and Wings With Tip Tanks

JOHN F. McCARTHY, JR.
GARABED ZARTARIAN
JOHN R. MARTUCCELLI
GIFFORD W. ASHER

MASSACHUSETTS INSTITUTE OF TECHNOLOGY

DECEMBER 1955

AIRCRAFT LABORATORY
CONTRACT AF 33(038)-22955
PROJECT 1370

WRIGHT AIR DEVELOPMENT CENTER
AIR RESEARCH AND DEVELOPMENT COMMAND
UNITED STATES AIR FORCE
WRIGHT-PATTERSON AIR FORCE BASE, OHIO

FOREWORD

This report, which presents the experimental and theoretical results of a program of supersonic flutter testing, was prepared by the Aeroelastic and Structures Research Laboratory, Massachusetts Institute of Technology, Cambridge 39, Massachusetts for the Aircraft Laboratory, Wright Air Development Center, Wright-Patterson Air Force Base, Ohio. The work was performed at the MIT under the direction of Professor R. L. Halfman, and the project was supervised by Mr. J. F. McCarthy, Jr. The research and development work was accomplished under Air Force Contract No. AF 33(038)-22955, Project No. 1370, (Unclassified Title) "Aeroelasticity, Vibration and Noise," and Task No. 13474, (Unclassified Title) "Three-Dimensional Supersonic Flutter Model Tests at Mach Number 1.5". Mr. Niles R. Hoffman of the Dynamics Branch, Aircraft Laboratory, is task engineer. This task covers a continuing effort on flutter research at supersonic speeds. Research was started in March 1951. The test data presented in this report was obtained during the period from December 1952 to December 1954. This is Part II of a report to be issued in three separate parts. Part I of this report, WADC TR 54-113, (Unclassified Title) "Three-Dimensional Supersonic Flutter Model Tests Near Mach Number 1.5, Part I. Model Design and Testing Techniques," was issued in December 1955. Technical Report WADC TR 54-114, "(Unclassified Title)" A Variable Mach Number Supersonic Test Section for Flutter Research" was issued in December 1954.

The authors are indebted to Mr. O. Wallin, and Mr. C. Fall for their help in the model construction and in keeping the wind tunnel in operation; to Mr. G. M. Falla for the photograph; to Messrs. A. Heller and H. Hagerup for their help in the calculations; to Messrs. J. R. Friery, G. Anitole, and W. Marchant for their help in preparing the tables and figures; and to Miss K. Roberts and Mrs. B. Marks for their help in typing this report.

This document is classified CONFIDENTIAL in its entirety (excepting the title) because results of supersonic flutter tests generally indicate limiting performance capabilities of present and future military aircraft and have application in the form of design criteria.

ABSTRACT

Three-dimensional supersonic flutter tests were made on over 75 semi-span models in the MIT blowdown wind tunnel facility. The testing technique involved injecting the model into a stable region of flow and decreasing the Mach number until instability occurred. Experimental flutter stability boundaries are defined for bare straight, swept and delta-wing planforms in the Mach number range, 1.3 - 2.0. Exploratory tests were also made on wings with ailerons for all planforms, and on straight and swept wings with tip tanks for both cantilever and free-to-roll root conditions. Except for absolute stiffness, the dimensionless flutter parameters were chosen so as to be typical of present-day high-speed aircraft.

Extensive theoretical calculations were made on the straight-wing planform using two-dimensional supersonic oscillatory aerodynamic coefficients and three-dimensional structural properties. The qualitative prediction by the theory of the effect of various parameter changes generally agrees with experiment, but the quantitative prediction is generally poor. The theoretical calculations are unconservative in that they predict smaller regions of instability than those obtained experimentally at Mach numbers above 1.4. No theoretical calculations were made for the swept and delta planforms.

Comparison of the experimental data with the results of other flutter tests shows that in the Mach number range of 0.6 to 2.0 for wings with parameters similar to those tested the following conclusions may be drawn:

1). At constant altitude, the critical flutter region for straight wings lies at about M ≅ 1.7

2). At constant altitude, the critical flutter region for swept wings lies in the transonic regime at about M ≅ 1.1

3). At constant altitude, the critical flutter region for 60° delta wings lies at the highest Mach number tested, M ≅ 2.0

4). At constant dynamic pressure, the critical flutter region lies in the transonic regime close to M ≅ 1.0, for all the straight, swept, and delta planforms tested

A complete tabulation of the design properties for all the models tested is presented along with the results of static, vibration, and flutter tests.

PUBLICATION REVIEW

This report has been reviewed and is approved.

FOR THE COMMANDER:

DANIEL D. McKEE
Colonel, USAF
Chief, Aircraft Laboratory

TABLE OF CONTENTS

TABLE OF CONTENTS (Contd.)

[redacted]

LIST OF ILLUSTRATIONS

[redacted]

LIST OF ILLUSTRATIONS (Contd.)

LIST OF ILLUSTRATIONS (Contd.)

LIST OF TABLES

LIST OF SYMBOLS

$\underline{A}$, $\underline{B}$, $\underline{C}$, etc.	Elements of three-dimensional flutter determinant expressed in dimensionless form
$\overline{\underline{A}}$, $\overline{\underline{B}}$, $\overline{\underline{C}}$, etc.	Elements of three-dimensional flutter determinant expressed in dimensional form
a	Distance the wing elastic axis is aft of the wing mid-chord, as a fraction of the wing semi-chord
a	Speed of sound
B	Base of rectangular spar measured parallel to the root chord
b	Semi-chord of wing
b_T	Semi-chord of tip tank
c	Distance the aileron hinge line is aft of the wing mid-chord, as a fraction of the wing semi-chord
c.g.	Center of gravity
E	Modulus of elasticity in bending
EI	Bending stiffness
e.a.	Elastic axis
f_h	Assumed uncoupled mode shape of wing in bending
f_α	Assumed uncoupled mode shape of wing in torsion
f_β	Assumed uncoupled aileron mode shape
G	Modulus of elasticity in shear
GJ	Torsional stiffness

LIST OF SYMBOLS (Contd.)

g_h, g_α, g_β	Structural damping coefficients in the wing bending, wing torsion, and aileron-rotational degrees of freedom, respectively
H	Height of rectangular spar measured parallel to the root chord
H.L.	Hinge line
h	Vertical displacement of elastic axis, positive down
$\bar{h}$	Amplitude of assumed bending mode at wing tip station
$(I_{c.g.})_T$	Mass moment of inertia in pitch of tip tank about its center of gravity
I_s	Mass moment of inertia of wing support about roll axis
I_T	Mass moment of tip tank about wing elastic axis
I_α	Mass moment of inertia in pitch of wing section about elastic axis per unit length of span
I_β	Mass moment of inertia of aileron about the aileron hinge line per unit span
I_1	Volume moment of inertia in pitch of tip tank about its geometrical center
KE	Kinetic energy
k	Reduced flutter frequency, $k = \frac{\omega b}{V}$
L	Lift per unit span, positive down

LIST OF SYMBOLS (Contd.)

L_h, L_α, L_β, M_h, M_α, M_β, T_h, T_α, T_β	Aerodynamic coefficients defined in Reference 26
L_1, L_2, L_3, L_4, L_5, L_6, M_1, M_2, M_3, M_4, M_5, M_6, N_1, N_2, N_3, N_4, N_5, N_6.	Aerodynamic coefficients defined in Reference 7
L. E.	Leading edge
ℓ	Semi-span of wing
ℓ_1	Distance from wing root chord to inboard end of aileron
ℓ_2	Distance from wing root chord to outboard end of aileron
M	Free-stream Mach number
M'	Aerodynamic moment about elastic axis per unit span, positive nose up
M_T	Total mass of tip tank
M_W	Total mass of bare wing
m, m(y)	Mass of wing per unit span
m (x,y)	Mass of wing per unit area
$m_T(x)$	Mass of tip-tank per unit chordwise distance

LIST OF SYMBOLS (Contd.)

n_T	Distance the geometrical center of the tip tank lies aft of the elastic axis of the wing
PE	Potential energy
p	pressure
Q_i	i^{th} generalized force
Q_{ij}	Generalized force in the i^{th} mode per unit displacement of the j^{th} mode
$\overline{q}_i$	Magnitude of the i^{th} generalized coordinate at wing tip station
R	Gas constant
$\frac{RN}{L}$	Reynolds number per unit length
r_α	Dimensionless radius of gyration of wing section about the elastic axis, $\sqrt{\frac{I_\alpha}{mb^2}}$
$(r_{\alpha_{c.g.}})_T$	Dimensionless radius of gyration in pitch of tip tank about its center of gravity, $\sqrt{\frac{(I_{c.g.})_T}{M_T (b_T)^2}}$
r_β	Dimensionless radius of gyration of aileron about aileron hinge line, $\sqrt{\frac{I_\beta}{mb^2}}$
S_T	Static unbalance of tip tank about elastic axis of wing, positive nose up
$\overline{S}_T$	Dimensionless static unbalance of tip tank, $\frac{S_T}{mb\ell}$
$S_\alpha(y)$	Static unbalance per unit span of wing section about the elastic axis, positive nose up
S_β	Static unbalance per unit span of aileron about the aileron hinge line
T	Absolute temperature

LIST OF SYMBOLS (Contd.)

t	Time
V_T	Volume of tip tank
v	Free-stream velocity
W	Work
x	Coordinate measured perpendicular to elastic axis from mid-chord of airfoil, positive aft
x_o	Fraction of chord elastic axis of wing is behind leading edge
x_α	Dimensionless distance the center of gravity of the wing section lies aft of the elastic axis, $\frac{S_\alpha}{mb}$
x_β	Dimensionless distance the center of gravity of the aileron lies aft of the aileron hinge line, $\frac{S_\beta}{mb}$
y	Coordinate measured parallel to elastic axis from root chord of right wing
Z	Frequency ratio, $\left(\frac{\omega_\alpha}{\omega}\right)^2$
z	Vertical displacement of wing, positive down
α	Twist about elastic axis, positve nose up
$\overline{\alpha}$	Amplitude of assumed torsion mode at wing tip station
β	Rotation of aileron about its hinge line, positive for increasing angle of attack
γ	Ratio of specific heats
η	Dimensionless spanwise variable, $\frac{y}{\ell}$

LIST OF SYMBOLS (Contd.)

θ	Rigid-body angular rotation about wing root, positive right wing down
$\bar{\theta}$	Amplitude of assumed θ-mode at wing tip station
λ	Wing taper ratio, ratio of wing tip chord to wing root chord
μ	Wing mass-density ratio, $\frac{m}{\pi \rho b^2}$
$\bar{\mu}$	Wing mass-density ratio, $\frac{m}{4 \rho b^2}$
ν	Kinematic viscosity
ρ	Free-stream air density
ρ_{BA}	Density of balsa wood
τ	Thickness ratio of airfoil
Ω	Frequency ratio, $(\frac{\omega_\alpha}{\omega})^2 (1 + ig)$
ω, ω_f	Flutter frequency .
$\bar{\omega}$	Reduced frequency, parameter, $\frac{2k M^2}{M^2-1}$
ω_h, ω_{h_1}	First bending frequency of bare wing
ω_{h_2}	Second bending frequency of bare wing
$\omega_\alpha, \omega_{\alpha_1}$	First torsional frequency of bare wing
ω_{α_2}	Second torsional frequency of bare wing
ω_β	First aileron frequency of wing

Subscripts

A	Airplane
BA	Balsa Wood
c	Wing chord

LIST OF SYMBOLS (Contd.)

c.g.	Center of gravity
f	Flutter
h	First bending mode
M	Model
o	Wing root
o	Refers to stagnation conditions in wind tunnel
T	Tip tank
α	First torsional mode
0.75	3/4 span station

SECTION I

INTRODUCTION

The phenomenon of flutter, the self-excited oscillation of an elastic structure in an airstream, appeared early in the development of aircraft. At first, designers could apply only crude corrective measures, and it was not until the early 1930's that aeronautical scientists were able to fashion promising theoretical approaches to the problem of flutter. Although experimental work lagged behind the theoretical attack, the flutter problem in incompressible flow had become quite tractable by the end of the Second World War. Both the theoretical and experimental approaches were well developed and understood. Until the advent of transonic and supersonic aircraft, these techniques were adequate for the airplane designer.

Unfortunately, the trend towards higher speeds, increased structural flexibility and lower aspect-ratio lifting surfaces as well as the growing use of large external stores so aggravate the flutter problem that it is now often a primary design consideration rather than an occurrence that can be remedied fairly easily. Because of the questionable reliability of existing methods of flutter analysis in the high-speed range, the airplane designer calls upon the experimentalist to provide data that are immediately useful and that can be used to confirm theory. A reasonable amount of experimental flutter data exists, but attempts to correlate this data with calculations made with incompressible unsteady aerodynamic coefficients have not been too successful (see Ref. 4).

In the low supersonic speed range, M = 1.2 to M = 2.0, basic flutter theory may be used successfully with linearized

---

Manuscript released by the authors December 1955 for publication as a WADC Technical Report.

aerodynamic forces provided the perturbation velocities on the system to be studied are small compared to the free stream velocity. Flutter analyses using two-dimensional supersonic aerodynamic coefficients (Ref. 7) have been done for some time, but there has been little confirmation of the theory with experiment over a range of Mach numbers and for dimensional parameters which are typical of present-day aircraft, especially in the case of the mass ratio, which has generally been much higher for the models tested than that encountered in practice (Refs. 8-11).

Experimental investigations of flutter in the supersonic speed range at first glance appear to be as difficult as those in the transonic range. Models mounted on rockets, bombs, or sleds must go through the transonic range before encountering supersonic speeds so that the same problems of complexity and expense (mounting, data recording, expendable models, etc.) are still present. For tests conducted in the wind tunnel, there are the large-power requirements for continuous-flow tunnels of reasonable size, the aerodynamic problems of obtaining uniform flow in the test section, and the potential damage that could be inflicted on the testing facility by models which are lost. For supersonic flow, the Mach number in the test section is a function only of the geometry of the nozzle, so it might appear that many nozzles of fixed geometry would have to be used to get useful data. The model designer is again confronted with the problem of building efficient structure into thin wings in order to obtain the very high natural frequencies required when Mach number must be simulated (see Reference 12).

Some of the complexity and expense of testing flutter models in the low supersonic speed range was eliminated by designing the facility described in Reference 13. Briefly, a supersonic nozzle of variable geometry was built for installa-

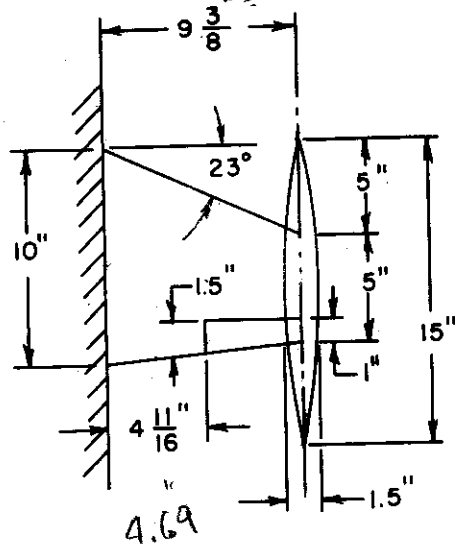

STRAIGHT WING

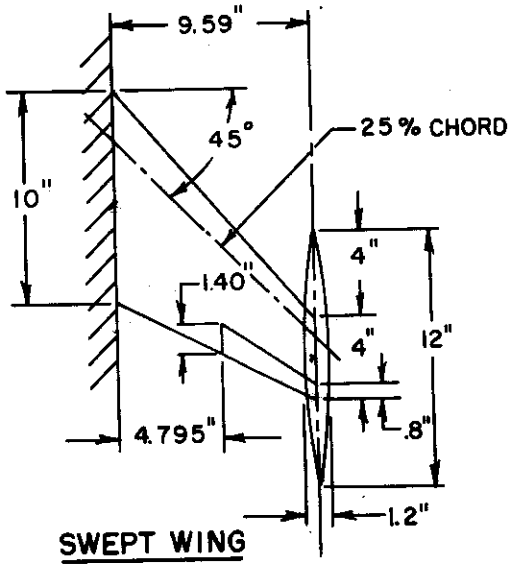

SWEPT WING

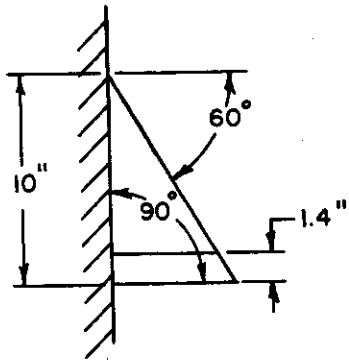

DELTA WING

AIRFOIL SECTION SYMMETRICAL DOUBLE WEDGE ON ALL MODELS, 6% THICK EXCEPT AS NOTED FOR DELTA WINGS IN TABLE D.6

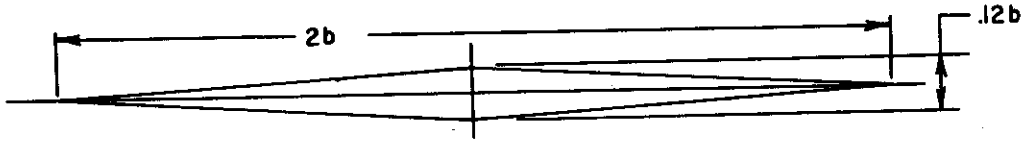

FIGURE 1.1 WING PLANFORMS

tion in a blowdown wind tunnel. It is of the asymmetric sliding-block type, and the Mach number can be varied through the complete range of the nozzle during a run (M=1.2 - 2.1) without any change in the dimensions of the test section. The testing technique involves injection of the model into the airstream in order to avoid destruction of the model by the violent starting shock. Thus, the problems of large power, damage from broken models, and testing at fixed Mach number were immediately solved. Also, the difficulty of obtaining low mass ratios is somewhat alleviated because of the high air density in the test section, which is characteristic of a blowdown wind tunnel. The approaches for designing, building, and testing inexpensive supersonic flutter models with desired parameters are discussed in References 14-17.

The planforms shown in Figure 1.1 were chosen for investigation (Ref. 18). These are typical of present-day high-speed fighters and proposed supersonic bombers. Although most of the work was done on the bare wings, some exploratory tests were made on models with ailerons and, in the case of the straight and swept wings, on models with tip tanks for both cantilever and free-to-roll root conditions. The 10-inch root chord represents the model of maximum size that can be tested in the facility without shock interference (see Reference 14). The symmetrical double wedge airfoil section was used because of its simplicity. The range of flutter parameters built into the models are typical of current high-speed aircraft.

Theoretical flutter calculations were made only for the straight-wing, since it was felt that two dimensional aerodynamic coefficients could be used successfully for this planform. No theoretical work was done on the swept or delta planforms because the primary emphasis of the research program was on experimental results. However, enough theoretical work was done

on the straight wing so that the complete range of experimental parameters was covered and a reasonable comparison between theory and experiment could be made for this planform. The theoretical trends exhibited by the straight wing were compared with those obtained experimentally for the swept and delta wings.

In subsonic and low transonic flutter testing wings are brought from a stable to an unstable region by increasing the speed or Mach number. Figure 1.2, which shows a hypothetical flutter boundary, demonstrates a peculiarity of supersonic flutter testing. A wing is generally brought from a stable region to an unstable region (see Reference 14) by decreasing the speed or Mach number along a tunnel operating curve. From Fig. 1.2

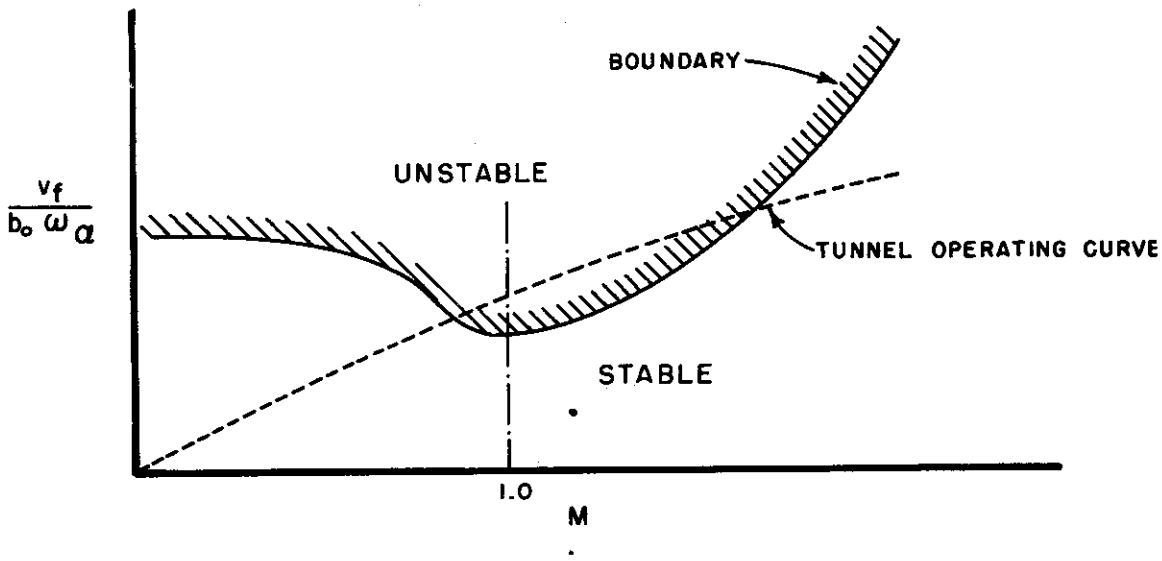

FIGURE 1.2 HYPOTHETICAL FLUTTER BOUNDARY

it can also be seen that decreasing the region of instability over the whole Mach number range will lower the Mach number for flutter in the supersonic speed range and raise the Mach number for flutter in the subsonic and low transonic speed range.

These facts explain some of the conclusions of Sections 3 and 4 that at first glance may appear unreasonable.

SECTION II

FORMULATION

The dimensionless answers which one hopes to obtain from a flutter model test are the values of the Mach number, M, the reduced frequency, k, and the frequency ratio, Z, at flutter and the flutter mode shape. These dimensionless quantities can be derived from basic flutter theory (see Reference 19 and Appendix A.1) along with other parameters which define the physical properties of the lifting surface. For bare wings of reasonably large aspect ratio, the physical properties evolve as dimensionless parameters which must be defined at every spanwise station, viz.,

planform, $\frac{b}{b_o}$

mass distribution, $\frac{m}{m_o}$

location of the chordwise center of gravity, x_α

dimensionless moment of inertia in pitch, r_α

bending stiffness distribution, $\frac{EI}{(\overline{EI})_o}$

torsional rigidity distribution, $\frac{GJ}{(\overline{GJ})_o}$

location of the elastic axis, a

For wings of low aspect ratio or for surfaces where chordwise deformations are appreciable, the concepts of bending stiffness, torsional rigidity and elastic axis are not valid, and the chordwise as well as the spanwise distributions of mass and stiffness must be defined.

For given distributions of mass and stiffness, the model has a discrete set of eigenfrequencies with associated eigenfunctions and a distinct set of influence coefficients. For both models and full-scale airplanes, these latter parameters are relatively easy to obtain experimentally compared to obtaining mass and stiffness distributions, especially when the chordwise as well as the spanwise variations must be considered. Therefore, in the usual formulation of the flutter problem, natural frequencies and mode shapes or matrices of influence coefficients replace stiffness distributions. Through the years, flutter engineers have become used to thinking of the flutter problem in terms of natural frequencies and mode shapes rather than in terms of stiffnesses. The concept of attacking the problem with matrices of influence coefficients is relatively new, since lifting surfaces of low aspect ratio have only recently become popular. The tendency is to treat this latter type of planform in the same way, i.e., in terms of natural frequencies and mode shapes when attacking the problem physically or when interpreting results. This tendency is still valid since coupled frequencies and mode shapes evolve as theoretical solutions to the flutter equations at zero airspeed, even though the problem has been formulated in terms of influence coefficients.

It is the intention of this report to adhere to the classical concepts of natural frequencies and mode shapes and elastic-axis location, rather than to consider matrices of influence coefficients or stiffness distributions. Valid criticism may accompany the concept of an elastic axis for any of the planforms considered because of sweep and low aspect ratio. Also, in the interest of simplicity, all models were designed to have identical spanwise distributions of mass and stiffness. The former varies as the square of the chord, and the latter varies as the fourth power of the chord. These distributions, which

were accomplished by tapering all dimensions linearly from root to tip, are typical of present-day aircraft. The absolute values of bending and torsional stiffness are measured by the magnitude of the first bending and the first torsional frequency, respectively, and that of the mass by the value of the flow parameter, μ . The models were designed to have constant values of chordwise center-of-gravity location, dimensionless moment of inertia in pitch and elastic-axis location at every spanwise station. No attempt was made to design chordwise distributions of mass or stiffness into the models although matrices of influence coefficients were measured in some cases.

With these simplifications, the parameters which were considered for each bare wing planform are:

mass ratio, μ

location of the chordwise center of gravity, x_α

dimensionless moment of inertia in pitch, r_α

first torsional frequency, ω_α

frequency ratio, $\frac{\omega_h}{\omega_\alpha}$

location of the elastic axis, a.

The ranges of the values of these parameters were chosen to be typical of present-day aircraft. By virtue of the design, the quantities, μ , x_α , r_α, and a are constant at all spanwise stations; the frequencies ω_h and ω_α , are three-dimensional structural properties. Natural frequencies higher than first bending and first torsion were not considered separately in the model design since their values are dictated by the choice of the mass and the stiffness distributions already mentioned. We also note that the mass and stiffness distributions determine the values of the mode shapes associated with each natural fre-

quency.

Other parameters which evolve from basic flutter theory are:

airfoil shape

structural-damping coefficients

Reynolds number

Prandtl number

ratio of specific heats.

For simplicity, the airfoil section was taken as a symmetrical double wedge for all the models, since it is probably of secondary importance in the flutter problem. For the structural-damping coefficients, the correct order of magnitude was obtained through discriminate choice of structural material. As high a Reynolds number as possible was obtained by using as large a scale model and as high a fluid density as practical with the available facility (Reference 13). Control of the values of Prandtl number and the ratio of specific heats was not considered since air was used as the testing medium.

For wings with control surfaces, additional parameters evolve out of model theory (see Appendix A.1), viz.,

location of the aileron hinge line, c

chordwise location of the aileron center of gravity, x_β

dimensionless radius of gyration of the aileron about its hinge line, r_β

frequency ratio, $\frac{\omega_\beta}{\omega_\alpha}$

Again, the problem has been formulated in terms of mode shapes and frequencies, and for the control surface, the stiffness chordwise is considered large with respect to the stiffness spanwise. The values of c, x_β and r_β were made constant at each spanwise station in the model-design procedure.

For wings with tip tanks (see Appendix A.2) in the cantilever or free-to-roll condition, we must define the geometry and mass of the tip tank in addition to the bare wing parameters already considered:

volume, $\frac{V_T}{4b^2\ell}$

location, $\frac{n_T}{b}$

mass, $\frac{M_T}{m\ell}$

static unbalance, $\bar{S}_T = \frac{S_T}{mb\ell}$

moment of inertia in pitch, $\frac{I_T}{mb^2\ell}$

moment of inertia in roll of the root support, $\frac{I_s}{m\ell^3}$

These parameters have been non-dimensionalized in a somewhat arbitrary fashion because of the simple theoretical model considered.

Having formulated the problem in terms of explicit parameters for all configurations, it now remains for us to devise a scheme of model design whereby desired values of the parameters can be obtained. Also, techniques of testing the models at zero airspeed and in the wind tunnel must be developed to verify our design values and to obtain the desired answers. Detailed con-

sideration of model design and testing techniques are presented in Reference 14. A cursory glance at the highlights, sufficient for this report, is given in Appendix D.

Since the emphasis of the research program was on experimental results, the theory was used primarily as a guide for model design. Only the straight-wing planform was treated theoretically since it is most amenable to analysis. The calculations were based on three-dimensional structural properties and two-dimensional supersonic aerodynamic forces since experience has shown that a similar procedure gives reasonable results for subsonic flutter below the transonic range. Also, other more complicated methods of analysis which are presently being developed, (e.g. Reference 20) were considered far too premature to be used on the present program. Some calculations based on Piston Theory were made because of its simplicity. In formulating the theory, only those degrees of freedom which experience had shown to be essential in the analysis were included. Thus, for the bare-wing and cantilever tip-tank calculations, only first bending and first torsion were included. For wings with control surfaces, the aileron degree of freedom was added, and for wings with freedom to roll, the rigid-body roll motion was added.

The choice of eigenvalues was such that most useful information for a given effort could be obtained from a model-design viewpoint. For example, in the theoretical analysis of the bare wing, the problem was set up so that the bending and torsional frequencies, which are measures of stiffness level were obtained as results for each set of assumed conditions (frequency and Mach number at flutter). In the analysis of wings with ailerons and wings with tip tanks, the torsional frequency along with the aileron frequency for the former and the tip-tank static unbalance for the latter were chosen as unknowns. This choice of eigenvalues still allows for a comparison between

theory and experiment so long as the complete range of experimental parameters is covered.

The theoretical results are presented in terms of the flutter coefficient, $\frac{V_F}{b_o \omega_\alpha}$, rather than in terms of a velocity ratio, as has been done in the past. This procedure eliminates the necessity of treating velocity (v), size (b) and stiffness level (ω_α) as separate parameters. Also, this dimensionless quantity evolves out of the theory (see Appendix C.1).

SECTION III

PRESENTATION OF RESULTS

3.1 Bare Wings

3.1.1 Straight

In designing the bare straight-wing models, an attempt was made to vary the first torsional frequency of the wing keeping all other pertinent dimensionless parameters constant, viz.,

mass ratio, μ

location of chordwise center of gravity, x_α

dimensionless mass moment of inertia in pitch, r_α

frequency ratio, $\frac{\omega_h}{\omega_\alpha}$

location of elastic axis, a

spanwise mass and stiffness distributions.

In this way, experimental curves of the flutter coefficient, $\frac{V_f}{b_o \omega_\alpha}$, and the reduced frequency, k, could be determined as a function of Mach number. These experimental curves could then be compared with those obtained by theory in order to test the validity of the theory and, if necessary, aid in the development of a criterion for torsional rigidity.

This choice of parametric variation was particularly difficult to accomplish insofar as model design was concerned because of the interdependence of the parameters and the requirement that the frequency ratio, $\frac{\omega_h}{\omega_\alpha}$, be held constant, so that some variations occurred in the parameters which were to be held constant. Control of the mass ratio, μ, was difficult

because of the change in air density with Mach number and the fact that the Mach number at flutter could not be accurately predicted beforehand. The values of other mass parameters, center-of-gravity location, c.g., and moment of inertia in pitch, r_α , as well as the spanwise distributions of mass and stiffness could be controlled accurately. Insofar as elastic axis is concerned, there was some question as to how this concept should be handled for real wings. After some research late in the program, it was decided that, based on classical flutter theory, the elastic axis should be treated as the locus of shear centers rather than as that point on the wing where bending and torsion is statically uncoupled, "apparent" elastic axis (see Reference 21). Experiments showed that the locus of this latter point varied slightly along the wing because of sweep and root effects. Furthermore, accurate control of the locus of shear centers could be maintained by careful construction of the models, since the location of the shear center is a function of the position of the structural elements of the model. Both measured "apparent elastic axis" and calculated locus of shear centers are tabulated in Appendix D where available. Good control of the frequency ratio, $\frac{\omega_h}{\omega_\alpha}$, also evolved with experience. Careful selection of balsa wood and realistic estimates of the effect of glue were made late in the program. A detailed tabulation of the parameters for all the models tested is given in Appendix D.

In order to determine the effects on flutter of those parameters which were difficult to control accurately in the models, theoretical straight wing studies were made varying these parameters. Figure 3.1 presents a systematic variation of,

frequency ratio, $\frac{\omega_h}{\omega_\alpha}$

mass ratio, μ

elastic axis, a

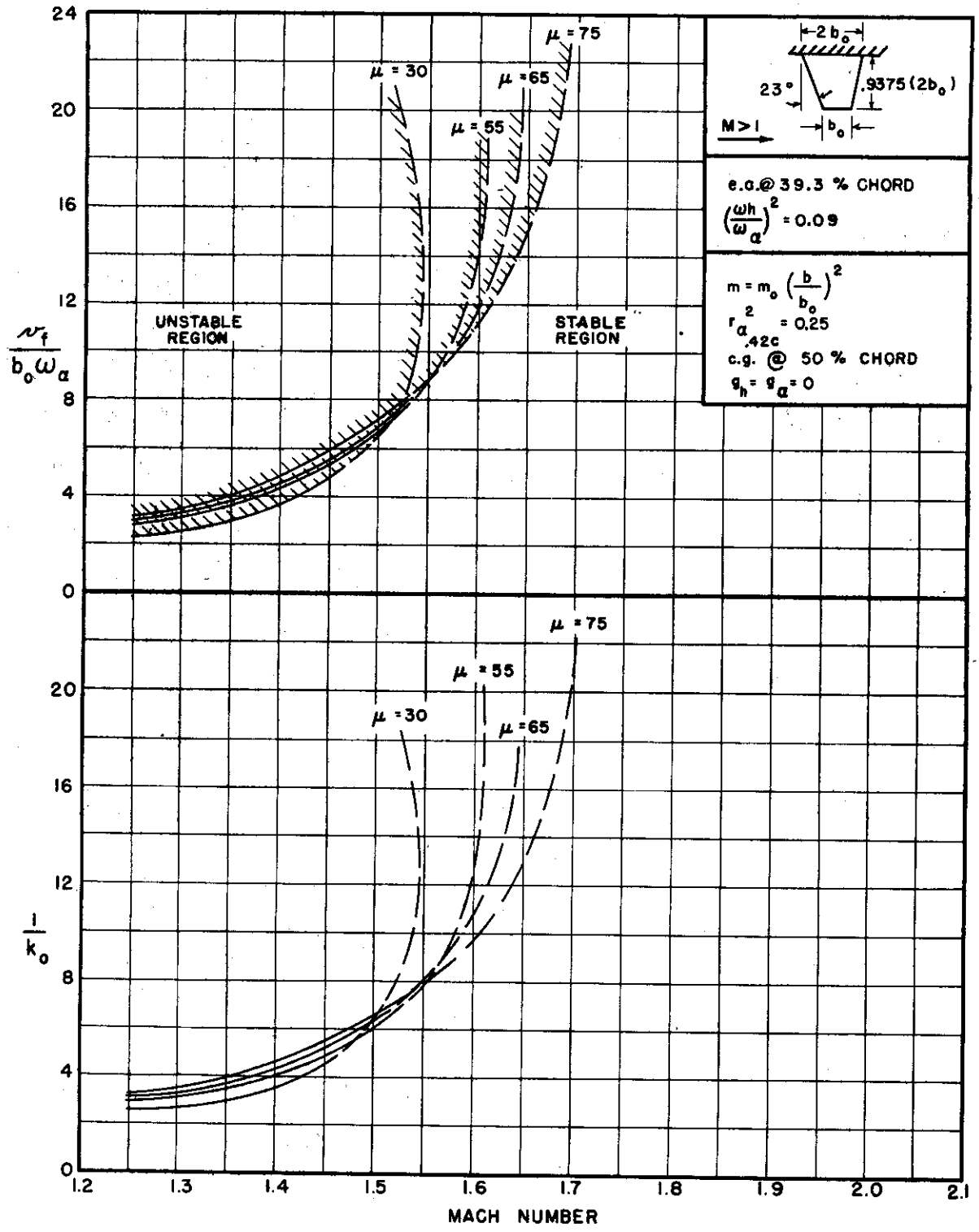

FIGURE 3.1(a) THEORETICAL RESULTS FOR BARE STRAIGHT-WING PLANFORM, e.a. AT 39.3% CHORD, $\left(\frac{\omega_h}{\omega_\alpha}\right)^2 = 0.09$

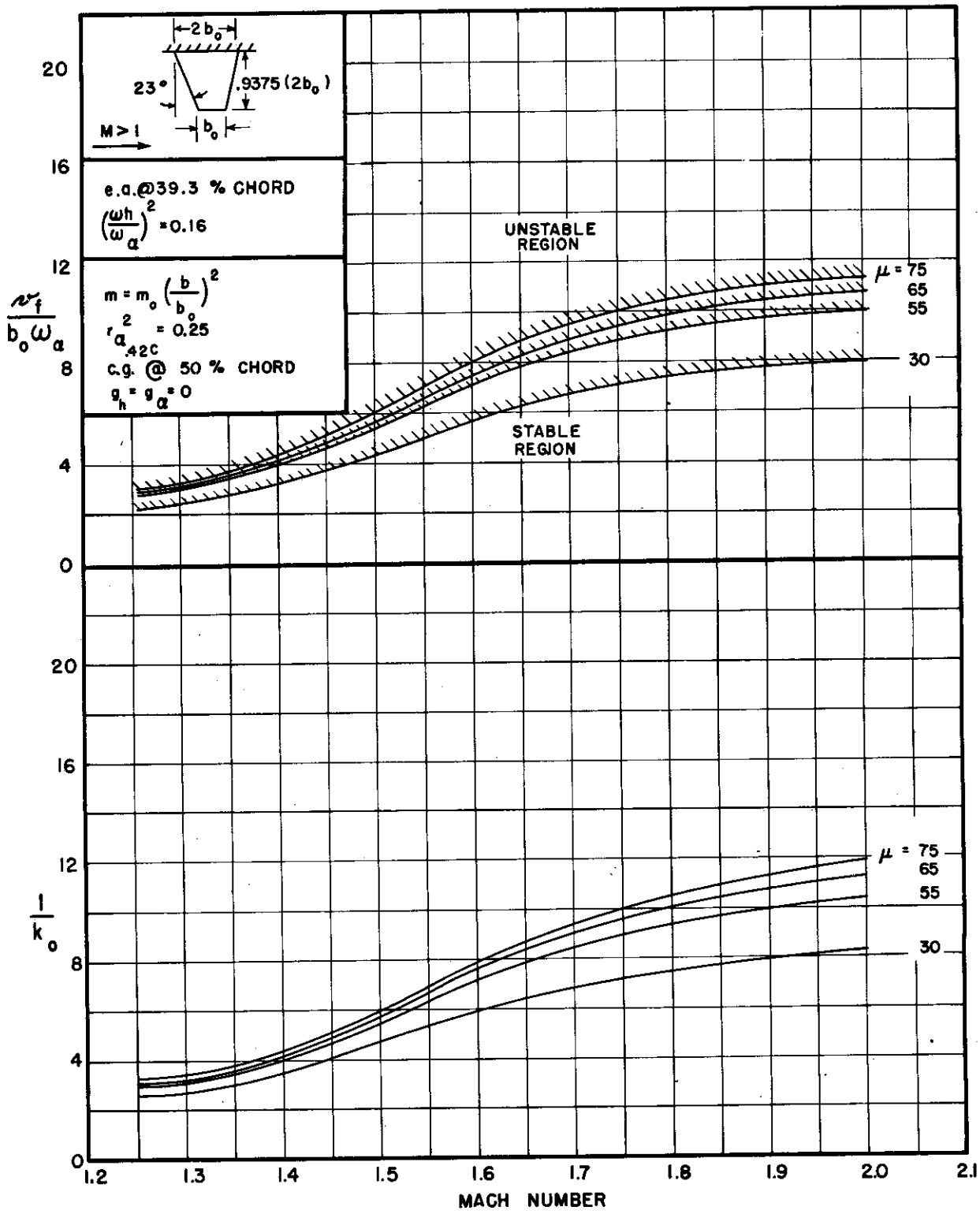

FIGURE 3.1(b) THEORETICAL RESULTS FOR BARE STRAIGHT-WING PLANFORM, e.a. AT 39.3% CHORD, $\left(\frac{\omega_h}{\omega_\alpha}\right)^2 = 0.16$

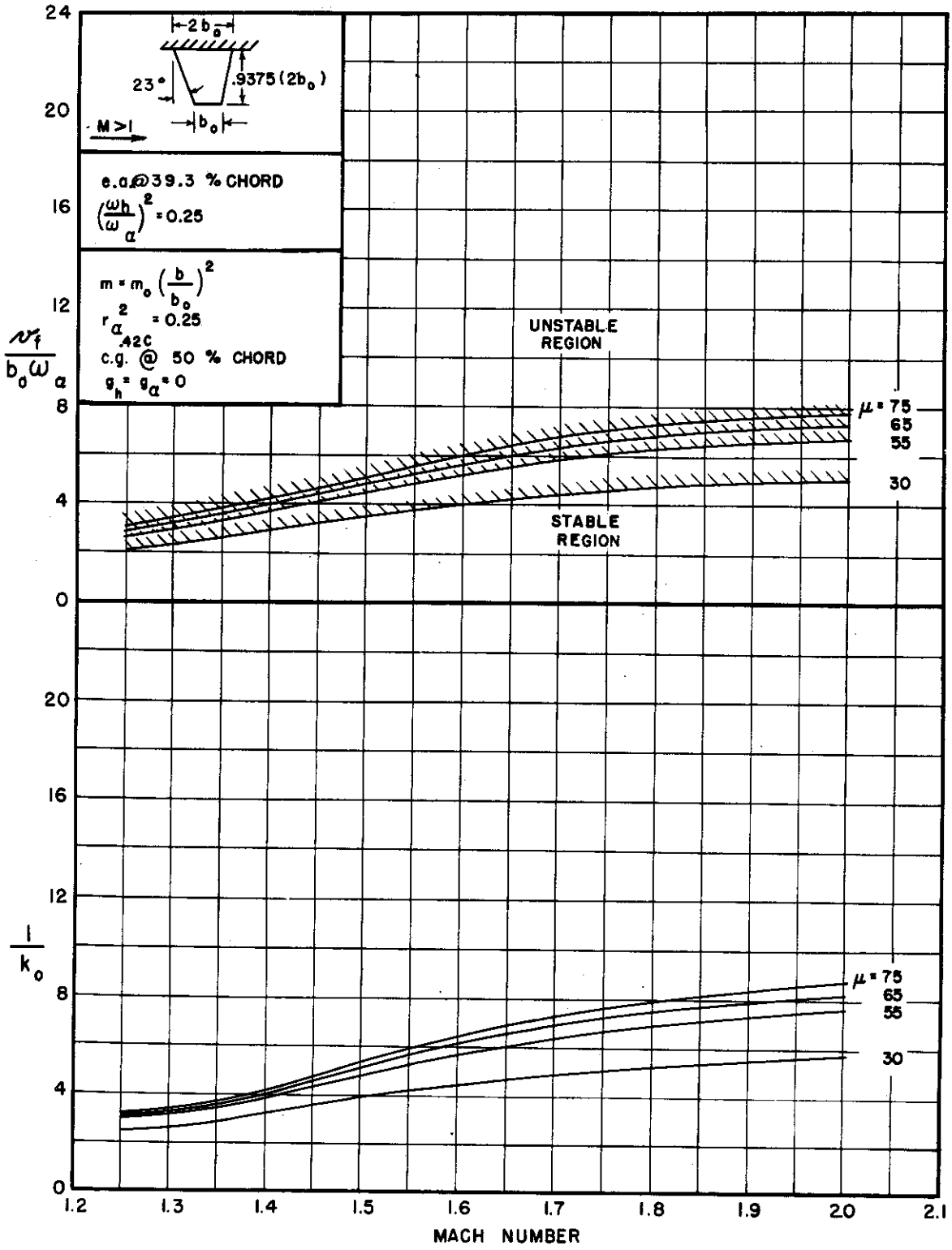

FIGURE 3.1(c) THEORETICAL RESULTS FOR BARE STRAIGHT-WING PLANFORM, e.a. AT 39.3% CHORD, $\left(\frac{\omega_h}{\omega_\alpha}\right)^2 = 0.25$

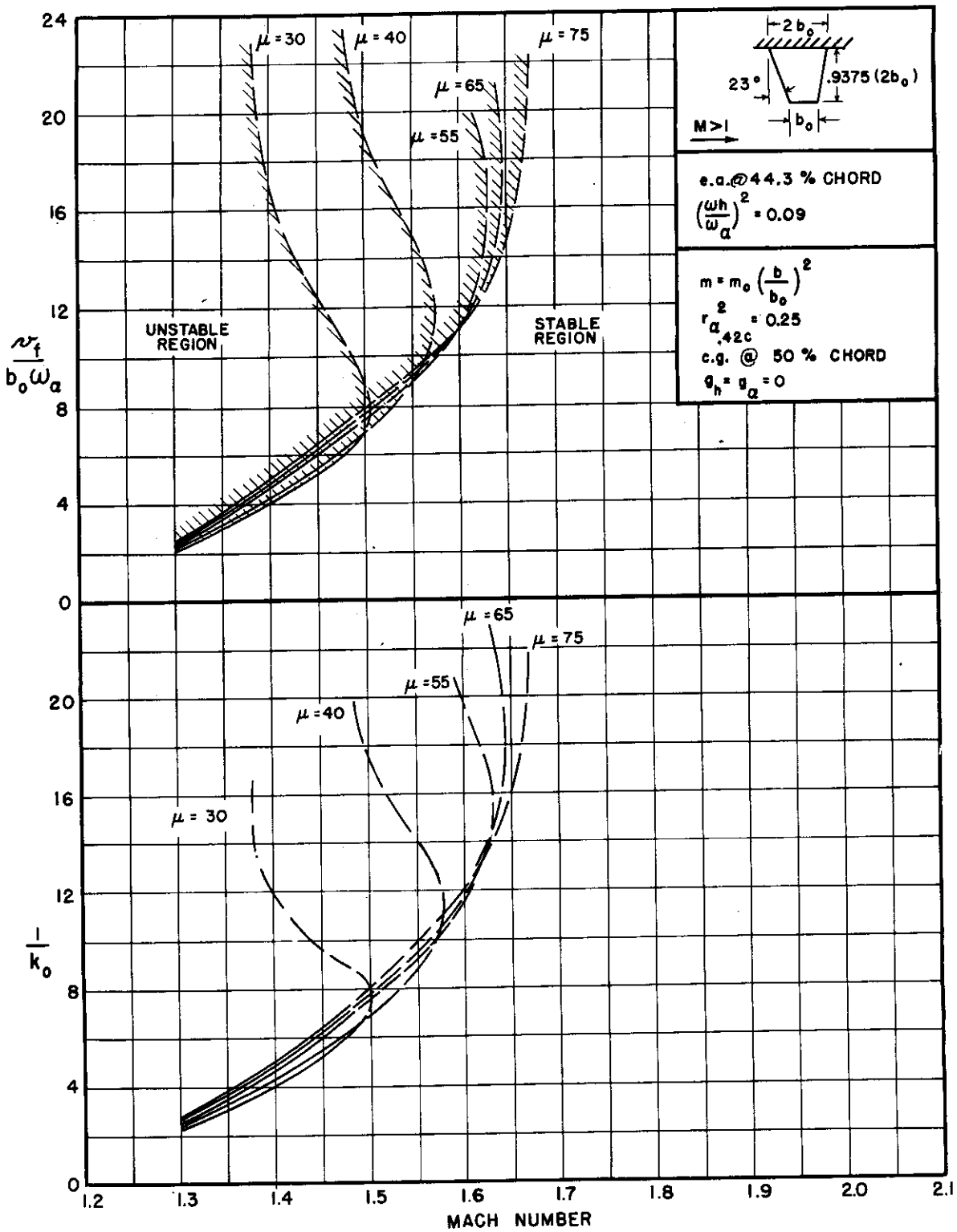

FIGURE 3.1(d) THEORETICAL RESULTS FOR BARE STRAIGHT-WING PLANFORM, e.a. AT 44.3% CHORD, $\left(\frac{\omega_h}{\omega_\alpha}\right)^2 = 0.09$

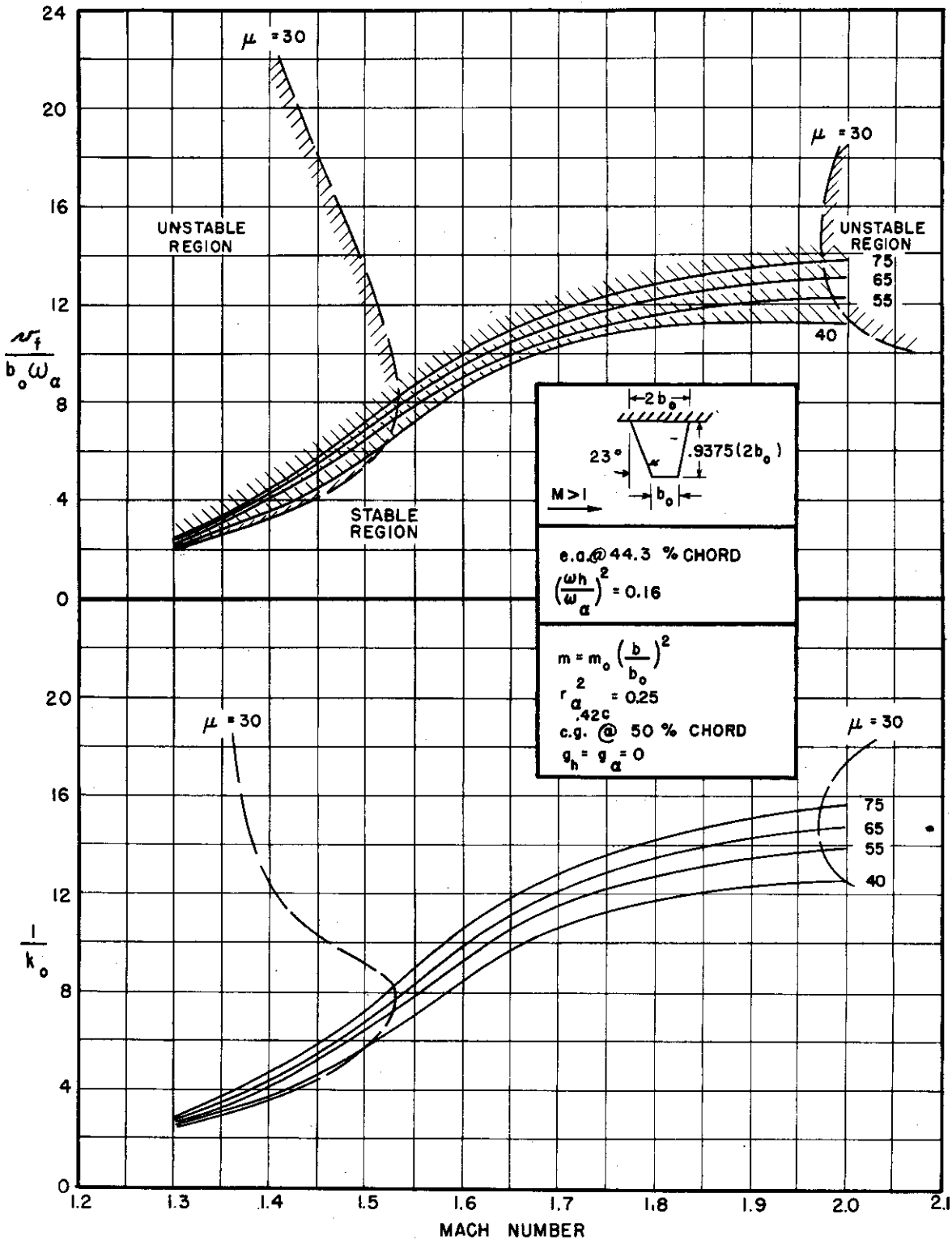

FIGURE 3.1(e) THEORETICAL RESULTS FOR BARE STRAIGHT-WING PLANFORM, e.a. AT 44.3% CHORD, $\left(\frac{\omega_h}{\omega_\alpha}\right)^2 = 0.16$

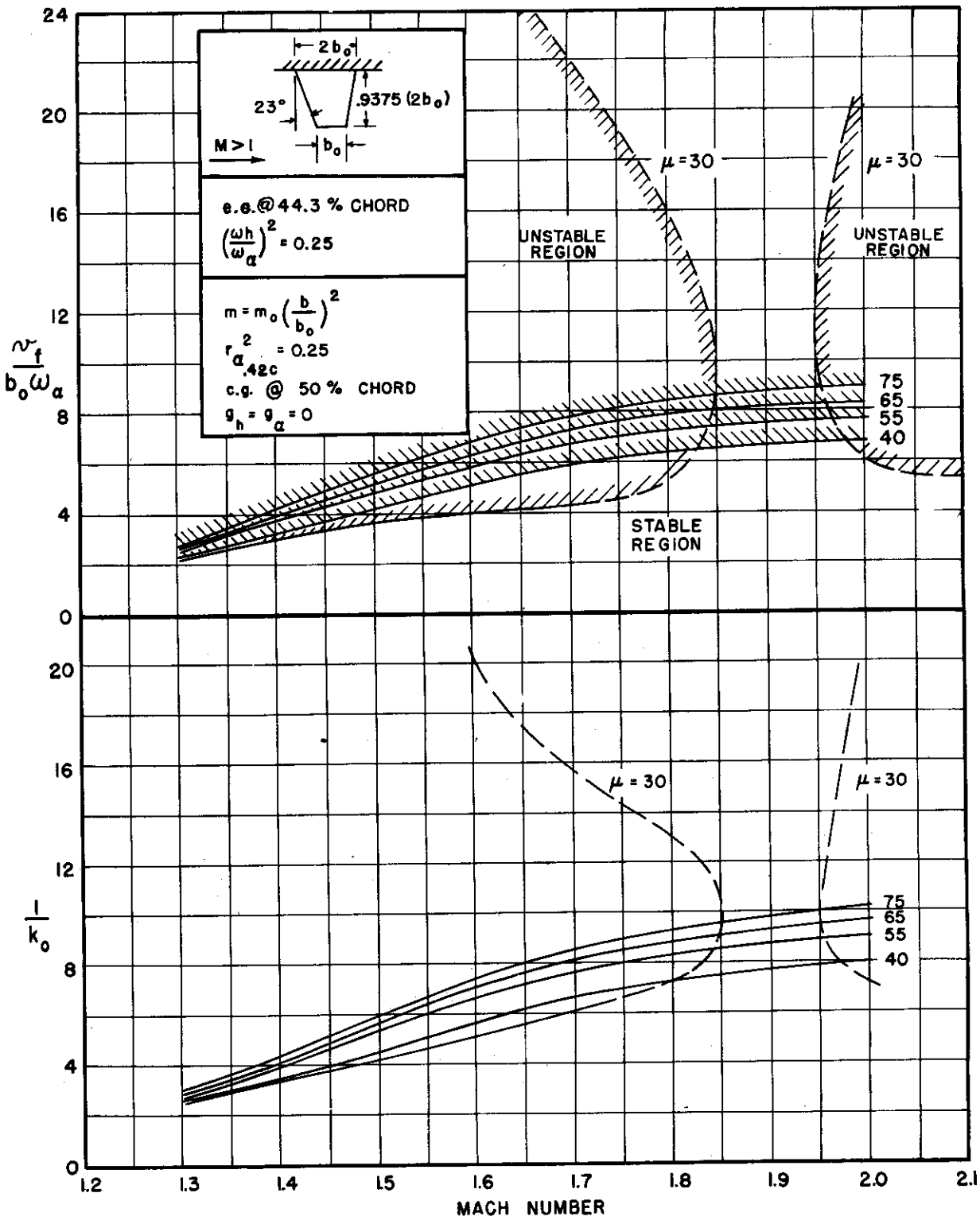

FIGURE 3.1(f) THEORETICAL RESULTS FOR BARE STRAIGHT-WING PLANFORM, e.a. AT 44.3% CHORD, $\left(\frac{\omega_h}{\omega_\alpha}\right)^2 = 0.25$

for fixed spanwise mass and stiffness distributions, fixed moment of inertia in pitch and fixed chordwise center-of-gravity location. Taper was taken into account in determining the aerodynamic forces. All the curves of Figure 3.1 were based on zero structural damping. However, spot checks showed that inclusion of a small amount of structural damping ($g = 0.01$) in the analysis did not alter the answers appreciably, probably because all of the calculated cases had reasonable amounts of positive static unbalance. Two-dimensional aerodynamic coefficients and three-dimensional structural properties were used in the theoretical calculations. The detailed formulation of the theory is given in Appendix A.1, and an example analysis is presented in Appendix C.2. Theoretical results for values of frequency ratio, $\frac{\omega_h}{\omega_\alpha}$, other than those presented in Figure 3.1 can be obtained by cross-plotting the curves of Figure C.1. Because available tabulated values of the supersonic oscillatory aerodynamic coefficients were limited (Ref. 7), portions of the curves of Figure 3.1 could not be defined accurately. These doubtful portions are presented as dashed lines.

Figure 3.1 shows that, in the range of practical interest ($\frac{V_f}{b_o \omega_\alpha} \leq 5$), the theoretical stability boundaries are not very sensitive to changes in the parameters, mass ratio and elastic-axis location (for the ranges considered) but do vary somewhat with frequency ratio, $\frac{\omega_h}{\omega_\alpha}$. We also notice that the trends are comparable to those to be expected from experience in subsonic flow (Ref. 22), i.e., the region of instability increases with,

decreasing mass ratio, μ

increasing distance between the elastic axis and the center of gravity, x_α

increasing frequency ratio, $\frac{\omega_h}{\omega_\alpha}$

The theoretical curves of Fig. 3.1 may be used to predict the onset of flutter which will be given by the intersection of an operating line and the flutter boundary. The operating line for a model with a given set of mass and stiffness parameters depends on the velocity- Mach number relationship of the environment in which the model is tested. Velocity at a given Mach number is a function of the ambient temperature only. Velocity versus Mach number for extreme ranges of the atmosphere and of the facility used for flutter testing on this program is given in Figure 3.2. In the tunnel the stagnation temperature is roughly that of the atmosphere, and at a given Mach number the static temperature, and hence the speed of sound and velocity, is less than atmospheric in accordance with isentropic flow relations. Figure 3.2 shows graphically the difference between the velocity- Mach number relationship in the atmosphere and the wind tunnel. A given model will then have a different operating line in the tunnel than it

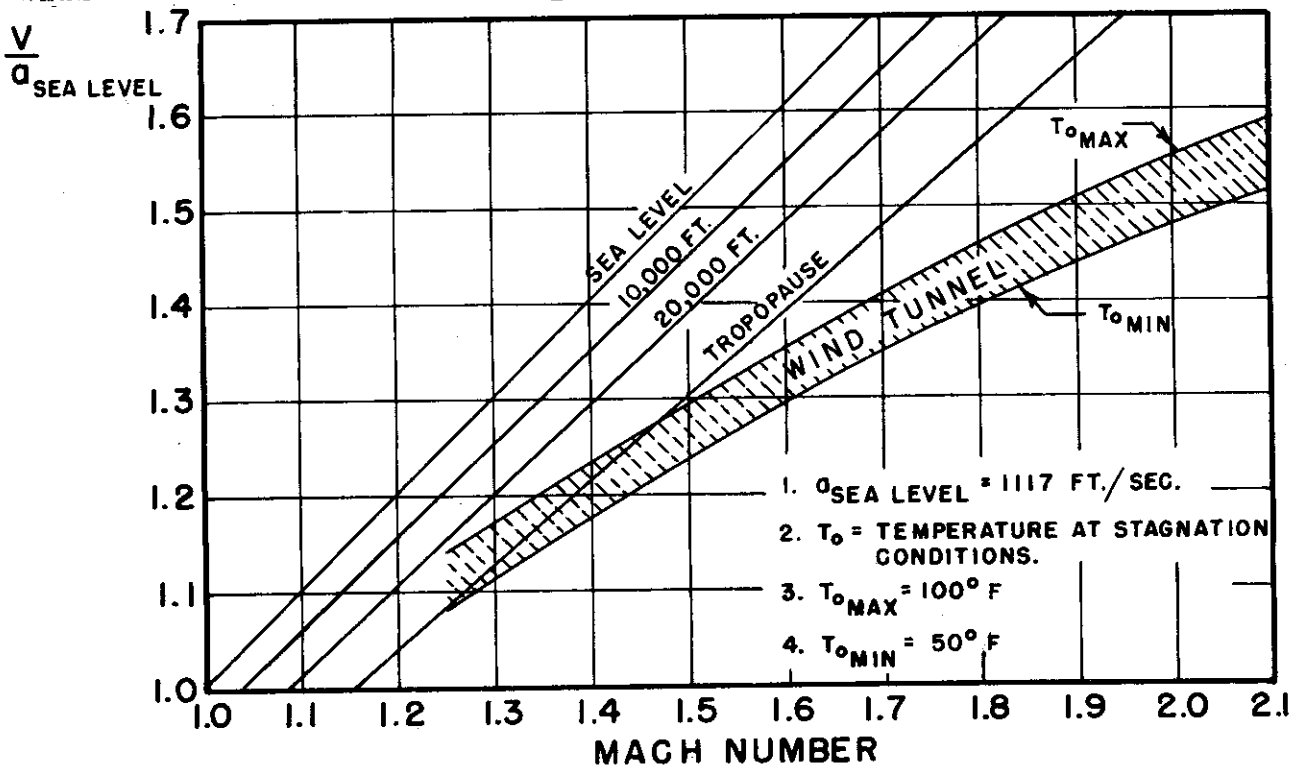

FIGURE 3.2 VELOCITY VERSUS MACH NUMBER FOR EXTREME RANGES OF ATMOSPHERIC AND WIND TUNNEL CONDITIONS

has in the atmosphere. Figure 3.3, illustrates this point. It shows the operating lines for a model in the wind tunnel and in the standard atmosphere at sea level and at the tropopause. Since these operating lines are not the same they intersect the flutter boundary at different values of Mach number. It is also interesting to note that if the flutter boundary is to be approached from a stable region at either constant altitude in the atmosphere or in the tunnel, it must be approached by decreasing the Mach number.

For all of the straight wing models tested on the present program the theoretical Mach number of flutter has been determined from curves similar to Figure 3.3. The flutter Mach number has been determined for conditions in the tunnel and in the standard atmosphere. The theoretical Mach numbers of flutter so determined are compared with the flutter Mach number of the actual tests. These results are given in Table 3.1.

An even more graphic comparison between theory and experiment is given in Figure 3.4. All the legitimate experimental flutter points were obtained by injecting the model into a stable region and decreasing the Mach number until flutter occurred. All the straight wings built on this program fluttered, and no single-degree-of-freedom torsion flutter was encountered experimentally (see Ref. 23, p. 6). The scatter of the data is small and most of the deviations from the mean can be explained. The models which fluttered during injection would have their marginally stable condition at higher Mach number. These injection flutters generally occurred at frequencies closer to the first torsional frequency than would otherwise be expected. Models ST-1d and ST-1d-1 were designed with elastic axes forward so that they had slightly higher values of the coefficient, $\frac{V_f}{b_o \omega_\alpha}$, than the other models, verifying the trend predicted by the theory. Model ST-12 was a low-density, μ_f=30, wing designed to have a margin of safety against flutter based on the test results of models with mass ratio on the order of 65 and on the theoretical effect of lowering the mass

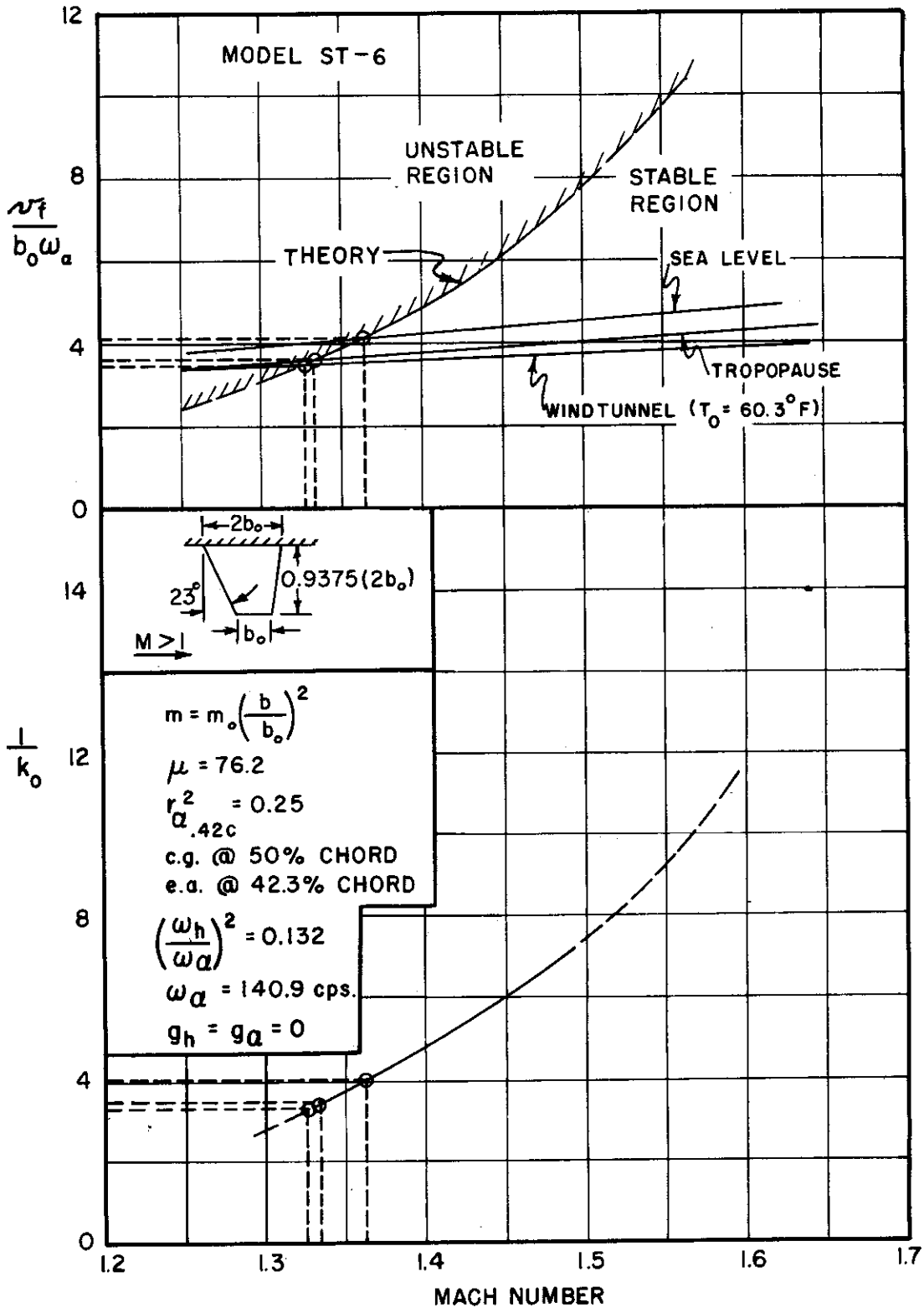

FIGURE 3.3 EXAMPLE USE OF THEORETICAL CURVES

TABLE 3.1

MACH NUMBER AND FREQUENCY AT FLUTTER FOR STRAIGHT-WING PLANFORM, THEORY AND EXPERIMENT

	Experiment		Theory						Structural-Damping Coefficient in Theory
	Wind Tunnel		Wind Tunnel		Tropopause		Sea Level		
	Bare Wings								
Model	M_f	ω_f cps	M_f	ω_f cps	M_f	ω_f cps	M_f	ω_f cps	
ST-1	1.52	85.7	1.33	150	1.33	130	1.36	145	0
ST-1d	1.59	82.7	1.29	135	1.31	120	1.38	125	0
ST-1d-1	1.52	86.2	1.35	150	1.35	135	1.41	140	0
ST-2*	1.71	110	1.39	115	1.39	95	1.44	95	0
ST-4	1.52	93.7	1.32	165	1.33	140	1.37	145	0
ST-4-1	1.30	98.4	1.33	170	1.33	145	1.37	145	0
ST-5	1.44	83.3	1.33	155	1.33	130	1.37	135	0
ST-5-1	1.47	89.5	1.35	150	1.35	130	1.38	135	0
ST-6	1.72	78.3	1.33	140	1.34	120	1.37	120	0
ST-7-1*	1.88	76.9	1.38	115	1.39	100	1.43	100	0
ST-7-2*	1.92	108.0	1.39	115	1.39	95	1.44	95	0
ST-7-3	1.94	81.5	1.36	130	1.39	105	1.42	105	0
ST-12	1.45	120.8	1.30	215	1.30	190	1.33	195	0
Wings with Tip Tanks (Cantilever)									
ST-1a*	1.80	21.4	unstable 1.59	-- 36	unstable unstable	-- --	unstable unstable	-- --	0 0.01
ST-1c*	1.83	18.1	1.54 1.43	48 38	1.56 1.43	49 38	1.62 1.48	47 37	0 0.01
ST-4a	1.43	26.3	1.50 stable	63 --	1.40 stable	61 --	1.48 stable	67 --	0 0.01
ST-4b*	1.83	29.4	unstable 1.60	-- 38	unstable unstable	-- --	unstable unstable	-- --	0 0.01
Wings with Tip Tanks (free-to-roll)									
ST-4c-1	1.33	33.9	1.57	50	1.60	52	1.62	59	0
ST-4c-2	1.32	30.0	1.57	49	1.60	52	1.62	59	0
ST-4c-3	1.32	32.7	1.57	50	1.60	52	1.62	59	0
Wings with Ailerons									
ST-1b*	1.80	200.0	1.34	190	1.34	185	1.35	195	0
ST-1e	1.72	87.9	1.37	140	1.38	135	1.44	135	0
ST-1f	1.65	87.5	1.36	160	1.36	145	1.38	150	0

*Injection flutter

Note: tip-tank solutions attempted only inside interval $1.3 < M < 1.8$

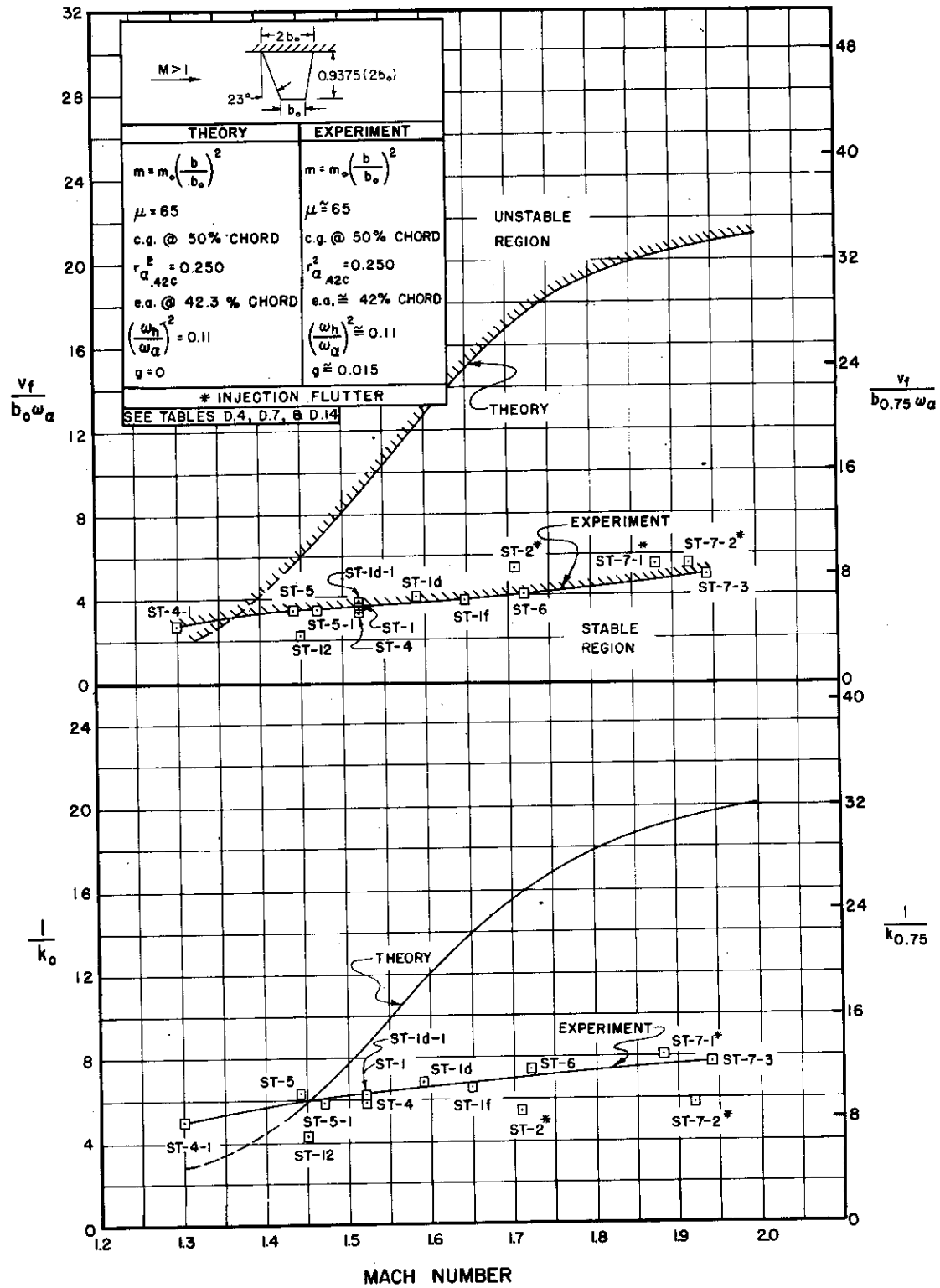

FIGURE 3.4 THEORETICAL AND EXPERIMENTAL FLUTTER STABILITY BOUNDARIES FOR BARE STRAIGHT-WING PLANFORM

ratio. When the model fluttered, the experimental results were re-interpreted on the basis of the parameter, $\frac{V_f}{b_o \omega_\alpha} \sqrt{\frac{1}{\mu_f}}$. Theoretically, the flutter coefficient and the mass ratio are independent parameters and consequently cannot be combined into a single quantity. Piston theory shows, however, that for the case of high supersonic bending-torsion flutter of a representative two-dimensional section, this combination can be demonstrated analytically for some special cases (Ref. 24, p. 81 ff). The semi-empirical flutter formula proposed in Reference 22 (p. 17) for subsonic flow also suggests this combination.

Figure 3.5 shows the results of plotting the experimental data on the basis of this parameter. We see that the scatter of Model ST-12 is considerably reduced with no appreciable loss of consistency in the other data points. The range of mass ratio is not large enough to determine if this trend is general however.

Figure 3.4 emphatically shows the value of being able to vary the Mach number during a flutter model test. If a fixed nozzle of low supersonic Mach number were used, we might conclude that the theory gave good agreement with experiment, and there would be some doubt as to the location of the neutrally stable region. The gross deviation between theory and experiment at higher Mach numbers led to a theoretical investigation using Piston theory. The theoretical formulation is presented in Appendix A.3, and a numerical example is given in Appendix C.6. The results of this investigation are shown in Figure 3.6. It should be emphasized that this theory is valid only at high Mach numbers, well out of the range of the experimentation of this program. We see that if thickness is taken into account, the results of Piston Theory give better agreement with experiment than the results of the classical theory near Mach 2. Piston Theory certainly does not apply at Mach numbers below 2.0.

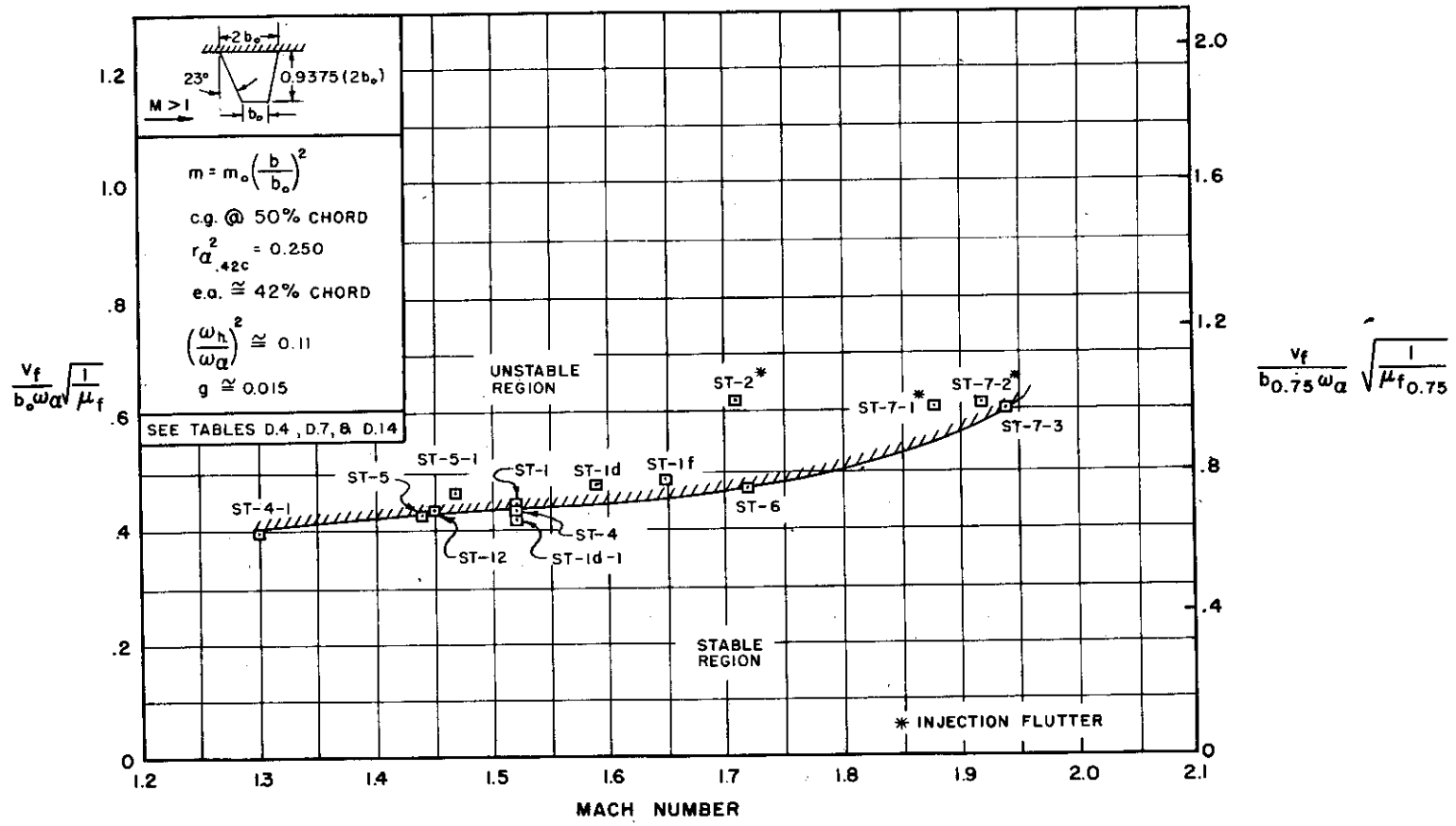

FIGURE 3.5 EXPERIMENTAL FLUTTER STABILITY BOUNDARY FOR BARE STRAIGHT-WING PLANFORM BASED ON THE COEFFICIENT, $\frac{V_f}{b_0 \omega_\alpha}\sqrt{\frac{1}{\mu_f}}$

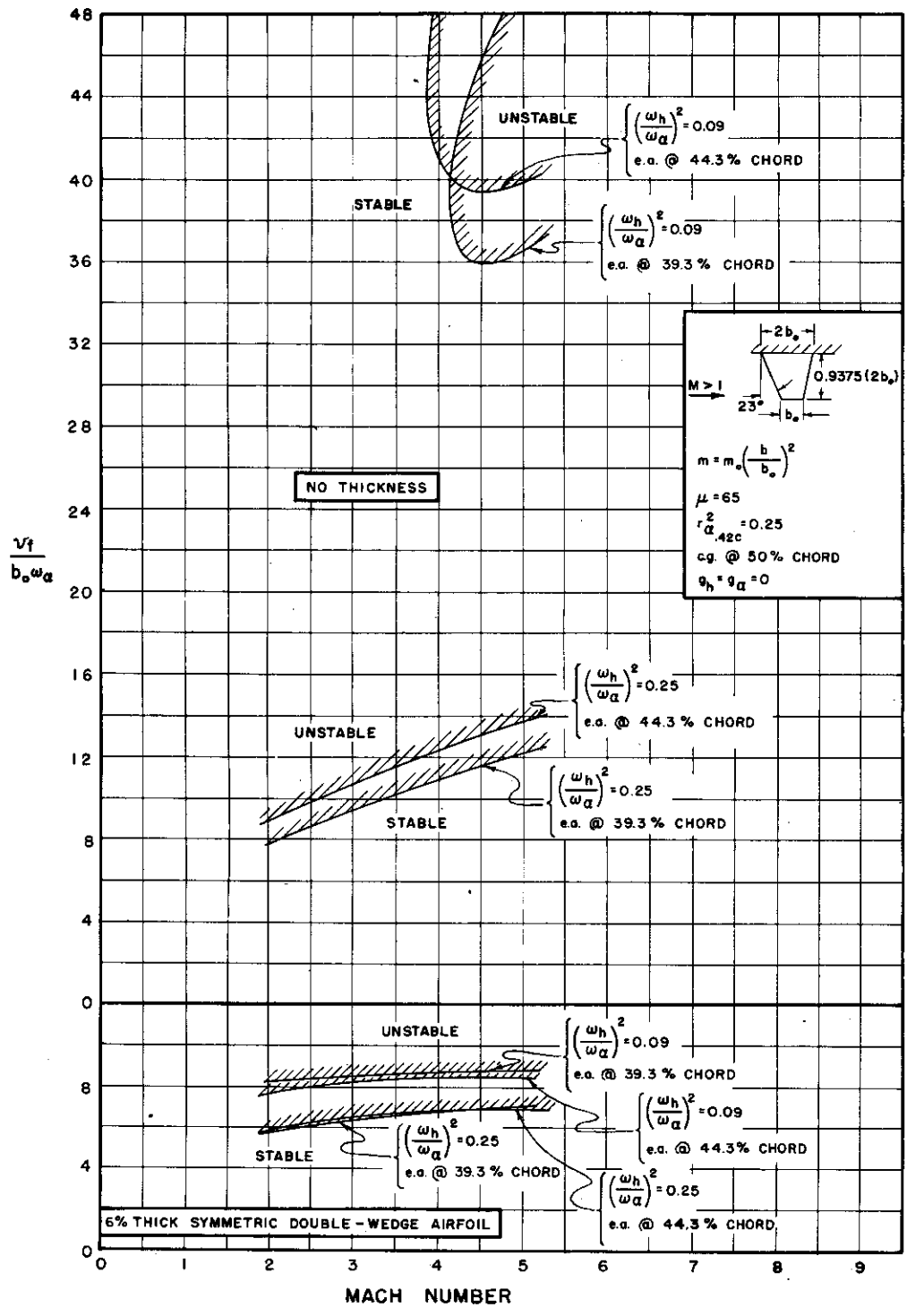

FIGURE 3.6 THEORETICAL RESULTS FOR BARE STRAIGHT-WING PLANFORM BASED ON PISTON THEORY

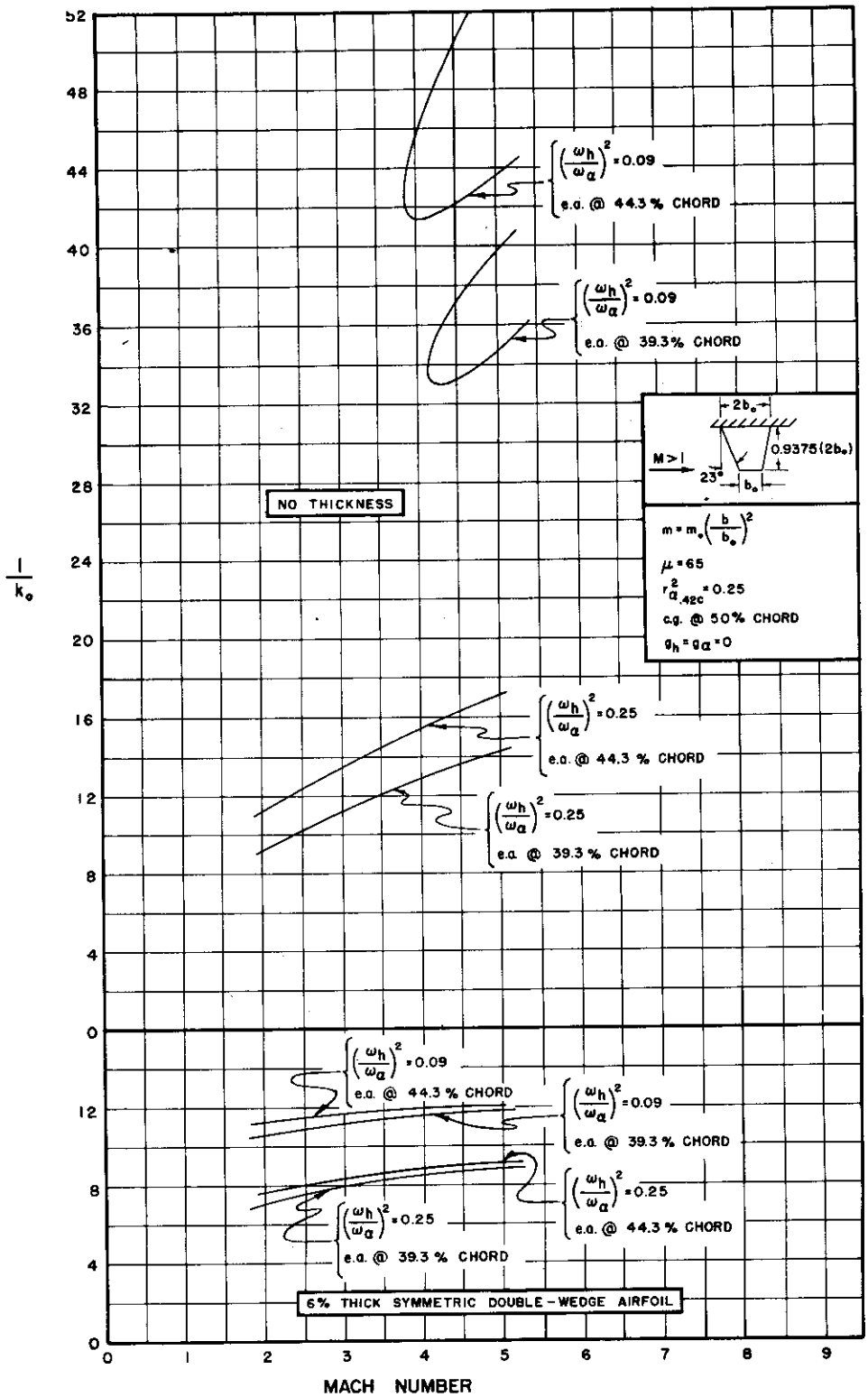

FIGURE 3.6 (Continued) THEORETICAL RESULTS FOR BARE STRAIGHT-WING PLANFORM BASED ON PISTON THEORY

Reference 25, based on potential flow solutions, shows that the effect of thickness on the damping of an oscillating airfoil in the range of Mach number from 2.0 to about 1.2 may be either stabilizing or destabilizing depending on the Mach number, reduced frequency, and other parameters. Reference 33, based on Piston Theory, shows that the effect of thickness, for the cases considered there, is destabilizing and that the effect increases with increasing Mach number. It should also be mentioned that even though the Piston Theory shows a tremendous effect due to thickness, this effect may not be as large as the results indicate, because terms have been neglected in the analysis which could be of the same order of magnitude as the thickness terms. The results are presented in order to determine trends for a better insight into what happens at high Mach number.

For purposes of comparison, Figure 3.7 gives the results of a theoretical flutter analysis based on incompressible aerodynamic coefficients (Ref. 26). A numerical example is given in Appendix C.1. It is interesting to note that the incompressible theory gives almost the same results as the supersonic theory near Mach number 1.35.

It is interesting to compare the flutter parameters of the models tests on this program with those of some actual high-speed airplanes. Table 3.2 gives flutter parameters for three representative airplanes. The data in Table 3.2 has been derived from actual airplane data, averaged to give representative straight, swept and delta wing airplanes. The torsional frequency of the scaled model, $(\omega_\alpha)_M$, is included in Table 3.2 so that a direct comparison could be made of the model and actual airplane stiffness. From dimensional analysis it can be shown that if Mach

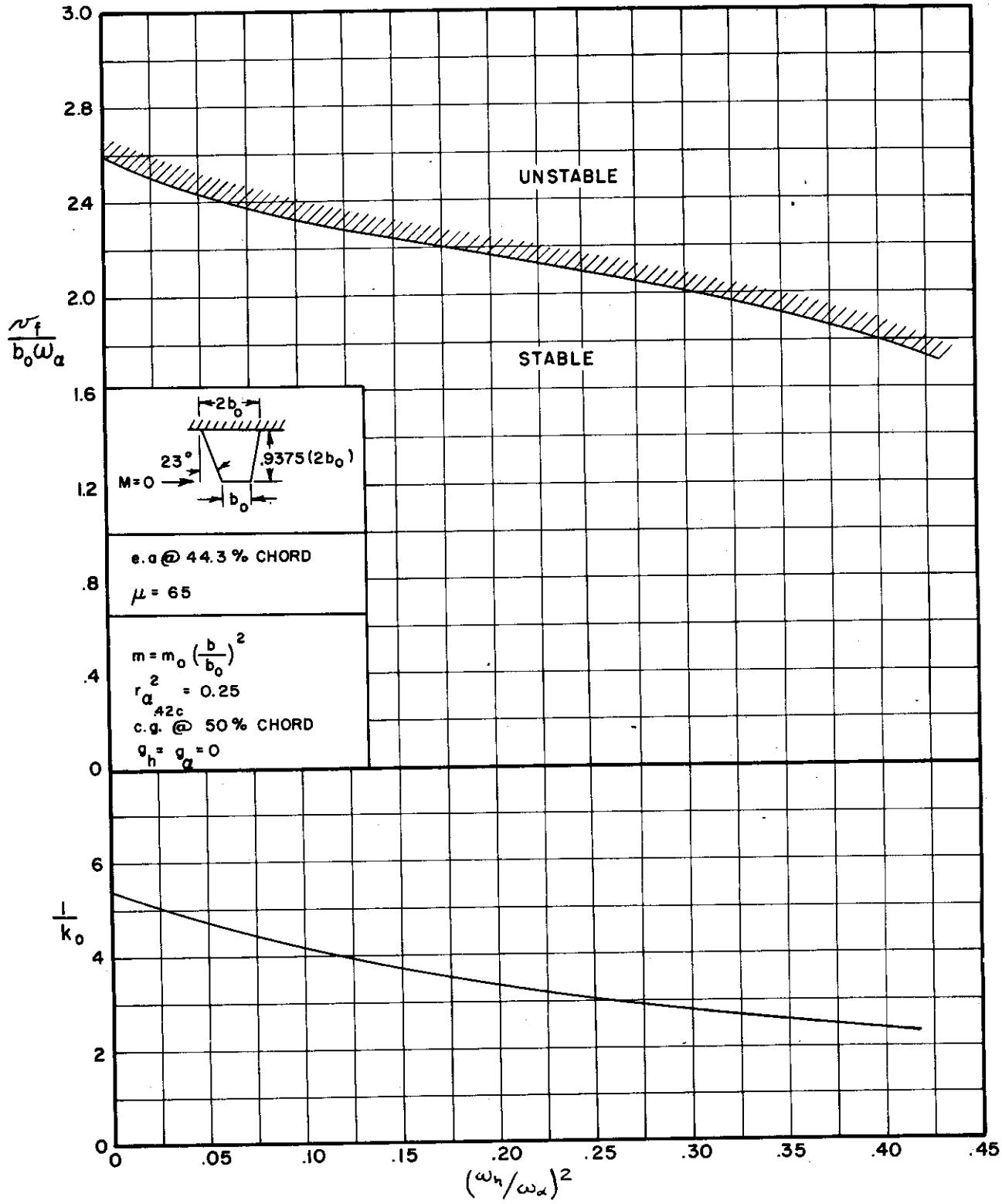

FIGURE 3.7 THEORETICAL RESULTS FOR BARE STRAIGHT-WING PLANFORM BASED ON INCOMPRESSIBLE THEORY

number is to be kept constant from model to airplane, the following relationship holds,

$$\frac{(\omega_\alpha)_M}{(\omega_\alpha)_A} = \frac{L_A}{L_M}\sqrt{\frac{T_A}{T_M}} \qquad \text{Eq. (3.1)}$$

where

ω_α is the first torsional frequency of the wing
L is length
T is temperature

The subscripts, M and A, refer to model and airplane, respectively. The scaled model frequencies, $(\omega_\alpha)_M$, of Table 3.2 were calculated assuming a scaled model of the airplane with a root chord equal to that of the wings tested on this program (10 inches). Air was assumed as the model testing medium. The air was assumed to expand adiabatically from a stagnation temperature equal to room temperature (70^oF) (See Reference 12).

3.1.2 Swept

The experimental data for the bare swept wings are presented graphically in Figure 3.8; no theoretical work was done for this planform. Less extensive tests were conducted on the swept than on the straight wings, and some of the models tested did not flutter (see Table D.8). Again, all legitimate flutter points were obtained by injecting the model into a stable region and decreasing the Mach number until flutter occurred. The remarks made above pertaining to control of the parameters for the straight wings are also applicable to this planform.

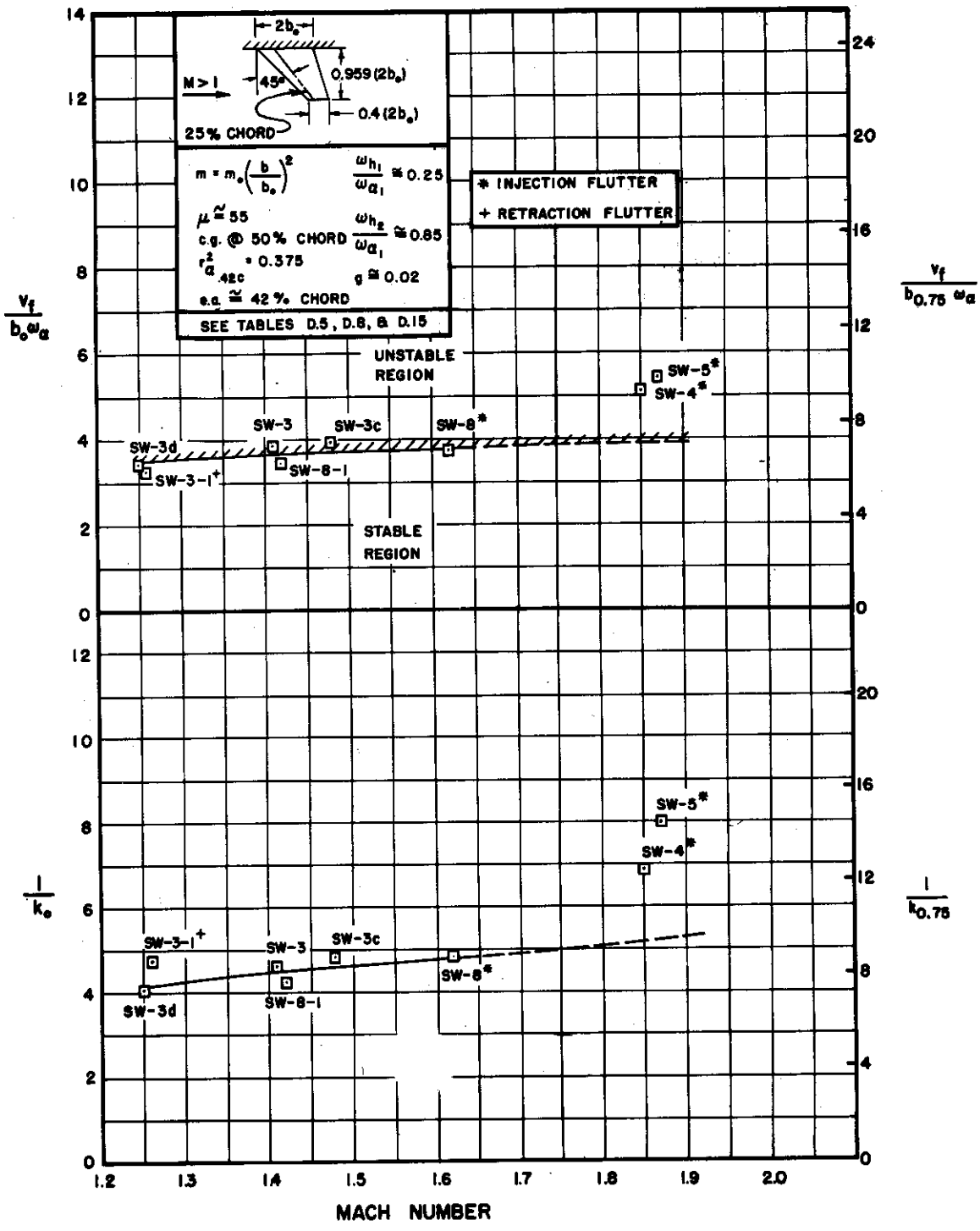

FIGURE 3.8 EXPERIMENTAL FLUTTER STABILITY BOUNDARY FOR BARE SWEPT-WING PLANFORM

In Figure 3.8 those models which fluttered during injection would probably be neutrally stable at higher values of Mach number, and the model which fluttered during retraction would probably be neutrally stable at a lower Mach number. Models SW-3c, SW-3 and SW-3d were purposely designed to have three different elastic-axis locations (loci of shear centers). All other parameters were held very nearly constant (see Tables D.5 & D.8). The theoretical and experimental trend evidenced by

Model	e.a. % chord	M_f	ω_α cps
SW-3c	37.0	1.48	135
SW-3	42.0	1.41	132
SW-3d	47.0	1.25	137

the straight-wing planform holds, i.e., moving the elastic axis forward from a given center-of-gravity location is equivalent to a decrease in stiffness. Therefore, on Figure 3.8, Model SW-3c should have a slightly higher and Model SW-3d a slightly lower value of the flutter coefficient, $\frac{V_f}{b_o \omega_\alpha}$, than the mean.

The destabilizing effect of lowering the mass ratio, is evidenced by Model SW-8 (See Table D.8) which was tested once without flutter. In a second test during which the mass ratio was lowered by raising the air density in the test section, the model fluttered during injection. If the experimental results are plotted on the basis of the parameter, $\frac{V_f}{b_o \omega_\alpha}\sqrt{\frac{1}{\mu_f}}$, (Figure 3.9), there is no appreciable increase in scatter, but again there is no sound theoretical basis for this choice of parameter, and it should be used cautiously because of the scantiness of the data.

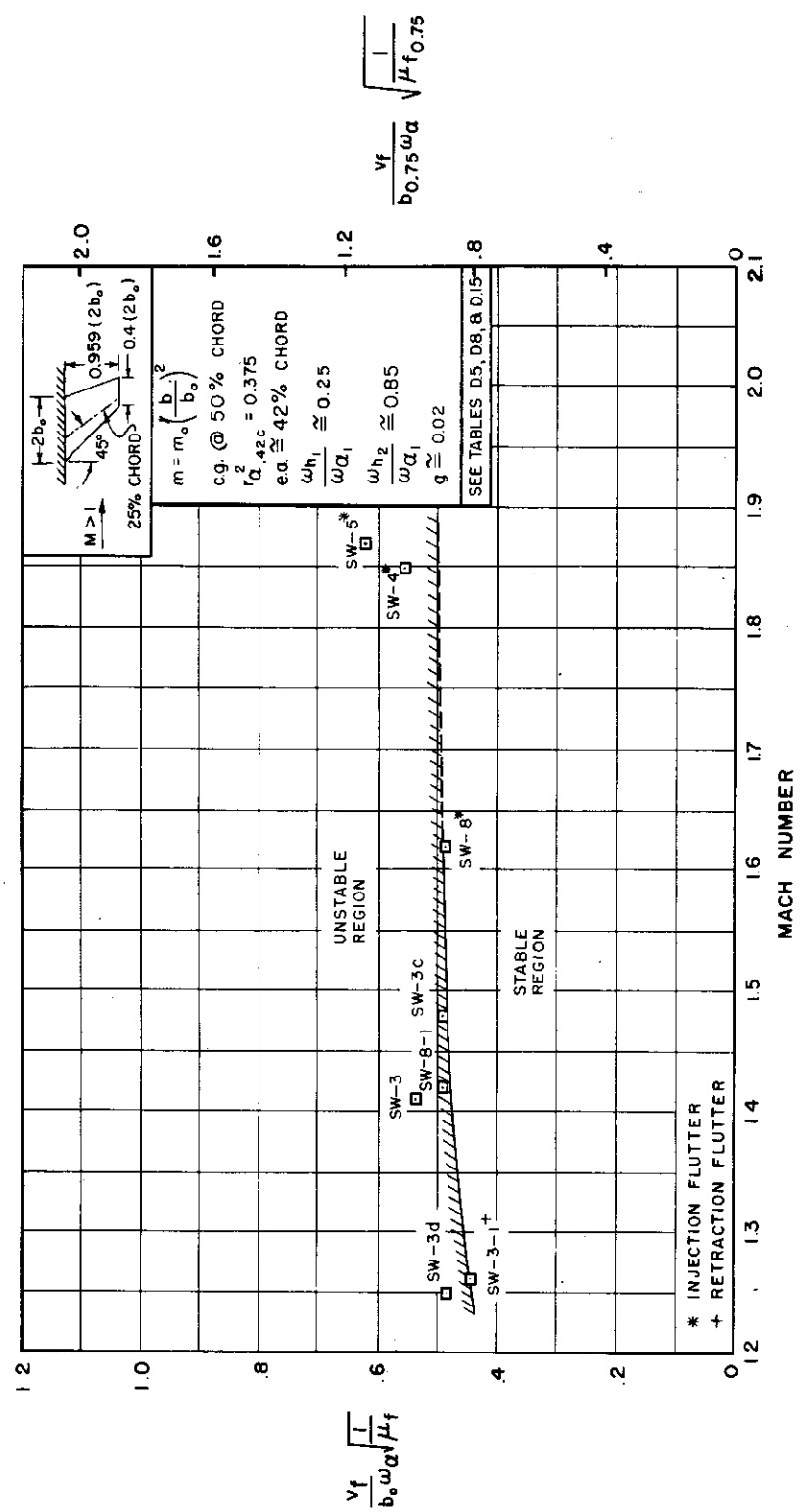

FIGURE 3.9 EXPERIMENTAL FLUTTER STABILITY BOUNDARY FOR BARE SWEPT-WING PLANFORM BASED ON THE COEFFICIENT, $\frac{v_f}{b_o \omega_\alpha} \sqrt{\frac{1}{\mu_f}}$

The experimental stability boundary for the swept planform occurs at about the same values of the flutter coefficients, $\frac{V_f}{b_o \omega_\alpha}$ and $\frac{V_f}{b_o \omega_\alpha}\sqrt{\frac{1}{\mu_f}}$, as for the straight planform at low supersonic Mach number while the slope of the boundary with increasing Mach number does not appear to be as steep as that for the straight wing. The same effect of sweepback has also been obtained from flutter tests at transonic speeds (see Reference 4, p. 27 and Reference 6). The numerical equivalence of flutter coefficients probably means that the swept wing is slightly less desirable from a flutter viewpoint than the straight wing. While it is difficult to compare wings of different geometry, some remarks can be made. From elementary rod considerations, the following relation can be deduced for a wing of given root stiffness and of given root chord,

$$\omega_\alpha \sim \frac{f_1(\lambda)\sqrt{\cos\psi}}{\ell r_\alpha \sqrt{\mu}} \qquad \text{Eq. (3.1)}$$

where

ψ is the sweep of the elastic axis

ℓ is the semi-span of the wing, measured from the root chord.

The effect of taper, λ, on the torsional frequency has been estimated from the relation,

$$(\omega_\alpha)_{\text{tapered}} = (\omega_\alpha)_{\text{untapered}}\, f_1(\lambda) \qquad \text{Eq. (3.2)}$$

where the function, $f_1(\lambda)$, is obtained from Reference 27 as

$$f_1(\lambda) = 1 + 1.87\,(1 - \lambda)^{1.6} \qquad \text{Eq. (3.3)}$$

It should be mentioned that the effect of taper on the bending frequency is more difficult to estimate, and the methods of Reference 28 are suggested. On the basis of equation 3.2, for the experimental parameters of Figures 3.4 and 3.8, the straight wing should have a higher torsional frequency by about 10 percent than the swept wing for the same root stiffness and the same root chord.

3.1.3 Delta

Considerable difficulty was encountered precipitating delta-wing flutter. Some twenty models were flown before successful flutter was obtained, utilizing the extreme values of center-of-gravity and elastic-axis locations available with the model-design procedure. Even models made only of balsa and lead were flutter-free. Lead was added to some of the wings which had been tested without event in an attempt to lower the second bending frequency without significantly changing first bending or first torsion, since there was some evidence that a critical condition might be one where the second bending frequency is below first torsion (Ref. 29).

Successful flutter was finally obtained by reducing the thickness ratio of the wings to 4 percent, thus reducing the stiffness well below that which would be encountered in practice. To illustrate this point one need only compare the scaled torsional frequency of the delta-wing airplane presented in Table 3.2 with those of the delta-wing models tested on this program (Table D.9). The frequency of the model of the actual aircraft, where Mach number is kept constant from model to airplane, is an order of magnitude higher than those of any model built on this program. A similar conclusion can be drawn by comparing the flexibility influence coefficients of the models tested.

(Table D.18) with those of the XF-92A airplane (Table D.19) using the relation,

$$\frac{(C_{ij})_M}{(C_{ij})_A} = \frac{\rho_A}{\rho_M} \frac{T_M}{T_A} \qquad \text{Eq. (3.4)}$$

where

C_{ij} is the force-deflection influence coefficient
ρ is the air density.

Equation 3.4, which is based on dimensional-analysis considerations, assumes that the mass ratio as well as the Mach number is held constant from model to airplane. It is interesting to note that the ratio of influence coefficients depends only on flow parameters and is independent of the length scale factor. This ratio is equal to 1/3 if the XF-92A airplane is simulated at an altitude of 35,000 in a wind tunnel where air is expanded isentropically from a stagnation temperature equal to room temperature (70°) and a stagnation pressure equal to 10 psig.

Figure 3.10 shows the flutter stability boundaries obtained experimentally. Again, each successful flutter point, except those otherwise indicated, represents a model which was injected into the airstream, flutter-free. Flutter was then approached by decreasing the Mach number until instability occurred. Figure 3.11 presents the results of plotting the experimental data on the basis of the coefficient, $\frac{V_f}{b_o \omega_\alpha} \sqrt{\frac{1}{\mu_f}}$ Experimental evidence of the destabilizing effect of lowering the mass ratio, μ , was obtained in the case of Model De-2d-2 which was tested once, flutter-free, at higher mass ratio than that obtained at flutter during a second test (see Table D.9).

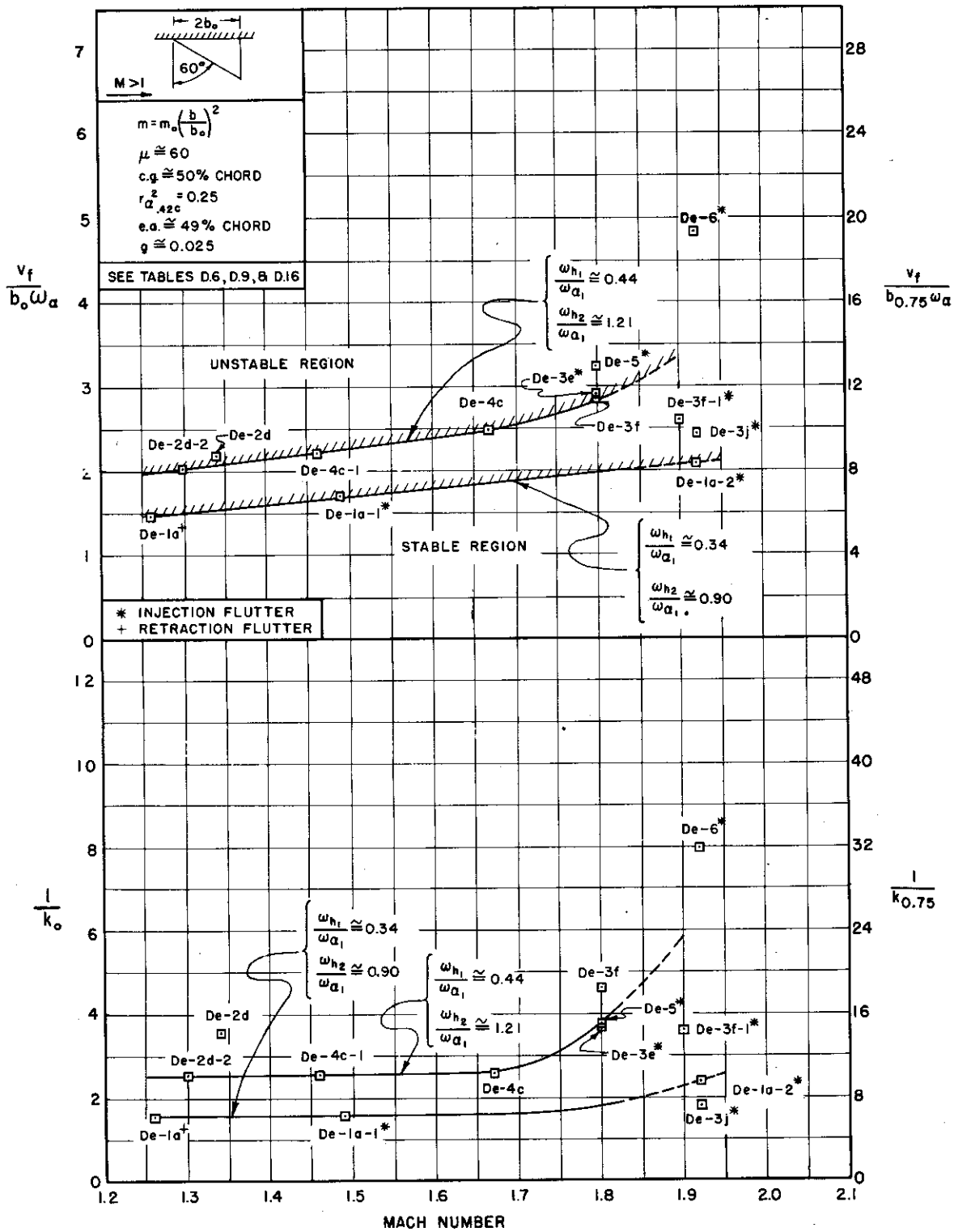

FIGURE 3.10 EXPERIMENTAL FLUTTER STABILITY BOUNDARIES FOR BARE DELTA-WING PLANFORM

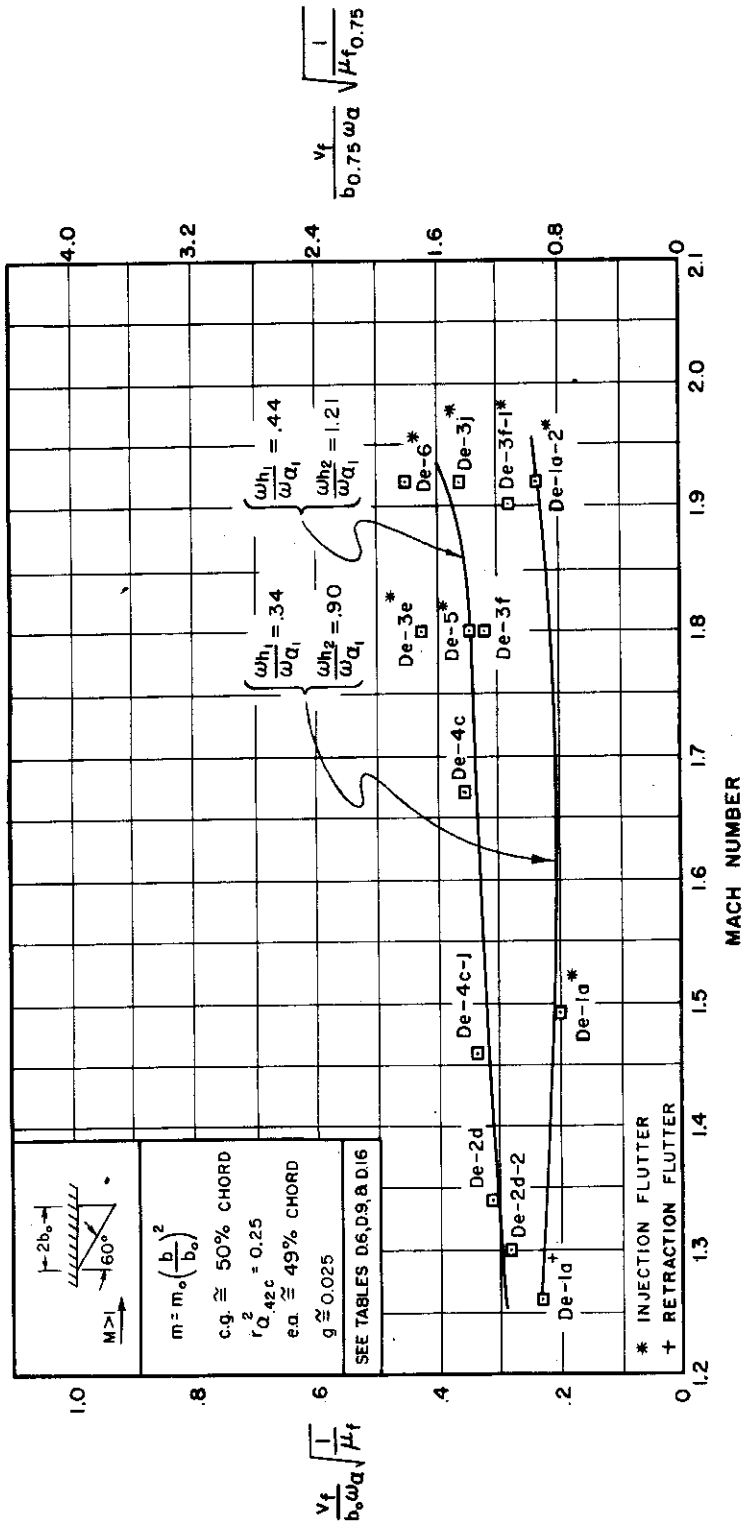

FIGURE 3.11 EXPERIMENTAL FLUTTER STABILITY BOUNDARIES FOR BARE DELTA-WING PLANFORM BASED ON THE COEFFICIENT, $\frac{v_f}{b_o\omega_\alpha}\sqrt{\frac{1}{\mu_f}}$

The curves of Figures 3.10 and 3.11 are not as well defined as those of the straight and swept-wing planforms because of the inherent difficulty, with a simple design procedure, of accurately controlling the natural frequencies of delta-wing models where the effects of plate-type vibratory modes become significant. While there is little justification for quantitatively comparing the stability boundary of the delta wing with those of the straight and swept wings, even on the basis of equation 3.1, the delta wing should have its stability boundary at much lower values of the coefficient, $\frac{V_f}{b_o \omega_\alpha}$, than that obtained experimentally (about 1/4 that of the straight wing) for the same root chord and the same root torsional rigidity. It is interesting to note that the same general changes in stability boundary with sweepback as those obtained on this program have also been obtained from transonic tests (see Reference 4, p. 27 and Reference 6).

3.2 Wings with Ailerons

3.2.1 Straight

In the theoretical formulation of the straight wing with aileron, the frequency ratio, $\frac{\omega_\beta}{\omega_\alpha}$, was considered as an unknown in the analysis with the fixed parameters shown on Figure 3.12. The detailed formulation of the theory is given in Appendix A.2, and a numerical example is given in Appendix C.3. Only three models were tested so that a direct graphical comparison between theory and experiment could not be made as in the case of the bare straight wing. A tabulated comparison of the Mach number and the frequency at flutter is given in Table 3.1, and a detailed tabulation of the experimental parameters is given in Appendix D.

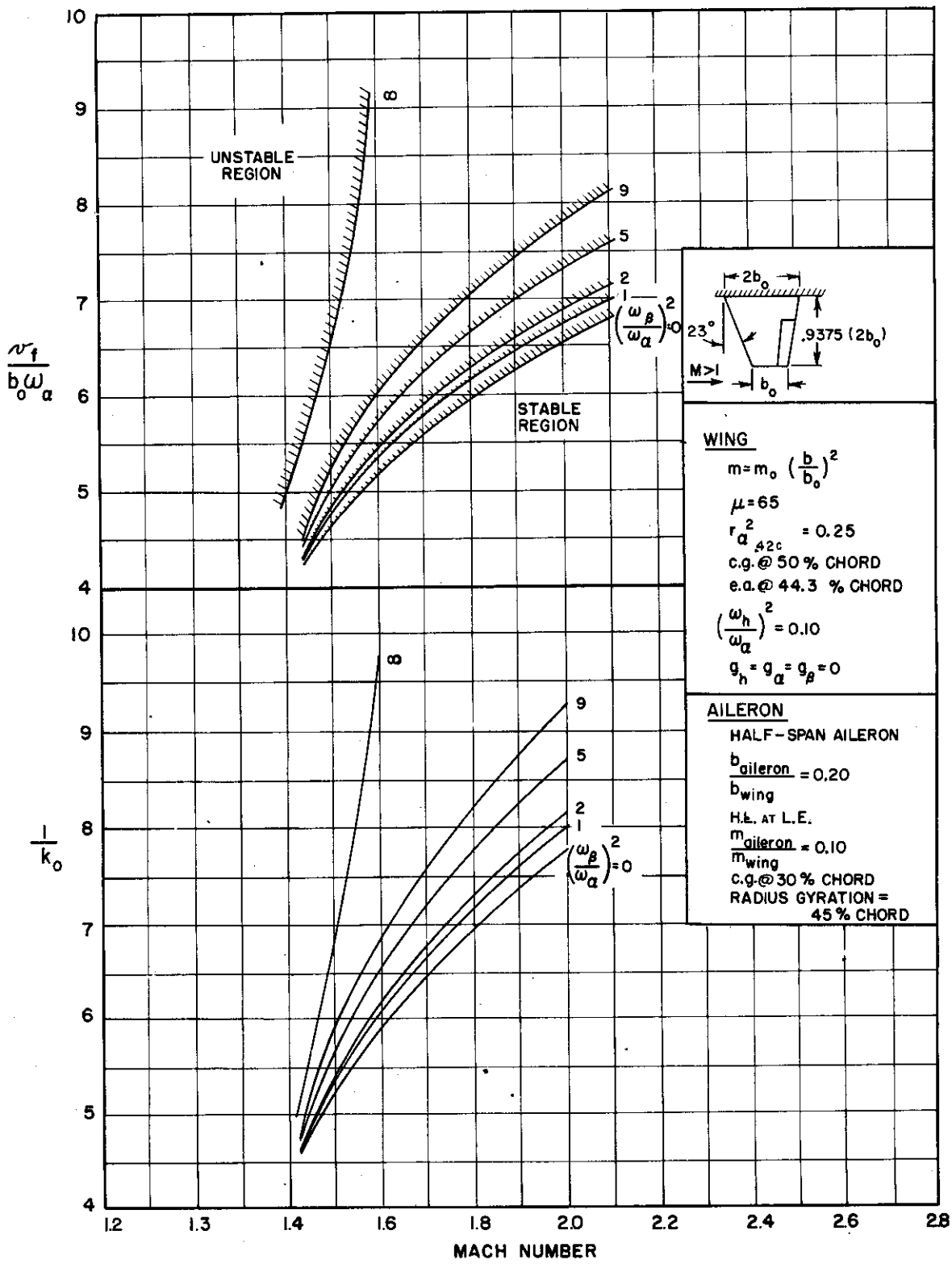

FIGURE 3.12 THEORETICAL RESULTS FOR STRAIGHT WING WITH AILERON

Again, the theory shows that for flutter at supersonic Mach numbers, instability must be approached from high Mach number. Decreasing the frequency ratio, $\frac{\omega_\beta}{\omega_\alpha}$, is an effective decrease in torsional stiffness, and no significant change occurs near the condition, $\frac{\omega_\beta}{\omega_\alpha} \cong 1.0$, as would be expected from subsonic experience.

These trends have been verified by experiment for the three models tested.

Model	$\frac{\omega_\beta}{\omega_\alpha}$	M_f
ST-1b	0.691	1.80*
ST-1e	1.49	1.72
ST-1f	∞	1.65

* Injection Flutter

Model ST-1f was the result of the repairing Model ST-1e and locking the aileron. Increasing the frequency ratio, $\frac{\omega_\beta}{\omega_\alpha}$, lowers the Mach number at flutter or has the same effect as increasing the absolute stiffness, ω_α. Although the trends are correct, the theory is again unconservative in that experiment shows a larger region of instability than the theory (see Table 3.1). The experimental flutter frequencies are also lower than those predicted by the theory except in the case of Model ST-1b which fluttered during injection near the first torsional frequency.

In the design of the aileron models, the aileron frequency was controlled by flexures even though such a design was difficult, especially since all the models had sealed gaps, typical of high-speed aircraft. If the aileron frequency were

controlled from outside the wind tunnel, a real wing would not be simulated because the aileron would rotate relative to a line fixed in space rather than relative to the wing itself.

3.2.2 Swept and Delta

The trends obtained for the straight wing with aileron were also evidenced for the swept and delta planforms, although no theoretical work was done and only one model with aileron was tested for each of these planforms. The data show that Model SW-3b, which had roughly the same parameters as Models SW-3 and SW-8-1 except for finite aileron frequency (see Tables D.5 and D.8), fluttered at a higher Mach number than either of these latter two. The delta-wing elevon model, DE-2e, fluttered during injection in a mode in which aileron motion predominated at much higher Mach number than the experimental results of the bare delta wings would indicate.

3.3 Wings with Tip Tanks

In addition to tests on bare wings and on wings with ailerons, some exploratory tests were made on straight and swept wings with tip tanks for both cantilever and free-to-roll root conditions. Some theoretical work was done on the straight wing for a simplified model (see Figure 3.13) so that trends useful for model design could be obtained. In the theoretical formulation of the problem, the dimenionless static unbalance of the tip tank, $\overline{S}_T$, and the first torsional frequency of the bare wing, ω_α, were treated as unknowns. The frequencies of the bare wing were chosen as independent parameters because those of the wing with tip tank depend on the tip-tank static unbalance, which was to be varied both theoretically and experimentally.

3.3.1 Cantilever Root Condition

The results of the theoretical calculations on the simplified model of the straight-wing planform for zero structural damping are presented in Figure 3.13. The detailed formulation of the theory is given in Appendix A.2, and a numerical example is given in Appendix C.4. It should be mentioned that the aerodynamic forces on the tip tank were taken into account in the calculations (see Appendix B) and were significant, especially insofar as the pitching moment was concerned. Theoretical results for values of the dimensionless tip-tank static unbalance, $\bar{S}_T$, other than those presented in Figure 3.13 can be obtained by cross-plotting the curves of Figure C.4.

The curves of Figure 3.13 are at best confusing. It can be shown mathematically that the curves must be continuous, so that the theory seems to indicate that the wing with tip tank is unstable even for infinite stiffness ($\frac{V_f}{b_o \omega_\alpha} = 0$). Considerable difficulties were encountered in the calculations because of the limited tabulated values of the supersonic oscillatory aerodynamic coefficients (Ref. 7) and the choice of eigenvalues.

The extreme sensitivity of the theoretical curves and the disappointing results led to the decision to do some of the calculations including a small amount of structural damping. The results of these calculations are presented in Figure 3.14. Theoretical curves for values of dimensionless tip-tank static unbalance, $\bar{S}_T$, other than those presented can be obtained by cross-plotting the curves of Figure C.5. The curves of Figure 3.14 are more encouraging, following the trends typified by bare wings and by wings with ailerons.

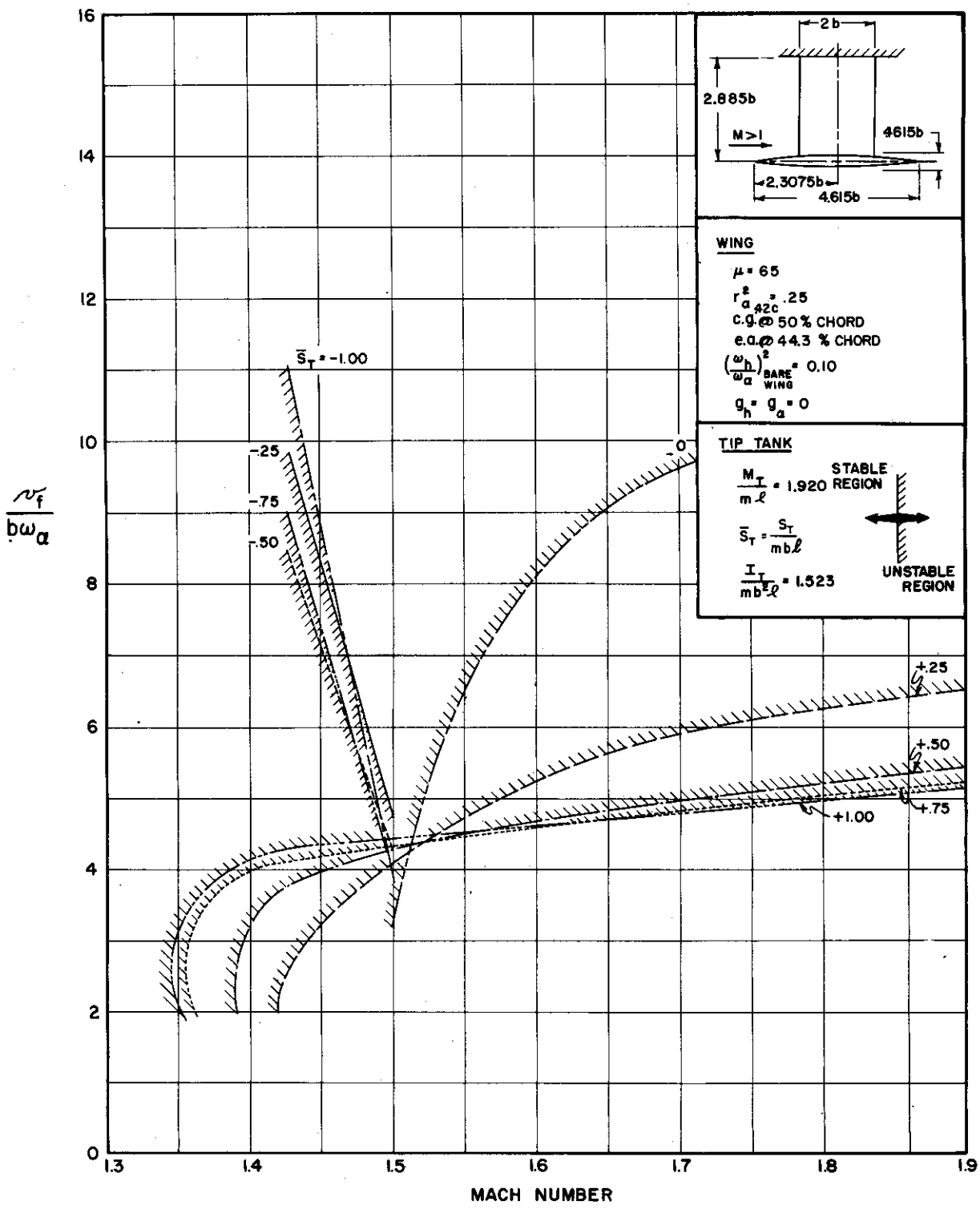

FIGURE 3.13 THEORETICAL RESULTS FOR STRAIGHT WING WITH TIP TANK, NO STRUCTURAL DAMPING

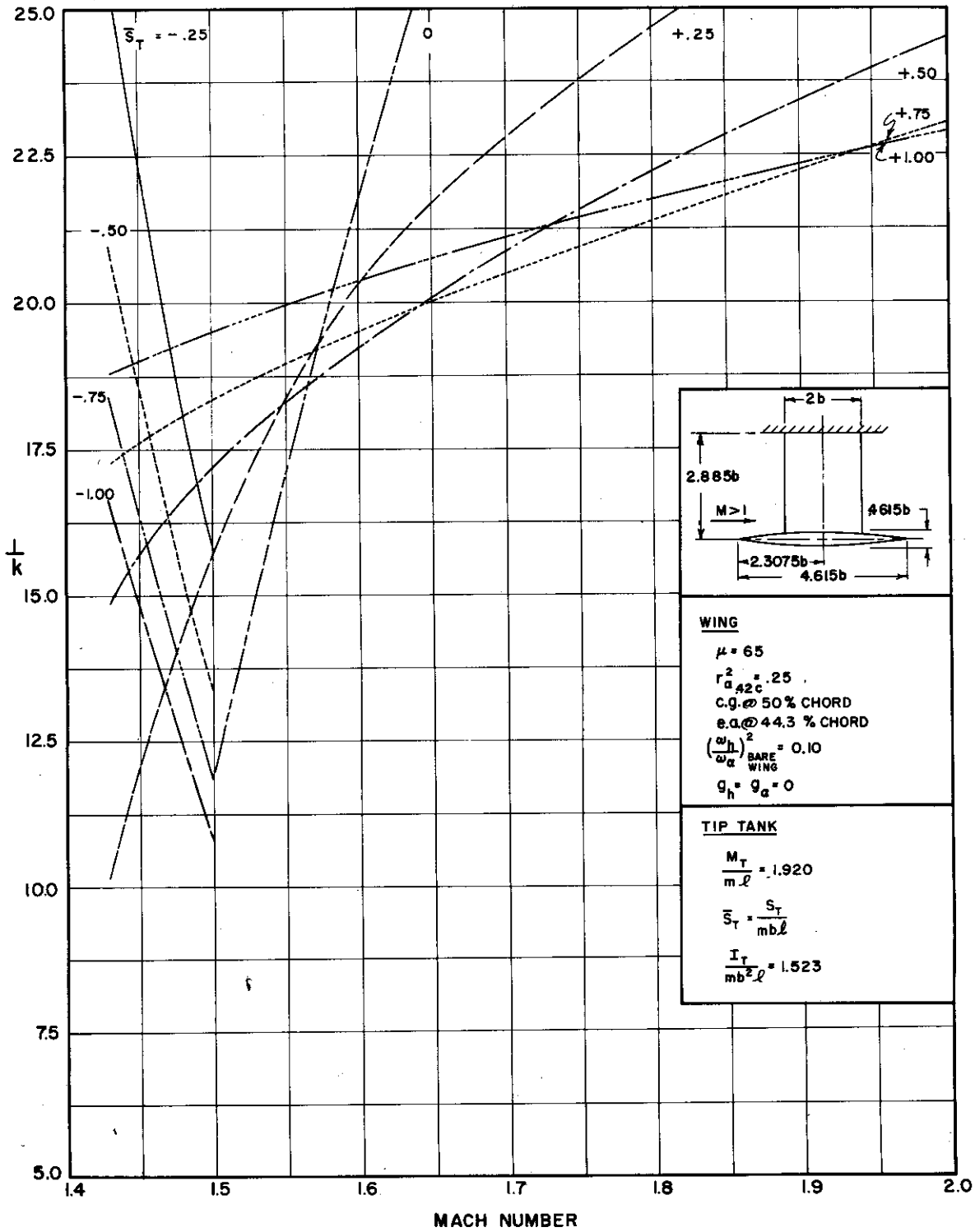

FIGURE 3.13 (Continued) THEORETICAL RESULTS FOR STRAIGHT WING WITH TIP TANK, NO STRUCTURAL DAMPING

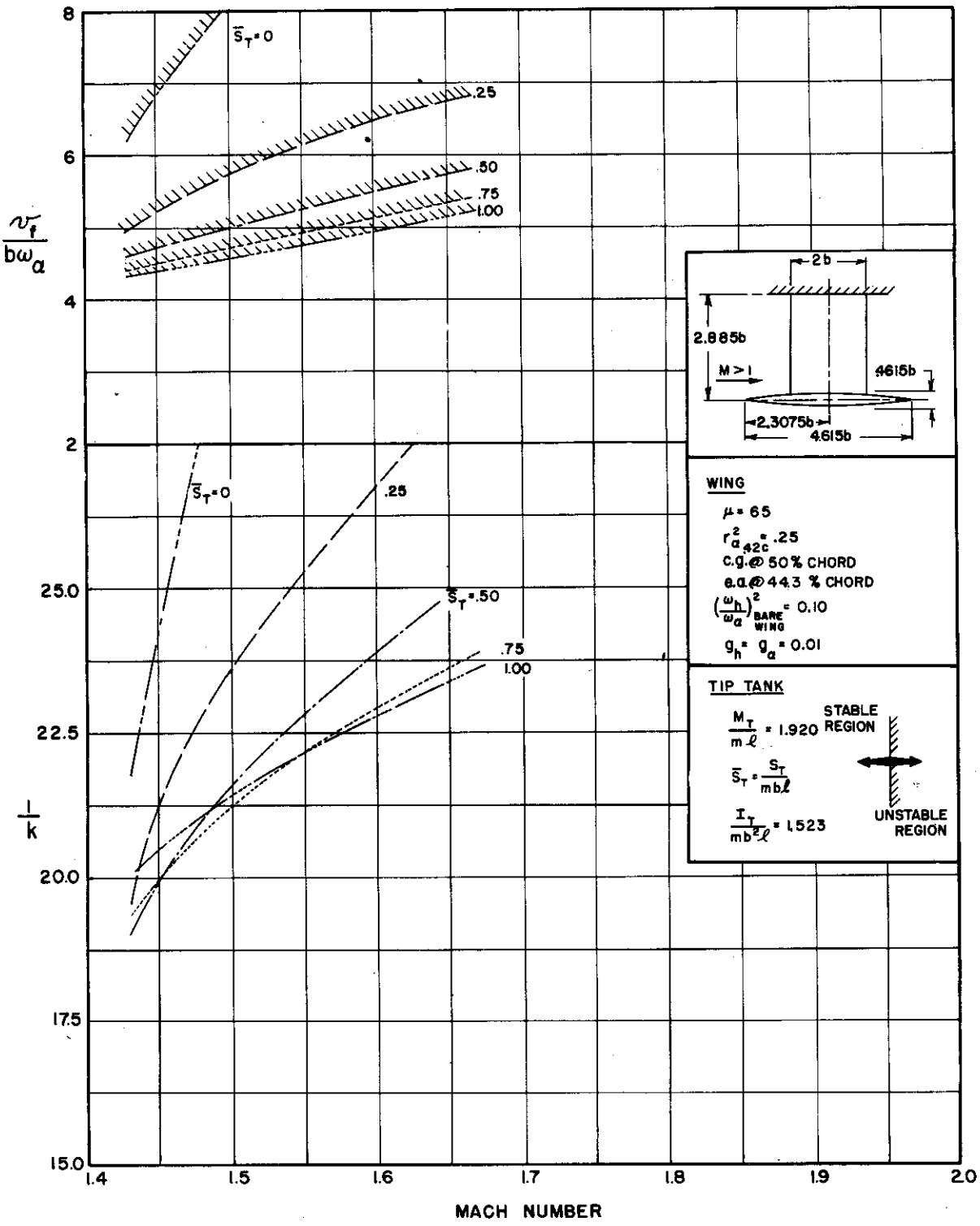

FIGURE 3.14 THEORETICAL RESULTS FOR CANTILEVER STRAIGHT WING WITH TIP TANK, STRUCTURAL DAMPING INCLUDED

The theory shows that instability increases with increasing tip-tank static unbalance, S_T, corresponding to rearward travel of the tip-tank center of gravity. Few real roots were obtained for negative tip-tank static unbalance, i.e. for tip-tank center-of-gravity locations ahead of the wing elastic axis (see Figure C.5), indicating that the wing is always stable if the center of gravity of the tip tank is far enough forward. The trends predicted by the theory were verified by experiment, but again the theory is unconservative if quantitative results are compared. Four cantilever tip-tank models were tested, from the most aft to the most forward tip-tank center-of-gravity location obtainable with the model design. All the configurations with tip-tank center of gravity aft of the wing elastic

Model	$\bar{S}_T$	Tip Tank c.g. % Wing Tip Chord	M_f
ST-4b*	1.05	77.5	1.83*
ST-1a*	0.401	56.0	1.80*
ST-1c*	0.0506	39.1	1.83*
ST-4a	-0.511	25.0	1.43

* Injection Flutter

axis fluttered during injection, even the model with a tip-tank static unbalance of very nearly zero (Model ST-1c). The only successful flutter was obtained with a model whose tip-tank center of gravity was well forward (Model ST-4a). According to the theory, this latter model should have been stable for all Mach numbers above 1.3. A tabulated comparison of theory and experiment is presented in Table 3.1, and detailed parameters for the models tested are given in Appendix D.

The stabilizing effect of moving the tip-tank center of gravity forward has also been demonstrated experimentally at high subsonic speeds (Ref. 30).

Three swept-wing models with tip tanks were tested; no theoretical studies were made for this planform. Although the tip-tank center-of-gravity location was not varied as above for the straight wings, the models did have different values of the torsional frequency of the bare wing, with essentially constant values of other parameters (see Table D.11). The trend predicted by the theory was verified, i.e. increasing the torsional frequency of the wing lowered the Mach number at flutter.

Model	$\bar{S}_T$	Tip-Tank c.g. % Wing Tip Chord	ω_α cps	M_f
SW-3a*	-0.51	25.0	145	1.92*
SW-7	-0.51	25.0	161	1.44
SW-6	-0.53	25.0	189	1.30

* Injection Flutter

3.3.2 Free-to-Roll Root Condition

The results of the theoretical calculations for the simplified straight-wing model with free-to-roll root condition are presented in Figure 3.15. The theoretical formulation is given in Appendix A.2, and a numerical example is given in Appendix C.5. The calculations were made for zero structural

damping only.

Again the theoretical results are confusing, but it did not seem worthwhile to expend additional effort redoing the calculations with structural damping included since the major effort of the research program was on experimental results. The solution of the three-degree-of-freedom flutter determinant for the free-to-roll root condition involves tedious graphical solutions of simultaneous equations for each set of assumed conditions, i.e. the Mach number and the frequency at flutter (see Appendix C.5).

Some preliminary calculations indicated that with the inclusion of structural damping in the analysis, one of the branches of the curves would disappear (see Figure C.6) and a general shift similar to that for the cantilever root condition would occur. The condition is one which is fairly common in flutter analyses, where small changes in input give erratic changes in results.

In the theoretical formulation, no account was taken of the canted hinge, which was used to give the models aerodynamic stability in roll, although this would be possible in a more refined analysis. The amount of cant was kept as low as possible, $2\ 1/2^{o}$, consistent with the change in flow direction with Mach number, about $\pm\ 0.1^{o}$ (see Reference 13). For small angles it can be shown that there is a simple relation between cant angle, roll angle, and angle of attack,

$$\frac{\alpha}{\theta} = \varepsilon \qquad \text{Eq. (3.6)}$$

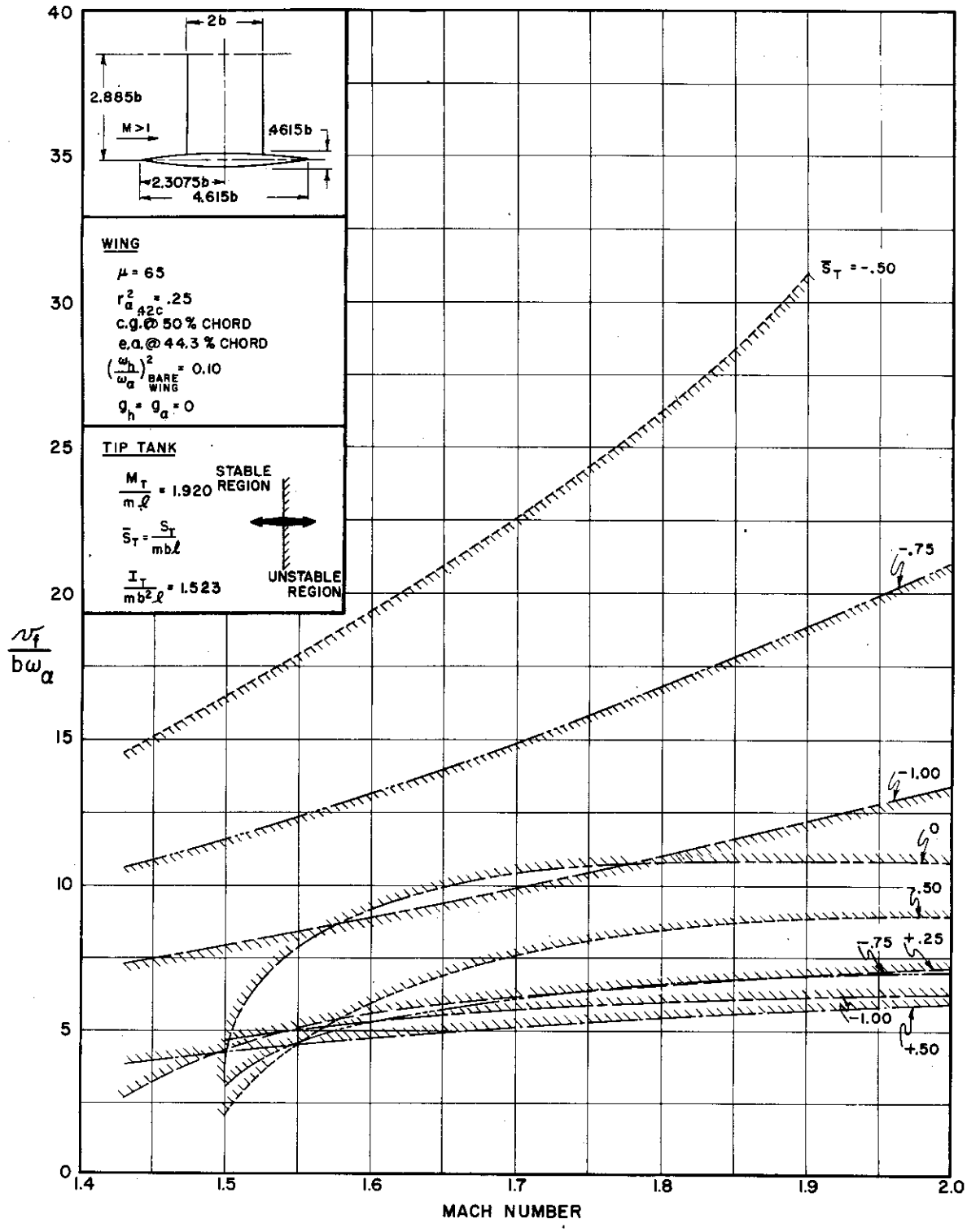

FIGURE 3.15 THEORETICAL RESULTS FOR STRAIGHT WING WITH TIP TANK, FREE TO ROLL

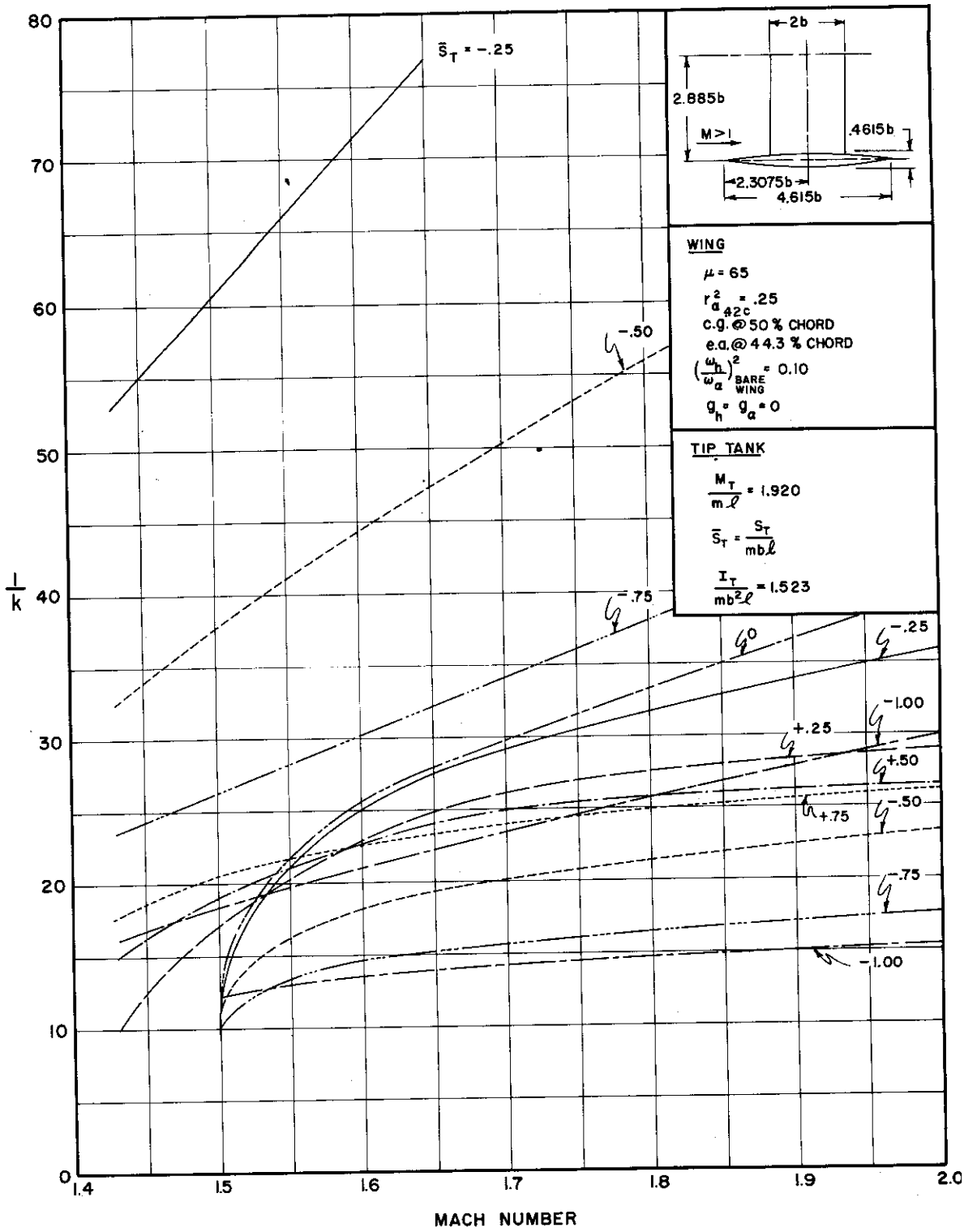

FIGURE 3.15 (Continued) THEORETICAL RESULTS FOR STRAIGHT WING WITH TIP TANK, FREE TO ROLL

where

α is the angle of attack

θ is the angle of roll

ε is the angle of cant in radians.

In any wind tunnel test where a semi-span model is given freedom to roll, the classical question of whether or not the anti-symmetrical degrees-of-freedom are adequately simulated always arises. This uncertainty comes from the fact that the model plus its mirror image are actually represented (see Figure 3.16). Because of this doubt along with the canted hinge, the results for the models which were tested probably lie somewhere

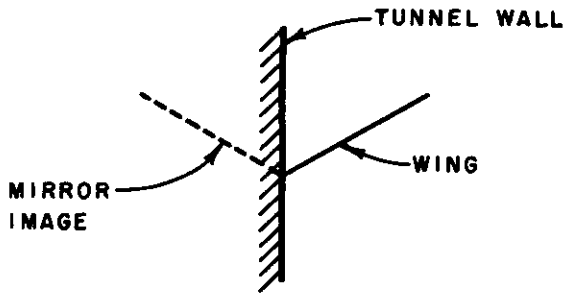

FIGURE 3.16 SEMI-SPAN MODEL WITH FREEDOM TO ROLL IN WIND TUNNEL

between the cantilever and the ideal free-to-roll configurations.

The experimental results for the free-to-roll tip-tank models are as inconclusive as the theoretical results. The four straight-wing models tabulated in Appendix D actually represent one model which was repaired after each flutter so that small changes in the experimental parameters occurred (see Appendix D).

The straight-wing free-to-roll model fluttered at a lower Mach number than its cantilever counterpart, while the opposite is true for the swept wing.

Model	Root Condition	M_f
ST-4a	Cantilever	1.43
ST-4c-2	Free-to-Roll	1.32
SW-7	Cantilever	1.44
SW-7a	Free-to-Roll	1.92

3.4 Comparison with Other Experimental Results

In assessing the value of any experimental program of high speed testing the question always arises as to whether the results obtained are representative of what would be obtained for a full scale airplane, or merely represent the peculiarities of the testing facility or the models tested. Little or no full scale airplane flutter data is available, but a considerable body of flutter experience for models of various geometry and construction methods is available. In particular, Reference 4, 5, 47, 48 49 and 50 give flutter data for straight, swept, and delta wings whose characteristics are similar to those tested under the present program. A variety of model construction methods are represented; from the solid plate models of Reference 47 to the wrapped aluminum foil, foam plastic core models of Reference 5. A number of different testing facilities have been used to obtain the test data. Figures 3.17, 3.18, and 3.19 are plots of the parameter, $\frac{b_{0.75}\,\omega_\alpha}{a_f}\sqrt{\left(\frac{\mu_f}{\mu_{ref.}}\right)_{0.75}}$ versus Mach number for the straight swept and delta wing models of this report and for similar models from References 4, 5, 47, 48, 49, and 50. This parameter, suggested in Reference 47, is an extremely convenient one for the plotting of flutter results, but it must be remembered that the use of the factor $\sqrt{\mu_f}$ has no firm theoretical basis. Figures 3.17, 3.18 and 3.19 represent a collection of data for wings that are similar but not identical. Therefore some differences in the data are bound to occur. Even so the correlation of the various test results is

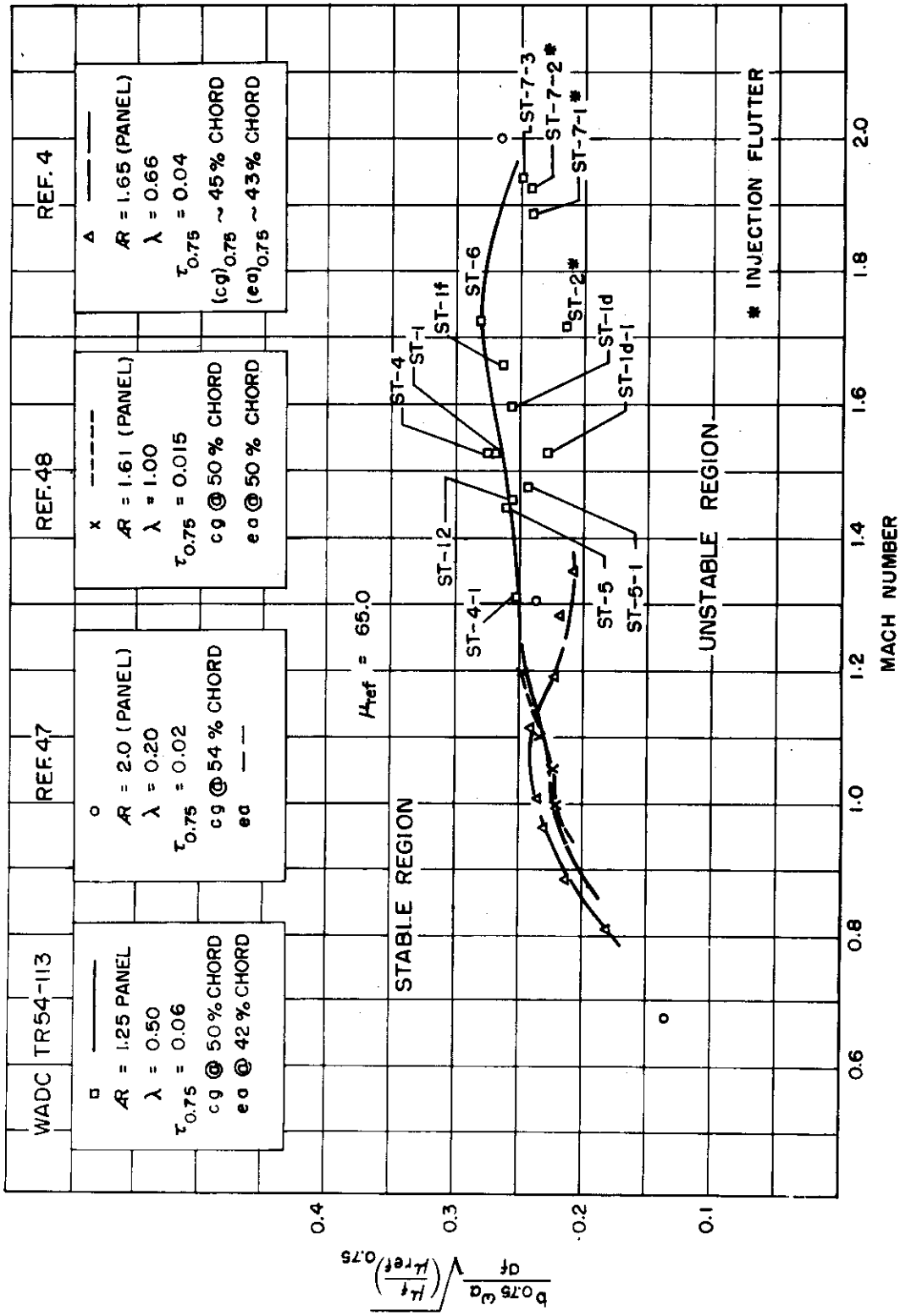

FIGURE 3.17 COMPARISON OF STRAIGHT WING RESULTS WITH SIMILAR TESTS

quite good.

Figure 3.17 shows the results for the straight wing models. The data of Reference 47 is too sparse to draw a curve since only three points are available from M = 0.67 to M = 2.0. The level of this data agrees quite well with that of the present report. The data of References 4 and 48 agree very well with each other in the transonic range. In the low supersonic range, the data of Reference 4 shows that a smaller ω_α is needed at a given Mach number to reach the stable region than for the models of this report. The trend of the data obtained in this report with increasing Mach numbers up to about 1.7 is somewhat disturbing since it indicates that higher and higher ω_α's are needed to prevent flutter. Since no data was obtained at Mach numbers below 1.3, it is not possible to say whether there is a peak in the boundary at about M = 1.0 which is higher than the peak in the boundary at about 1.7. The data of Reference 47 is too widely separated in Mach number to determine whether or not a peak exists. The extended curve for the straight-wing models of this report, given as the heavy dash line on Fig. 3.17, shows a slight peak. The extension is based on the results of Ref. 48 and some unpublished data. Such an extension shows that an airplane, flying at constant altitude or constant density may encounter bending-torsion flutter in the low supersonic range at about M = 1.6 after having passed through the transonic range without flutter. On the whole the agreement of the straight wing data obtained on this program with that of References 4, 47, and 48 is quite good. There seem to be no major discrepancies that cannot be explained by the differences in the model parameters.

Figure 3.18 shows similar curves of the parameter,

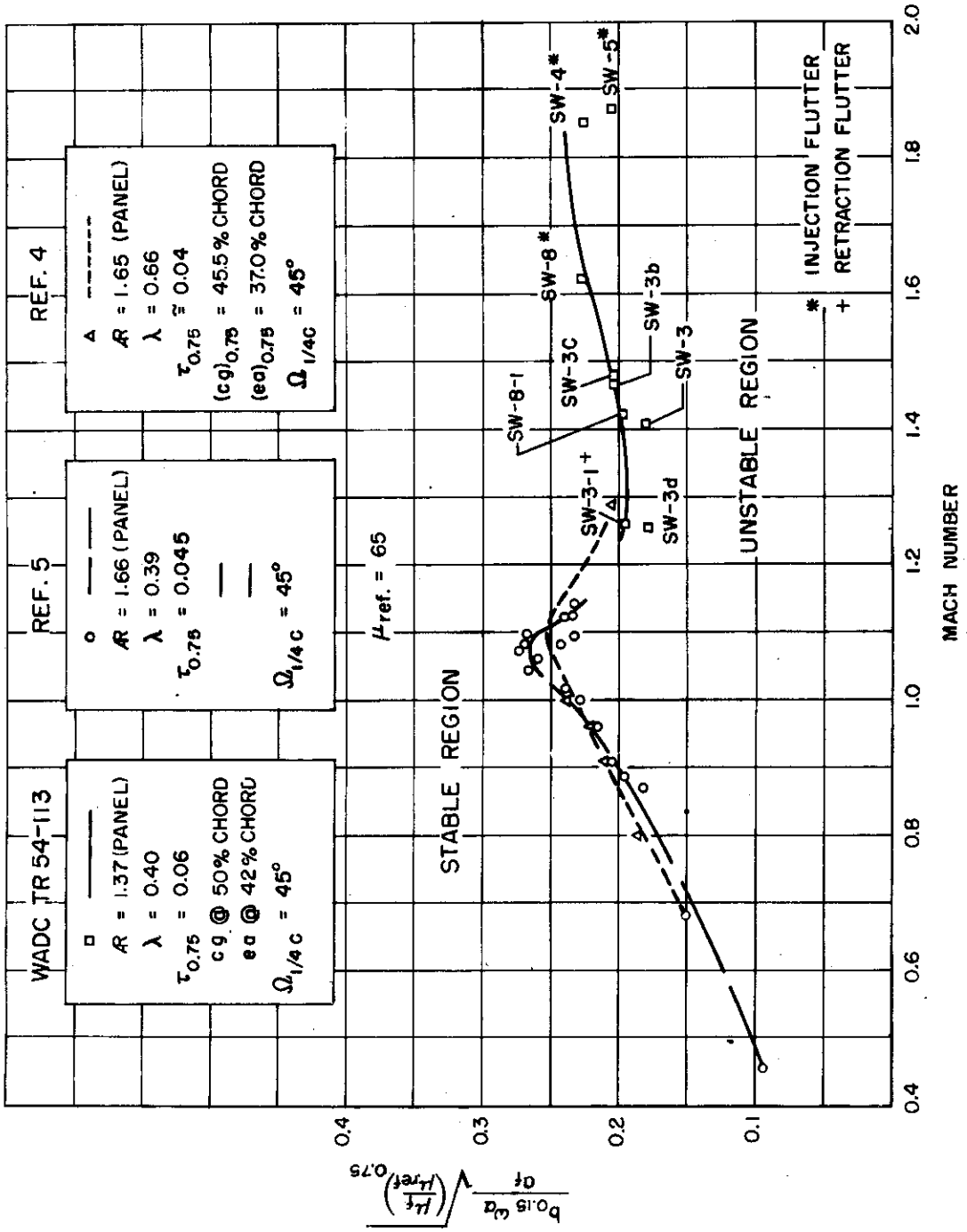

FIGURE 3.18 COMPARISON OF SWEPT WING RESULTS WITH SIMILAR TESTS

$\frac{b_{0.75}\omega_\alpha}{q_f}\sqrt{\left(\frac{\mu_f}{\mu_{ref}}\right)_{0.75}}$ vs. Mach number of the swept wing models. The agreement between the present data and that of References 4 and 5 is very good. The three sets of data could easily be represented by a single curve. In spite of a slight tendency towards increasing ω_α's necessary to prevent flutter at the higher Mach numbers covered by the present data, the critical region for flutter appears to be the transonic range.

Figure 3.19 shows the comparison of the delta wing data of the present report with that of Refs. 47, 49, and 50. Less delta wing data is available for comparison because of the apparently heavy dependence of delta wing flutter speed on second bending to first torsion and first bending to first torsion frequency ratios noted in Figs. 3.10 and 3.11. This heavy dependence on these frequency ratios means that if delta wing flutter data is to be compared on a rational basis these ratios must be similar. Data for only those models from Refs. 47, 49, and 50 which have frequency ratios and mode shapes similar to those of the delta wings of the present program have been used in Fig. 3.19. In general the agreement is not too bad. The data of Ref. 47 shows a level of the flutter parameter about equal to that of the present report at Mach numbers of 1.3 and 2.0. The data of Refs. 49 and 50 indicates that there is a peak in boundary around M = 1.0.

The curves of Figs. 3.17, 3.18, and 3.19, are also extremely useful for practical airplane design in that they show clearly the critical conditions for flutter. A straight line from the origin M = 0, $\frac{b_{0.75}\omega_\alpha}{q_f}\sqrt{\left(\frac{\mu_f}{\mu_{ref}}\right)_{0.75}} = 0$ of the curves can easily be shown to be a line of constant dynamic pressure. A straight line parallel to the abscissa represents a line of constant altitude.

It is then apparent that for the straight wing data shown in Fig. 3.17 that the critical flutter region for a con-

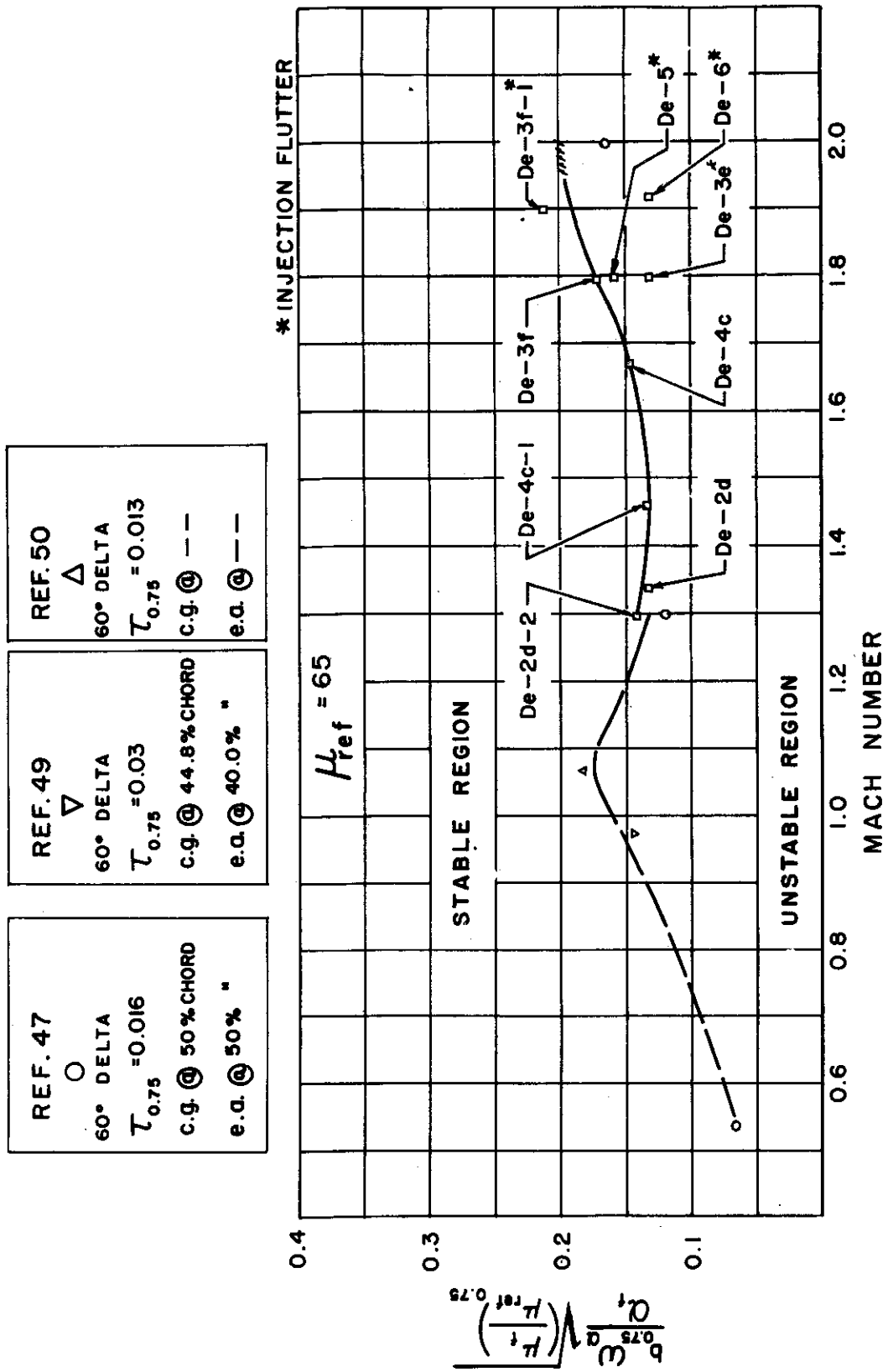

FIGURE 3.19 COMPARISON OF DELTA WING RESULTS WITH SIMILAR TESTS

stant altitude airplane condition occurs at about M = 1.7. At constant dynamic pressure the critical flutter region occurs at Mach numbers slightly less than 1.0.

For the swept wing data shown in Fig. 3.18 the critical flutter region for both constant altitude and constant dynamic pressure conditions occurs at about Mach number 1.1.

For the delta wing data shown in Fig. 3.19, the peak in the boundary at a Mach number of about 1.1 is very close to being at the same level as the boundary at a Mach number of about 2.0. Therefore, it is difficult to say with any assurance whether the most critical flutter region at constant altitude is in the transonic region or at higher Mach numbers. The data of Ref. 47 indicates that the boundary continues to rise beyond M = 2.0 since the flutter point obtained in Ref. 47 for M = 3.0 occurs at a higher value of $\frac{b_{0.75}\,\omega_\alpha}{a_f}\sqrt{\left(\frac{\mu_f}{\mu_{ref}}\right)_{0.75}}$ than the point at M = 2.0 shown. It would appear, then, that the critical region for flutter at constant altitude lies at the higher Mach numbers around M = 2.0 in the range covered by Fig. 3.19. This conclusion should be used with care because of the scatter in the data at the higher Mach numbers and the general scarcity of data on equivalent delta wings in the transonic range.

As a further illustration of the usefulness of the boundaries of Figs. 3.17, 3.18, and 3.19 for airplane design, a simple design example is discussed below. Figure 3.20 shows the consolidated flutter boundaries for straight wings, drawn from the data of Fig. 3.17. The critical constant altitude and constant dynamic pressure lines are shown. The following airplane characteristics and desired performance are given:

$$\mu_{sea\ level} = 20.0$$
$$b_{0.75} = 5.0 \text{ (ft.)}$$
$$M_{max.} = 2.0 \text{ at } 30{,}000 \text{ (ft.)}$$

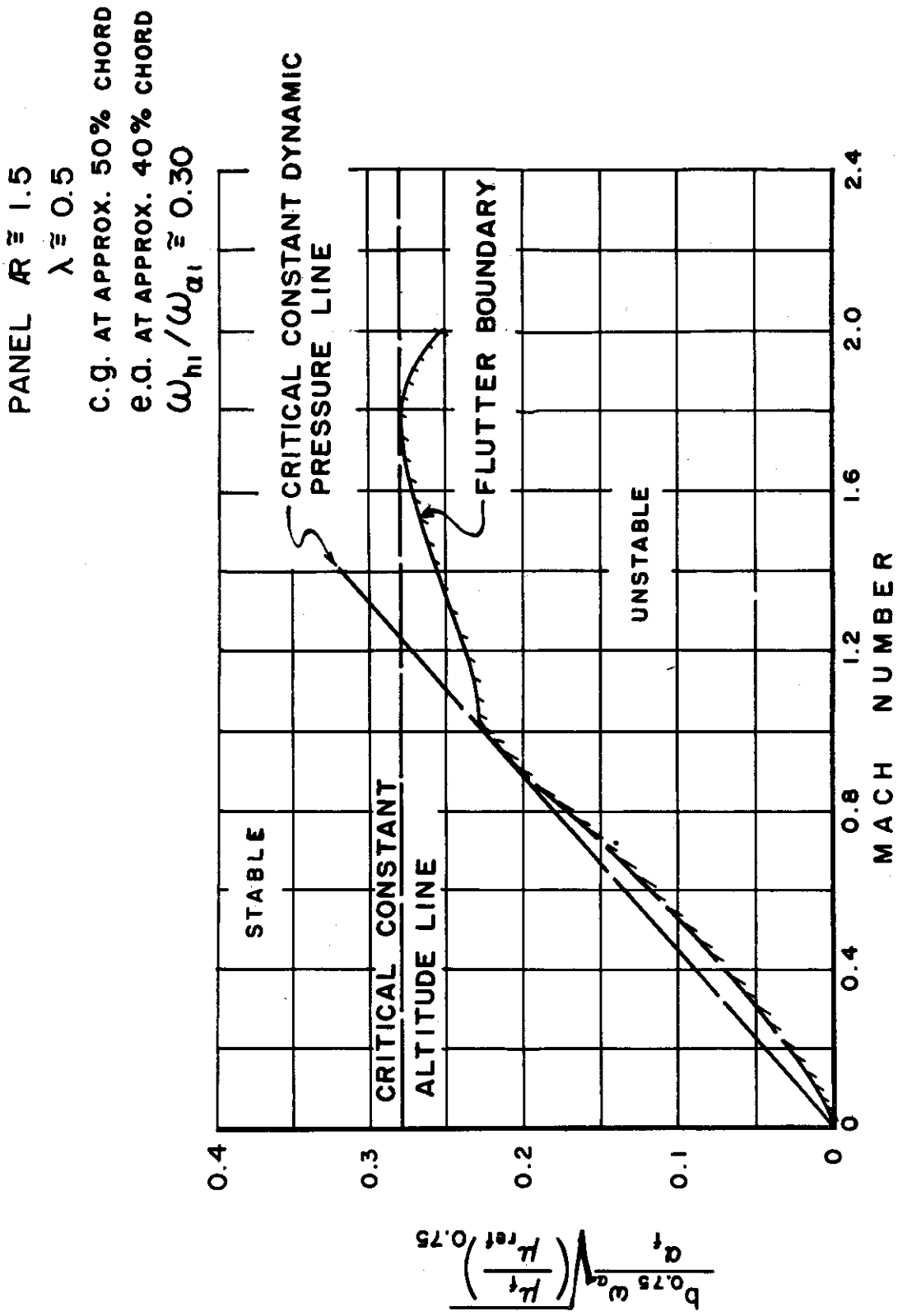

FIGURE 3.20 CONSOLIDATED STRAIGHT WING FLUTTER BOUNDARY

The level of wing torsional frequency required to prevent flutter for the high-speed condition will be determined, and then the speed and dynamic pressure restrictions that occur will be noted. The standard atmosphere is assumed.

For the constant altitude condition the critical value of $\frac{b_{0.75}\,\omega_\alpha}{a_f}\sqrt{\left(\frac{\mu_f}{\mu_{ref}}\right)_{0.75}}$ is 0.28 at M = 1.75 as can be seen from Fig. 3.20. The resulting value of ω_α needed to just prevent flutter is 9.8 cps. For this value of ω_α, the airplane must be limited in both speed and dynamic pressure to prevent flutter at altitudes below 30,000 ft. For example, with this value of ω_α, the Mach number for flutter at sea level is 0.81 and the critical dynamic pressure is 670 pounds per square foot.

If the example airplane is to be flutter free at a sea level Mach number of 1.1, then the critical value of the parameter $\frac{b_{0.75}\,\omega_\alpha}{a_f}\sqrt{\left(\frac{\mu_f}{\mu_{ref}}\right)_{0.75}}$ is 0.23. The value of ω_α necessary to prevent flutter for this condition is 14.8 cps, about 50% greater than the previous case.

TABLE 3.2

ESTIMATED FLUTTER PARAMETERS FOR REPRESENTATIVE HIGH-SPEED AIRPLANES

Airplane	Wing Planform	Max Speed Range	$\frac{V_{max}}{b_o \omega_\alpha}$	h kilofeet	μ	$\frac{\omega_{h1}}{\omega_\alpha}$	$\frac{\omega_{h2}}{\omega_\alpha}$	c.g.	e.a.	$(\omega_\alpha)_M$ cps
A	Straight	High Subsonic	0.70	35	125	0.22	0.71	50	40	390
B	Swept	Low Supersonic	0.93	35	71	0.27	0.89	51	40	540
C	Delta	Low Supersonic	0.52	32	22	0.38	0.71	50	--	840

V_{max} = Maximum speed at combat weight

b_o = wing semichord taken at fuselage skin

ω_α = first torsional frequency of wing

$(\omega_\alpha)_M$ = first torsinal frequency of wing for scaled model

$\omega_{h_1}, \omega_{h_2}$ = first and second bending frequencies of wing, respectively

h = altitude corresponding to V_{max}

μ = mass-density ratio of wing, $\frac{m}{\pi \rho b^2}$, taken at 3/4 semispan at altitude corresponding to V_{max}

c.g. = chordwise location of the wing center of gravity at 3/4 semispan

e.a. = chordwise location of the elastic axis at 3/4 semispan

Note: Scale is for model with 10-inch root chord.

SECTION IV

CONCLUSIONS

It is possible to draw a number of conclusions from the data presented in this report. The experimentally obtained flutter boundaries for the straight wing planform can be compared with the boundaries obtained from theoretical studies. This comparison can serve to indicate in what Mach number ranges theoretical calculations can be expected to give good quantitative correlation with experimental results. Figure 3.4 shows graphically that good correlation between theoretical studies and experimental results is found at Mach numbers between 1.3 and 1.4. Outside of this Mach number regime the correlation appears to be progressively poorer with the theoretical results being unconservative, showing too small a region of instability, above $M = 1.4$, and conservative below $M = 1.3$. The results of Table 3.1 show that because of the steeper slope of the theoretical curve on Figure 3.4 nearly all the bare wings have theoretical flutter Mach numbers between 1.3 and 1.4.

Some other conclusions can be drawn from the trends of the theoretical and experimental data. Both the theory for the straight wing and the experimentation for all three planforms show that, for the ranges of parameters considered, which are typical of present-day high-speed aircraft, the region of instability increases with the following independent parametric variations:

1. decreasing torsional frequency
2. decreasing mass ratio
3. rearward movement of the tip-tank center of gravity
4. decreasing aileron frequency
5. forward movement of the elastic axis

These items are listed in order of importance based on the experimental results.

In general, the straight wings fluttered in bending-torsion; the swept wings sometimes had a small amount of second bending in the flutter mode. It is difficult to say what modes were involved in the flutter of the delta wings since all the motion was near the tip, and very few cycles were required to damage the models. One delta-wing with aileron fluttered on injection in a mode in which aileron motion predominated, but even in this case the mode shape of flutter is not too clear since wing torsion and bending motions are involved in the flutter. The experimental values of the reduced frequency at flutter were much lower than those characteristic of subsonic flow. Some of the trends noted above and the same general changes in the stability boundaries with sweepback as those obtained on this program have also been obtained from transonic tests.

In Section 3.4 the data obtained on the present program is compared with that obtained in other tests on similar models with similar parameters. In that section the flutter boundaries are drawn from M = 0.60 to M = 2.0 using all this data. Some scatter exists but the general trends may be noted. Conclusions can only be made for models whose parameters compare well with those presented. The following general conclusions may be reached:

(1) For straight wings with the parameters,
Panel AR = 1.50
center of gravity at about 50% chord
elastic axis at about 42% chord
$\left(\frac{\omega_h}{\omega_\alpha}\right)$ = 0.3

The critical flutter condition at constant altitude lies at Mach numbers of about 1.7.

(2) For swept wings with parameters similar to the straight wings given above, the critical flutter condition at constant altitude probably lies in the transonic region.

(3) For 60^{o} deltas with mode shapes and natural frequency ratios similar to those of the subject program, the critical flutter condition probably lies near M = 2.0. As noted in Section 3.4 this conclusion must be used with care because of the scarcity of delta wing flutter data for models with characteristics similar to those tested on the subject program.

(4) For all those planforms, straight, swept, and delta, the critical flutter condition at constant dynamic pressure lies in the transonic regime at Mach numbers close to 1.0.

[redacted]

BIBLIOGRAPHY

1. Garrick, I. E. Some Research on High-Speed Flutter. Paper Presented at the Third Anglo-American Aeronautical Conference, 1951.

2. Cunningham, H. J. and Brown, H. H. A Compilation of Experimental Flutter Information. NACA R.M. L53K02a, January 11, 1954 (Confidential).

3. Molyneux, W. G. and Ruddlesden, F. Some Flutter Tests on Sweptback Wings using Ground Launched Rockets. Royal Aircraft Establishment, Report No. Structures 155, October 1953 (Confidential).

4. Jones, G. W., Jr. and DuBose, H. C. Investigation of Wing Flutter at Transonic Speeds for Six Systematically Varied Plan Forms. NACA RM L53G10a, August 13, 1953 (Confidential)

5. Maier, H. G. and King, S. R. Special Progress Report, The Critical Flutter Mach Number for 45° Sweptback Wings, Transonic Flutter Model Tests. Cornell Aeronautical Laboratory, Inc. Report No. C.A.L. - 70 on Contract No. AF 33(616)-179, January 1955 (Confidential).

6. Loftin, L. K., Jr. Flutter Characteristics of Swept Wings at Transonic Speeds. NACA Conference on Aircraft Loads, Flutter, and Structures, Langley Aeronautical Laboratory, Langley Field, Virginia, March 2-4, 1955 (Confidential).

7. Garrick, I. E. and Rubinow, S. I. Flutter and Oscillating Air-Force Calculations for an Airfoil in a Two-Dimensional Supersonic Flow. NACA T.R. 846, May 1946.

8. Pengelley, C. D., Benun, D., D'Ewart, B. B. Jr., and Blackwell, E.; Supersonic Flutter Model Tests at M = 1.5. Curtiss-Wright Corporation, USAF Technical Report No. 5793, April 1951.

9. Tuovila, W. J., Baker, J. E. and Regier, A. A. Initial Experiments on Flutter of Unswept Cantilever Wings at Mach Number 1.3. NACA T.N. 3312, November 1954.

10. Nelson, H. C. and Rainey, R. A. Comparison of Flutter Calculations Using Various Aerodynamic Coefficients with Experimental Results for Some Rectangular Cantilever Wings at Mach Number 1.3. NACA T.N. 3301, November 1954.

BIBLIOGRAPHY (Contd.)

11. Andreopoulos, T. C., and Targoff, W. P.; Flutter at M = 1.72 Two-Dimensional Tests, WADC Technical Report 53-306 Sept. 1953.

12. McCarthy, J. F., Jr. and Halfman, R. L. The Design and Testing of Supersonic Flutter Models. Paper presented at the 23rd Annual Meeting of the Institute of Aeronautical Sciences, New York City, July 1955. I.A.S. Preprint No. 513.

13. Halfman, R. L., McCarthy, J. F., Jr., Prigge, J. S., Jr., and Wood, G. A., Jr. A Variable Mach Number Supersonic Test Section for Flutter Research. Aeroelastic and Structures Research Laboratory, Massachusetts Institute of Technology, WADC Technical Report 54-114, December 1954.

14. McCarthy, J. F., Jr., Asher, G. W., Prigge, J. S., Jr. and Levey, G. M. Three-Dimensional Supersonic Flutter Model Tests Near Mach Number 1.5 Part I Model Design and Testing Techniques. Aeroelastic and Structures Research Laboratory, Massachusetts Institute of Technology, WADC Technical Report 54-113, Part I (to be published).

15. McCarthy, J. F., Jr., Prigge, J. S., Jr., Halfman, R. L. Three-Dimensional Flutter Tests Near Mach No. 1.5. Massachusetts Institute of Technology, Preliminary Report on Contract No. AF33 (038)-22955, March 1952 (Confidential).

16. Aeroelastic and Structures Research Laboratory, Massachusetts Institute of Technology. The Design and Testing of Supersonic Flutter Models. 16 mm sound-colored movie, 22 minutes, November 1954.

17. Prigge, J. S. Jr. The Design of Supersonic Flutter Models, M.I.T., Department of Aeronautical Engineering, A. E. Thesis, August 1954.

18. Wright Air Development Center. General and Detail Requirements for Three-Dimensional Flutter Model Tests Near M=1.5. Exhibit "A", Attachment to PR: 123716, March 19, 1951.

19. Bisplinghoff, R. L., Ashley, H. and Halfman, R. L. Aeroelasticity. Addison Wesley Press, Inc., Cambridge, 1955.

20. Pines, S., Dugundji, J., and Neuringer, J. Aerodynamic Flutter Derivatives for a Flexible Wing with Subsonic and Supersonic Edges, Jour. Aero. Sci., Vol. 22, No. 10, October 1955, pp. 693-700.

BIBLIOGRAPHY (Contd.)

21. Martin, H. C. and Gursahaney, H. J. On the Deflection of Swept Cantilevered Surfaces. Jour. Aero. Sci., Vol. 18 No. 12, December 1951, pp. 805-812.

22. Theodorsen, T. and Garrick, I. E. Mechanism of Flutter, A Theoretical and Experimental Investigation of the Flutter Problem. NACA T.R. 685, September 1940.

23. The Staff of the Johns Hopkins University, Applied Physics Laboratory, Silver Spring, Maryland. Handbook of Supersonic Aerodynamics, Volume 4, Section 12 - Aeroelastic Phenomena. NAVORD Report 1488 (Vol. 4), 1 January 1952.

24. Landahl, M., Mollo-Christensen, E. L. and Ashley, H. Parametric Studies of Viscous Nonviscous Unsteady Flows. M.I.T. Fluid Dynamic Research Group, OSR Technical Report No. 55-13 Group Report No. 55-1, Office of Scientific Research Contract No. AF 18(600)-961, April 1955.

25. Van Dyke, M. D., Supersonic Flow Past Oscillating Airfoils Including Nonlinear Thickness Effects. NACA T.N. 2982 July 1953.

26. Smilg, B. and Wasserman, L. S. Application of Three-Dimensional Flutter Theory to Aircraft Structures. Air Corps Technical Report No. 4798, July 1942.

27. Martin, D. J. Summary of Flutter Experiences as a Guide to the Preliminary Design of Lifting Surfaces on Missiles. NACA RM L51J30, November 1951

28. Marks, L. S. Mechanical Engineers' Handbook. McGraw-Hill Book Company, Inc., New York 1951, p. 499.

29. Judd, J. H. and Lauten, W. T., Jr. Flutter of a 60° Delta Wing (NACA 65A003 Airfoil) Encountered at Supersonic Speeds During the Flight Test of a Rocket-Propelled Model. NACA RM L52E06a, 1952 (Confidential).

30. Sewall, J. L., Herr, R. W., and Igoe, W. B.; Flutter Investigation of a True Speed Dynamic Model with Various Tip Tank Configurations. NACA RML54I19, March 1955 (Confidential).

31. Scanlan, R. T. and Rosenbaum, R. Aircraft Vibration and Flutter. First Edition. The Macmillan Company, New York, 1951.

BIBLIOGRAPHY (Contd.)

32. Zartarian, G., Hsu, P. T., and Voss, H. M. Comparative Flutter Calculations on Low-Aspect-Ratio Wings in Incompressible and Supersonic Flows. Aeroelastic and Structures Research Laboratory, Massachusetts Institute of Technology, Technical Report 52-2, Bureau of Aeronautics Contract NOa(s) 53-564-c, 1 October 1954.

33. Zartarian, G., Heller, A., and Ashley, H. Application of Piston Theory to Certain Elementary Aeroelastic Problems. Paper presented at the Midwestern Conference on Fluid Mechanics. Purdue University, West Lafayette, Indiana, September 1955.

34. Lighthill, M. J. Oscillating Airfoils at High Mach Number. Jour. Aero. Sci., Vol. 20 No. 6, June 1953, pp. 402-406.

35. Miles, J. W. Unsteady Supersonic Flow Past Slender Pointed Bodies. U. S. Naval Ordnance Test Station, Inyokern, China Lake, California, NAVORD Report 2031, 11 May 1953.

36. Rauscher, M. Introduction to Aeronautical Dynamics. First Edition. John Wiley & Sons, Inc., New York 1953.

37. Milne-Thomson, L. M. Theoretical Hydrodynamics. First Edition. Macmillan and Co., Limited, London 1938.

38. Ashley, H., Zartarian, G., and Neilson, D. O. Investigation of Certain Unsteady Aerodynamic Effects in Longitudinal Dynamic Stability. Aeroelastic and Structures Research Laboratory, Massachusetts Institute of Technology, USAF Technical Report No. 5986, December 1951.

39. Bisplinghoff, R. L., Isakson, G., Pian, T. H. H., Flomenhoft, H. I., and O'Brien, T. F. Report on an Investigation of Stresses in Aircraft Structures under Dynamic Loading. Aeroelastic and Structures Research Laboratory, Massachusetts Institute of Technology, Bureau of Aeronautics Contract NOa(s) 8790, 21 January 1949.

40. Huckel, V. and Durling, B. J. Tables of Wing-Aileron Coefficients of Oscillating Air Forces for Two-Dimensional Supersonic Flow. NACA T. N. 2055, March 1950.

41. Zartarian, G. and Voss, H. M. On the Evaluation of the Function $f_{\lambda}(M, \bar{\omega})$. Readers Forum, Jour. Aero. Sci., Vol. 20, No. 11, November 1953, pp. 781-782.

BIBLIOGRAPHY (Contd.)

42. Wylie, C. R., Jr. Advanced Engineering Mathematics. First Edition. McGraw-Hill Book Company, Inc., New York, 1951.

43. Munitions Board Aircraft Committee. Design of Wood Aircraft Structures. ANC-18. June 1951.

44. Tolve, L. A. XF-92A Vibration Tests. WADC Memorandum Report No. MCREXA 5-4302-64-20, 9 January 1950 (Confidential).

45. Spielberg, I. N. Structural Influence Coefficients of the XF-92A Delta Wing. WADC Memorandum Report No. WCNSY-4595-7-2, 4 September 1951.

46. Voss, H. M., and Zartarian, G. Flutter Analyses of Two Low-Aspect-Ratio Wings. M.I.T. Aeroelastic and Structures Research Laboratory Report for the Bureau of Aeronautics, U. S. Navy on Contract No. NOa(s) 53-564-c, October 1, 1953 (Confidential).

47. Tuovila, W. J., and McCarty, J. L., Experimental Flutter Results for Cantilever-Wing Models at Mach Numbers up to 3.0, NACA RML55E11, June 1955, (Confidential).

48. Pratt, G. L., Experimental Flutter Investigation of a Thin Unswept Wing at Transonic Speeds, NACA RML55A18, April 1955, (Confidential).

49. Lauten, W. J. Jr., and O'Kelley, B. R., Free-Flight Flutter Tests in the Transonic and Low Supersonic Speed Range of Three Low-Aspect-Ratio, Swept, Tapered Wings on Rocket Propelled Vehicles, NACA RM L55J21, March 1956.

50. Judd, J. H., and Lauten, W. J. Jr., Flutter of a 60° Delta Wing (NACA 65A008 Airfoil) Encountered at Supersonic Speeds during the Flight Test of a Rocket-Propelled Model. NACA RM L52E06a, September 1952.

APPENDIX A

THEORETICAL FLUTTER ANALYSES FOR STRAIGHT-WING PLANFORM IN SUPERSONIC FLOW

A.1 Aileron and Bare Wing

Using the standard nomenclature of Figure A.1, the elements of the three-dimensional flutter determinant of Reference 26 can be written directly for our case by a straightforward substitution of the two-dimensional supersonic aerodynamic coefficients of Reference 7. A comparison of the expressions for the lift and the moments in incompressible flow (Ref. 26, p. 25 ff) and supersonic flow (Ref. 7, p. 7) shows that the following aerodynamic terms are equivalent,

Incompressible	Supersonic	
πL_h	$-4(L_1 + iL_2)$	Eq. (A.1)
$\pi\left[L_\alpha - L_h\left(\frac{1}{2}+a\right)\right]$	$-4(L_3 + iL_4)$	Eq. (A.2)
πL_β	$-4(L_5 + iL_6)$	Eq. (A.3)
$\pi\left[\frac{1}{2} - L_h\left(\frac{1}{2}+a\right)\right]$	$-4(M_1 + iM_2)$	Eq. (A.4)
$\pi\left[M_\alpha - L_\alpha\left(\frac{1}{2}+a\right) - \frac{1}{2}\left(\frac{1}{2}+a\right) + L_h\left(\frac{1}{2}+a\right)^2\right]$	$-4(M_3 + iM_4)$	Eq. (A.5)
$\pi\left[M_\beta - L_\beta\left(\frac{1}{2}+a\right)\right]$	$-4(M_5 + iM_6)$	Eq. (A.6)

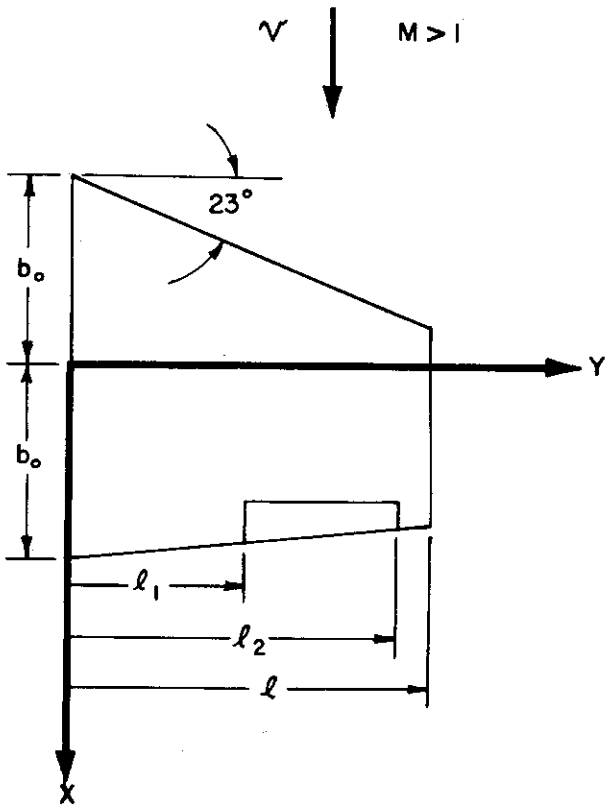

(a) Plan View of Wing

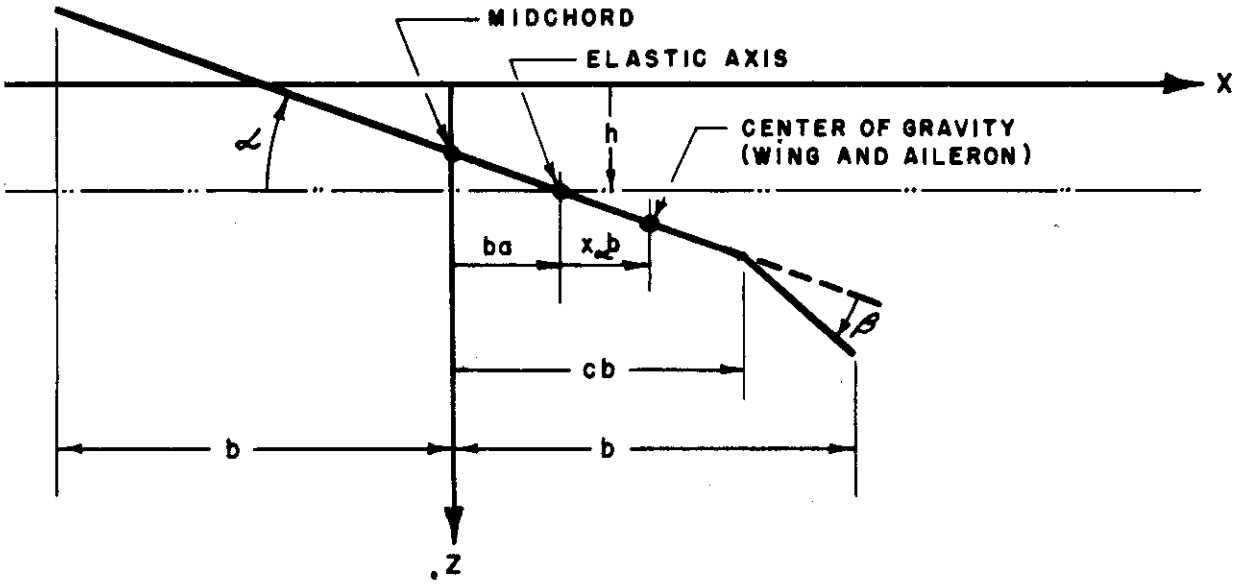

(b) Streamwise Section

FIGURE A.1 NOMENCLATURE AND CONVENTIONS FOR THEORY

Incompressible	Supersonic	
πT_h	$-4(N_1 + iN_2)$	Eq. (A.7)
$\pi [T_\alpha - T_h(\frac{1}{2} + a)]$	$-4(N_3 + iN_4)$	Eq. (A.8)
πT_β	$-4(N_5 + iN_6)$	Eq. (A.9)

Equations (A.1) through (A.9) assume that the leading edge of the aileron lies on the hinge line. The coefficient, M_h, is taken equal to 1/2 (Ref. 7, p. 29). With this equivalence, the flutter determinant can be written as (Ref. 7, pp. 62, 63),

$$\begin{vmatrix} \underline{A} & \underline{B} & \underline{C} \\ \underline{D} & \underline{E} & \underline{F} \\ \underline{G} & \underline{H} & \underline{I} \end{vmatrix} = 0 \qquad \text{Eq. (A.10)}$$

where

$$\underline{A} = \left[1 - \left(\frac{\omega_\alpha}{\omega}\right)^2 \left(\frac{\omega_h}{\omega_\alpha}\right)^2 (1 + ig_h)\right] \int_0^\ell m(y) f_h^2(y)\, dy - 4\rho \int_0^\ell (L_1 + iL_2) b^2(y) f_h^2(y)\, dy \qquad \text{Eq. (A.11)}$$

$$\underline{B} = \int_0^\ell S_\alpha(y) f_h(y) f_\alpha(y)\, dy - 4\rho \int_0^\ell (L_3 + iL_4) b^3(y) f_h(y) f_\alpha(y)\, dy \qquad \text{Eq. (A.12)}$$

$$\overline{C} = \int_{l_1}^{l_2} S_\beta(y)\, f_h(y)\, f_\beta(y)\, dy - 4\rho \int_{l_1}^{l_2} (L_5 + iL_6)\, b^3(y)\, f_h(y)\, f_\beta(y)\, dy \qquad \text{Eq. (A.13)}$$

$$\overline{D} \int_0^{l} S_\alpha(y)\, f_h(y)\, f_\alpha(y)\, dy - 4\rho \int_0^{l} (M_1 + iM_2)\, b^3(y)\, f_h(y)\, f_\alpha(y)\, dy \qquad \text{Eq. (A.14)}$$

$$\overline{E} = \left[1 - \left(\frac{\omega_\alpha}{\omega}\right)^2 (1 + ig_\alpha)\right] \int_0^{l} I_\alpha(y)\, f_\alpha^2(y)\, dy - 4\rho \int_0^{l} (M_3 + iM_4)\, b^4(y)\, f_\alpha^2(y)\, dy \qquad \text{Eq. (A.15)}$$

$$\overline{F} = \int_{l_1}^{l_2} \left[I_\beta(y) + (c-a)\, b(y)\, S_\beta(y)\right] f_\alpha(y)\, f_\beta(y)\, dy - 4\rho \int_{l_1}^{l_2} (M_5 + iM_6)\, b^4(y)\, f_\alpha(y)\, f_\beta(y)\, dy \qquad \text{Eq. (A.16)}$$

$$\overline{G} = \int_{l_1}^{l_2} S_\beta(y)\, f_h(y)\, f_\beta(y)\, dy - 4\rho \int_{l_1}^{l_2} (N_1 + iN_2)\, b^3(y)\, f_h(y)\, f_\beta(y)\, dy \qquad \text{Eq. (A.17)}$$

$$\overline{H} = \int_{l_1}^{l_2} \left[I_\beta(y) + (c-a)\, b(y)\, S_\beta(y)\right] f_\alpha(y)\, f_\beta(y)\, dy - 4\rho \int_{l_1}^{l_2} (N_3 + iN_4)\, b^4(y)\, f_\alpha(y)\, f_\beta(y)\, dy \qquad \text{Eq. (A.18)}$$

$$\overline{I} = \left[1 - \left(\frac{\omega_\beta}{\omega_\alpha}\right)^2 \left(\frac{\omega_\alpha}{\omega}\right)^2 (1 + ig_\rho)\right] \int_{l_1}^{l_2} I_\beta(y)\, f_\beta^2(y)\, dy - 4\rho \int_{l_1}^{l_2} (N_5 + iN_6)\, b^4(y)\, f_\beta^2(y)\, dy \qquad \text{Eq. (A.19)}$$

The assumed bending and torsion mode shapes are taken as approximations to the uncoupled first bending and first torsion mode shapes of an ideal beam; the aileron mode is assumed to be a constant rigid-body motion, i.e.,

$$f_h(y) = y^2 \qquad \text{Eq. (A.20)}$$

$$f_\alpha(y) = y \qquad \text{Eq. (A.21)}$$

$$f_\beta(y) = 1 \qquad \text{Eq. (A.22)}$$

The mass parameters of the models were built to be typical of actual wings, hence,

$$b(y) = b_o\left[1 - (1-\lambda)\frac{y}{\ell}\right] \qquad \text{Eq. (A.23)}$$

$$m(y) = m_o\left[\frac{b(y)}{b_o}\right]^2 \qquad \text{Eq. (A.24)}$$

$$S_\alpha(y) = S_{\alpha o}\left[\frac{b(y)}{b_o}\right]^3 \qquad \text{Eq. (A.25)}$$

$$S_\beta(y) = S_{\beta o}\left[\frac{b(y)}{b_o}\right]^3 \qquad \text{Eq. (A.26)}$$

$$I_\alpha(y) = I_{\alpha o}\left[\frac{b(y)}{b_o}\right]^4 \qquad \text{Eq. (A.27)}$$

$$I_\beta(y) = I_{\beta o}\left[\frac{b(y)}{b_o}\right]^4 \qquad \text{Eq. (A.28)}$$

where

λ is the ratio of the tip chord to the root chord. The subscript, o, refers to conditions at the root chord of the wing. In the case of the aileron, these are fictitious values since the aileron extends over the outboard half of the wing only. Taking $\lambda = 1/2$, introducing the dimensionless variable,

$$\eta = \frac{y}{\ell} \qquad \text{Eq. (A.29)}$$

and dividing the columns and rows of the flutter determinant by appropriate constants, the elements of the flutter determinant can be rewritten in the following dimensionless form,

$$\underline{A} = \left[1-\left(\frac{\omega_h}{\omega_\alpha}\right)^2\left(\frac{\omega_k}{\omega}\right)^2(1+ig_h)\right]\bar{\mu}\int_0^1\left(1-\eta/2\right)^2\eta^4\,d\eta - \int_0^1(L_1+iL_2)\left(1-\frac{\eta}{2}\right)^2\eta^4\,d\eta \qquad \text{Eq. (A.30)}$$

$$\underline{B} = \bar{\mu}x_\alpha\int_0^1\left(1-\frac{\eta}{2}\right)^3\eta^3\,d\eta - \int_0^1(L_3+iL_4)\left(1-\frac{\eta}{2}\right)^3\eta^3\,d\eta \qquad \text{Eq. (A.31)}$$

$$\underline{C} = \bar{\mu}x_\beta\int_{0.5}^1\left(1-\frac{\eta}{2}\right)^3\eta^2\,d\eta - \int_{0.5}^1(L_5+iL_6)\left(1-\frac{\eta}{2}\right)^3\eta^2\,d\eta \qquad \text{Eq. (A.32)}$$

$$\underline{D} = \bar{\mu}x_\alpha\int_0^1\left(1-\frac{\eta}{2}\right)^3\eta^3\,d\eta - \int_0^1(M_1+iM_2)\left(1-\frac{\eta}{2}\right)^3\eta^3\,d\eta \qquad \text{Eq. (A.33)}$$

$$\underline{E} = \left[1-\left(\frac{\omega_\alpha}{\omega}\right)^2(1+ig_\alpha)\right]\bar{\mu}r_\alpha^2\int_0^1\left(1-\frac{\eta}{2}\right)^4\eta^2\,d\eta - \int_0^1(M_3+iM_4)\left(1-\frac{\eta}{2}\right)^4\eta^2\,d\eta \qquad \text{Eq. (A.34)}$$

$$\underline{F} = \bar{\mu} r_\beta^2 \int_{0.5}^{1} \left(1 - \frac{\eta}{2}\right)^4 \eta \, d\eta + \bar{\mu} \chi_\beta (c-a) \int_{0.5}^{1} \left(1 - \frac{\eta}{2}\right)^4 \eta \, d\eta - \int_{0.5}^{1} (M_5 + i M_6)\left(1 - \frac{\eta}{2}\right)^4 \eta \, d\eta \qquad \text{Eq. (A.35)}$$

$$\underline{G} = \bar{\mu} \chi_\beta \int_{0.5}^{1} \left(1 - \frac{\eta}{2}\right)^3 \eta^2 d\eta - \int_{0.5}^{1} (N_1 + i N_2)\left(1 - \frac{\eta}{2}\right)^3 \eta^2 \, d\eta \qquad \text{Eq. (A.36)}$$

$$\underline{H} = \bar{\mu} r_\beta^2 \int_{0.5}^{1} \left(1 - \frac{\eta}{2}\right)^4 \eta \, d\eta + \bar{\mu} \chi_\beta (c-a) \int_{0.5}^{1} \left(1 - \frac{\eta}{2}\right)^4 \eta \, d\eta - \int_{0.5}^{1} (N_3 + i N_4)\left(1 - \frac{\eta}{2}\right)^4 \eta \, d\eta \qquad \text{Eq. (A.37)}$$

$$\underline{I} = \left[1 - \left(\frac{\omega_\beta}{\omega_\alpha}\right)^2 \left(\frac{\omega_\mu}{\omega}\right)^2 (1 + i g_\beta)\right] \bar{\mu} r_\beta^2 \int_{0.5}^{1} \left(1 - \frac{\eta}{2}\right)^4 d\eta - \int_{0.5}^{1} (N_5 + i N_6)\left(1 - \frac{\eta}{2}\right)^4 d\eta \qquad \text{Eq. (A.38)}$$

where

$\bar{\mu}$ is the wing mass-density ratio in supersonic flow, $\frac{m}{4\rho b^2}$. It should be noted that by virtue of the linear taper of all dimensions (see Figure 1.1) and the spanwise mass variations of equations (A.23) through (A.28), the parameters, μ, χ_α, χ_β, r_α, r_β, c and a, are constant along the span.

The integrals multiplying the mass parameters are definite integrals and can be evaluated in closed form. Their values are:

$$\int_0^1 \left(1 - \frac{\eta}{2}\right)^2 \eta^4 d\eta = \frac{29}{420} \qquad \text{Eq. (A.39)}$$

$$\int_{0.5}^{1} \left(1 - \frac{\eta}{2}\right)^3 \eta^2 d\eta = \frac{997}{15,360} \qquad \text{Eq. (A.40)}$$

$$\int_0^1 \left(1-\frac{\eta}{2}\right)^3 \eta^3 d\eta = \frac{2}{35} \qquad \text{Eq. (A.41)}$$

$$\int_{0.5}^1 \left(1-\frac{\eta}{2}\right)^4 d\eta = \frac{211}{2560} \qquad \text{Eq. (A.42)}$$

$$\int_{0.5}^1 \left(1-\frac{\eta}{2}\right)^4 \eta \, d\eta = \frac{1739}{30,720} \qquad \text{Eq. (A.43)}$$

$$\int_0^1 \left(1-\frac{\eta}{2}\right)^4 \eta^2 d\eta = \frac{33}{560} \qquad \text{Eq. (A.44)}$$

The integrals containing the aerodynamic coefficients cannot be evaluated directly because the aerodynamic coefficients are functions of the reduced-frequency parameter , $\bar{\omega}$, which varies along the span.

The flutter determinant for the case of the bare cantilever wing can be obtained by setting the aileron terms equal to zero. Thus, the determinant is,

$$\begin{vmatrix} \underline{A} & \underline{B} \\ \underline{D} & \underline{E} \end{vmatrix} = 0 \qquad \text{Eq. (A.45)}$$

where the elements, $\underline{A}$, $\underline{B}$, $\underline{D}$, $\underline{E}$, are as defined for the wing-aileron flutter determinant.

A.2 Tip Tank; Free-to-Roll and Cantilever Conditions

Assuming that the motion of the wing at flutter can be represented by the superposition of the fundamental uncoupled bending mode (h), the uncoupled torsion mode (α) and the rigid body rotational mode about the wing root (θ), the vertical deflection of the wing illustrated in Figure A.2 may be written as

$$z(x,y,t) = y\theta(t) + h(y,t) + (x - ba)\alpha(y,t) \qquad \text{Eq. (A.46)}$$

Equation (A.46) assumes that the elastic axis of the wing is straight and is perpendicular to the wing root chord.

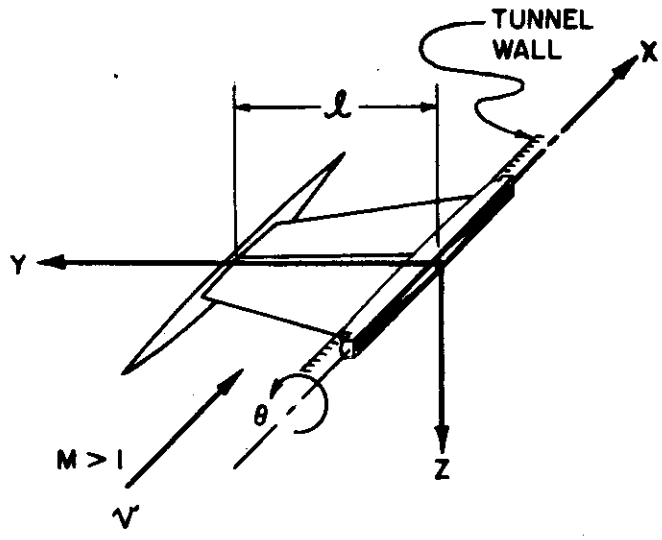

FIGURE A.2 AXIS SYSTEM FOR WING WITH TIP TANK

With the introduction of assumed modes, the kinetic energy of the mechanical system becomes

$$KE = \frac{1}{2}\int_0^{\ell}\int_{-b}^{b} m(x,y)\left[y\,\dot{\bar{\theta}}(t) + f_h(y)\,\dot{\bar{h}}(t) + (x-ba)f_\alpha(y)\dot{\bar{\alpha}}(t)\right]^2 dx\,dy$$
$$+ \frac{1}{2} I_s \left[\dot{\bar{\theta}}(t)\right]^2 \qquad \text{Eq. (A.47)}$$
$$+ \frac{1}{2}\int_T m_T(x)\left[\ell\,\dot{\bar{\theta}}(t) + \dot{\bar{h}}(t) + (x-ba)\dot{\bar{\alpha}}(t)\right]^2 dx$$

where

$m_T(x)$ is the mass of the tip tank per unit chordwise distance

I_s is the rolling moment of inertia of the wing support

Each motion has been separated into a time-dependent variation (superscript $-$) and a space-dependent variation (mode shape). For the case of simple harmonic motion, equation (A.47) may be differentiated with respect to time and integrated along the chord to give the following results

$$\frac{d}{dt}\left(\frac{\partial(KE)}{\partial\dot{\bar{\theta}}}\right) = -\omega^2 e^{i\omega t}\left[\bar{\theta}\int_0^{\ell} m(y)\,y^2 dy + \bar{h}\int_0^{\ell} m(y) f_h(y)\,y\,dy\right. \qquad \text{Eq. (A.48)}$$
$$+ \bar{\alpha}\int_0^{\ell} S_\alpha(y) f_\alpha(y)\,y\,dy + \bar{\theta}\dot{I}_s + \bar{\theta}\ell^2 M_T$$
$$\left. + \bar{h}\ell M_T + \bar{\alpha}\ell S_T\right]$$

$$\frac{d}{dt}\left(\frac{\partial(KE)}{\partial\dot{\bar{h}}}\right) = -\omega^2 e^{i\omega t}\left[\bar{\theta}\int_0^{\ell} m(y) f_h(y)\,y\,dy + \bar{h}\int_0^{\ell} m(y) f_h^2(y)\,dy\right. \qquad \text{Eq. (A.49)}$$
$$+ \bar{\alpha}\int_0^{\ell} S_\alpha(y) f_h(y) f_\alpha(y)\,dy + \bar{\theta}\ell M_T + \bar{h} M_T$$
$$\left. + \bar{\alpha} S_T\right.$$

$$\frac{d}{dt}\left(\frac{\partial(KE)}{\partial \dot{\bar{\alpha}}}\right) = -\omega^2 e^{i\omega t}\left[\bar{\theta}\int_0^{\ell} S_\alpha(y) f_\alpha(y)\, y\, dy + \bar{h}\int_0^{\ell} S_\alpha(y) f_h(y) f_\alpha(y)\, dy\right.$$

$$\left. + \bar{\alpha}\int_0^{\ell} I_\alpha(y) f_\alpha^2(y)\, dy + \bar{\theta}\,\ell\, S_T + \bar{h}\, S_T\right. \qquad \text{Eq. (A.50)}$$

$$\left. + \bar{\alpha}\, I_T\right]$$

where

M_T is the total mass of the tip tank

S_T is the static unbalance of the tip tank about the elastic axis of the wing, positive nose up

I_T is the mass moment of inertia of the tip tank about the elastic axis of the wing.

The assuming of fundamental mode shapes to describe the flutter motion is a Rayleigh-type approximation, and it can be shown (Ref. 31, p. 19) that the variation of the potential energy with respect to the assumed modes may be written as

$$\frac{\partial(PE)}{\partial \bar{\theta}} = 0 \qquad \text{Eq. (A.51)}$$

since the rigid-body rolling mode cannot affect the internal potential-energy level of the system, and

$$\frac{\partial(PE)}{\partial \bar{h}} = \omega_h^2 e^{i\omega t}\bar{h}\int_0^{\ell} m(y) f_h^2(y)\, dy \qquad \text{Eq. (A.52)}$$

$$\frac{\partial(PE)}{\partial \bar{\alpha}} = \omega_\alpha^2 e^{i\omega t}\bar{\alpha}\int_0^{\ell} I_\alpha(y) f_\alpha^2(y)\, dy \qquad \text{Eq. (A.53)}$$

Because the potential energy is a function only of the elastic deflection of the wing, it is convenient to choose the mode shapes and thus the frequencies in equations (A.52) and (A.53) as those of the bare wing without the tip tank. This assumption implies that the uncoupled mode shapes are the same for the wing with and without the tip tank. By eliminating the necessity of estimating new mode shapes and frequencies for each change in the parameters of the tip tank, theoretical trends for variations in tip-tank parameters can be obtained with a minimum of effort.

The equations of motion are derived by applying Lagrange's equation,

$$\frac{d}{dt}\left(\frac{\partial(KE)}{\partial \dot{\bar{q}}_i}\right) - \frac{\partial(KE)}{\partial \bar{q}_i} + \frac{\partial(PE)}{\partial \bar{q}_i} = Q_i \qquad \text{Eq. (A.54)}$$

where Q_i is the generalized force of the i^{th} mode and represents all the forces not included in the potential-energy or kinetic-energy functions, and $\bar{q}_i$ is the magnitude of the i^{th} generalized coordinate at the wing tip station. Expressions for the generalized force, Q_i, are obtained from virtual-work considerations (Ref. 31, p. 56). The virtual work done on the wing as it moves through the virtual displacements, $\delta\theta$, δh and $\delta\alpha$ is

$$\delta W = \int_0^\ell \left\{ L(y)\left[y\,\delta\theta(y) + \delta h(y)\right] + M'(y)\,\delta\alpha(y) \right\} dy \qquad \text{Eq. (A.55)}$$

$$\delta W = \int_0^\ell L(y)\,y\,dy\,\delta\bar{\theta} + \int_0^\ell L(y)\,f_h(y)\,dy\,\delta\bar{h} + \int_0^\ell M'(y)\,f_\alpha(y)\,dy\,\delta\bar{\alpha} \qquad \text{Eq. (A.56)}$$

$$\delta W = Q_{\bar{\theta}}\,\delta\bar{\theta} + Q_{\bar{h}}\,\delta\bar{h} + Q_{\bar{\alpha}}\,\delta\bar{\alpha} \qquad \text{Eq. (A.57)}$$

where

L is the lift on the wing per unit span, positive down

M' is the moment about the elastic axis of the wing per unit span, positive nose up.

These generalized forces, which, for a system with zero damping, consist only of aerodynamic forces may be written as

$$Q_{\bar{\theta}} = Q_{\theta\theta}\bar{\theta} + Q_{\theta h}\bar{h} + Q_{\theta\alpha}\bar{\alpha} \qquad \text{Eq. (A.58)}$$

$$Q_{\bar{h}} = Q_{h\theta}\bar{\theta} + Q_{hh}\bar{h} + Q_{h\alpha}\bar{\alpha} \qquad \text{Eq. (A.59)}$$

$$Q_{\bar{\alpha}} = Q_{\alpha\theta}\bar{\theta} + Q_{\alpha h}\bar{h} + Q_{\alpha\alpha}\bar{\alpha} \qquad \text{Eq. (A.60)}$$

where Q_{ij} is the generalized force in the i^{th} mode per unit displacement of the j^{th} mode. For the aerodynamic forces acting on the wing and on the tip tank,

$$Q_{\theta\theta} = \int_0^\ell \bar{L}_h(y)\, y^2\, dy + \bar{L}_{h_T}\ell^2 \qquad \text{Eq. (A.61)}$$

$$Q_{\theta h} = \int_0^\ell \bar{L}_h(y)\, f_h(y)\, y\, dy + \bar{L}_{h_T}\ell \qquad \text{Eq. (A.62)}$$

$$Q_{\theta\alpha} = \int_0^\ell \bar{L}_\alpha(y)\, f_\alpha(y)\, y\, dy + \bar{L}_{\alpha_T}\ell \qquad \text{Eq. (A.63)}$$

$$Q_{h\theta} = \int_0^\ell \bar{L}_h(y)\, f_h(y)\, y\, dy + \bar{L}_{h_T}\ell \qquad \text{Eq. (A.64)}$$

$$Q_{hh} = \int_0^\ell \bar{L}_h(y)\, f_h^2(y)\, dy + \bar{L}_{h_T} \qquad \text{Eq. (A.65)}$$

$$Q_{h\alpha} = \int_0^\ell \bar{L}_\alpha(y)\, f_h(y)\, f_\alpha(y)\, dy + \bar{L}_{\alpha_T} \qquad \text{Eq. (A.66)}$$

$$Q_{\alpha\theta} = \int_0^\ell \bar{M}_h(y)\, f_\alpha(y)\, y\, dy + \bar{M}_{h_T} \qquad \text{Eq. (A.67)}$$

$$Q_{\alpha h} = \int_0^\ell \bar{M}_h(y)\, f_h(y)\, f_\alpha(y)\, dy + \bar{M}_{h_T} \qquad \text{Eq. (A.68)}$$

$$Q_{\alpha\alpha} = \int_0^{\ell} \bar{M}_{\alpha}(y)\, f_{\alpha}^2(y)\, dy + \bar{M}_{\alpha_T} \qquad \text{Eq. (A.69)}$$

where explicit expressions for $\bar{L}_h$, $\bar{L}_\alpha$, $\bar{M}_h$ and $\bar{M}_\alpha$ are obtained from Reference 7 (p. 7) for the wing and those for $\bar{L}_{h_T}$, $\bar{L}_{\alpha_T}$, $\bar{M}_{h_T}$ and $\bar{M}_{\alpha_T}$ from equations (B.26) and (B.27) for the tip tank,

$$\bar{L}_h = -\frac{m}{\bar{\mu}}\omega^2 e^{i\omega t}(L_1 + iL_2) \qquad \text{Eq. (A.70)}$$

$$\bar{L}_\alpha = -\frac{m}{\bar{\mu}}\omega^2 b e^{i\omega t}(L_4 + iL_4) \qquad \text{Eq. (A.71)}$$

$$\bar{M}_h = -\frac{m}{\bar{\mu}}\omega^2 b e^{i\omega t}(M_1 + iM_2) \qquad \text{Eq. (A.72)}$$

$$\bar{M}_\alpha = -\frac{m}{\bar{\mu}}\omega^2 b^2 e^{i\omega t}(M_3 + iM_4) \qquad \text{Eq. (A.73)}$$

$$\bar{L}_{h_T} = \rho V_T \omega^2 e^{i\omega t} \qquad \text{Eq. (A.74)}$$

$$\bar{L}_{\alpha_T} = \rho \bar{V}_T \omega^2 e^{i\omega t}\left(n_T - i\frac{v}{\omega}\right) \qquad \text{Eq. (A.75)}$$

$$\overline{M}_{h_T} = \rho \bar{V}_T \omega^2 e^{i\omega t} \left(n_T + i\frac{v}{\omega}\right) \qquad \text{Eq. (A.76)}$$

$$\overline{M}_{\alpha_T} = \rho V_T \omega^2 e^{i\omega t} \left(n_T^2 + \frac{I_1}{V_T} + \frac{v^2}{\omega^2}\right) \qquad \text{Eq. (A.77)}$$

where

V_T is the volume of the tip tank

T is the distance that the geometrical center of the tip tank lies aft of the elastic axis of the wing

v is the free-stream velocity

I_1 is the volume moment of inertia in pitch of the tip tank about its geometrical center.

To simplify the theory, the wing is assumed to be uniform with constant chord (see Figure C.3). If the non-rigid bending and torsion modes are taken as the fundamental bending and torsion modes of a uniform cantilever beam (see Reference 32, pp. 65, 66), then

$$\int_0^\ell f_h^2(y)\, dy = \frac{\ell}{4} \qquad \text{Eq. (A.78)}$$

$$\int_0^\ell f_h(y)\, f_\alpha(y)\, dy = 0.338,93\,\ell \qquad \text{Eq. (A.79)}$$

$$\int_0^{\bar{\ell}} f_h(y)\, y\, dy = 0.284,41\, \ell^2 \qquad \text{Eq. (A.80)}$$

$$\int_0^{\ell} f_\alpha^2(y)\, dy = \frac{\ell}{2} \qquad \text{Eq. (A.81)}$$

$$\int_0^{\ell} f_\alpha(y)\, y\, dy = \frac{4\ell^2}{\pi^2} \qquad \text{Eq. (A.82)}$$

Using these results, the generalized aerodynamic forces become

$$Q_{\theta\theta} = \omega^2 m \ell^3 e^{i\omega t}\left[-\frac{1}{3\bar{\mu}}(L_1 + iL_2) + \frac{1}{\bar{\mu}}\left(\frac{\bar{V}_T}{4b^2\ell}\right)\right] \qquad \text{Eq. (A.83)}$$

$$Q_{\theta h} = \omega^2 m \ell^2 e^{i\omega t}\left[-\frac{0.284,41}{\bar{\mu}}(L_1 + iL_2) + \frac{1}{\bar{\mu}}\left(\frac{\bar{V}_T}{4b^2\ell}\right)\right] \qquad \text{Eq. (A.84)}$$

$$Q_{\theta\alpha} = \omega^2 m \ell^3 e^{i\omega t}\left[-\frac{4}{\pi^2\bar{\mu}}\left(\frac{b}{\ell}\right)(L_3 + iL_4) + \frac{1}{\bar{\mu}}\left(\frac{\bar{V}_T}{4b^2\ell}\right)\left(\frac{n_T}{\ell} - \frac{i}{k}\frac{b}{\ell}\right)\right] \qquad \text{Eq. (A.85)}$$

$$Q_{h\theta} = \omega^2 m \ell^2 e^{i\omega t}\left[-\frac{0.284,41}{\bar{\mu}}(L_1 + iL_2) + \frac{1}{\bar{\mu}}\left(\frac{\bar{V}_T}{4b^2\ell}\right)\right] \qquad \text{Eq. (A.86)}$$

$$Q_{hh} = \omega^2 m \ell e^{i\omega t}\left[-\frac{1}{4\bar{\mu}}(L_1 + iL_2) + \frac{1}{\bar{\mu}}\left(\frac{V_T}{4b^2\ell}\right)\right] \qquad \text{Eq. (A.87)}$$

$$Q_{h\alpha} = \omega^2 m \ell^2 e^{i\omega t}\left[-\frac{0.338,93}{\bar{\mu}}\left(\frac{b}{\ell}\right)(L_3 + iL_4) + \frac{1}{\bar{\mu}}\left(\frac{V_T}{4b^2\ell}\right)\left(\frac{n_T}{\ell} - \frac{i}{k}\frac{b}{\ell}\right)\right] \qquad \text{Eq. (A.88)}$$

$$Q_{\alpha\theta} = \omega^2 m \ell^3 e^{i\omega t}\left[-\frac{4}{\pi^2\bar{\mu}}\left(\frac{b}{\ell}\right)(M_1 + iM_2) + \frac{1}{\bar{\mu}}\left(\frac{V_T}{4b^2\ell}\right)\left(\frac{n_T}{\ell} + \frac{i}{k}\frac{b}{\ell}\right)\right] \qquad \text{Eq. (A.89)}$$

$$Q_{\alpha h} = \omega^2 m \ell^2 e^{i\omega t}\left[-\frac{0.338,93}{\bar{\mu}}\left(\frac{b}{\ell}\right)(M_1 + iM_2) + \frac{1}{\bar{\mu}}\left(\frac{V_T}{4b^2\ell}\right)\left(\frac{n_T}{\ell} + \frac{i}{k}\frac{b}{\ell}\right)\right] \qquad \text{Eq. (A.90)}$$

$$Q_{\alpha\alpha} = \omega^2 m \ell^3 e^{i\omega t}\left\{-\frac{1}{2\bar{\mu}}\left(\frac{b}{\ell}\right)^2(M_3 + iM_4) + \frac{1}{\bar{\mu}}\left(\frac{V_T}{4b^2\ell}\right)\left[\left(\frac{n_T}{\ell}\right)^2 + \frac{1}{k^2}\left(\frac{b}{\ell}\right)^2 + \frac{1}{\bar{\mu}}\left(\frac{I_1}{4b^2\ell}\right)\left(\frac{b}{\ell}\right)^2\right]\right\} \qquad \text{Eq. (A.91)}$$

The equations of motion for simple harmonic motion of the system can be derived by the application of Lagrange's equation (Eq. (A.54) with the following results,

$$\bar{\theta}\left[\omega^2 m\frac{\ell^3}{3} + \omega^2 I_s + \omega^2 M_T \ell^2 + \frac{Q_{\theta\theta}}{e^{i\omega t}}\right] + \bar{h}\left[0.284,41\,\omega^2 m \ell^2 + \omega^2 M_T \ell + \frac{Q_{\theta h}}{e^{i\omega t}}\right] + \bar{\alpha}\left[\frac{4}{\pi^2}\omega^2 S_\alpha \ell^2 + \omega^2 S_T \ell + \frac{Q_{\theta\alpha}}{e^{i\omega t}}\right] = 0 \qquad \text{Eq. (A.92)}$$

$$\bar{\theta}\left[0.284{,}41\,\omega^2 m\ell^2 + \omega^2 M_T \ell + \frac{Q_{h\theta}}{e^{i\omega t}}\right] + \bar{h}\left[(\omega^2-\omega_h^2)\frac{m\ell}{4} + \omega^2 M_T + \frac{Q_{hh}}{e^{i\omega t}}\right] + \bar{\alpha}\left[0.338{,}93\,\omega^2 S_\alpha \ell + \omega^2 S_T + \frac{Q_{h\alpha}}{e^{i\omega t}}\right] = 0 \qquad \text{Eq. (A.93)}$$

$$\bar{\theta}\left[\frac{4}{\pi^2}\omega^2 S_\alpha \ell^2 + \omega^2 S_T \ell + \frac{Q_{\alpha\theta}}{e^{i\omega t}}\right] + \bar{h}\left[0.338{,}93\,\omega^2 S_\alpha \ell + \omega^2 S_T + \frac{Q_{\alpha h}}{e^{i\omega t}}\right] + \bar{\alpha}\left[(\omega^2-\omega_\alpha^2) I_\alpha \frac{\ell}{2} + \omega^2 I_T + \frac{Q_{\alpha\alpha}}{e^{i\omega t}}\right] = 0 \qquad \text{Eq. (A.94)}$$

Introducing equations (A.83) through (A.91) into equations (A.92) through (A.94), the equations of motion become, after proper non-dimensionalization and simplification,

$$K_{\theta\theta}\bar{\theta} + K_{\theta h}\left(\frac{\bar{h}}{\ell}\right) + K_{\theta\alpha}\left(\bar{\alpha}\frac{b}{\ell}\right) = 0 \qquad \text{Eq. (A.95)}$$

$$K_{h\theta}\bar{\theta} + K_{hh}\left(\frac{\bar{h}}{\ell}\right) + K_{h\alpha}\left(\bar{\alpha}\frac{b}{\ell}\right) = 0 \qquad \text{Eq. (A.96)}$$

$$K_{\alpha\theta}(\bar{\theta}) + K_{\alpha h}\left(\frac{\bar{h}}{\ell}\right) + K_{\alpha\alpha}\left(\bar{\alpha}\frac{b}{\ell}\right) = 0 \qquad \text{Eq. (A.97)}$$

where

$$K_{\theta\theta} = \frac{1}{3} + \frac{I_s}{m\ell^3} + \frac{M_T}{m\ell} - \frac{1}{3\bar{\mu}}(L_1 + iL_2) + \frac{1}{\bar{\mu}} \frac{V_T}{4b^2\ell} \qquad \text{Eq. (A.98)}$$

$$K_{\theta h} = 0.284,41 + \frac{M_T}{m\ell} - \frac{0.284,41}{\bar{\mu}}(L_1 + iL_2) + \frac{1}{\bar{\mu}} \frac{V_T}{4b^2\ell} \qquad \text{Eq. (A.99)}$$

$$K_{\theta\alpha} = \frac{4}{\pi^2} \chi_\alpha + \overline{S_T} - \frac{4}{\pi^2\bar{\mu}}(L_3 + iL_4) + \frac{1}{\bar{\mu}} \frac{V_T}{4b^2\ell}\left(\frac{n_T}{b} - \frac{i}{k}\right) \qquad \text{Eq. (A.100)}$$

$$K_{h\theta} = 0.284,41 + \frac{M_T}{m\ell} - \frac{0.284,41}{\bar{\mu}}(L_1 + iL_2) + \frac{1}{\bar{\mu}} \frac{V_T}{4b^2\ell} \qquad \text{Eq. (A.101)}$$

$$K_{hh} = \frac{1}{4}\left[1 - \left(\frac{\omega_h}{\omega_\alpha}\right)^2 Z\right] - \frac{1}{4\bar{\mu}}(L_1 + iL_2) + \frac{M_T}{m\ell} + \frac{1}{\bar{\mu}} \frac{V_T}{4b^2\ell} \qquad \text{Eq. (A.102)}$$

$$K_{h\alpha} = 0.338,93\, \chi_\alpha + \overline{S_T} - \frac{0.338,93}{\bar{\mu}}(L_3 + iL_4) + \frac{1}{\bar{\mu}} \frac{V_T}{4b^2\ell}\left(\frac{n_T}{b} - \frac{i}{k}\right) \qquad \text{Eq. (A.103)}$$

$$K_{\alpha\theta} = \frac{4}{\pi^2}\chi_\alpha + \overline{S_T} - \frac{4}{\pi^2\bar{\mu}}(M_1 + iM_2) + \frac{1}{\bar{\mu}}\frac{\overline{V_T}}{4b^2\ell}\left(\frac{n_T}{b} + \frac{i}{k}\right) \qquad \text{Eq. (A.104)}$$

$$K_{\alpha h} = 0.338,93\,\chi_\alpha + \overline{S_T} - \frac{0.338,93}{\bar{\mu}}(M_1 + iM_2) + \frac{1}{\bar{\mu}}\frac{\overline{V_T}}{4b^2\ell}\left(\frac{n_T}{b} + \frac{i}{k}\right) \qquad \text{Eq. (A.105)}$$

$$K_{\alpha\alpha} = \frac{1}{2}(1 - z)r_\alpha^2 + \frac{I_T}{mb^2\ell} - \frac{1}{2\bar{\mu}}(M_3 + iM_4) + \frac{1}{\bar{\mu}}\frac{\overline{V_T}}{4b^2\ell}\left[\left(\frac{n_T}{b}\right)^2 + \frac{1}{k^2}\right] + \frac{1}{\bar{\mu}}\frac{I_1}{4b^2\ell} \qquad \text{Eq. (A.106)}$$

where

$$\overline{S_T} \equiv \frac{S_T}{mb\ell} \qquad \text{Eq. (A.107)}$$

$$\overline{Z} \equiv \left(\frac{\omega_\alpha}{\omega}\right)^2 \qquad \text{Eq. (A.108)}$$

It should be remembered that the problem has been formulated so that the frequencies, ω_h and ω_α, are those of the bare wing without the tip tank. Structural damping can be introduced by merely replacing the frequency ratio, $\overline{Z}$, by (Ref. 31, p. 196)

$$\Omega_h = \left(\frac{\omega_\alpha}{\omega}\right)^2 (1 + i g_h) \qquad \text{for } K_{hh} \qquad \text{Eq. (A.109)}$$

$$\Omega_\alpha = \left(\frac{\omega_\alpha}{\omega}\right)^2 (1 + i g_\alpha) \qquad \text{for } K_{\alpha\alpha} \qquad \text{Eq. (A.110)}$$

For the cantilever condition, $\bar{\theta} = 0$, and the equations of motion degenerate to

$$K_{hh}\left(\frac{\bar{h}}{\ell}\right) + K_{h\alpha}\left(\bar{\alpha}\,\frac{b}{\ell}\right) = 0 \qquad \text{Eq. (A.111)}$$

$$K_{\alpha h}\left(\frac{\bar{h}}{\ell}\right) + K_{\alpha\alpha}\left(\bar{\alpha}\,\frac{b}{\ell}\right) = 0 \qquad \text{Eq. (A.112)}$$

A.3 Piston Theory

It has been shown in Reference 33 that the application of Piston Theory (Ref. 34) to the flutter analysis of a typical section results in great simplifications. The technique is applied here to the straight tapered wing of this report.

Using the first bending and the first torsion modes, the flutter determinant from Appendix A.1 is

$$\begin{vmatrix} \underline{A} & \underline{B} \\ \underline{D} & \underline{E} \end{vmatrix} = 0 \qquad \text{Eq. (A.113)}$$

where

$$\underline{A} = \frac{29}{420}\bar{\mu}\left[1-\left(\frac{\omega_h}{\omega_\alpha}\right)^2 \bar{z}\right] - I_1 \qquad \text{Eq. (A.114)}$$

$$\underline{B} = \frac{2}{35}\bar{\mu}\,\chi_\alpha - I_2 \qquad \text{Eq. (A.115)}$$

$$\underline{D} = \frac{2}{35}\bar{\mu}\,\chi_\alpha - I_3 \qquad \text{Eq. (A.116)}$$

$$\underline{E} = \frac{33}{560}\bar{\mu}\,r_\alpha^2\,(1-\bar{z}) - I_4 \qquad \text{Eq. (A.117)}$$

and the aerodynamic terms are

$$I_1(M,k) = \int_0^1 (L_1 + iL_2)\left(1-\frac{\eta}{2}\right)^2 \eta^4\, d\eta \qquad \text{Eq. (A.118)}$$

$$I_2(M,k) = \int_0^1 (L_3 + iL_4)\left(1-\frac{\eta}{2}\right)^3 \eta^3\, d\eta \qquad \text{Eq. (A.119)}$$

$$I_3(M,k) = \int_0^1 (M_1 + iM_2)\left(1-\frac{\eta}{2}\right)^3 \eta^3\, d\eta \qquad \text{Eq. (A.120)}$$

$$I_4(M,k) = \int_0^1 (M_3 + i M_4)\left(1 - \frac{\eta}{2}\right)^4 \eta^2 \, d\eta \qquad \text{Eq. (A.121)}$$

If any one of the conditions,

$$M^2 >> 1 \qquad M^2 k >> 1 \qquad M^2 k^2 >> 1 \qquad \text{Eq. (A.122)}$$

holds, Piston Theory can be applied, and the aerodynamic terms are greatly simplified. From Reference 33 (p. 6), the aerodynamic coefficients for a symmetrical double-wedged airfoil at zero angle of attack are

$$L_1 + i L_2 = \frac{i}{Mk} F \qquad \text{Eq. (A.123)}$$

$$L_3 + i L_4 = \frac{1}{Mk^2} F + \frac{i}{Mk}\left[-G + F(1 - 2x_0)\right] \qquad \text{Eq. (A.124)}$$

$$M_1 + i M_2 = \frac{i}{Mk}\left[-G + F(1 - 2x_0)\right] \qquad \text{Eq. (A.125)}$$

$$M_3 + i M_4 = \frac{1}{Mk^2}\left[-G + F(1 - 2x_0)\right] + \frac{i}{Mk}\left[-2G(1 - 2x_0) + F\left(\frac{4}{3} - 4x_0 + 4x_0^2\right)\right] \qquad \text{Eq. (A.126)}$$

where

$$F = 1 + \frac{\gamma + 1}{4}(M\gamma)^2 \qquad \text{Eq. (A.127)}$$

$$G = \frac{\gamma+1}{4} M\tau \qquad \text{Eq. (A.128)}$$

x_o is the fraction of the chord that the elastic axis of the wing is behind the leading edge

τ is the thickness ratio of the airfoil

For a flat plate, equations (A.126) and (A.127) reduce to

$$F = 1$$

$$G = 0$$

For the straight-wing planform of this report (Fig. 1.1),

$$b = b_o\left(1 - \frac{\eta}{2}\right) \qquad \text{Eq. (A.129)}$$

so that

$$k = k_o\left(1 - \frac{\eta}{2}\right) \qquad \text{Eq. (A.130)}$$

and the integrals of equations (A.118) through (A.121) can be evaluated exactly,

$$I_1(M, k_o) = \frac{i}{M k_o} \qquad \text{Eq. (A.131)}$$

$$I_2(M, k_o) = \frac{1}{M k_o^2}\frac{3}{20}F + \frac{i}{M k_o}\frac{11}{120}\left[-G + F(1-2x_o)\right] \qquad \text{Eq. (A.132)}$$

$$I_3(M, k_o) = \frac{i}{M k_o}\frac{11}{120}\left[-G + F(1-2x_o)\right] \qquad \text{Eq. (A.133)}$$

$$I_4(M, k_o) = \frac{1}{Mk_o^2}\frac{2}{15}\left[-G + F(1-2\chi_o)\right] \qquad \text{Eq. (A.134)}$$

$$+ \frac{i}{Mk_o}\frac{7}{80}\left[F\left(\frac{4}{3} - 4\chi_o + 4\chi_o^2\right) - 2G(1-2\chi_o)\right]$$

For a given set of wing parameters and a given Mach number, all the elements of the flutter determinant (Eq. (A.113) are known as simple functions of the parameters, ν and k_o. Therefore, the flutter determinant can be solved directly for its eigenvalues ν and k_o.

APPENDIX B

AERODYNAMIC FORCES ON THE TIP TANK

Expressions for the lift and the moment on the tip tank for simple harmonic motion in supersonic flow can be obtained by applying the results of Reference 35. In order to be consistent with the notation of Reference 35, a separate set of symbols is defined for this appendix.

The basic assumptions of the analysis are:

(a) The medium is continuous.
(b) The flow is frictionless.
(c) There is no heat transfer.
(d) There are no shock waves of finite strength.
(e) There are no body forces acting on the fluid.
(f) The undistrubed medium is homogeneous.
(g) The effect of wing interference on the tip tank is neglected.
(h) $\delta << 1$

where

δ is the body fineness ratio.

(i) $k\delta << 1$

where

k is the reduced frequency, $\frac{\omega(2c)}{U}$
ω is the frequency of the body motion
$2c$ is the body length
U is the free-stream velocity

(j) $(M\delta)^2 \ln \delta << 1$

where

M is the free-stream Mach number.

(k) $(kM\delta)^2 \ln \delta \ll 1$

With these assumptions, it is shown in Reference 35 (Eq.35) that linearization of the equations of motion, which results in the wave equation, in the neighborhood of the body for the general transient case further reduces the equations of motion to

$$\phi_{z\bar{z}} = 0 \qquad \text{Eq. (B.1)}$$

where

ϕ is the velocity potential
z is the complex coordinate, $x + iy$ (see Figure B.1)
$\bar{z}$ is the complex conjugate to z.

Equation (B.1) is Laplace's equation in the x-y plane, and solutions are known since it governs the case of irrotational incompressible steady flow. Solutions to the wave equation, which is applicable at large distances from the body, are needed for the determination of the drag only and need not concern us here.

Since the unsteady supersonic flow at any instant of time is approximated by an incompressible steady-state flow, expressions for the complex potential function can be obtained by resorting to classical incompressible aerodynamic theory. For the case at hand, i.e., a body of revolution in unaccelerated forward flight but with transverse motion, the flow can be considered as made up of two parts, viz.,

(1) the radial flow due to the free stream, U, and the change in radius along the s-axis,

(2) the transverse flow due to the motion of the body.

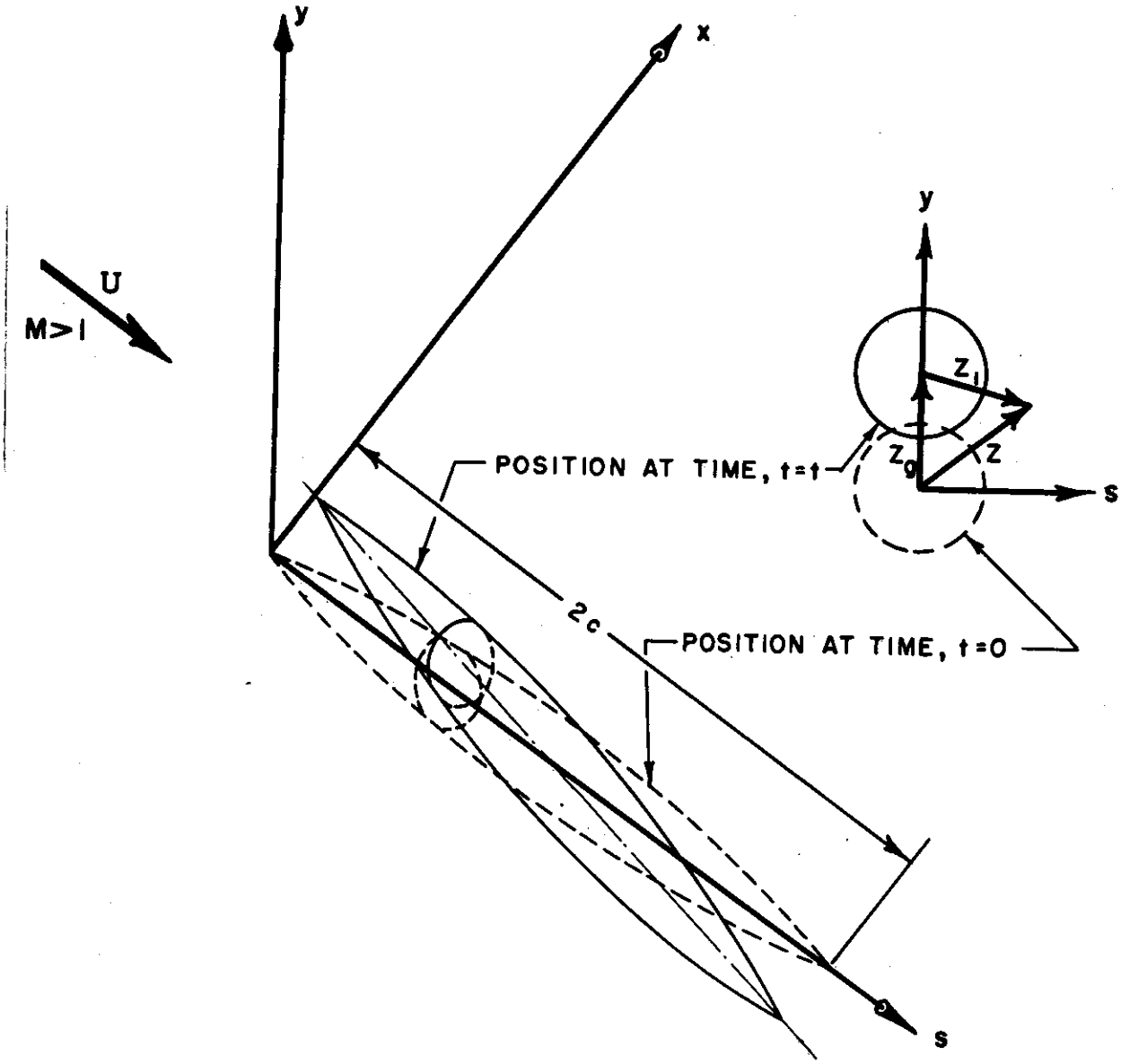

FIGURE B.1 AXIS SYSTEM FOR TIP-TANK AERODYNAMIC THEORY

The complex potential function for the radial flow can be obtained by considering a point source of such strength that the boundary conditions are satisfied on the surface of the cylinder (see Figure B.2). The complex potential function at

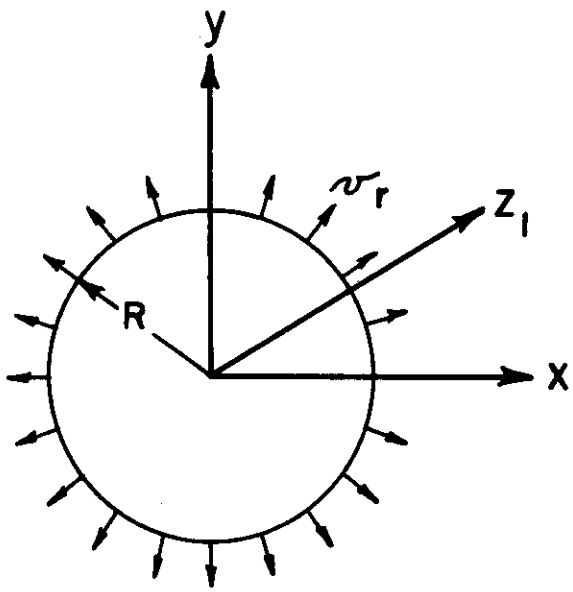

FIGURE B.2 RADIAL FLOW DUE TO A SOURCE

the point, z_1, for a point source at the origin of the z_1-vector is (Ref. 36, p. 212 ff and Ref. 37, p. 196 ff),

$$W = \frac{H}{2\pi} \ln z_1 \qquad \text{Eq. (B.2)}$$

where

W is the complex potential function, $\phi + i\psi$

ψ is the stream function

H is the volume of fluid spilled by the source in unit time.

The strength of the source, H, is determined by applying the boundary condition,

$$v_r = \frac{H}{2\pi R} = \frac{dR}{ds} U \qquad \text{Eq. (B.3)}$$

where

v_r is the radial velocity
R is the radius of the circular cross-section at station, s.

Therefore,

$$H = S' U \qquad \text{Eq. (B.4)}$$

where

S is the cross-sectional area of the body.

The prime denotes differentiation with respect to s. Hence,

$$W = \frac{S'}{2\pi} \ln z_1 \qquad \text{Eq. (B.5)}$$

since the velocity, U, is taken equal to one in Reference 35.

The complex potential function for the transverse flow due to the motion of the body can be found explicitly in Reference 37 (p. 246),

$$W = - \frac{R^2 \frac{D}{Dt}(z_g)}{z_1} \qquad \text{Eq. (B.6)}$$

where

$\frac{D}{Dt}(z_g)$ is the substantial derivative of z_g

Therefore, the solution to equation (B.1) for the case at hand is

$$W = \frac{S'(s)}{2\pi} \ln z_1 - \frac{S'(s)}{\pi} \frac{1}{z_1} \frac{D}{Dt}(z_g) \qquad \text{Eq. (B.7)}$$

which compares with equation 106 of Reference 35 except that it is for transverse motion in unaccelerated flight.

Reference 35 derives an explicit expression for the lift distribution associated with a more general complex potential (Eq. 40 of Ref. 35),

$$W(s,z,t) = a_0(s,t)\ln z + b_0(s,t) + \sum_{m=1}^{\infty} a_m(s,t)\, z^{-m} \qquad \text{Eq. (B.8)}$$

Here the term, $b_0(s,t)$, represents the solution which allows the inclusion of the radiation condition (zero disturbance at infinity), and for this analysis it need not be determined since it does not contribute to the lift.

In terms of the above series, the lift distribution may be written as (Eq. 92 of Ref. 35),

$$F_s(s,t) = q \frac{D}{Dt} \Gamma(s,t) \qquad \text{Eq. (B.9)}$$

where

F_s is the lateral force per unit length of the body
q is the dynamic pressure.

The circulation, Γ, is given by equation 99 of Reference 35,

$$\Gamma(s,t) = 4\pi a_1(s,t) + 2\frac{D}{Dt}\left[z_g(s,t)\, S(s) \right] \qquad \text{Eq. (B.10)}$$

It should be noted that the lift distribution depends only on the first term of the semi-infinite series of equation (B.8).

It now remains for us to express the complex potential for the case at hand, equation (B.7), in the form of equation (B.8). From Figure B.1,

$$z_1 = z - z_g \qquad \text{Eq. (B.11)}$$

so that

$$\ln z_1 = \ln(z - z_g) \qquad \text{Eq. (B.12)}$$

$$\frac{1}{z_1} = \frac{1}{z - z_g} \qquad \text{Eq. (B.13)}$$

Expansion of equations (B.12) and (B.13) yields,

$$\ln z_1 = \ln z - \frac{z_g}{z} - \frac{1}{2}\left(\frac{z_g}{z}\right)^2 + \cdots \qquad \text{Eq. (B.14)}$$

$$\frac{1}{z_1} = \frac{1}{z} + \frac{z_g}{z^2} + \cdots \qquad \text{Eq. (B.15)}$$

Comparison of equation (B.8) with equations (B.7), (B.14), and (B.15) shows that the coefficient of interest, a_1, must be,

$$a_1 = -\frac{S'(s)}{2\pi} - \frac{S(s)}{\pi}\frac{D}{Dt}(z_g) \qquad \text{Eq. (B.16)}$$

Inserting equations (B.16) and (B.10) into equation (B.9) and performing the indicated operations give,

$$\begin{aligned}\overline{F}_s(s) = 2q\Big[& S(s)k^2\bar{z}_g(s) - S(s)\bar{z}_g''(s) \\ & - ik\,S'(s)\bar{z}_g(s) - 2S(s)ik\,\bar{z}_g'(s) \\ & - S'(s)\bar{z}_g'(s)\Big]\end{aligned} \qquad \text{Eq. (B.17)}$$

Simple harmonic motion has been introduced by assuming

$$z_g = \bar{z}_g e^{ikt} \qquad \text{Eq. (B.18)}$$

$$F_s = \overline{F}_s e^{ikt} \qquad \text{Eq. (B.19)}$$

In the above presentation, the dimensionless parameters defined in Reference 35 have been used, i.e., all lengths are referred

to the body length, and all velocities are referred to the free-stream velocity. In dimensional form, equation (B.17) becomes

$$\bar{F}_s = 2\rho \left[S(s) \frac{\omega^2}{U^2} \bar{z}_g(s) - S(s) \bar{z}_g''(s) - \frac{i\omega}{U} S'(s) \bar{z}_g(s) \right. \qquad \text{Eq. (B.20)}$$
$$\left. - 2i \frac{\omega}{U} S(s) \bar{z}_g'(s) - S'(s) \bar{z}_g'(s) \right]$$

The motion of the body, z_g, can be expressed in terms of the assumed modes of vibration. For bending of, and torsion about the elastic axis of the wing,

$$h = \bar{h} f_h e^{i\omega t} \qquad \text{Eq. (B.21)}$$

$$\alpha = \bar{\alpha} f_\alpha e^{i\omega t} \qquad \text{Eq. (B.22)}$$

where

h is the vertical displacement of the wing elastic axis, positive down

α is the twist about the wing elastic axis, positive nose up.

The mode shapes, f_h and f_α, are normalized to be one at the wing tip. The frequency of oscillation in equations (B.21) and (B.22) is ω, not k as above, because the equations have been written in dimensional form. It should be noted that time, t, in equations (B.21) and (B.22) is dimensional, whereas time, t, in equations (B.18) and (B.19) is dimensionless. The motion of the centroid of the body in the complex plane is

$$\bar{z}_g = -i \left[\bar{h} + (s - s_{ea}) \bar{\alpha} \right] \qquad \text{Eq. (B.23)}$$

The subscript, e.a., refers to the elastic axis of the wing.

The amplitude of the lift is

$$\bar{L} = i \int_0^{2c} \bar{F}_s \, ds \qquad \text{Eq. (B.24)}$$

and the amplitude of the pitching moment about the center of the body is

$$\bar{M} = i \int_0^{2c} \bar{F}_s (s-c) \, ds \qquad \text{Eq. (B.25)}$$

When equations (B.20) and (B.23) are substituted into equations (B.24) and (B.25), certain integrals appear which are easily evaluated if one remembers that the body under consideration is symmetrical about s = c and that it is closed at both ends. The final expressions for the amplitudes of the total oscillatory lift and moment are

$$\bar{L} = \rho V_T \omega^2 \bar{h} + \rho V_T \omega^2 \left(n_T - i \frac{U}{\omega}\right) \bar{\alpha} \qquad \text{Eq. (B.26)}$$

$$\bar{M}_{e.a.} = n_T \bar{L} + i \rho U V_T \omega \bar{h} + \left(\rho \omega^2 I_1 + i \rho U V_T \omega n_T + \rho U^2 V_T\right) \bar{\alpha} \qquad \text{Eq. (B.27)}$$

where

ρ is the air density

V_T is the volume of the body

n_T is the distance that the geometrical center of the body lies aft of the elastic axis of the wing

I_1 is the volume moment of inertia in pitch of the body about its geometrical center,

The above results agree with those obtained by quasi-steady momentum theory for incompressible flow (Ref. 38, pp. 60, 61), as expected.

SYMBOLS FOR APPENDIX B

a_m	Coefficient in expansion of W, Eq. (B.8)
b_o	Coefficient in expansion of W, Eq. (B.8)
c	Half length of body
D/Dt	Substantial derivative,
f_h	Uncoupled bending mode of wing
f_α	Uncoupled torsion mode of wing
F_s	Lateral force per unit length of body
$\bar{F}_s$	Amplitude of F_s in simple harmonic motion
h	Vertical displacement of wing elastic axis, positive down
$\bar{h}$	Amplitude of wing bending mode at wing tip station
H	Strength of source, i.e., the volume of fluid spilled by the source in unit time
I_1	Volume moment of inertia in pitch of the body about its geometrical center
k	Reduced frequency,
$\bar{L}$	Amplitude of oscillatory lift, positive down
M	Free-stream Mach number

SYMBOLS FOR APPENDIX B (Contd.)

$\overline{M}$	Amplitude of oscillatory pitching moment about center of body, positive nose up
n_T	Distance the geometrical center of the tip tank lies aft of the elastic axis of the wing
q	Dynamic pressure,
R	Radius of body cross-section
s,x,y	Coordinates defined in Figure B.1
S	Cross-sectional area of body
t	Time
U	Free-stream velocity
v_r	Radial velocity
V_T	Volume of the body
W	Complex potential function, $\phi + i\psi$
z	Complex coordinate,
$\overline{z}$	Complex conjugate to z
z_g	Coordinate describing motion of centroid of area S
$\overline{z}_g$	Amplitude of z_g in simple harmonic motion

SYMBOLS FOR APPENDIX B (Contd.)

z_1	Complex coordinate referred to center of area (See Figure B.1)
α	Twist about wing elastic axis, positive nose up
$\overline{\alpha}$	Amplitude of wing torsion mode at wing tip station
Γ	Circulation
δ	Body fineness ratio, i.e., ratio of maximum cross-sectional length to body length
ρ	Air density
ϕ	Velocity potential
ψ	Stream function
ω	Frequency of the body motion

subscript e.a. Elastic axis of the wing

APPENDIX C

ARITHMETICAL EXAMPLES ILLUSTRATING USE OF THEORY

C.1 Bare Wing, Incompressible

Expressions for the elements of the three-dimensional flutter determinant in incompressible flow are given on page 65 of Reference 26. Thus, for the combined bending-torsion case, the flutter determinant is given by

$$\begin{vmatrix} \underline{A} & \underline{B} \\ \underline{D} & \underline{E} \end{vmatrix} = 0 \qquad \text{Eq. (C.1)}$$

The coefficients of the flutter determinant are the same as for the bare wing in supersonic flow, as given by equations (A.30), (A.31), (A.33) and (A.34), except that the aerodynamic coefficients are the incompressible coefficients tabulated in Reference 26, and μ is the incompressible wing mass ratio,

$$\mu = \frac{m}{\pi \rho b^2} \qquad \text{Eq. (C.2)}$$

The mass parameters are assumed to vary in the manner expressed by equations (A.23) through (A.28).

The eigenvalues of the two-degree-of-freedom system were chosen as $\bar{z}$ and $\left(\frac{\omega_h}{\omega_a}\right)^2$. Since the wing is tapered, the aerodynamic coefficients are functions of spanwise location, so that the aerodynamic integrals must be evaluated numerically for every value of k_o. Reference points for the numerical integrations were chosen as 0, 20, 40, 60 and 100% span. Simpson's Rule was used between 20% and 100% span since it requires an

odd number of stations, while the Trapezoidal Rule was used between 0% and 20% span. In evaluating the aerodynamic coefficients, L_h, L_α and M_α, for the specified spanwise stations, it was found that interpolation between tabulated values of reduced frequency, k, could be avoided by using the basic expressions given on page 29 of Reference 26 and by discriminately choosing the values of k_o. Convenient tables of Theordorsen's function can be found on page 342 of Reference 39.

For $k_o = 0.20$, the aerodynamic integrals are

$$\int_o^1 L_h \left(1-\frac{\eta}{2}\right)^2 \eta^4 d\eta = -0.139,46 - 0.943,94\, i \qquad \text{Eq. (C.3)}$$

$$\int_o^{1.0} \left[L_\alpha - L_h\left(\tfrac{1}{2}+a\right)\right]\left(1-\tfrac{\eta}{2}\right)^3 \eta^3 d\eta =$$

$$-6.139,56 + 0.438,36\, i \qquad \text{Eq. (C.4)}$$

$$\int_o^{1.0} \left[M_h - L_h\left(\tfrac{1}{2}+a\right)\right]\left(1-\tfrac{\eta}{2}\right)^3 \eta^3 d\eta =$$

$$0.070,56 + 0.313,14\, i \qquad \text{Eq. (C.5)}$$

$$\int_o^{1.0} \left[M_\alpha - M_h\left(\tfrac{1}{2}+a\right) - L_\alpha\left(\tfrac{1}{2}+a\right) + L_h\left(\tfrac{1}{2}+a\right)^2\right]\left(1-\tfrac{\eta}{2}\right)^4 \eta^2 d\eta =$$

$$2.105,37 - 0.577,17\, i \qquad \text{Eq. (C.6)}$$

Using the parameters,

$$\begin{aligned} \mu &= 65 \\ x_\alpha &= 0.114 \\ a &= -0.114 \\ r_\alpha^2 &= 0.237,40 \\ g_h &= g_\alpha = 0, \end{aligned} \qquad \text{Eq. (C.7)}$$

the flutter determinant can be expanded, and the real and imaginary parts can be set equal to zero, giving

$$4.057,38\left(\frac{\omega_h}{\omega_\alpha}\right)^2 Z^2 - 13.479,00\left(\frac{\omega_h}{\omega_\alpha}\right)^2 Z - 3.930,93\,Z + 15.468,65 = 0 \qquad \text{Eq. (C.8)}$$

$$2.582,85\left(\frac{\omega_h}{\omega_\alpha}\right)^2 Z + 0.855,84\,Z - 3.771,20 = 0 \qquad \text{Eq. (C.9)}$$

From the definition of Z,

$$\frac{v_f}{b_o\,\omega_\alpha} = \frac{1}{k_o\sqrt{Z}} \qquad \text{Eq. (C.10)}$$

Therefore, the following table can be calculated for the real solutions of equations (C.8) and (C.9).

Z	$\left(\frac{\omega_h}{\omega_\alpha}\right)^2$	$\frac{1}{k_o}$	$\frac{v_f}{b_o\,\omega_\alpha}$
4.026,63	0.031,25	5	2.492
0.778,04	1.545,28	5	5.669

Repeating the steps for different values of k_o results in the curves shown in Figure 3.7.

C.2 Bare Wing, Supersonic

The flutter determinant for the bare wing in supersonic flow is given by equation (A.45). The parameters, Z and $\left(\frac{\omega_h}{\omega_\alpha}\right)^2$ were again chosen as eigenvalues. The method of solution is the same as for the bare wing in incompressible flow except that a value of Mach number as well as frequency must be chosen. For high values of frequency, the aerodynamic coefficients, L_1, L_2, L_3, L_4, M_1, M_2, M_3, and M_4 were obtained from Reference 7 and linear interpolation was used. For low values of frequency, it

was found that linear or three-point interpolation between the tabulated values of the reduced-frequency parameter, $\bar{\omega}$ could not be used to evaluate the aerodynamic coefficients with sufficient accuracy because they are highly non-linear in the low-$\bar{\omega}$ range. Also, it has been pointed out in Reference 40 that a few errors exist in the tables of Reference 7 associated with the smallest values of $\bar{\omega}$

Therefore, for low values of $\bar{\omega}$ ($\bar{\omega} \leq 1/2$, approximately) and for Mach numbers not tabulated in Reference 7 ($M = \frac{4}{3}$ for the bare wing, $M = \frac{3}{2}$ for the wing with tip tank), resort was made to the basic expressions for the aerodynamic coefficients given in Reference 7 and to the method of Reference 41 for evaluating the basic function, $f_\lambda (M, \bar{\omega})$. It should be noted that the method of Reference 41 allows the evaluation of the function, f_λ, directly without the need of recursion formulae and that the labor required for a given accuracy decreases with decreasing $\bar{\omega}$. More extensive tables of the aerodynamic coefficients than those of Reference 7, particularly for the argument of Mach number, are given in Reference 23. This reference became available after the computations for the prescribed Mach numbers were well underway. The same method of integrating the aerodynamic coefficients across the span as outlined above in Appendix C.1 was used.

For $M = \frac{10}{7}$, $\bar{\omega}_o = 0.72835$ and $x_o = 0.443$, the aerodynamic integrals are

$$\int_0^1 (L_1 + iL_2)\left(1 - \frac{\eta}{2}\right)^2 \eta^4 d\eta = 0.062,68 + 0.601,80\,i \qquad \text{Eq. (C.11}$$

$$\int_0^1 (L_3 + iL_4)\left(1 - \frac{\eta}{2}\right)^3 \eta^3 d\eta = 4.159,59 - 0.388,07\,i \qquad \text{Eq. (C.12)}$$

$$\int_0^1 (M_1 + i M_2)\left(1 - \frac{\eta}{2}\right)^3 \eta^3 d\eta = 0.022,62 + 0.047,85\, i \qquad \text{Eq. (C.13)}$$

$$\int_0^1 (M_3 + i M_4)\left(1 - \frac{\eta}{2}\right)^4 \eta^2 d\eta = 0.372,06 - 0.021,96\, i \qquad \text{Eq. (C.14)}$$

Noting that the wing mass ratio is now that for the supersonic case,

$$\bar{\mu} = \mu \frac{\pi}{4} \qquad \text{Eq. (C.15)}$$

for the same parameters given in equation (C.7), expanding the flutter determinant and setting the real and imaginary parts equal to zero give

$$\left(\frac{\omega_h}{\omega_\alpha}\right)^2 Z^2 - 0.477,51\left(\frac{\omega_h}{\omega_\alpha}\right)^2 Z - 0.982,17\, Z + 0.939,43 = 0 \qquad \text{Eq. (C.16)}$$

$$Z - 0.180,06\left(\frac{\omega_h}{\omega_\alpha}\right)^2 Z - 1.007,85 = 0 \qquad \text{Eq. (C.17)}$$

The real solutions of equations (C.16) and (C.17) are

Z	$\left(\frac{\omega_h}{\omega_\alpha}\right)^2$
1.031,19	0.129,64

From the definitions of Z and $\bar{\omega}_o$

$$\frac{1}{k_o} = 5.384, \quad \frac{v_f}{b_o \omega_\alpha} = 5.300.$$

Repeating the steps for different values of M and $\bar{\omega}_o$ results in the curves shown in Figure C.1 (h). The parameters used for the remaining curves of Figure C.1 were chosen so that the complete experimental range of the models tested was covered.

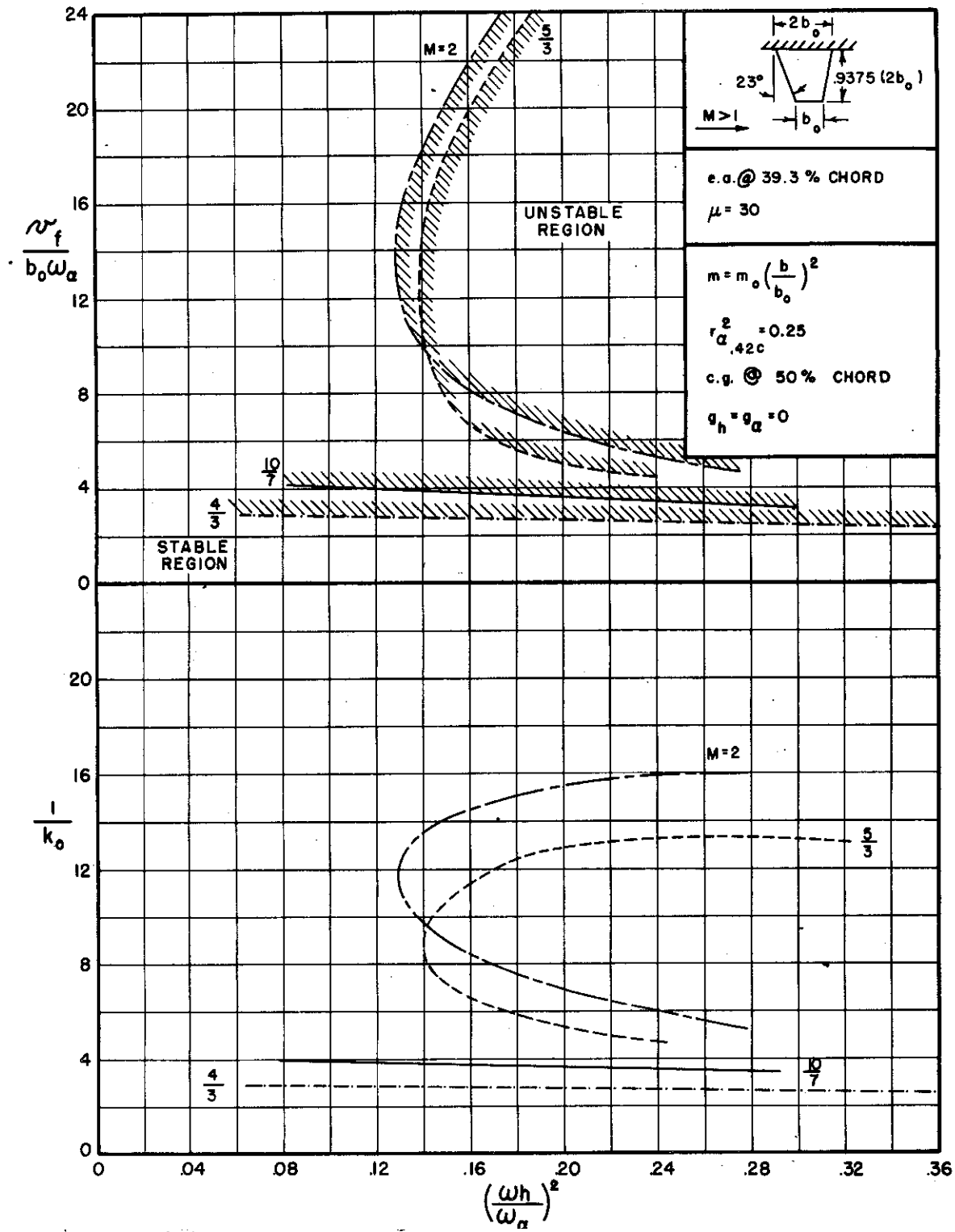

FIGURE C.1(a) FLUTTER COEFFICIENT AND REDUCED FREQUENCY VERSUS FREQUENCY RATIO FOR BARE STRAIGHT-WING PLANFORM, e.a. AT 39.3% CHORD, $\mu = 30$

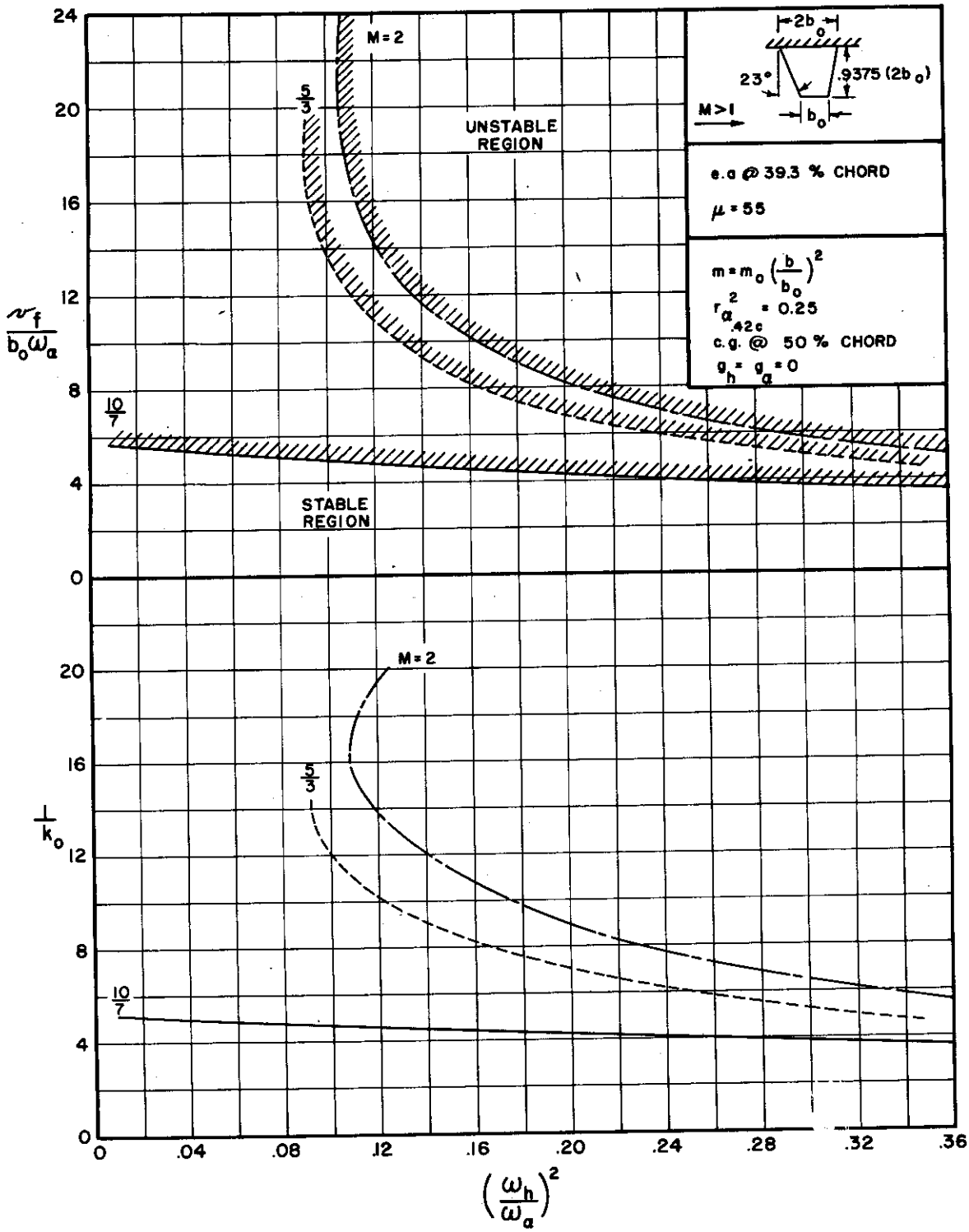

FIGURE C.1(b) FLUTTER COEFFICIENT AND REDUCED FREQUENCY VERSUS FREQUENCY RATIO FOR BARE STRAIGHT-WING PLANFORM, e.a. AT 39.3% CHORD, μ = 55

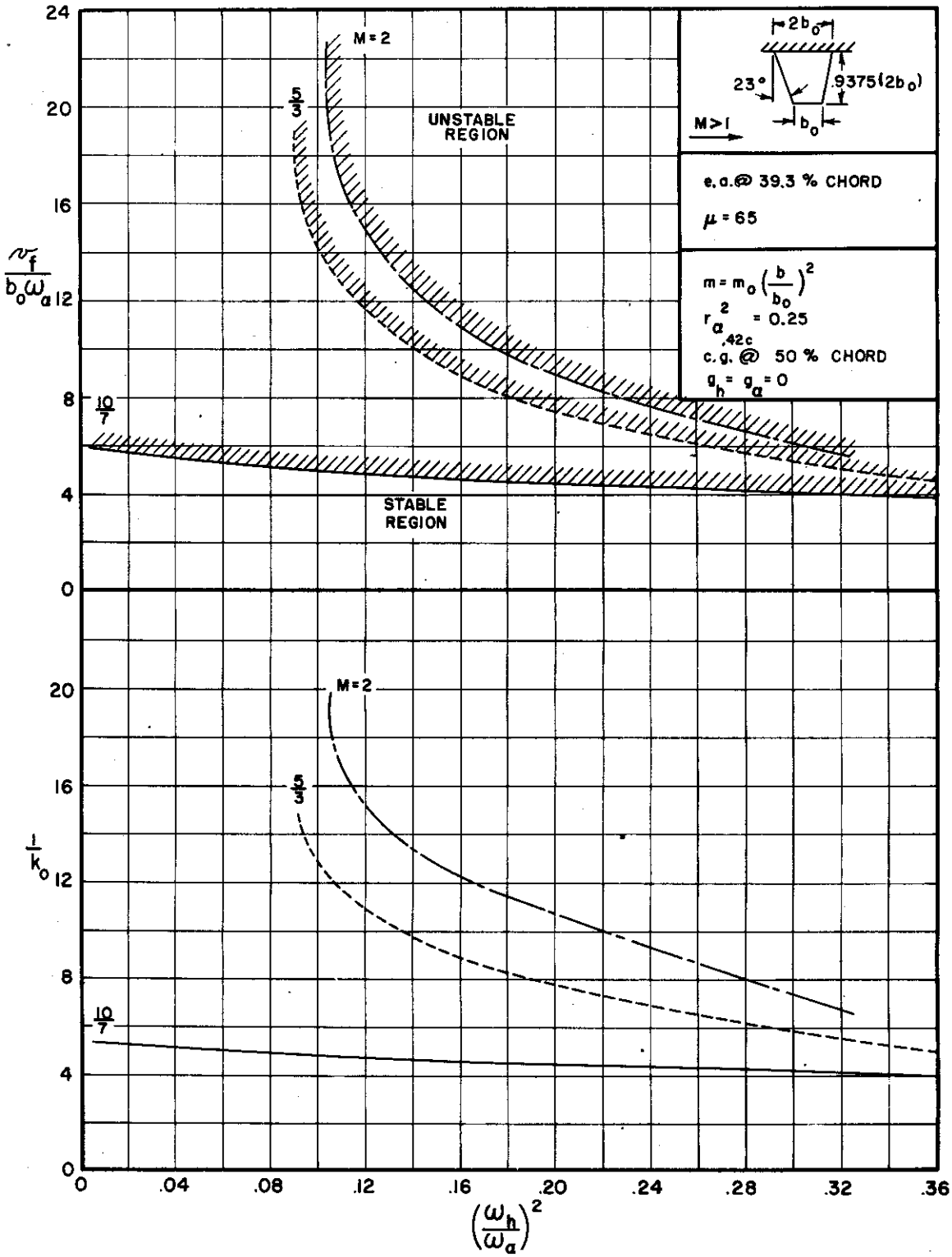

FIGURE C.1(c) FLUTTER COEFFICIENT AND REDUCED FREQUENCY VERSUS FREQUENCY RATIO FOR BARE STRAIGHT-WING PLANFORM, e.a. AT 39.3% CHORD, $\mu = 65$

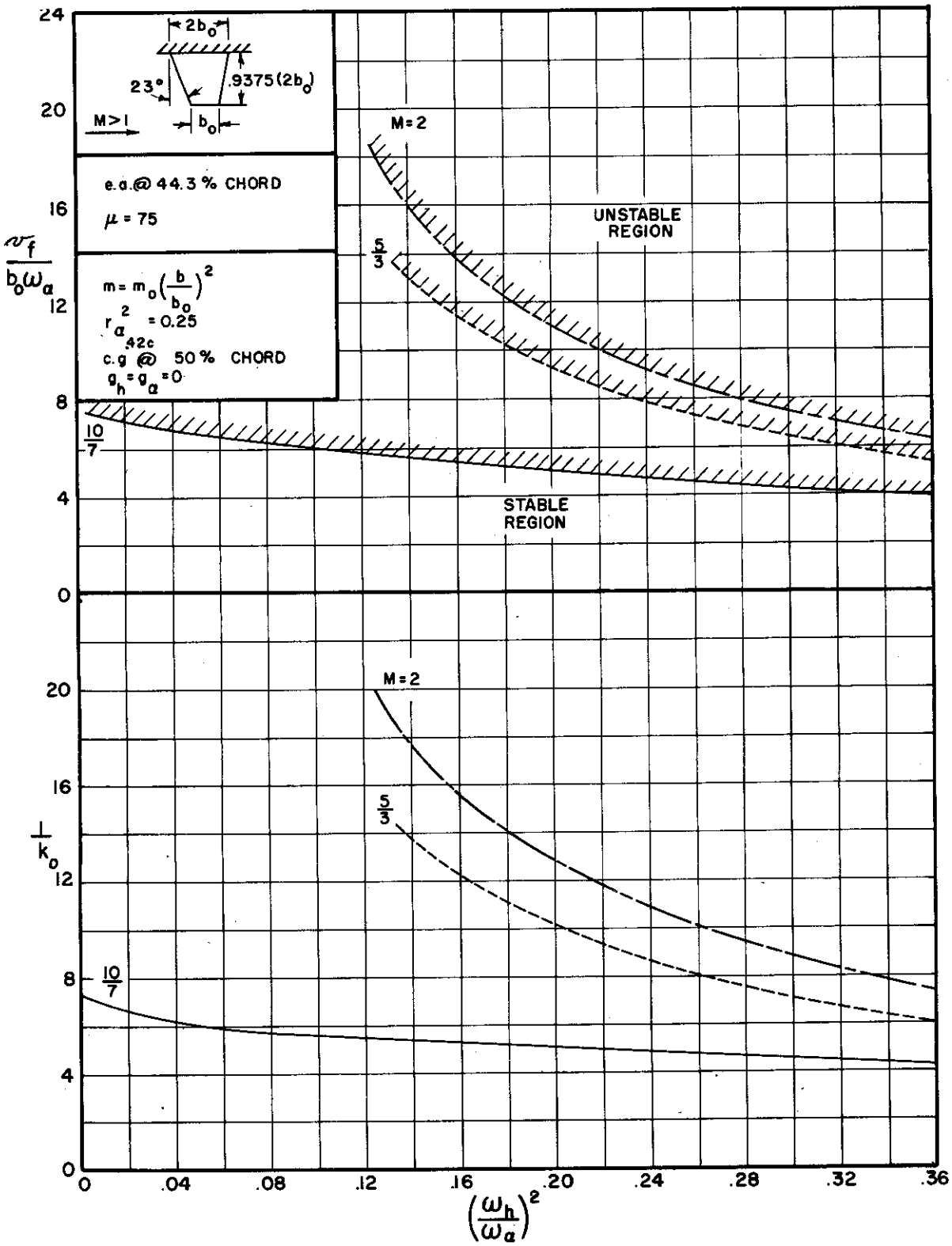

FIGURE C.1(d) FLUTTER COEFFICIENT AND REDUCED FREQUENCY VERSUS FREQUENCY RATIO FOR BARE STRAIGHT-WING PLANFORM, e.a. AT 39.3% CHORD, μ = 75

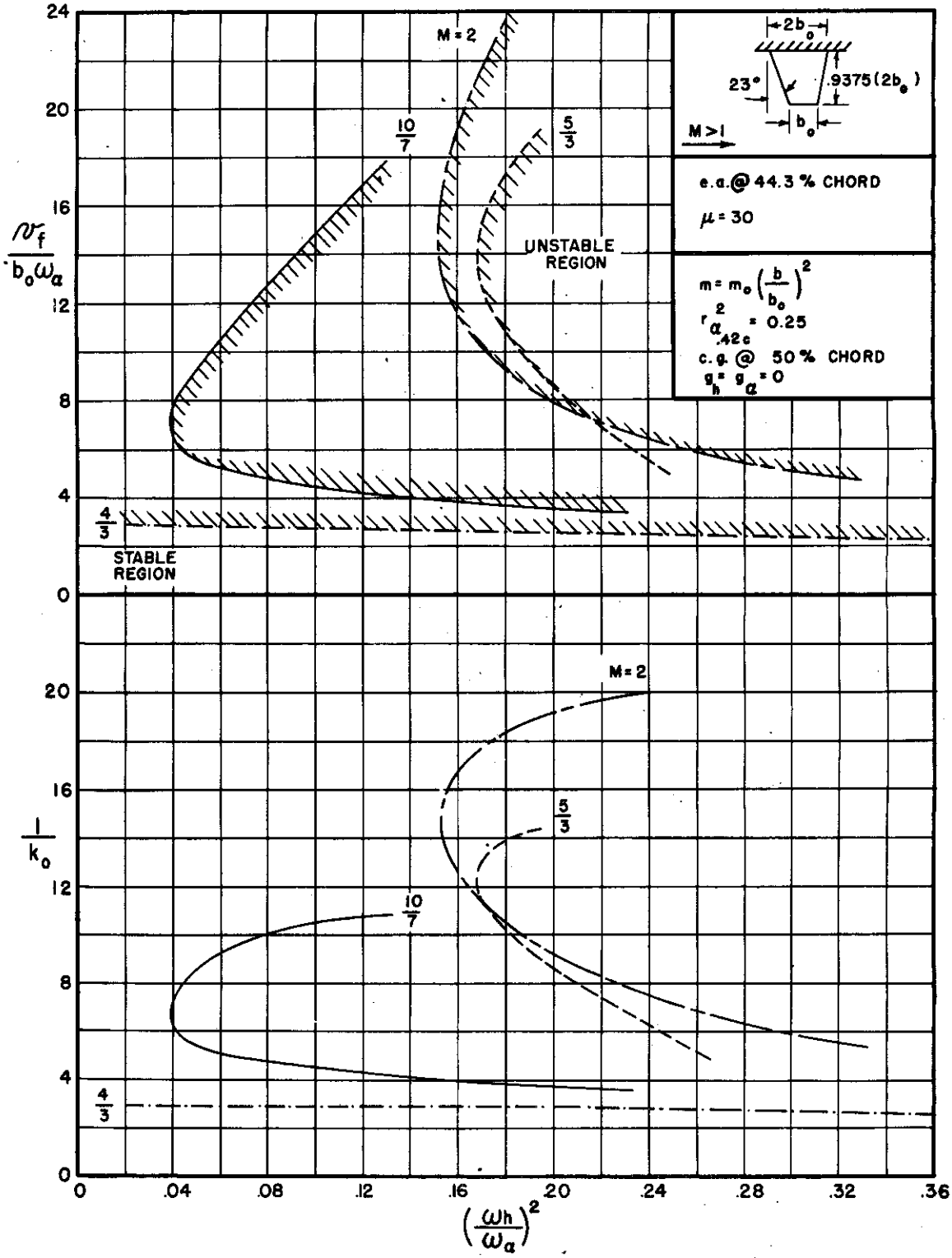

FIGURE C.1(e) FLUTTER COEFFICIENT AND REDUCED FREQUENCY VERSUS FREQUENCY RATIO FOR BARE STRAIGHT-WING PLANFORM, e.a. AT 44.3% CHORD, $\mu = 30$

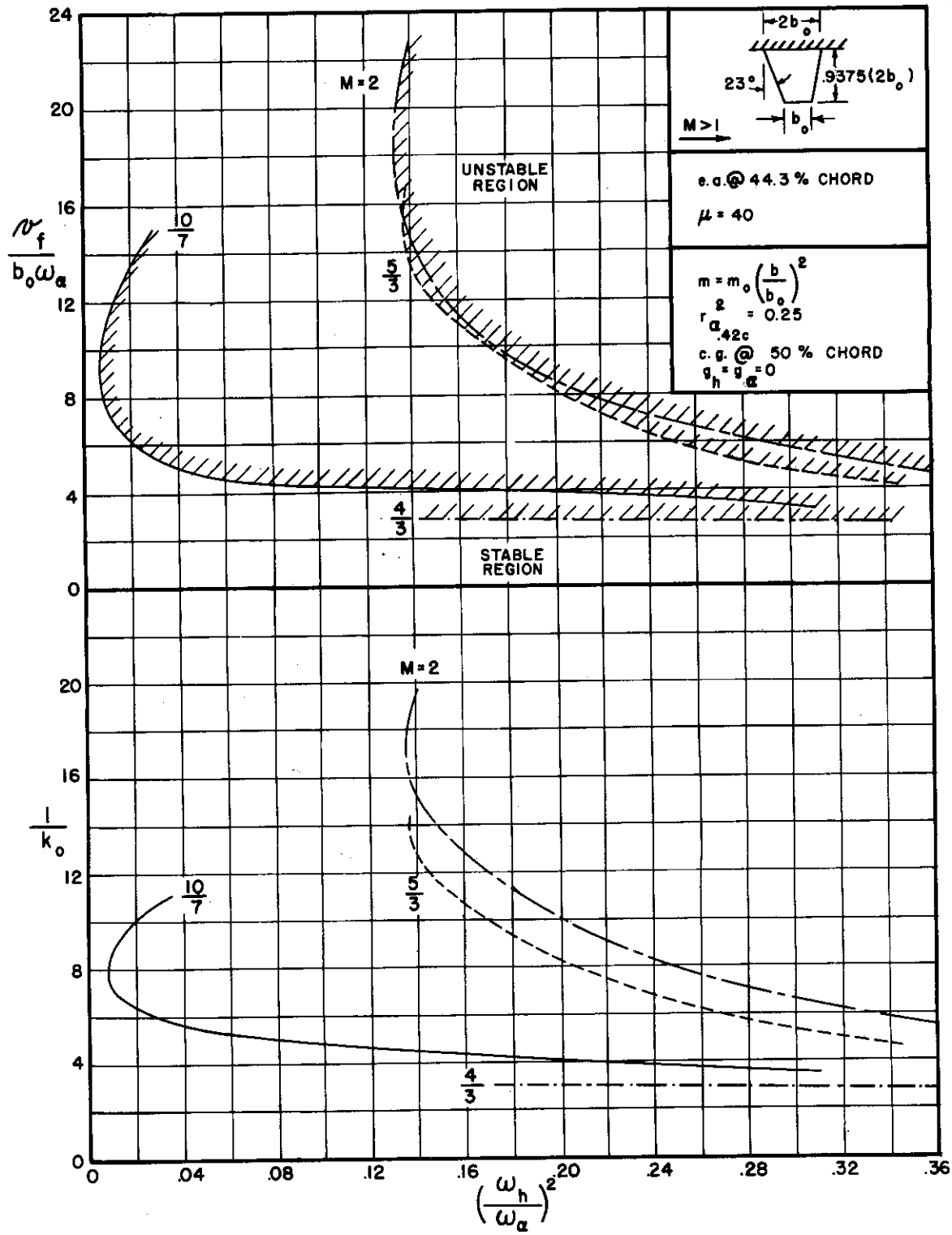

FIGURE C.1(f) FLUTTER COEFFICIENT AND REDUCED FREQUENCY VERSUS FREQUENCY RATIO FOR BARE STRAIGHT-WING PLANFORM, e.a. AT 44.3% CHORD, $\mu = 40$

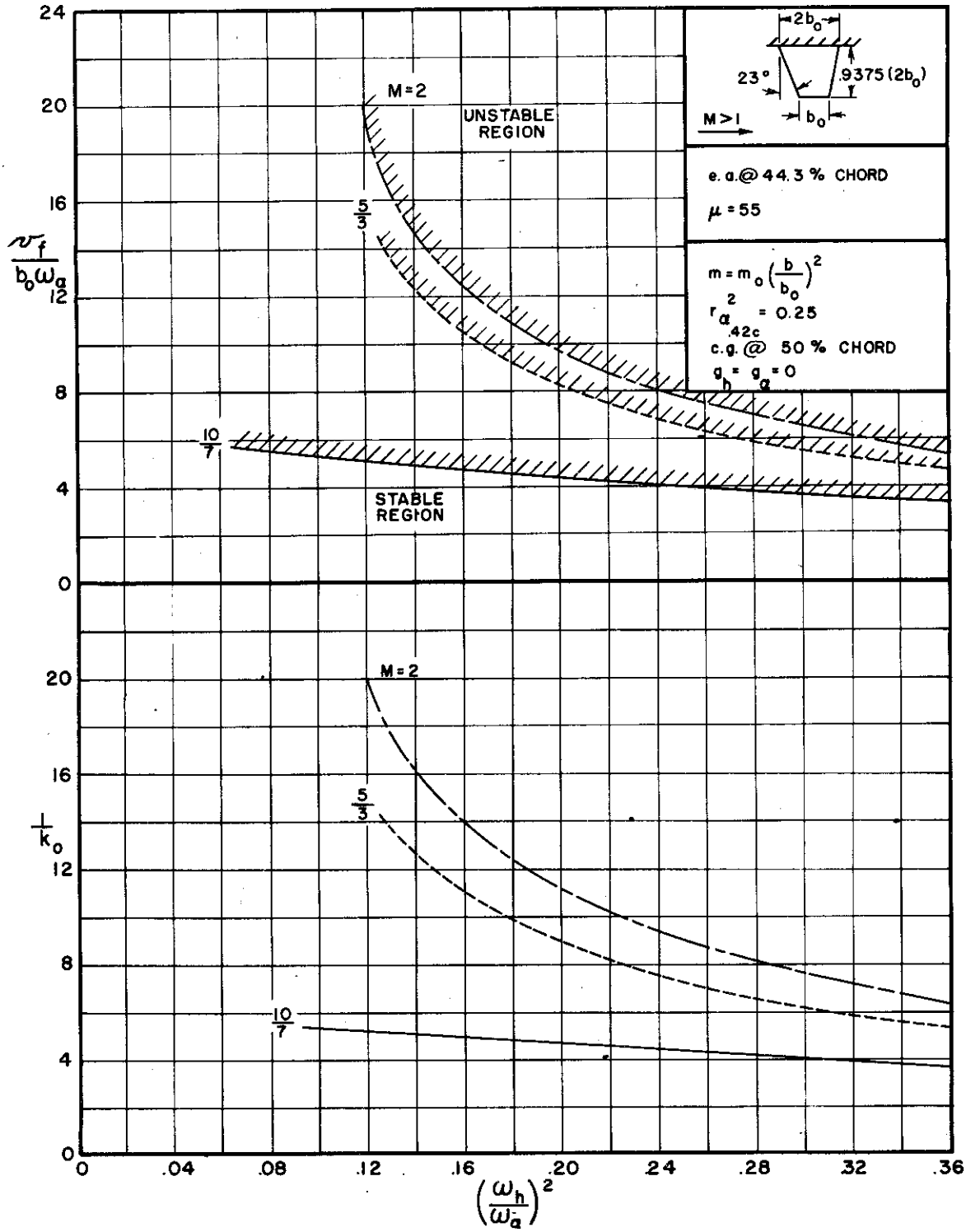

FIGURE C.1(g) FLUTTER COEFFICIENT AND REDUCED FREQUENCY VERSUS FREQUENCY RATIO FOR BARE STRAIGHT-WING PLANFORM, e.a. AT 44.3% CHORD, $\mu = 55$

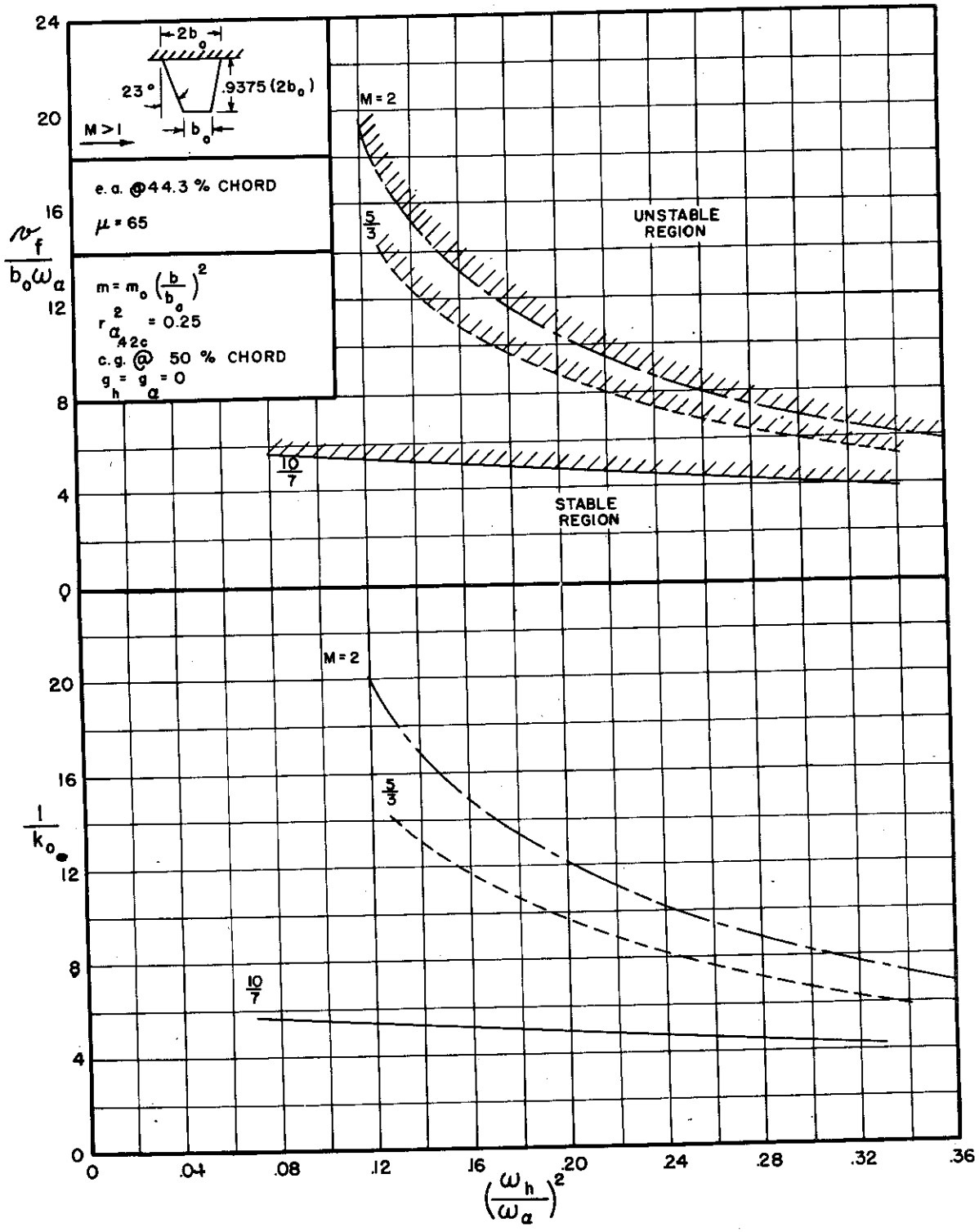

FIGURE C.1(h) FLUTTER COEFFICIENT AND REDUCED FREQUENCY VERSUS FREQUENCY RATIO FOR BARE STRAIGHT-WING PLANFORM, e.a. AT 44.3% CHORD, $\mu = 65$

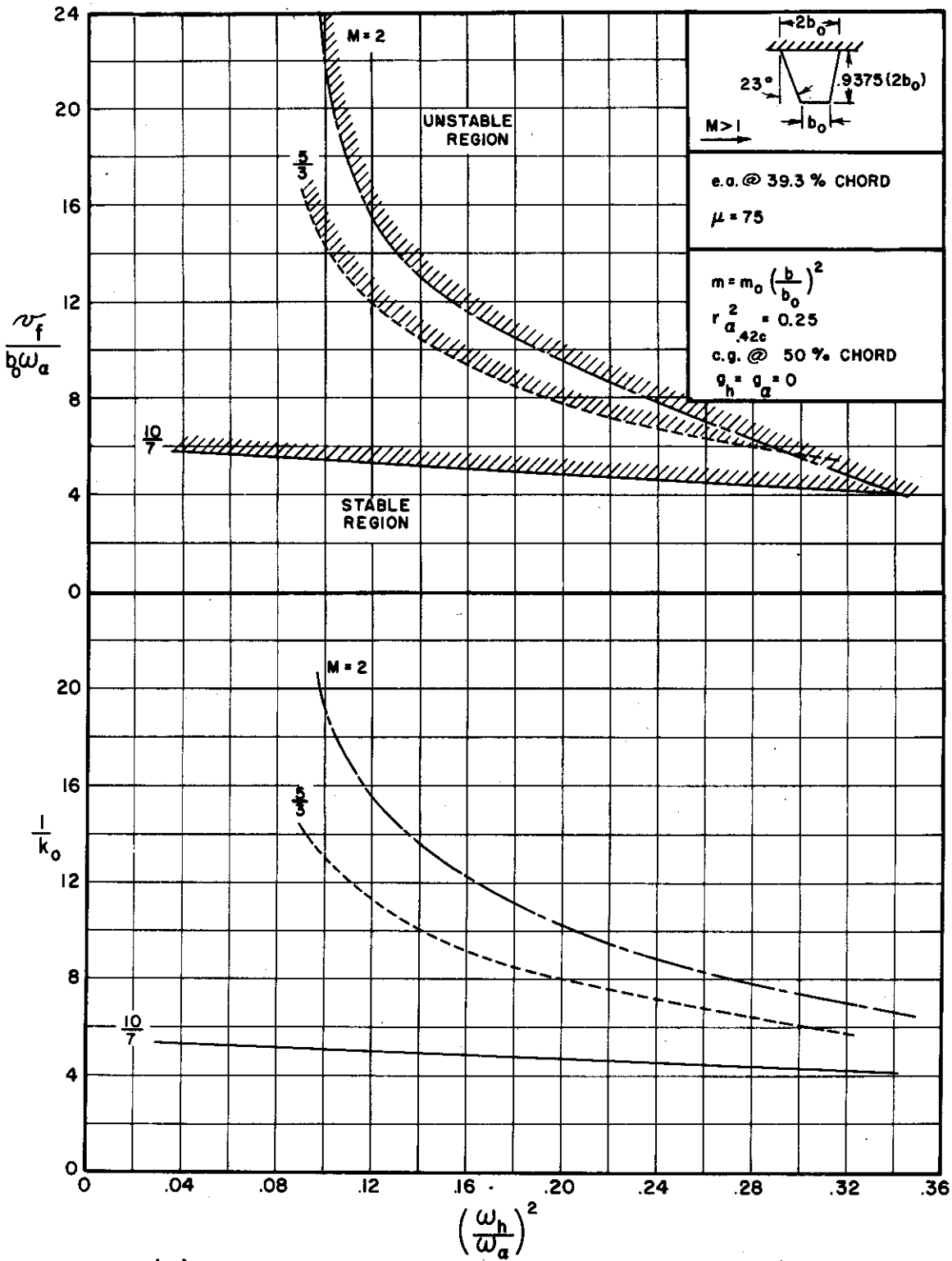

FIGURE C.1(i) FLUTTER COEFFICIENT AND REDUCED FREQUENCY VERSUS FREQUENCY RATIO FOR BARE STRAIGHT-WING PLANFORM, e.a. AT 44.3% CHORD, μ = 75

In all cases, not enough real solutions were obtained for Mach number $\frac{5}{4}$ to define the curves in the range of interest, so that $M = \frac{4}{3}$ was used when information below $M = \frac{10}{7}$ was considered necessary. The curves of Figure C.1 were then cross-plotted to obtain those of Figure 3.1.

It should be noted that the problem has been formulated completely on a dimensionless basis so that, in the computations, there is no need for using a curve of velocity versus Mach number for the wind tunnel or for the atmosphere (see Figure 3.2).

C.3 Wing with Aileron

The coefficients of the determinant for combined bending-torsion-aileron flutter are given by equations (A.30) through (A.38). In this case it was decided that the maximum amount of information for a given amount of effort could be obtained by choosing the frequency ratios, Z and $\left(\frac{\omega_3}{\omega_2}\right)^2$, as eigenvalues. The values of the integrals multiplying the mass parameters are given by equations (A.39) through (A.44). When the integration extended over the entire wing, the integrals containing aerodynamic coefficients were evaluated numerically for each value of the Mach number, M, and the reduced-frequency parameter, $\bar{\omega}$, as above for the bare wing. The integrals containing aerodynamic coefficients but with the integration extending only over the aileron were evaluated by assuming that $\bar{\omega}$ could be taken as a constant for a representative section of the wing. This representative section varied for each integral and was found by considering a weighted value of the integral. To illustrate,

$$\int_{0.5}^{1.0} (L_5 + iL_6)\left(1-\frac{\eta}{2}\right)^3 \eta^3 d\eta \cong (L_5 + iL_6)_{\bar{\eta}} \int_{0.5}^{1.0} \left(1-\frac{\eta}{2}\right)^3 \eta^3 d\eta^3 \qquad \text{Eq. (C.18)}$$

The complex coefficient, $(L_5 + i\, L_6)_{\bar{\eta}}$, was evaluated for the

value of $\bar{\omega}$ taken at station $\bar{\eta}$, where $\bar{\eta}$ was located at the centroid of the function,

$$\bar{\eta} = \frac{\int_{0.5}^{1.0} (1-\frac{\eta}{2})^3 \eta^3 \eta \, d\eta}{\int_{0.5}^{1.0} (1-\frac{\eta}{2})^3 \eta^3 \, d\eta} \qquad \text{Eq. (C.19)}$$

This method would give exact results if the aerodynamic coefficients varied linearly over the interval of integration.

For $M = \frac{10}{7}$, $\bar{\omega}_o = 0.849,76$ and $x_o = 0.443$, the aerodynamic integrals are,

$$\int_0^1 (L_1 + iL_2)(1-\tfrac{\eta}{2})^2 \eta^4 d\eta = 0.061,85 + 0.511,95\,i \qquad \text{Eq. (C.20)}$$

$$\int_0^1 (L_3 + iL_4)(1-\tfrac{\eta}{2})^3 \eta^3 d\eta = 3.031,34 - 0.325,92\,i \qquad \text{Eq. (C.21)}$$

$$\int_{0.5}^1 (L_5 + iL_6)(1-\tfrac{\eta}{2})^3 \eta^2 d\eta = 0.700,76 + 0.000,76\,i \qquad \text{Eq. (C.22)}$$

$$\int_0^1 (M_1 + iM_2)(1-\tfrac{\eta}{2})^3 \eta^3 d\eta = 0.022,07 + 0.038,82\,i \qquad \text{Eq. (C.23)}$$

$$\int_0^{1.0} (M_3 + iM_4)(1-\tfrac{\eta}{2})^4 \eta^2 d\eta = 0.257,90 - 0.013,80\,i \qquad \text{Eq. (C.24)}$$

$$\int_{0.5}^{1} (M_5 + i M_6)\left(1 - \frac{\eta}{2}\right)^4 \eta \, d\eta = 0.522,20 + 0.000,64i \qquad \text{Eq. (C.25)}$$

$$\int_{0.5}^{1} (N_1 + i N_2)\left(1 - \frac{\eta}{2}\right)^3 \eta^2 d\eta = 0.004,16 + 0.017,27i \qquad \text{Eq. (C.26)}$$

$$\int_{0.5}^{1} (N_3 + i N_4)\left(1 - \frac{\eta}{2}\right)^4 \eta \, d\eta = 0.104,33 - 0.009,87i \qquad \text{Eq. (C.27)}$$

$$\int_{0.5}^{1} (N_5 + i N_6)\left(1 - \frac{\eta}{2}\right)^4 d\eta = 0.159,26 + 0.000,25i \qquad \text{Eq. (C.28)}$$

Using the parameters,

wing plus aileron	aileron	
$\bar{\mu} = 65\left(\frac{\pi}{4}\right)$		
$x_\alpha = 0.114$	$x_\beta = 0.012$	
$a = -0.114$	$c = 0.60$	
$r_\alpha^2 = 0.237,40$	$r_\beta^2 = 0.003,24$	Eq. (C.29)
$\left(\frac{\omega_h}{\omega_\alpha}\right)^2 = 0.10$		
$g_h = g_\alpha = 0$	$g_\beta = 0$	

expanding the determinant and setting both the real and the imaginary parts equal to zero give

$$-0.003,43\left(\frac{\omega_\beta}{\omega_\alpha}\right)^2 Z^3 + 0.035,89\left(\frac{\omega_\beta}{\omega_\alpha}\right)^2 Z^2$$

$$-0.032,89\left(\frac{\omega_\beta}{\omega_\alpha}\right)^2 Z - 0.036,66\, Z^2 - 0.378,94\, Z - 0.398,41 = 0 \qquad \text{Eq. (C.30)}$$

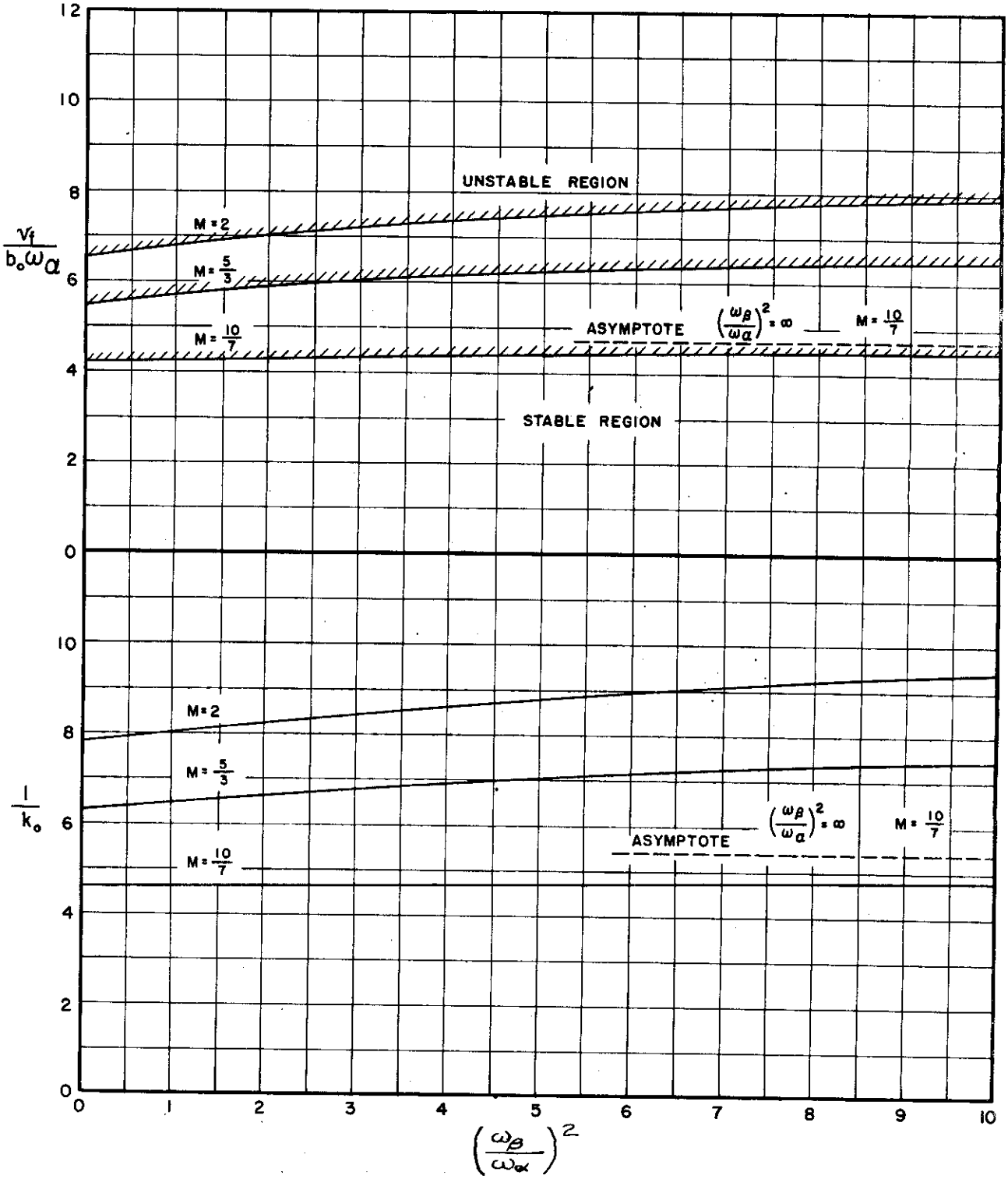

FIGURE C.2 FLUTTER COEFFICIENT AND REDUCED FREQUENCY VERSUS FREQUENCY RATIO FOR STRAIGHT WING WITH AILERON

$$0.049,18\left(\frac{\omega_\beta}{\omega_\alpha}\right)^2 Z^2 + 0.053,41\left(\frac{\omega_\beta}{\omega_\alpha}\right)^2 Z$$

$$-0.000,63\,Z^2 - 0.454,29\,Z + 0.534,83 = 0 \qquad \text{Eq. (C.31)}$$

Combining these two equations results in a quartic which can be solved by Graeffe's root-squaring process (Ref. 42, p. 484). Only the real positive solutions of equations (C.30) and (C.31) have any physical significance; they are

Z	$\left(\frac{\omega_\beta}{\omega_\alpha}\right)^2$
1.159	1.772

From the definitions of Z and $\overline{\omega_o}$,

$$\frac{1}{k_o} = 3.332, \qquad \frac{v_f}{b_o \omega_\alpha} = 3.095$$

By repeating this procedure for other values of M and $\overline{\omega_o}$, it is possible to obtain the curves shown in Figure C.2. The curves of Figure 3.12 were obtained by cross-plotting those of Figure C.2.

C.4 Wing with Tip Tank, Cantilever

The equations of motion for the cantilever wing with tip tank are given by equations (A.111) and (A.112). For simplification, the wing used for the theoretical calculations was assumed to have constant chord and constant mass properties in the formulation of the theory. The values for the chord and the mass properties were taken as representative of the seventy-percent-spanwise station of the actual planform (See Figure 1.1). The seventy-percent-spanwise station was chosen because experience has shown this location to be best for aerodynamic purposes. The tip-tank parameters were unchanged from the actual values so that

the ratio of the tip-tank mass to the total-wing mass was greater for the theoretical model than for the actual models. The fact that the theoretical bare wing is lighter and, as a consequence, would have higher vibratory frequencies, is partially rectified by having a greater proportion of the mass near the wing tip. The configuration of the theoretical model is given in Figure C.3.

It was decided that the most useful information could be obtained by leaving the static unbalance of the tip tank and the first torsional frequency of the bare wing as unknowns in the flutter equations. Thus, the parameters, $\bar{S}_T$ and Z, were taken as the two eigenvalues of the flutter determinant.

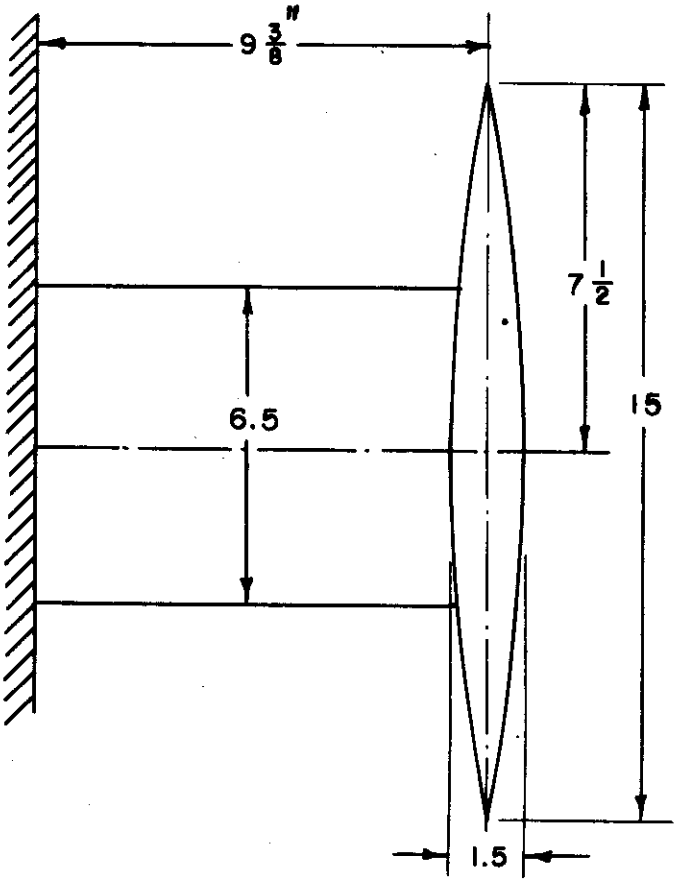

FIGURE C.3 TIP-TANK MODEL FOR CALCULATIONS

The parameters chosen for the analysis are

$m = 0.020,31$ slugs/ft $\quad V_T = 0.008,19$ ft^3

$\bar{\mu} = 65\left(\frac{\pi}{4}\right)$ $\quad M_T = 0.030,47$ slugs

$x_\alpha = 0.114$ $\quad I_1 = 0.000,46$ ft.^{5}

$r_\alpha^2 = 0.237,40$ $\quad I_T = 0.001,77$ slug-ft^2

$\left(\frac{\omega_h}{\omega_\alpha}\right)^2 = 0.10$ $\quad \frac{n_T}{b} = 0.114$

Eq. (C.32)

With these parameters, the coefficients of the flutter determinant become

$$K_{hh} = 2.170,72 - 0.025,00\bar{z} - 0.004,91(L_1 + iL_2) \qquad \text{Eq. (C.33)}$$

$$K_{h\alpha} = 0.038,72 + \bar{S}_T - 0.006,66(L_3 + iL_4) - 0.000,70\frac{i}{k} \qquad \text{Eq. (C.34)}$$

$$K_{\alpha h} = 0.038,72 + \bar{S}_T - 0.006,66(M_1 + iM_2) + 0.000,70\frac{i}{k} \qquad \text{Eq. (C.35)}$$

$$K_{\alpha\alpha} = 1.641,99 - 0.118,70\bar{z} - 0.009,82(M_3 + iM_4) + \frac{0.000,70}{k^2} \qquad \text{Eq. (C.36)}$$

For $M = \frac{10}{7}$, $\bar{\omega} = 0.34$ and $x_o = 0.443$, the aerodynamic coefficients are

$$L_1 + iL_2 = 0.921,57 + 11.147,60i \qquad \text{Eq. (C.37)}$$

$$L_3 + iL_4 = 128.379,49 - 9.279,93i \qquad \text{Eq. (C.38)}$$

$$M_1 + iM_2 = 0.406,87 + 1.192,13i \qquad \text{Eq. (C.39)}$$

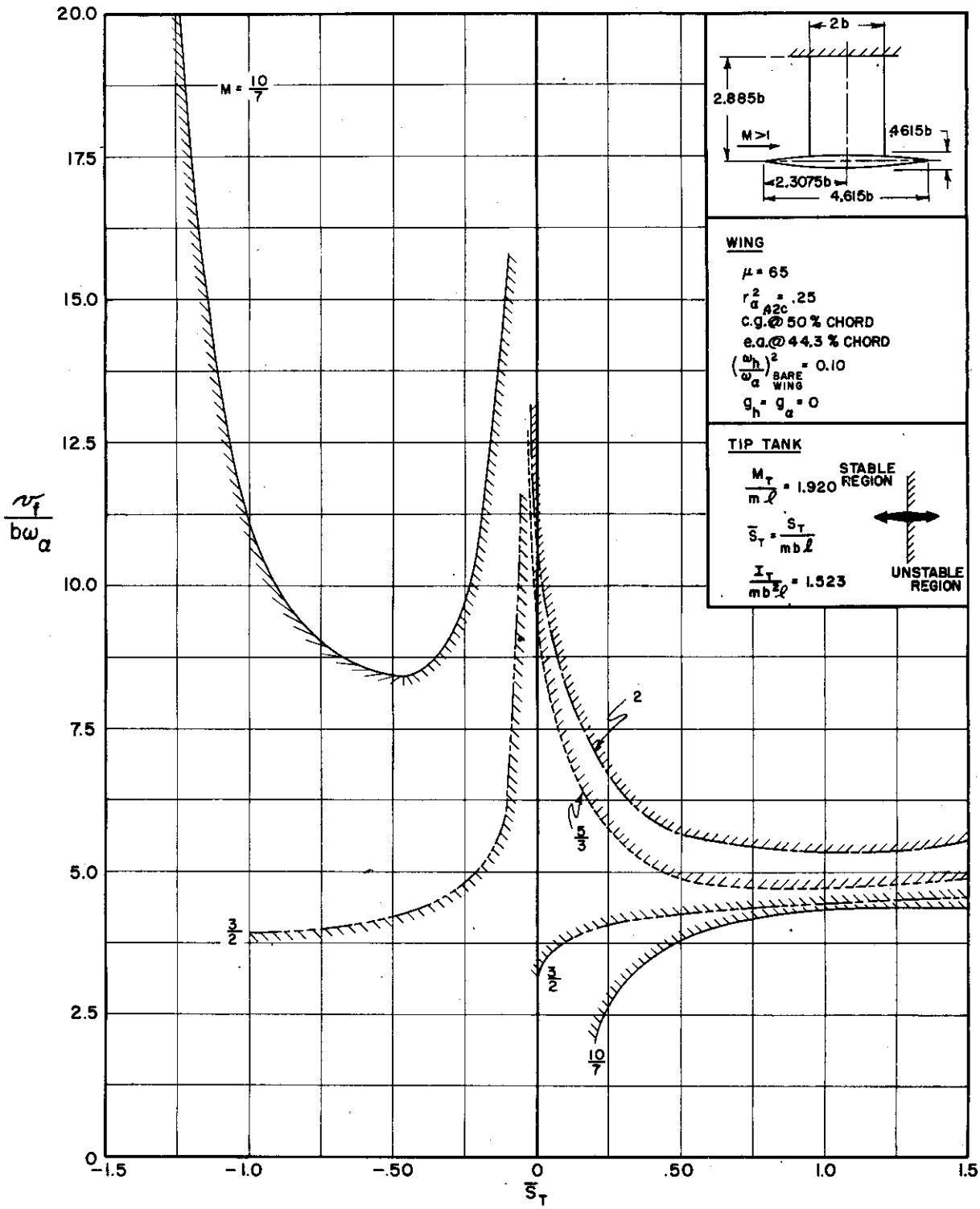

FIGURE C.4(a) FLUTTER COEFFICIENT VERSUS TIP-TANK STATIC-UNBALANCE PARAMETER FOR STRAIGHT-WING PLANFORM, NO STRUCTURAL DAMPING

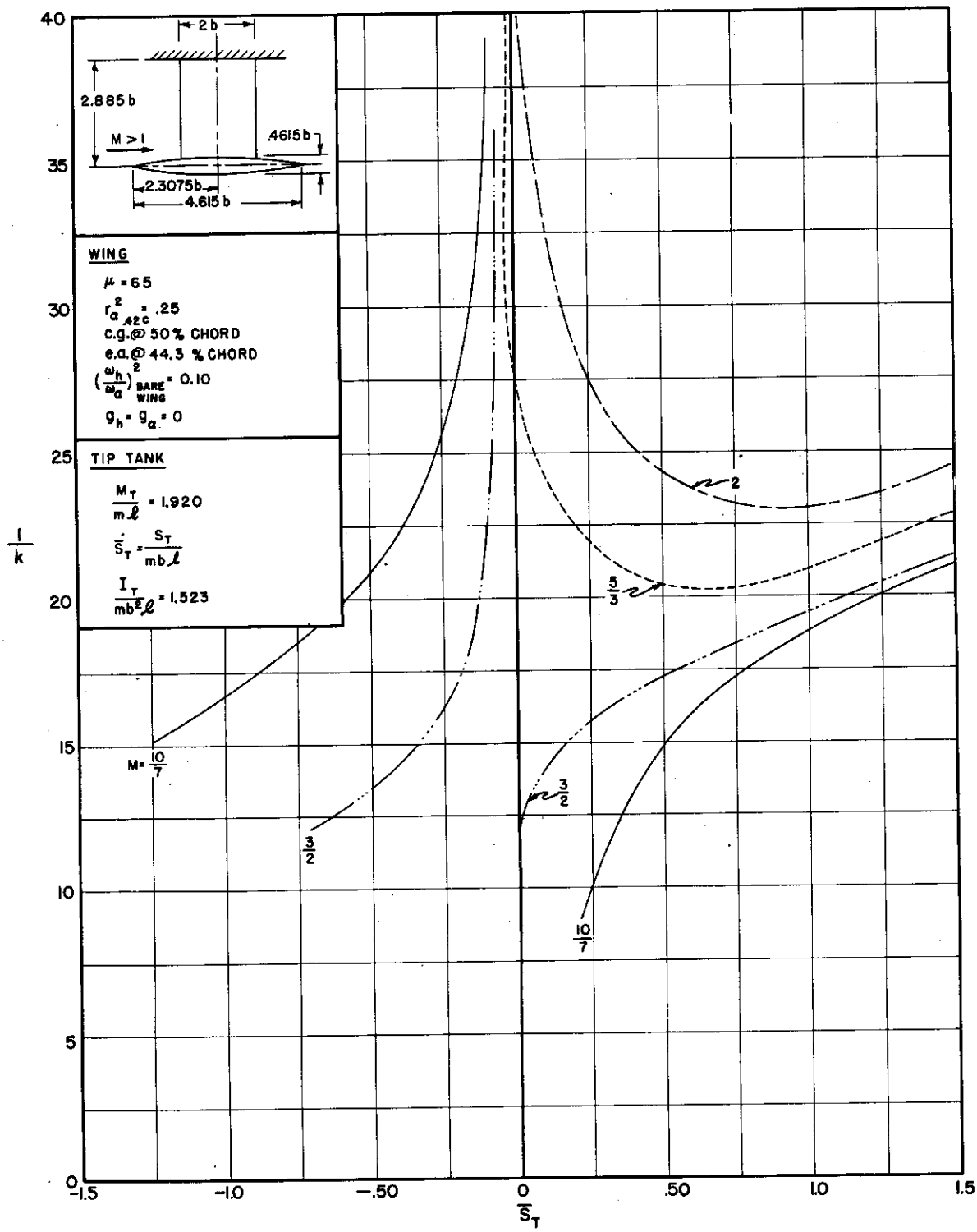

FIGURE C.4(b) REDUCED FREQUENCY VERSUS TIP-TANK STATIC-UNBALANCE PARAMETER FOR STRAIGHT-WING PLANFORM, NO STRUCTURAL DAMPING

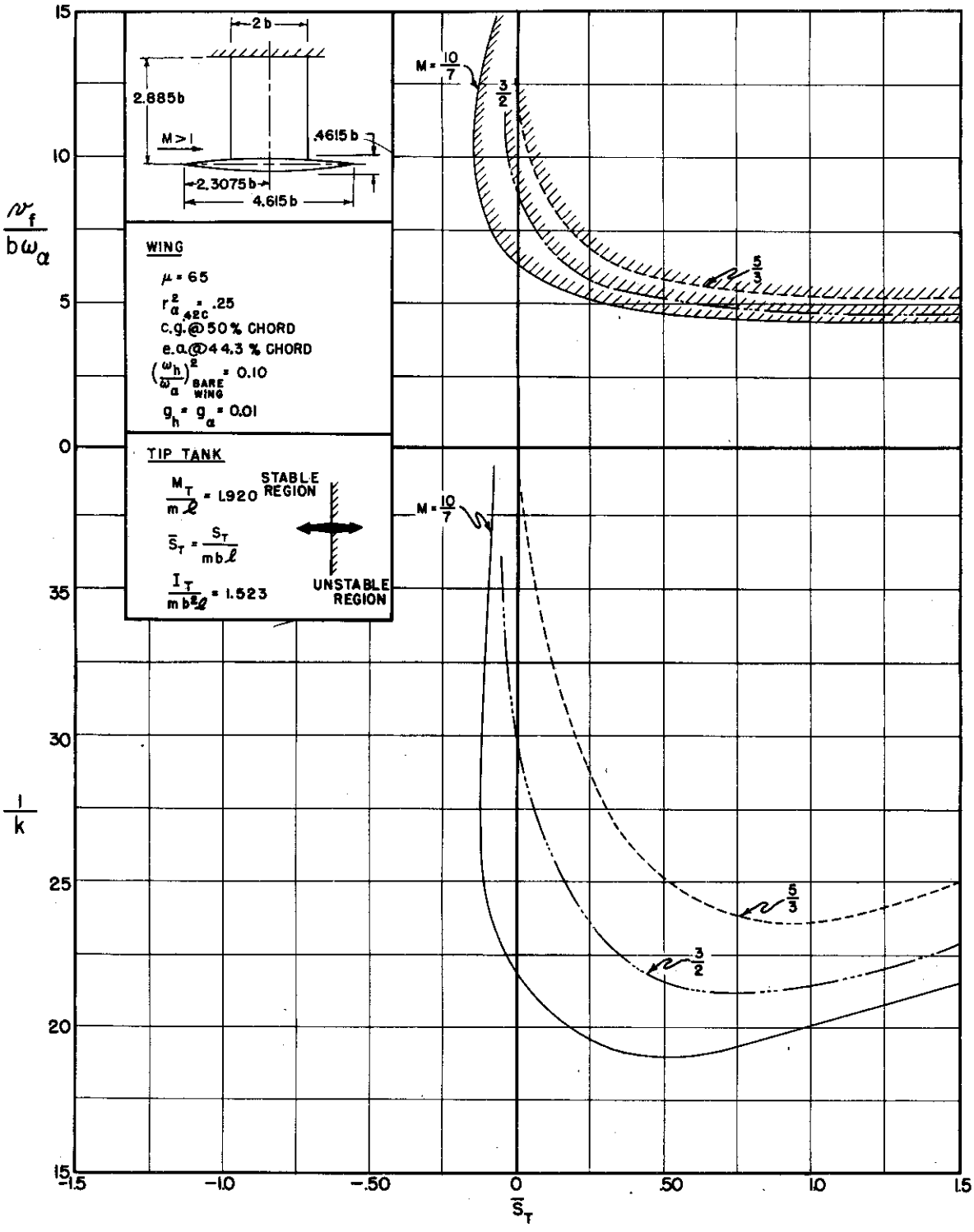

FIGURE C.5 FLUTTER COEFFICIENT AND REDUCED FREQUENCY VERSUS TIP-TANK STATIC-UNBALANCE PARAMETER FOR STRAIGHT-WING PLANFORM, STRUCTURAL DAMPING INCLUDED

$$M_3 + i\,M_4 = 13.769,86 - 0.748,82\,i \qquad \text{Eq. (C.40)}$$

Expanding the determinant and setting the real and imaginary parts equal to zero give

$$0.002,97\,Z^2 - 0.297,12\,Z + 0.780,12\,\bar{S}_T - \bar{S}_T^{\,2} + 3.495,73 = 0 \qquad \text{Eq. (C.41)}$$

$$0.063,15\,Z - 0.538,55\,\bar{S}_T - 0.734,82 = 0 \qquad \text{Eq. (C.42)}$$

The real roots of equations (C.41) and (C.42) are

Z	$\bar{S}_T$
14.298,94	0.312,28

Hence,

$$\frac{1}{k} = 11.534, \quad \frac{v_f}{b\,\omega_\alpha} = 3.050$$

Choosing other values for M and $\bar{\omega}$ and repeating the steps above result in the curves shown in Figure C.4. A small amount of structural damping was included in the analysis to obtain the curves of Figure C.5. The curves of Figures C.4 and C.5 were then cross-plotted to obtain those of Figures 3.13 and 3.14, respectively.

C.5 Wing with Tip Tank, Free-to-Roll

The equations of motion for the straight wing with tip tank are given by equations (A.95) through (A.97). Again, the wing is assumed to have constant chord and constant mass properties (see Figure C.3), and the quantities, $\overline{S}_T$ and Z, were chosen as eigenvalues. With the parameters of equation (C.32) and the value of the mass moment of inertia of the roll support about the roll axis,

$$I_s = 0.001,50 \text{ slug-ft}^2$$

the coefficients of the flutter determinant become

$$K_{\theta\theta} = 2.408,93 - 0.006,55(L_1 + iL_2) \qquad \text{Eq. (C.43)}$$

$$K_{\theta h} = 2.205,13 - 0.005,59(L_1 + iL_2) \qquad \text{Eq. (C.44)}$$

$$K_{\theta\alpha} = 0.046,28 + \overline{S_T} - 0.007,96(L_3 + iL_4) - 0.000,70\frac{i}{k} \qquad \text{Eq. (C.45)}$$

$$K_{h\theta} = 2.205,13 - 0.005,59(L_1 + iL_2) \qquad \text{Eq. (C.46)}$$

$$K_{hh} = 2.170,72 - 0.025,00Z - 0.004,91(L_1 + iL_2) \qquad \text{Eq. (C.47)}$$

$$K_{h\alpha} = 0.038,72 + \overline{S}_T - 0.006,66(L_3 + i L_4) - 0.000,70 \frac{i}{k} \qquad \text{Eq. (C.48)}$$

$$K_{\alpha\theta} = 0.046,28 + \overline{S}_T - 0.007,96(M_1 + i M_2) + 0.000,70 \frac{i}{k} \qquad \text{Eq. (C.49)}$$

$$K_{\alpha h} = 0.038,72 + \overline{S}_T - 0.006,66(M_1 + i M_2) + 0.000,70 \, i/k \qquad \text{Eq. (C.50)}$$

$$K_{\alpha\alpha} = 1.641,99 - 0.118,70Z - 0.009,82(M_3 + i M_4) + \frac{0.000,70}{k^2} \qquad \text{Eq. (C.51)}$$

For M = 2, $\overline{\omega} = 0.10$ and $x_o = 0.443$, the aerodynamic coefficients are found from Reference 7 (pp. 8 and 24) to be

$$L_1 + i L_2 = 0.192,11 + 15.386,40\, i \qquad \text{Eq. (C.52)}$$

$$L_3 + i L_4 = 410.262 - 3.363,85\, i \qquad \text{Eq. (C.53)}$$

$$M_1 + i M_2 = 0.085,66 + 1.749,05\, i \qquad \text{Eq. (C.54)}$$

$$M_3 + i M_4 = 46.653 + 3.039,95\, i \qquad \text{Eq. (C.55)}$$

Expanding the flutter determinant and separating the real and imaginary parts give

$$0.639,64 - 0.148,31Z + 0.007,14Z^2 + 0.431,72\overline{S}_T - 0.169,33\overline{S}_T^{\,2} - 0.079,37Z\overline{S}_T + 0.025,00Z\overline{S}_T^{\,2} = 0 \qquad \text{Eq. (C.56)}$$

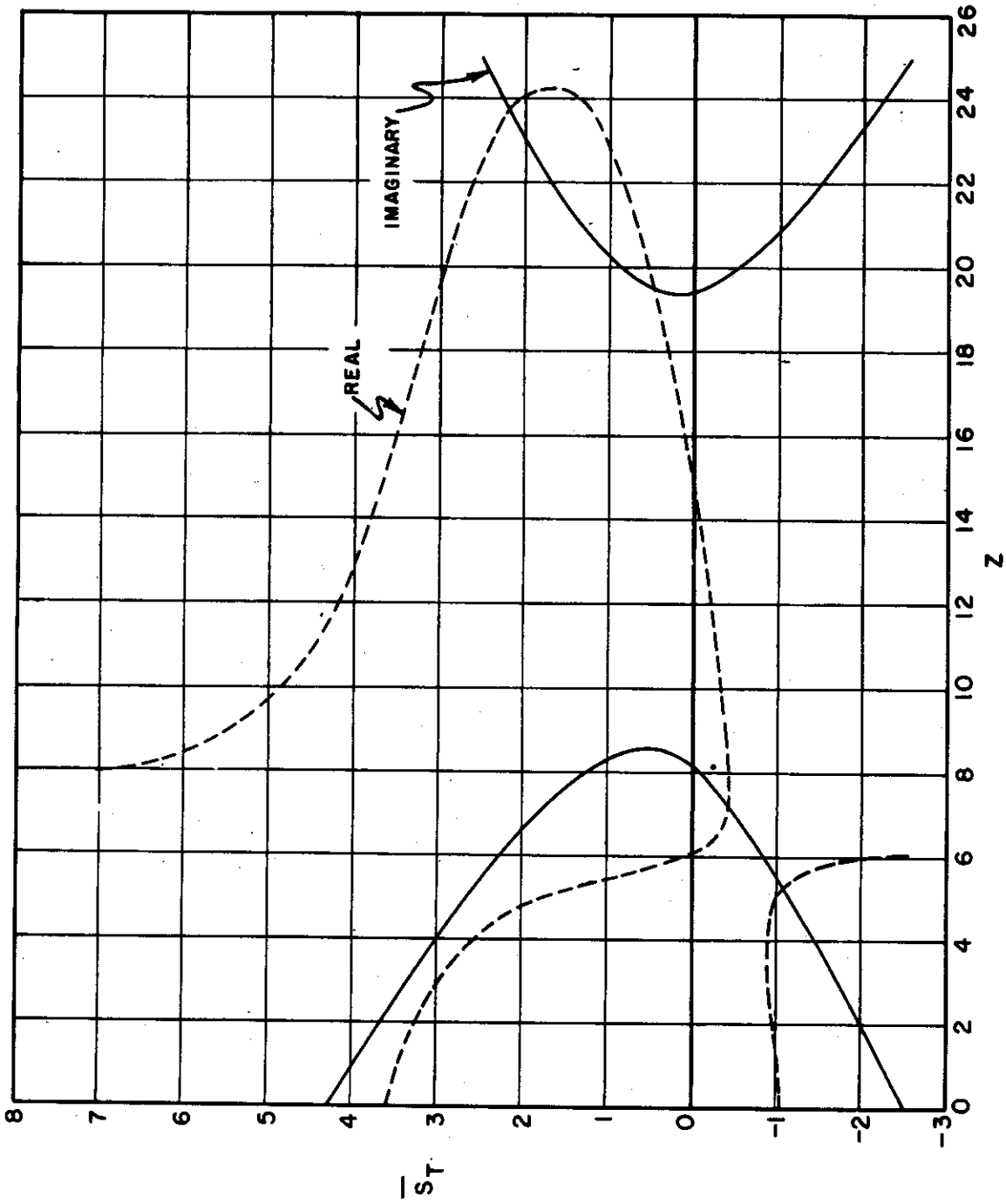

FIGURE C.6 GRAPHICAL SOLUTION OF SIMULTANEOUS EQUATIONS

$$-0.469,97 + 0.082,24 Z - 0.002,99 Z^2 - 0.079,88 \bar{S}_T + 0.043,87 \bar{S}_T^2 + 0.003,21 Z \bar{S}_T = 0 \qquad \text{Eq. (C.57)}$$

This set of simultaneous equations is most easily solved graphically (see Figure C.6). Additional accuracy can be obtained by iteration. The solutions are

Z	$\bar{S}_T$	$\frac{1}{k}$	$\frac{V_f}{b\omega_\alpha}$
5.300	-1.074	26.67	11.583
7.270	-0.405	26.67	9.890
19.46	0.479	26.67	6.045
23.75	2.191	26.67	5.472

Therefore, four points on the curves of $\frac{V_f}{b\omega_\alpha}$ and $\frac{1}{k}$ versus $\bar{S}_T$ have been determined. By assuming different values of $\bar{\omega}$, the process can be repeated until the curve for M = 2 has been defined (see Figure C.7). As explained in Appendix C.2 above, interpolation of the tables in Reference 7 is inaccurate, so the aerodynamic coefficients should be tabulated by the method of Reference 41 (or Reference 40 for low $\bar{\omega}$) for values of M and $\bar{\omega}$ not found in Reference 7. The curves of Figure 3.15 were obtained by cross-plotting those of Figure C.7.

C.6 Piston Theory

The coefficients of the two-degree-of-freedom flutter determinant for the straight-wing planform of this report (Fig. 1.1) are given by equations (A.114) through (A.117). The aerodynamic terms have been derived for the tapered planform with a symmetrical double-wedged air foil section at zero angle of attack in equations (A.131) through (A.134).

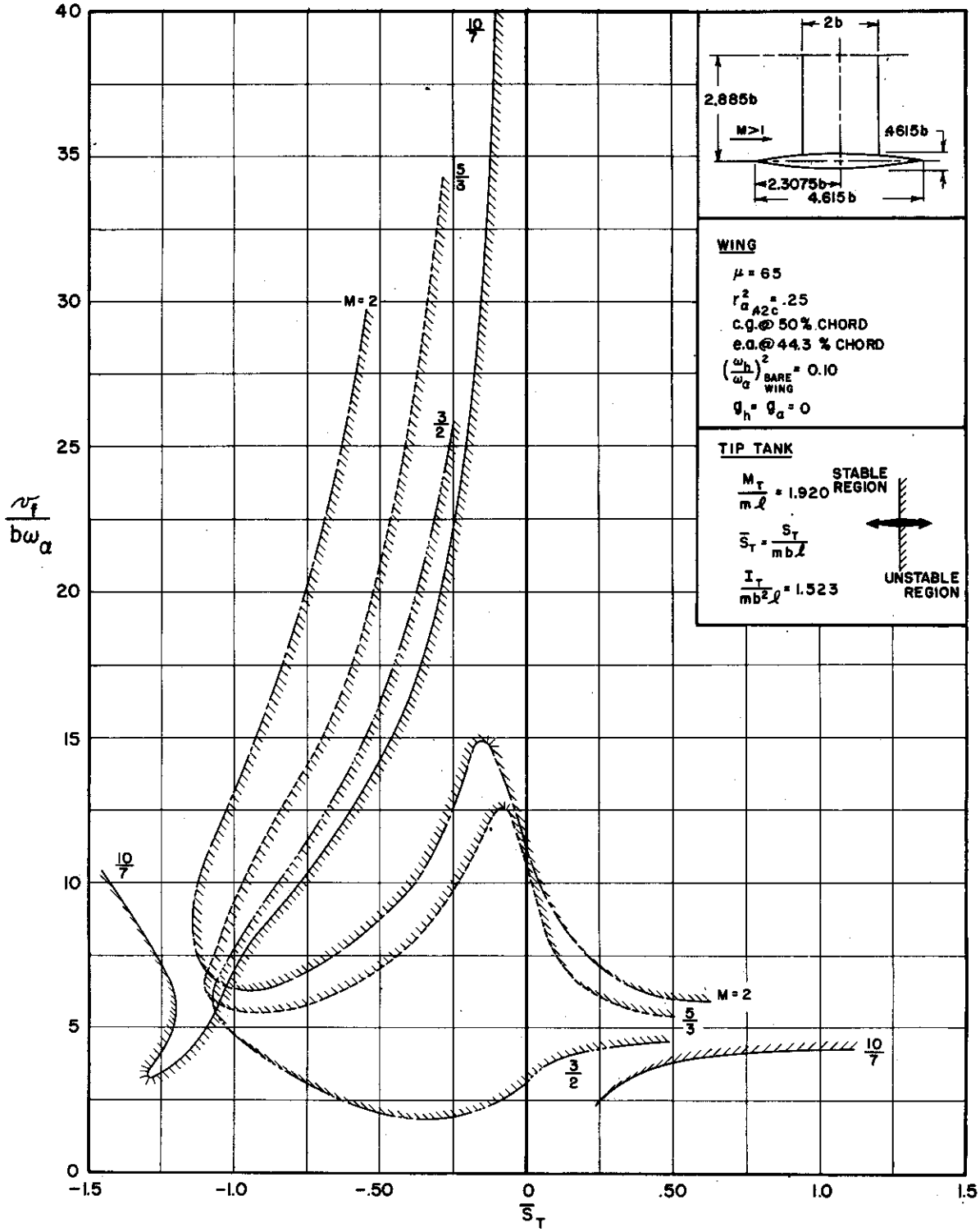

FIGURE C.7(a) FLUTTER COEFFICIENT VERSUS TIP-TANK STATIC-UNBALANCE PARAMETER FOR STRAIGHT-WING PLANFORM, FREE-TO-ROLL

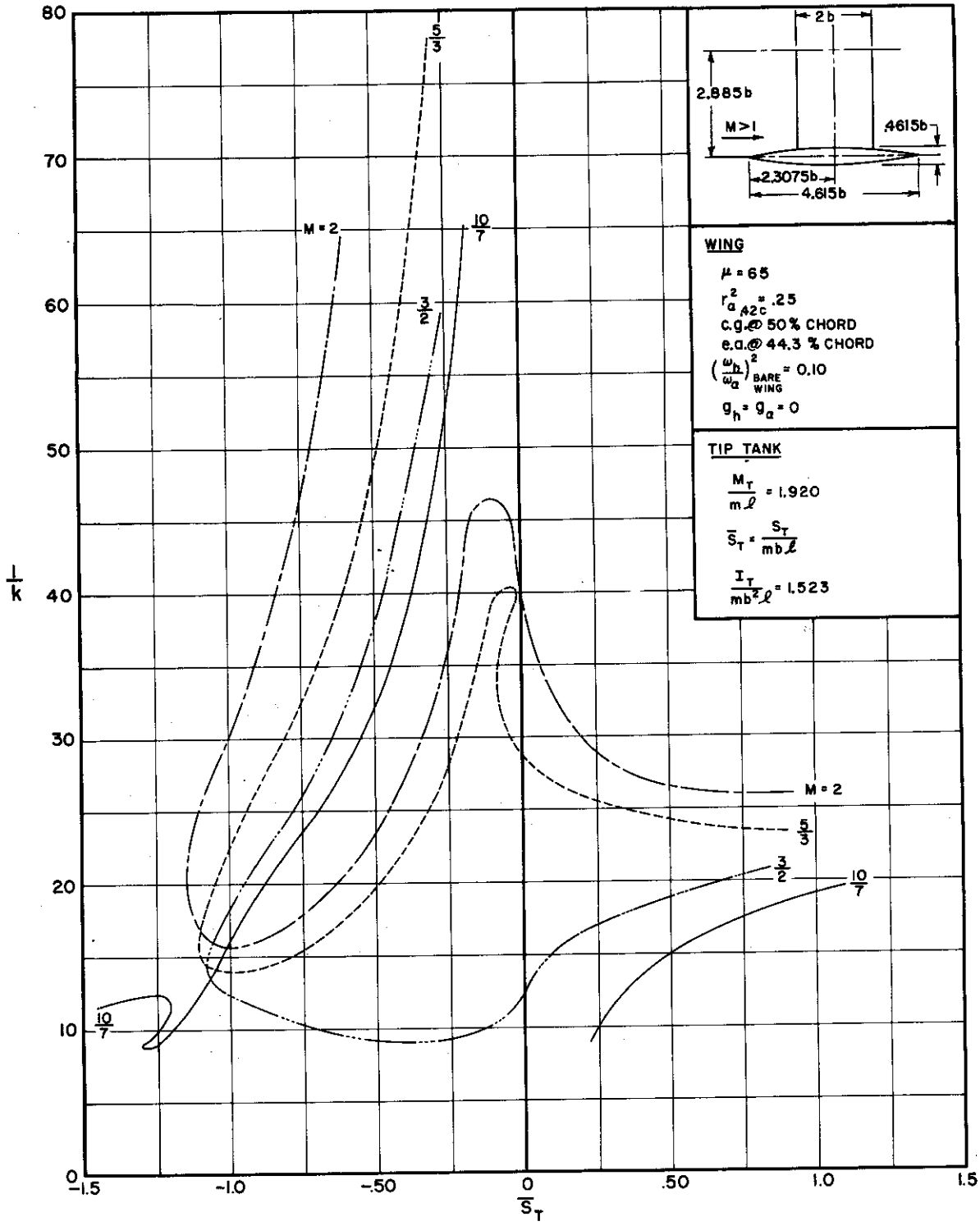

FIGURE C.7(b) REDUCED FREQUENCY VERSUS TIP-TANK STATIC-UNBALANCE PARAMETER FOR STRAIGHT-WING PLANFORM, FREE-TO-ROLL

With the following parameters,

$$\mu = 65\ (\tfrac{\pi}{4}) \qquad \gamma = 1.4 \text{ (air)}$$
$$x_\alpha = 0.114 \qquad \Upsilon = 0.06$$
$$r_\alpha^2 = 0.237,40 \qquad M = 2.0$$
$$\left(\frac{\omega_h}{\omega_\alpha}\right)^2 = 0.25 \qquad x_o = 0.443$$
$$g_h = g_\alpha = 0$$

Eq. (C.58)

the coefficients become

$$\underline{A} = 3.514,69 - 0.878,67\,\bar{z} - 0.058,84\,\frac{i}{k_o} \qquad \text{Eq. (C.59)}$$

$$\underline{B} = 0.331,59 - 0.075,65\,\frac{1}{k_o^2} - 0.001,97\,\frac{i}{k_o} \qquad \text{Eq. (C.60)}$$

$$\underline{D} = 0.331,59 - 0.001,97\,\frac{i}{k_o} \qquad \text{Eq. (C.61)}$$

$$\underline{E} = 0.712,10 - 0.712,10\,\bar{z} - 0.002,87\,\frac{1}{k_o^2} - 0.014,56\,\frac{i}{k_o} \qquad \text{Eq. (C.62)}$$

Expanding the determinant and setting the real and imaginary parts equal to zero give

$$-0.917,81 + 0.546,95\,\bar{z} + \frac{0.195,71}{10^3\,k_o^2} \qquad \text{Eq. (C.63)}$$

$$0.625,70\,Z^2 - 3.128,49\,Z + \frac{2.517,98\,Z}{10^3\,k_o^2} + \frac{14.159,43}{10^3\,k_o^2} + 2.392,84 = 0 \qquad \text{Eq. (C.64)}$$

The real, positive solutions to this set of equations are

Z	$\frac{1}{k_o}$
1.657	7.651

whence

$$\frac{v_f}{b_o\,\omega_\alpha} = 5.944$$

Repeating the process for other parameters (Eq. C.58) results in the curves of Figure 3.6.

APPENDIX D

DETAILED TABULATION FOR DATA FOR MODELS TESTED

D.1 General

In this appendix, a detailed tabulation of data is presented for all the models tested. The number of significant figures quoted is consistent with the experimental accuracy. See Reference 14 for a discussion of the testing techniques used to obtain these data.

The basic construction of balsa, aluminum and lead shown in Figure D.1 is the same for all the models tested. The balsa gives the desired aerodynamic shape. The airloads are transmitted by the balsa to the aluminum spar, whose dimensions, B and H, can be varied to control the torsional rigidity and the bending stiffness of the model, and whose chordwise location determines the elastic-axis position. 75ST aluminum alloy was selected for the spar because it is light and strong. Also, its yield strength is close to its ultimate strength, and thus a maximum linear range is available. The rectangular cross-section allows for ease of computation during the design and ease of fabrication in the shop. Two pairs of strain gages are mounted on the spar for use in the vibration and flutter tests; one pair along the elastic axis to pick up bending, and the other at 45° to the elastic to pick up torsion. Lead weights, fore and aft of the spar, are designed so as to give the desired mass and inertial properties at each spanwise station. The lead is slit before gluing so that its contribution to the model's stiffness is negligible.

Because the thickness ratio of the wing is constant, all dimensions are tapered linearly in thickness and in width.

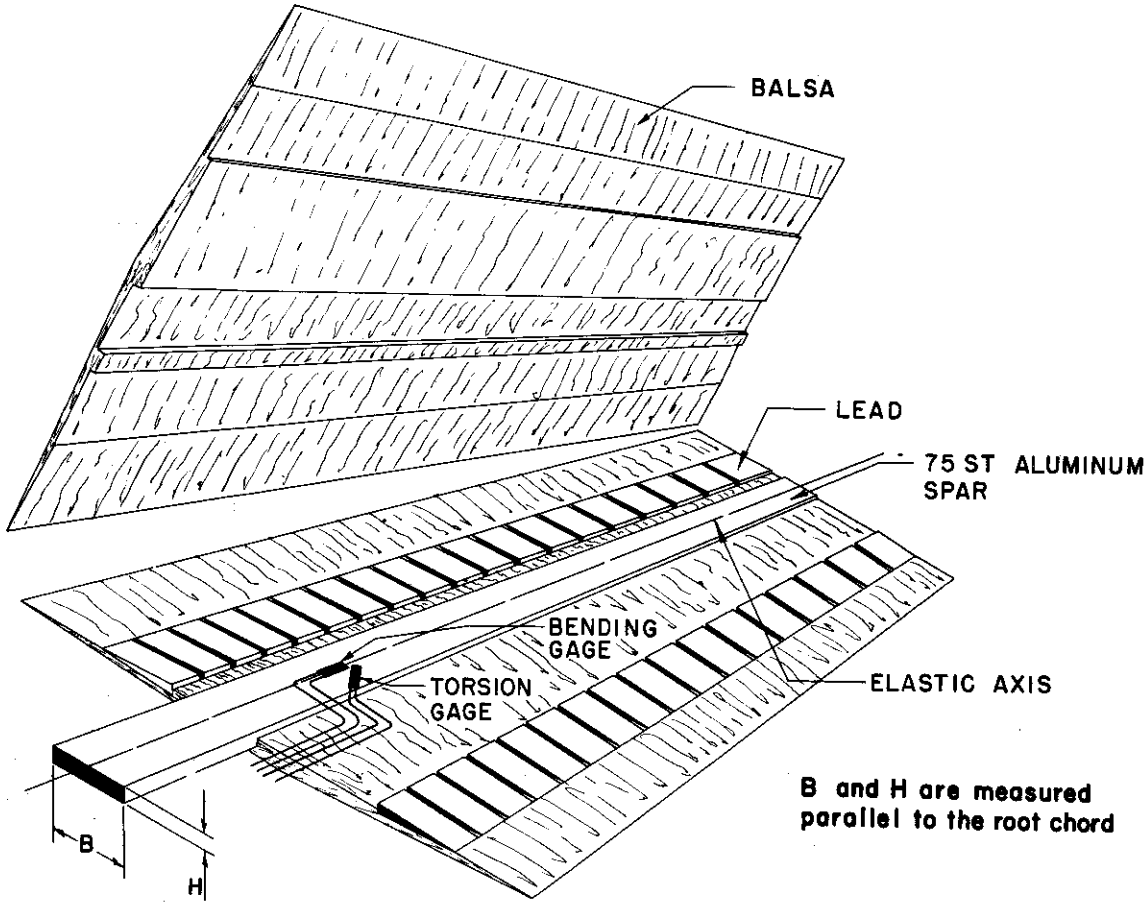

FIGURE D.1 A TYPICAL SUPERSONIC FLUTTER MODEL

Therefore, the mass varies as the square of the chord, and the stiffnesses vary as the fourth power of the chord,

$$m = m_o \left(\frac{b}{b_o}\right)^2 \qquad \text{Eq. (D.1)}$$

$$EI = (EI)_o \left(\frac{b}{b_o}\right)^4 \qquad \text{Eq. (D.2)}$$

$$GJ = (GJ)_o \left(\frac{b}{b_o}\right)^4 \qquad \text{Eq. (D.3)}$$

[redacted]

Model nomenclature is explained by the following example:

SW-2a-1

SW - denotes swept-wing model.

2 - denotes that the cross-sectional dimensions of the spar are the same as for model SW-2.

a - denotes the first basic modification of model SW-2 (but no change in spar dimensions).

1 - denotes the first duplicate model of SW-2a.

D.2 Design Data

Tables D.1, D.2 and D.3 present design data for all the models tested. Therefore, any model can be duplicated by the use of Tables D.1, D.2 and D.3 and the techniques discussed in References 14, 17, and 19 for designing lead weights to obtain the desired mass and inertial characteristics (see Tables D.4, D.5 and D.6). The spar dimensions, B_o and H_o, were measured in the streamwise direction for all the planforms. The elastic moduli of the balsa were obtained experimentally or were estimated using the methods of Reference 43. Except where indicated in Tables D.4, D.5 and D.6, the grain of the wood was parallel to the root chord for the straight wings, perpendicular to the spanwise centerline of the wing for the swept planforms, and parallel to the wing centerline for the delta models.

D.3 Mass and Stiffness Data

Tables D.4, D.5 and D.6 give mass and stiffness data. The

mass per unit length of the wing at the root chord, m_o, was obtained by weighting the wing and using the relation,

$$M_w = m_o \frac{l}{3}(1 + \lambda + \lambda^2) \qquad \text{Eq. (D.4)}$$

where

M_w is the total mass of the bare wing.

Equation (D.4) assumes that the mass varies as the square of the wing chord. The wing stiffnesses at the root, $(EI)_o$ and $(GJ)_o$, and the location of the measured elastic axis were obtained by static tests, assuming that the stiffnesses varied as the fourth power of the wing chord. The location of the measured elastic axis is that near the tip of the wing, and it varies slightly along the span because of sweep and root effects. Therefore, the locus of shear centers, which is constant along the span, was assumed to correspond to and was calculated as the locus of centroids of the bending stiffnesses. This latter parameter is probably more significant than the location of the measured elastic axis for the flutter engineer. Calculations were made to obtain the section center-of-gravity location and the dimensionless moment of inertia in pitch, r_α, which are constant along the span. Spot tests showed that the experimental values of these parameters coincided with the calculated values within the experimental accuracy.

In Table D.6, Models De-2b, De-3h and De-4a were duplicates of previous models except that lead was added to lower the second bending frequency without significantly changing the first torsional frequency in an attempt to precipitate flutter. The location of the lead depended on the mode shape for the second bending frequency, and lead was placed at points of maximum amplitude for the second-bending mode along the nodal line for first torsion. Therefore, the dimensionless radius of gy-

ration in pitch, r_α , and the chordiwse location of the center of gravity are not quoted for these models.

D.4 Flutter Data

Tables D.7, D.8 and D.9 present flutter data for the straight, swept and delta planforms, respectively. Enough data are presented so that other flow parameters can be calculated. For example,

$$v = Ma \qquad \text{Eq. (D.5)}$$

$$a = \sqrt{\gamma RT} \qquad \text{Eq. (D.6)}$$

$$\mu = \frac{m_o}{\pi \rho b_o^2} \qquad \text{Eq. (D.7)}$$

$$p = \rho RT \qquad \text{Eq. (D.8)}$$

$$\frac{RN}{L} = \frac{v}{\nu} \qquad \text{Eq. (D.9)}$$

$$\nu = \frac{1}{\rho} \frac{3.059 \times 10^{-8} T^{3/2}}{T + 114} \qquad \begin{pmatrix} \nu \text{ in ft}^2/\text{sec} \\ \rho \text{ in slugs/ft}^3 \\ T \text{ in } ^\circ\text{C absolute} \end{pmatrix} \qquad \text{Eq. (D.10)}$$

where

v is the free-stream velocity
M is the free-stream Mach number
a is the speed of sound
γ is the ratio of specific heats
R is the gas constant
T is the absolute static temperature of the gas
p is pressure

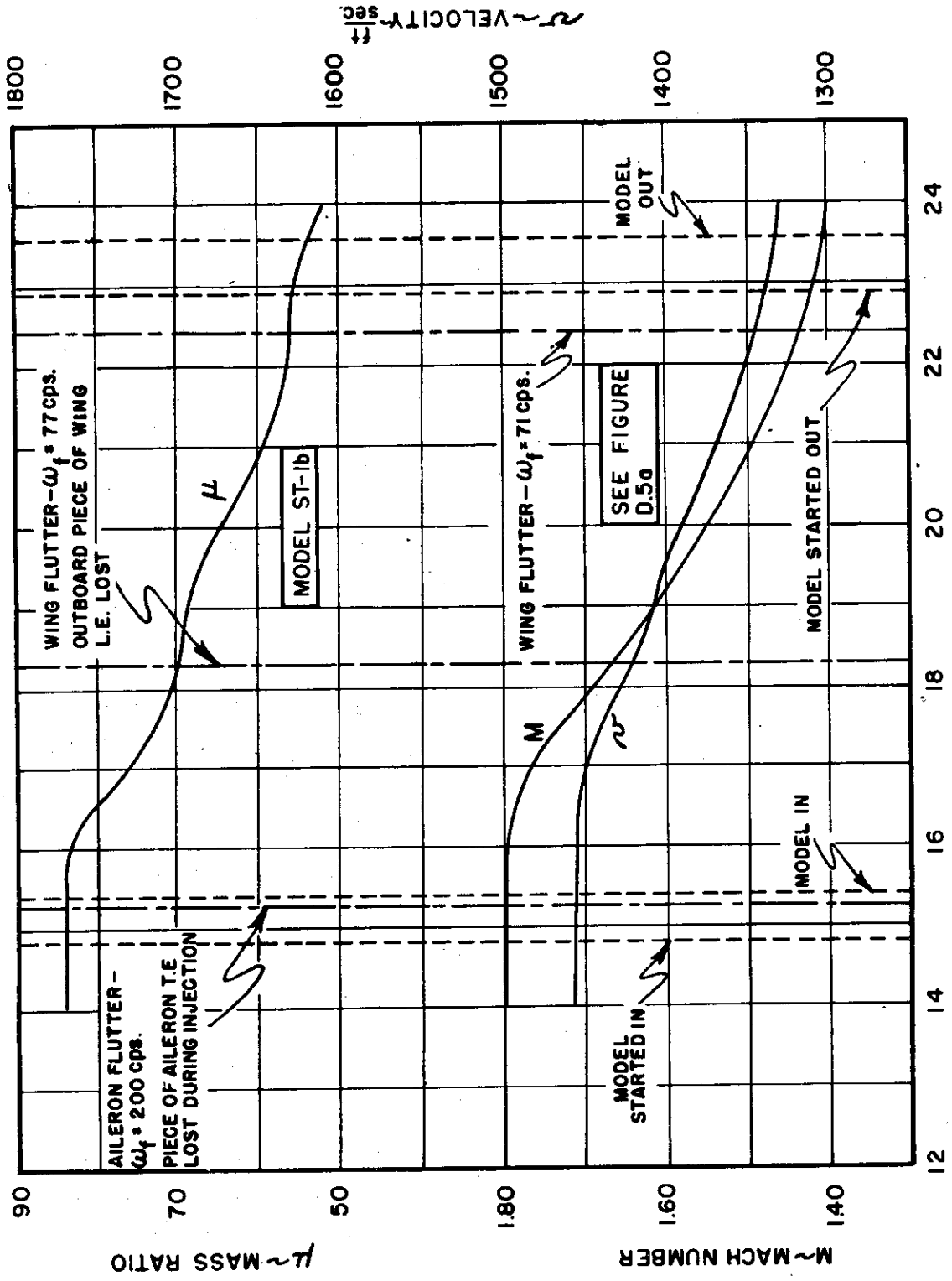

FIGURE D.2 TYPICAL TIME HISTORY OF FLOW PARAMETERS DURING FLUTTER TEST

$\frac{RN}{L}$ is the Reynolds number per unit length

ν is kinematic viscosity

The quantities, v, M and μ, are tabulated in Tables D.7, D.8 and D.9; the value of the parameter, m_o, can be found in Tables D.4, D.5 and D.6; for dry air,

$$\gamma = 1.4$$

$$R = 1718 \ \frac{ft^2}{sec^2 \ ^oF}$$

the wing semi-chord at the root, b_o, is 5/12 foot for all the models tested. The Reynolds number was on the order of 7.5×10^6 per foot of reference length during the flutter tests (see Reference 13, p. 51).

All legitimate flutter points were obtained by injecting the model into a stable region and approaching flutter from a high Mach number. The Mach number, velocity and wing mass ratio, μ, decreased during the tests. Figure.D.2 shows a typical time history of these parameters and also illustrates an interesting case. The model fluttered during injection in a three-degree-of-freedom flutter mode until a piece of the trailing edge of the aileron, which was of lead, was lost (see Figure D.5a). Loss of the trailing edge of the aileron changed the aileron mass and inertial characteristics, and the model became stable until it fluttered in a bending-torsion mode at a lower Mach number when a piece of the leading edge of the wing was lost. The model was again stable until it fluttered once more at a lower frequency and at a lower Mach number in a bending-torsion mode causing further damage.

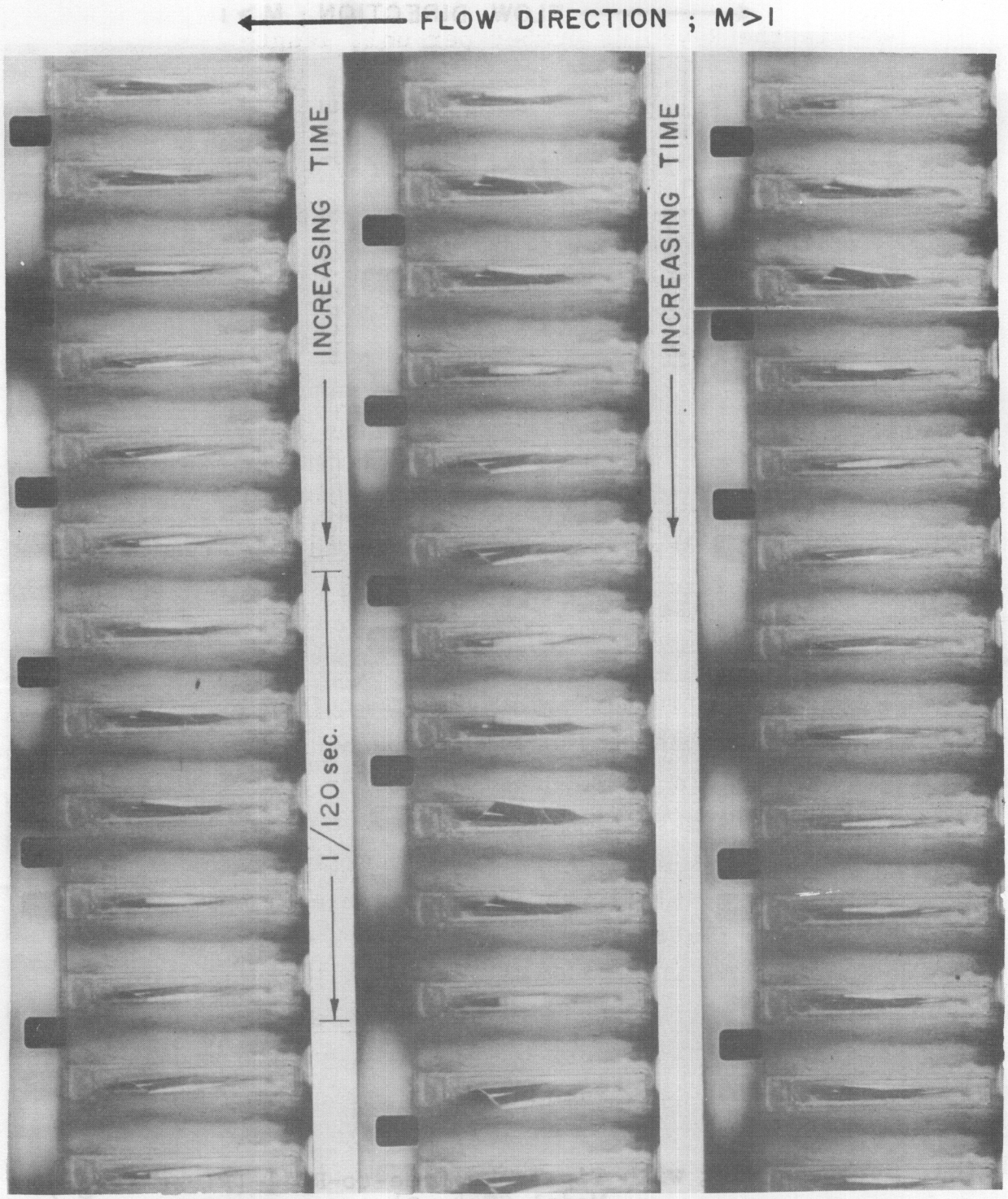

(a) Straight Wing with Free Aileron, Cantilever (Model ST-1e)

FIGURE D.3 SOME HIGH-SPEED MOVIES AT SUPERSONIC FLUTTER

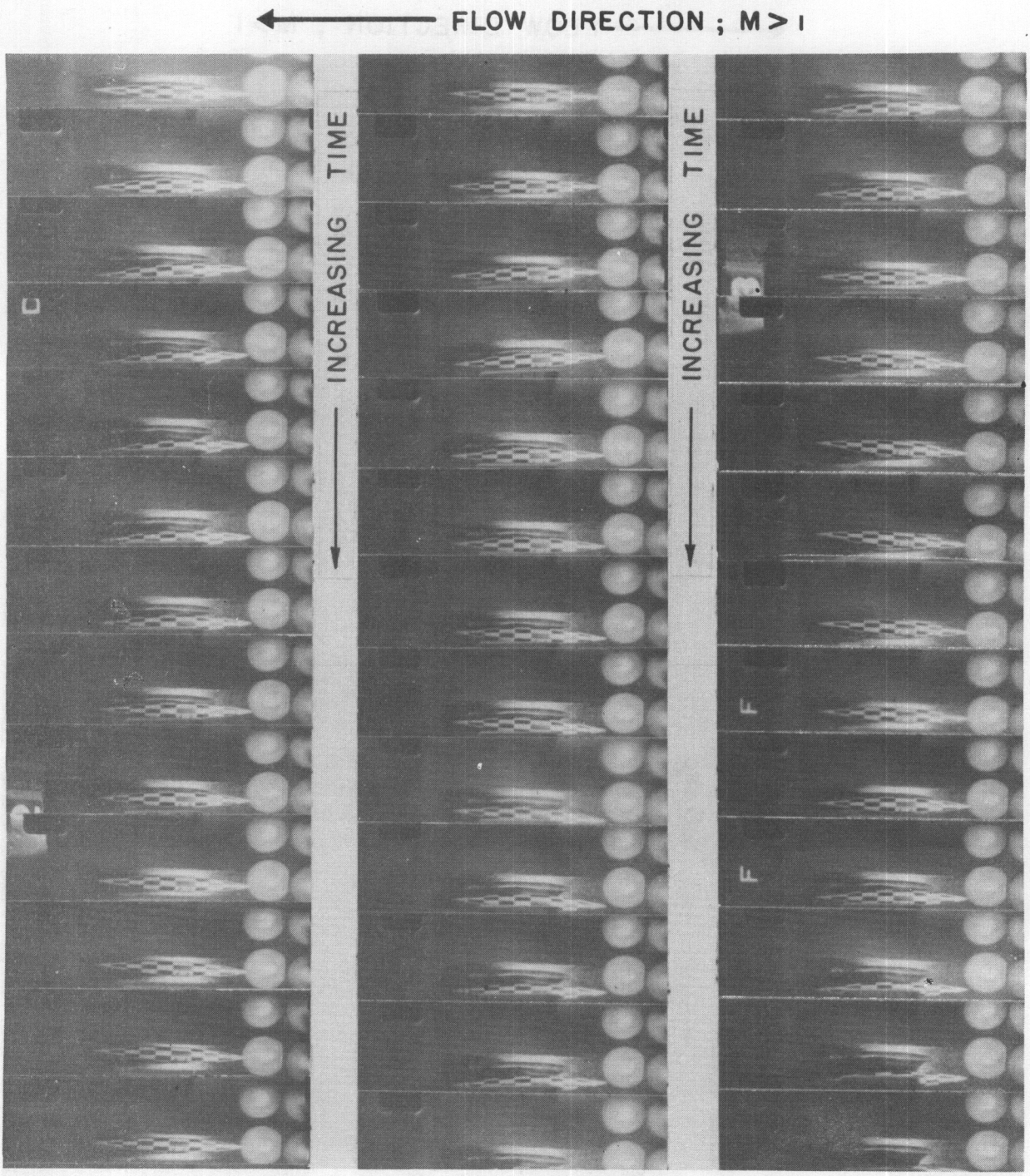

(b) Straight Wing with Tip Tank, Free-to-Roll (First Stage, Model ST-4c-3).

FIGURE D.3 (Continued) SOME HIGH-SPEED MOVIES AT SUPERSONIC FLUTTER

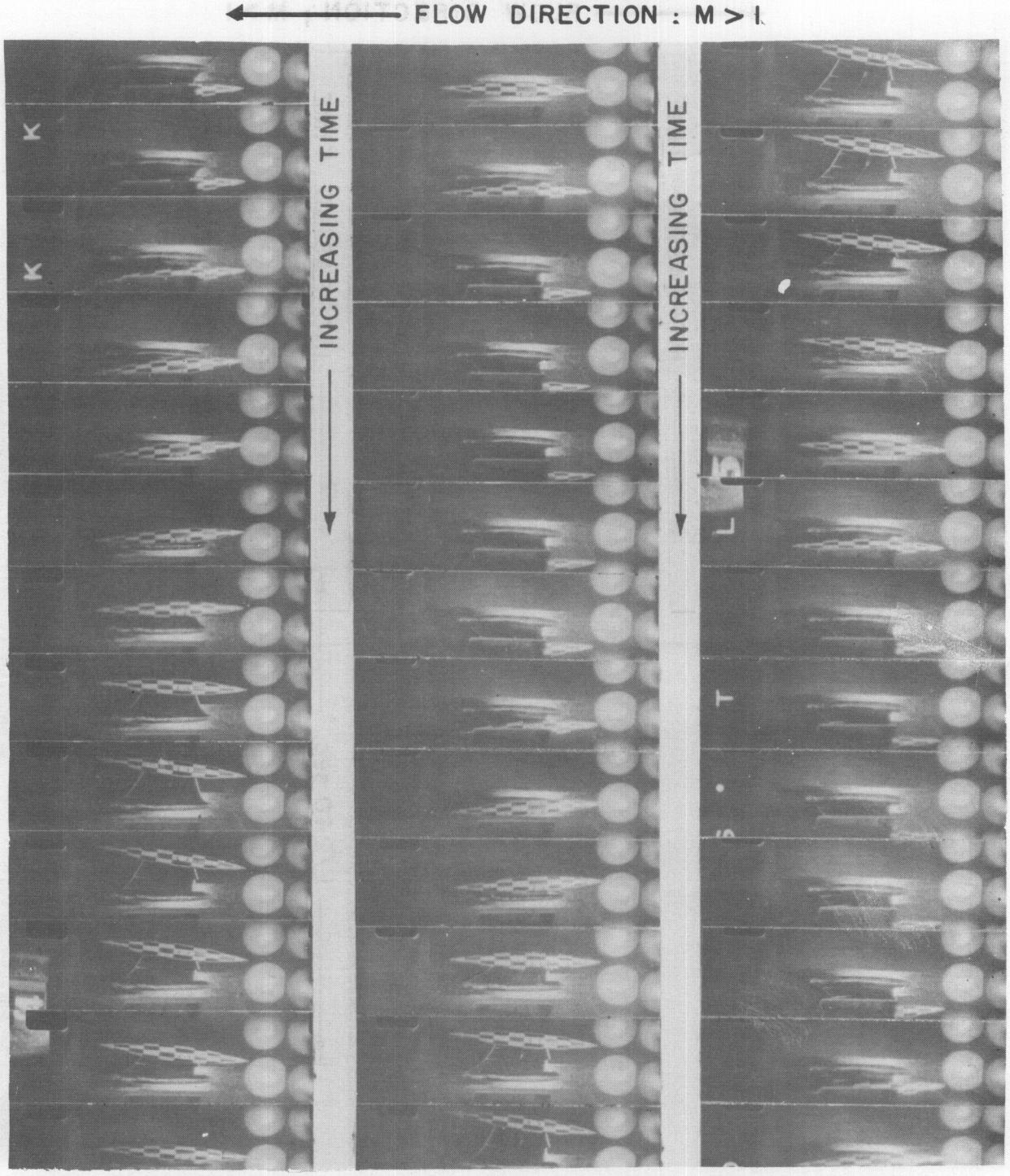

(c) Straight Wing with Tip Tank, Free-to-Roll (Second Stage, Model ST-4c-3)

FIGURE D.3 (Continued) SOME HIGH-SPEED MOVIES AT SUPERSONIC FLUTTER

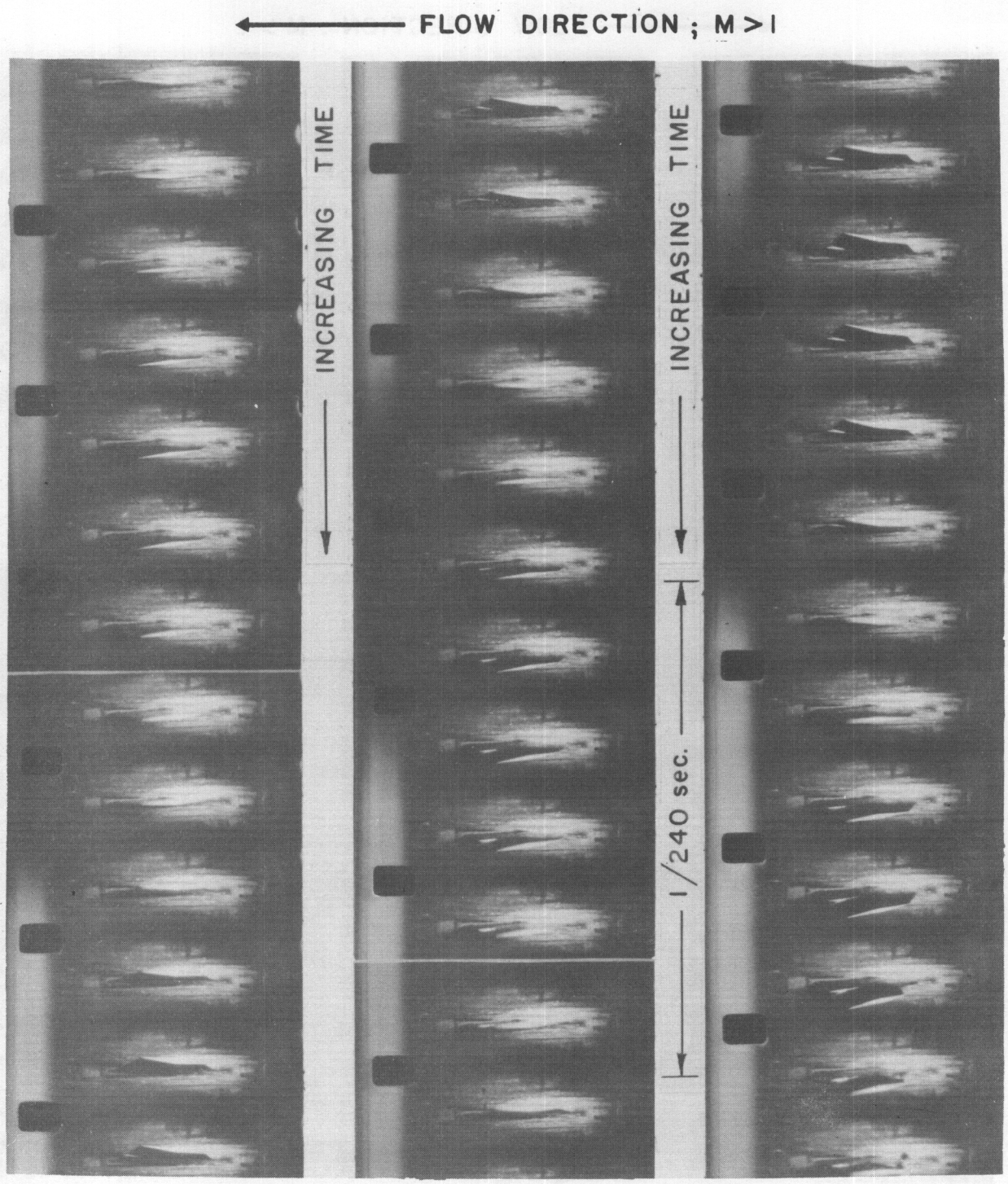

(d) Straight Wing with Locked Aileron, Cantilever (Model ST-1f)

FIGURE D.3 (Continued) SOME HIGH-SPEED MOVIES AT SUPERSONIC FLUTTER

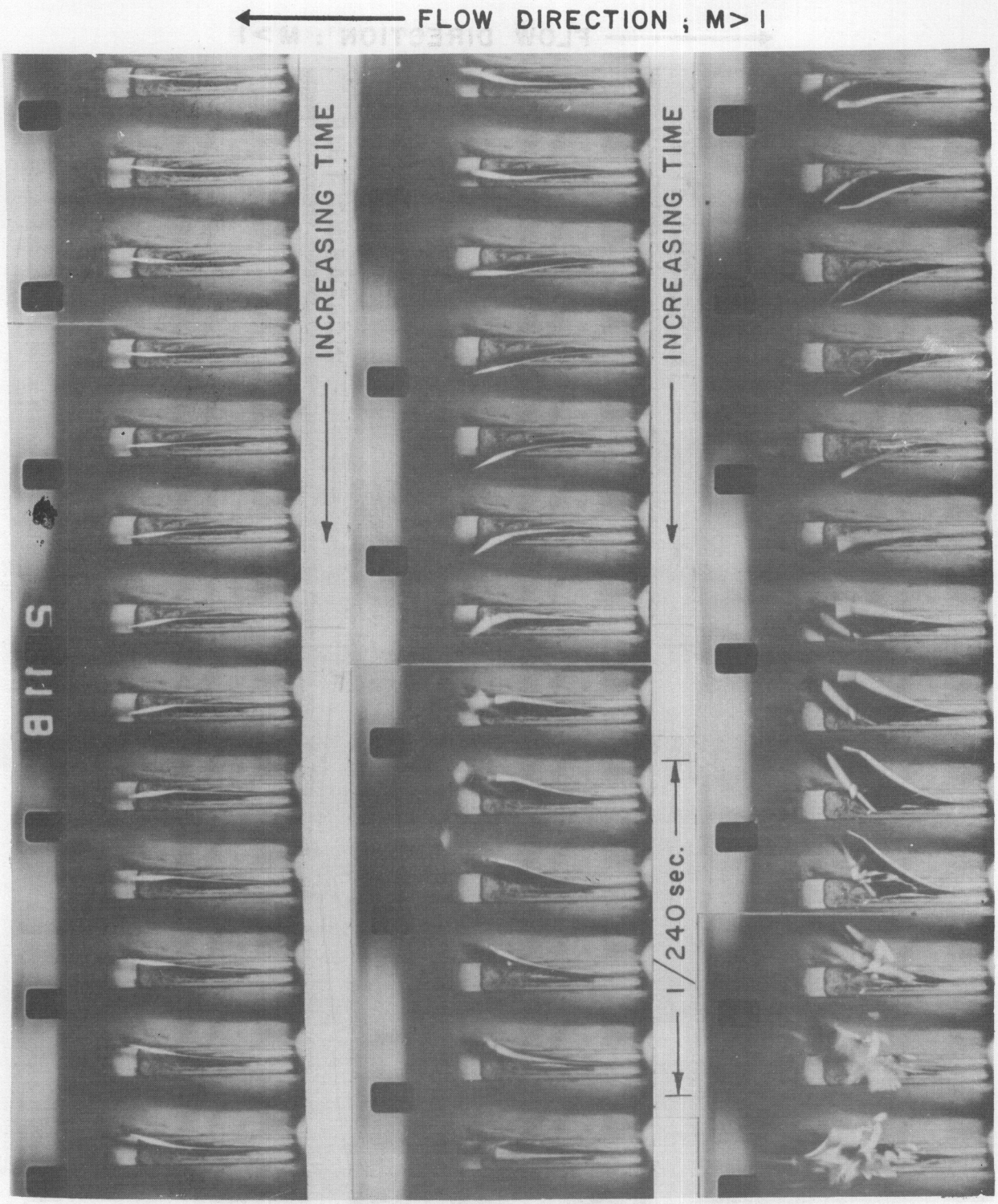

(e) Bare Swept Wing, Cantilever (Model SW-5, Injection Flutter)

FIGURE D.3 (Continued) SOME HIGH-SPEED MOVIES AT SUPERSONIC FLUTTER

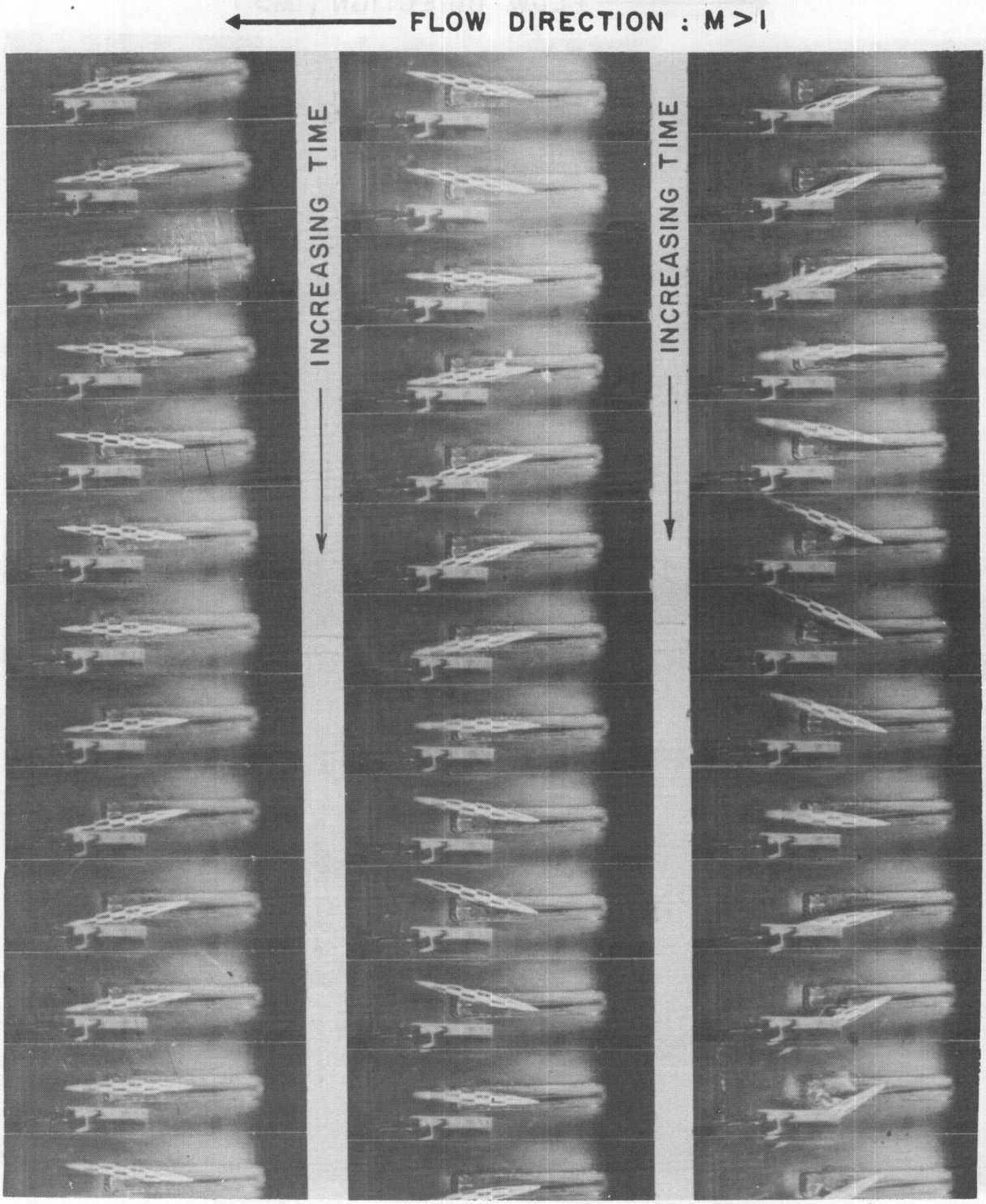

(f) Swept Wing with Tip Tank, Cantilever (Model SW-6)

FIGURE D.3 (Continued) SOME HIGH-SPEED MOVIES AT SUPERSONIC FLUTTER

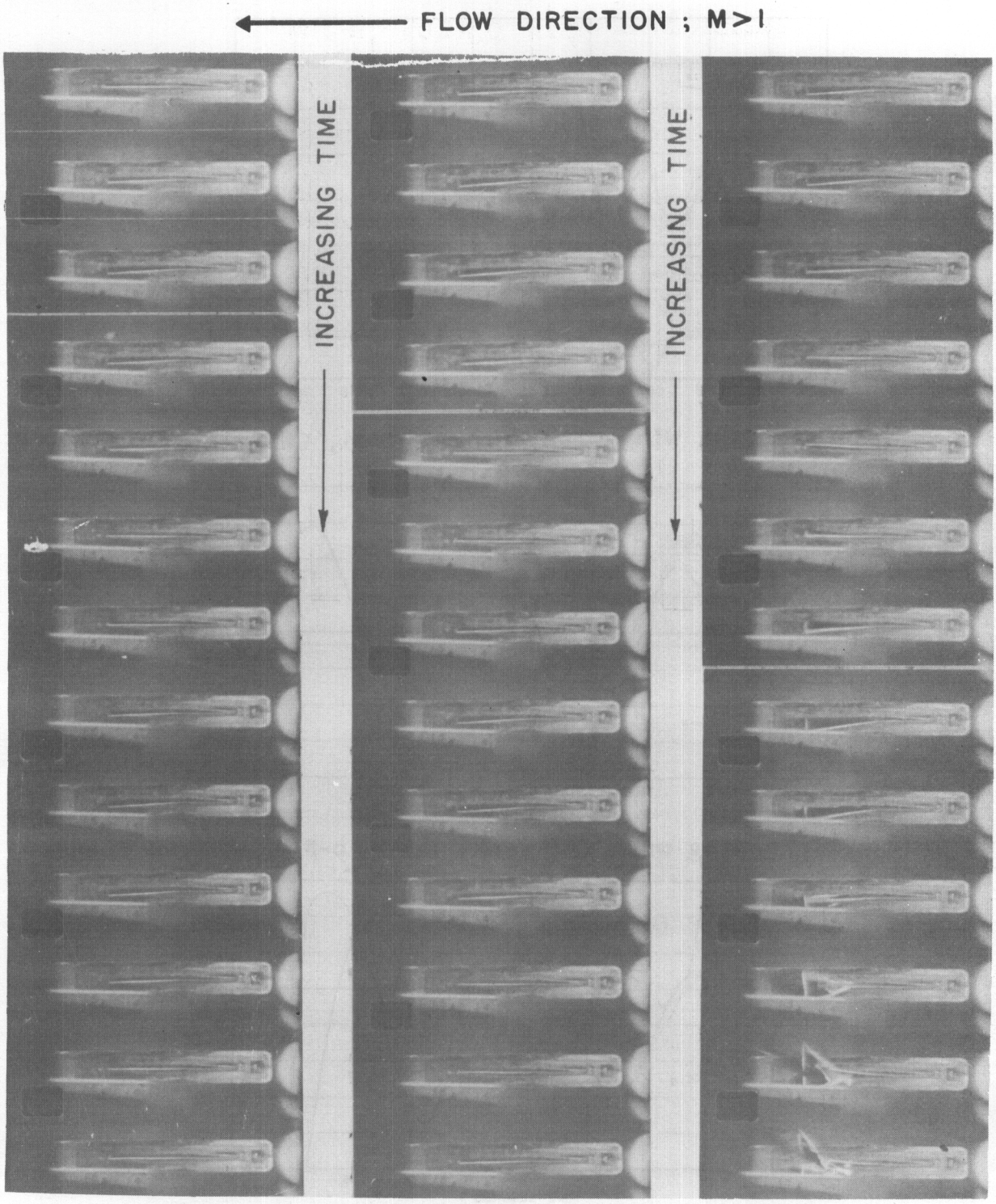

(g) Bare Delta Wing, Cantilever (Model De-4c)

FIGURE D.3 (Continued) SOME HIGH-SPEED MOVIES AT SUPERSONIC FLUTTER

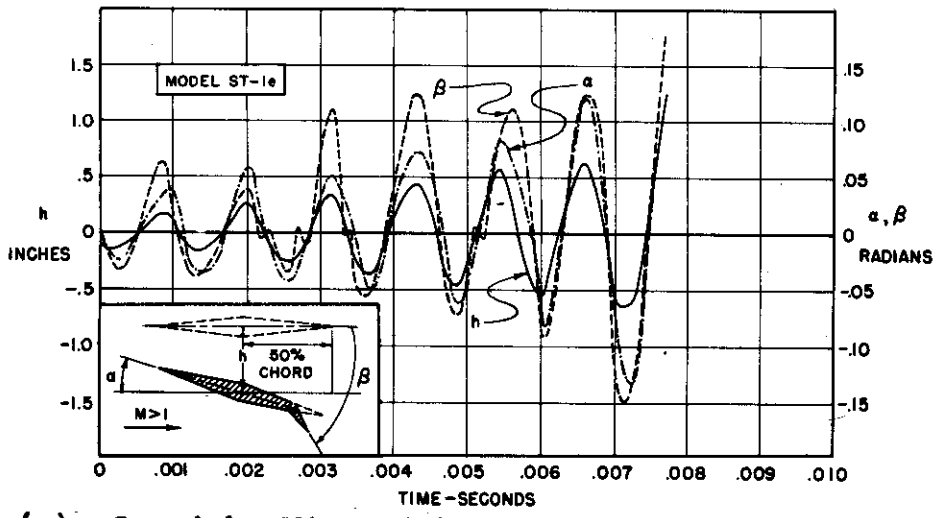

(a) Straight Wing with Free Aileron, Cantilever

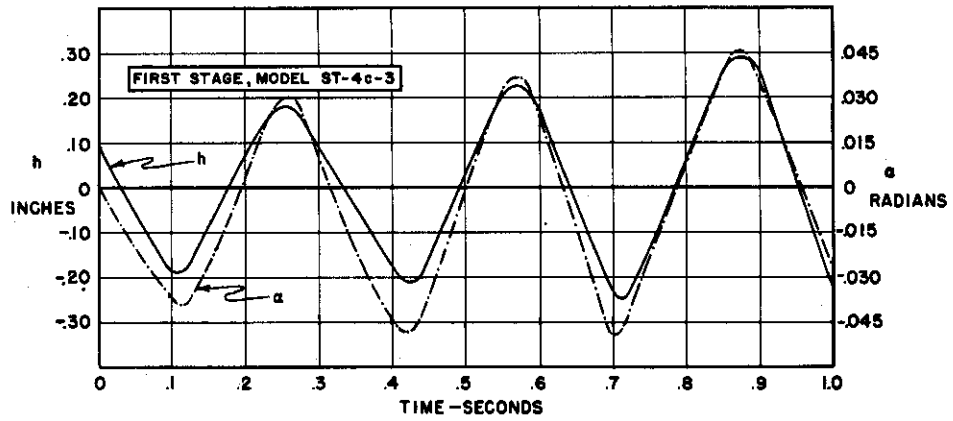

(b) Straight Wing with Tip Tank, Free-to-Roll (First Stage)

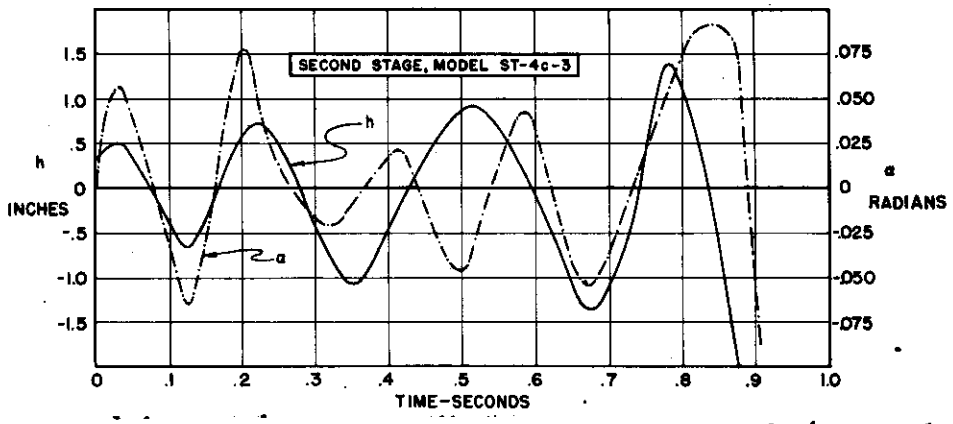

(c) Straight Wing with Tip Tank, Free-to-Roll (Second Stage)

FIGURE D.4 WING-TIP MOTION AT FLUTTER

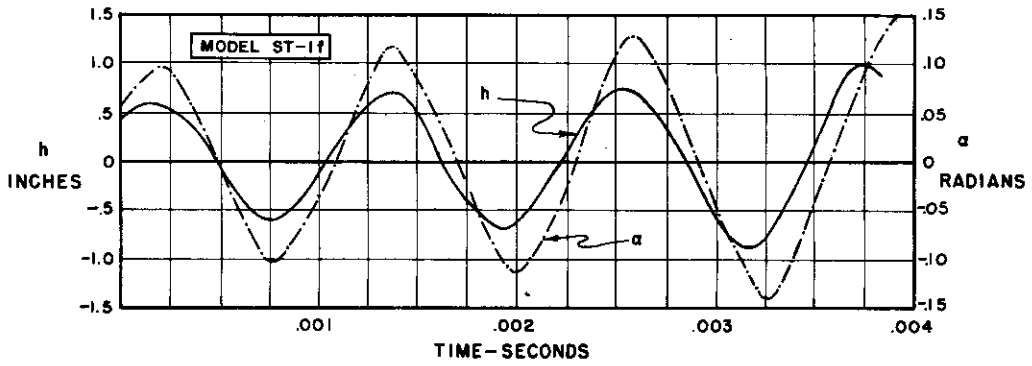

(d) Straight Wing with Locked Aileron, Cantilever

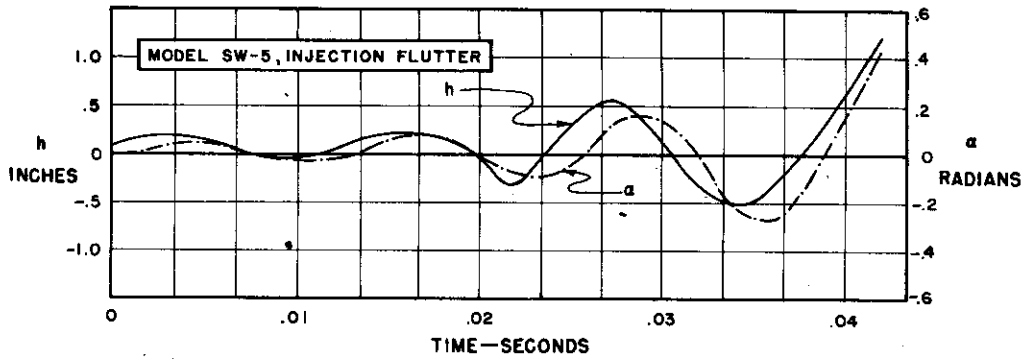

(e) Bare Swept Wing, Cantilever (Injection Flutter)

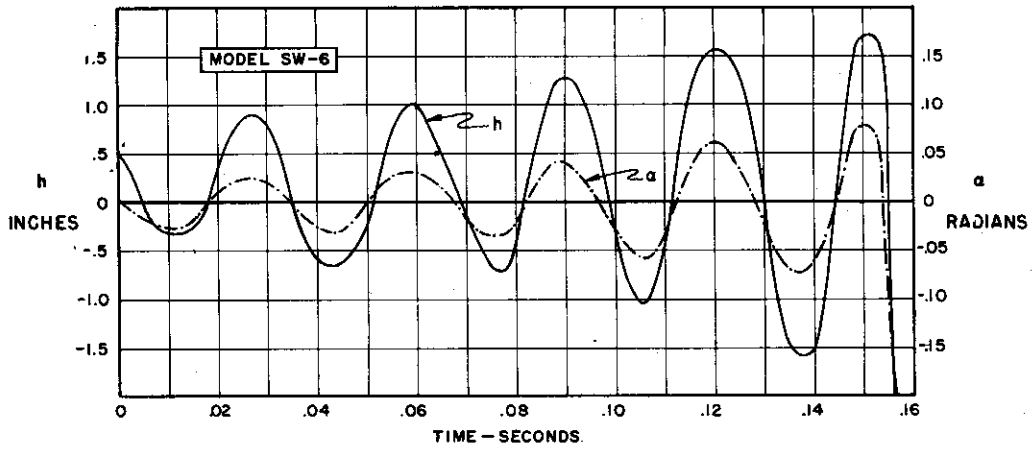

(f) Swept Wing with Tip Tank, Cantilever

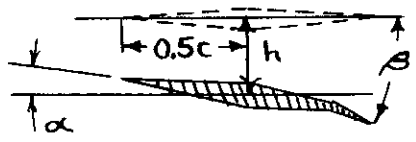

FIGURE D.4 (Continued) WING-TIP MOTION AT FLUTTER

High-speed movies were taken during most of the flutter tests. Besides giving evidence of model damage, the high-speed photography exhibited clearly the exact nature of the flutter mode shapes. Figure D.3 shows some high-speed movies of typical models at flutter. Timing lines could be obtained on the edge of the film for a check on flutter frequency, independent of the oscillograph records. On some of the sequences there is a record of Mach number at the bottom of each frame, which was recorded optically by a system of mirrors (see Reference 14).

Figure D.4, which was obtained from the high-speed movies, presents quantitatively the time history of the motion of the wing tip for some models at flutter. Measurements were taken from the high-speed films with the aid of a microreader. In general, the straight wings fluttered in bending-torsion; the swept wings sometimes had a small amount of second bending in the flutter mode, while it is difficult to say what modes were involved in the flutter of the delta wings since all the motion was near the tip, and very few cycles were required to damage the models.

Flutter of the bare straight wings was generally very violent, rarely reaching a constant amplitude before destruction; while the bare swept wings usually fluttered at constant amplitude for a number of cycles before the models were badly damaged. (The flutter of the bare swept wing which appears in Figure D.3e was an injection flutter, which was generally very violent, and, in this respect, is not typical of a legitimate flutter for this planform). The delta wings which fluttered were usually so weak that few cycles were required for damage. Flutter of models with tip tanks was always very violent.

A particular type of failure at flutter characterized each

a) STRAIGHT WING WITH AILERON (ST—1b)

b) BARE SWEPT WING (SW—4)

c) BARE DELTA WING

d) STRAIGHT WING WITH TIP TANK (ST—1a)

FIGURE D.5 TYPICAL MODELS AFTER FLUTTER

planform. Figure D.5 shows some typical models after flutter. For the bare straight wings an outboard piece of the wing at the leading edge was lost; for the bare swept wings an entire section of the model just inboard of the wing tip gave way; while for the delta wings a large section of the wing at the trailing edge was destroyed. Wings with ailerons often lost a piece of the aileron trailing edge at flutter, and those with tip tanks were usually totally destroyed. After damage the models often became stable, sometimes fluttering again at a lower Mach number before retraction.

D.5 Tip-Tank Parameters

Tables D.10 and D.11 give pertinent tip-tank parameters for the straight and swept wings, respectively. The total mass of the wing can be obtained by use of equation (D.4). Except for the location of the center of gravity of the tip tank, the models were designed to have constant dimensionless properties including the dimensionless tip-tank moment of inertia in pitch about the wing elastic axis. Some variation in this latter parameter occurred, however, because the tip tanks were designed for a moment of inertia in pitch about an estimated elastic-axis position, for the models were not statically tested until after the design stage. Later, after some research, it was decided that the locus of shear centers was more significant than the measured elastic-axis location. The center of gravity of the tip tank was changed by locating lead weights according to the design procedure outlined in Reference (19) and it was checked experimentally along with the weight and the mass moment of inertia in pitch. Therefore, the geometrical location of the tip tank with respect to the wing was constant for each model, even though the static unbalance of the tip tank varied. In Table D.10 the parameter, $\bar{S}_T$, is tabulated for convenience in

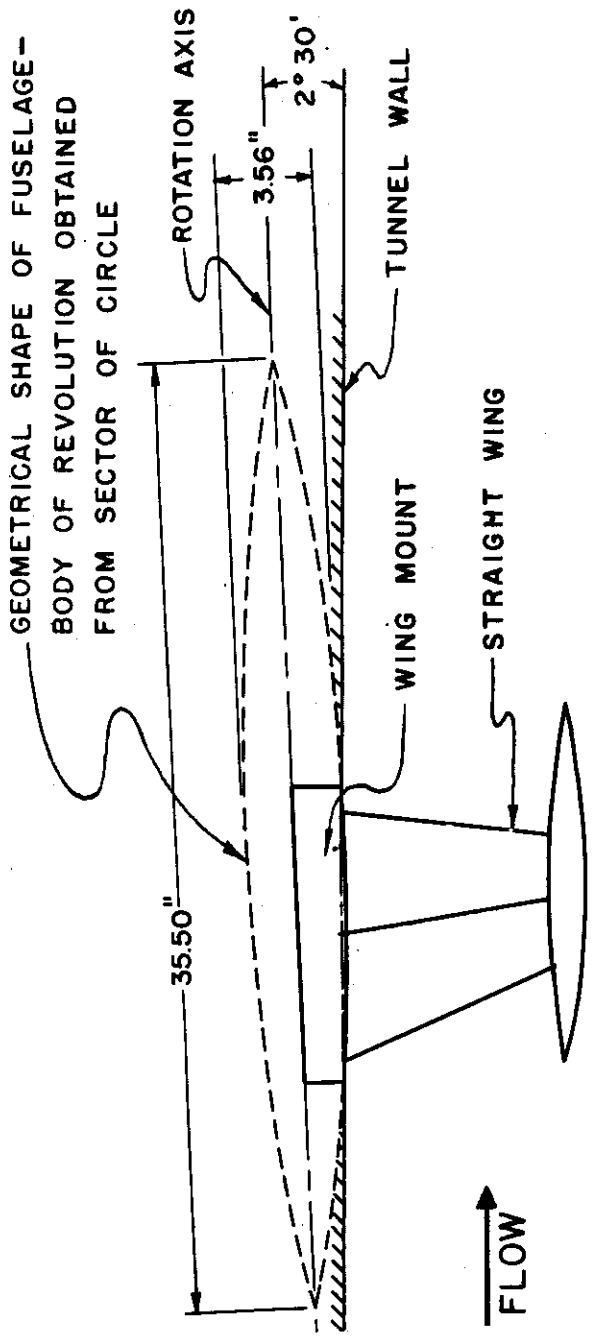

FIGURE D.6 GEOMETRY OF FREE-TO-ROLL MOUNT

using the theory.

For the free-to-roll models a 2 1/2-degree canted hinge was used to aerodynamically stabilize the wing (see Figure D.6). The models were mounted on a simulated fuselage which rolled with the model. Geometric parameters for the fuselage were chosen so as to be typical of supersonic aircraft, and the roll axis corresponded to the centerline of the fuselage. The value of the mass moment of inertia in roll of the root support was chosen so that its value corresponded to a fuselage radius of gyration in roll typical of present-day aircraft. Its value was also checked experimentally.

D.6 Aileron Parameters

Table D.12 gives pertinent aileron parameters for the models tested. In all cases the ailerons had sealed gaps. Again, lead weights were used to obtain the desired mass and inertial characteristics. The aileron was attached to the wing by flexures whose size determined the aileron frequency; no mechanism was used to adjust the aileron frequency from outside the tunnel. In the design of the lead weights, allowance was made for the weight of the flexures so that the dimensionless mass and inertial parameters for the total wing and aileron remained constant at all spanwise stations. Less accuracy is quoted for the elevon parameters of the delta wing (Table 12.b) since the design was complicated by the constant chord of the elevon. For the straight and swept wings, the chord and the thickness of the ailerons tapered linearly to the tip so that the lead weights had to be designed at only one spanwise station, for linear taper to the tip insured the mass variation of equation (D.1) and constant dimensionless parameters. For the delta wings with elevons, the advantages of linear taper are lost, and the lead-weight design must be made at more than one spanwise station.

D.7 Vibration Data

Tables D.14, D.15 and D.16 present nodal lines and structural-damping coefficients for the models tested. Only elastic frequencies are presented; for the free-to-roll models, the first natural frequency is a rigid-body rotation about the roll axis. The nodal lines are approximate, and no attempt was made to obtain mode shapes. The nodal lines were obtained optically with salt while the wing was vibrating at a natural frequency. Nodal areas as well as nodal lines appeared because of the limitation in applied shaking force. All the frequencies quoted are coupled, including those for the models with ailerons, since the ailerons were not clamped with respect to the wings during the shake tests. The first two uncoupled frequencies of all the bare straight wings were calculated from the coupled frequencies and the model parameters. Only the first two natural frequencies were considered. The results show that the first uncoupled frequency is about 1% higher than the first coupled frequency and that the second uncoupled frequency is about 1 1/2% lower than the second coupled frequency.

D.8 Influence Coefficients

Tables D.17 and D.18 and Figures D.7 and D.8 present influence-coefficient matrices with locations for some of the models tested. The influence coefficients were measured with linear variable differential transformers, and their accuracy is estimated at $\pm$ 0.0005 inch/# or less.

D.9 XF-92A Airplane

Table D.19 gives some available experimental data for the XF-92A airplane (References 44-46), since this airplane was used as a guide in designing the delta-wing models.

TABLE D.1

DESIGN DATA FOR STRAIGHT WINGS

Bare Wings

Model	℄ spar % chord	B_o spar inches	H_o spar inches	ρ_{BA} #/in^3	E_{BA} psi	G_{BA} psi
ST-1	41.8	2.721	0.171	0.0045*	8710*	22,300*
ST-1d	37.0	2.721	0.171	0.0052*	9590	29,600
ST-1d-1	37.0	2.721	0.171	0.0052*	9590*	29,600*
ST-2	42.0	0.664	0.251	0.0045*	8710*	22,300*
ST-3	42.0	0.257	0.300	0.0045*	8710*	22,300*
ST-4	42.0	4.214	0.160	0.0043	6380	16,800
ST-4-1	42.0	4.214	0.160	0.0043*	6380*	16,800*
ST-5	42.0	3.141	0.175	0.0041	6750	21,800
ST-5-1	42.0	3.141	0.175	0.0041*	6750*	21,800*
ST-6	42.0	1.049	0.229	0.0048	9510	26,900
ST-7	42.0	0.618	0.252	0.0049	10,700	27,400
ST-7-1	42.0	0.618	0.252	0.0045*	8710*	22,300*
ST-7-2	42.0	0.618	0.252	0.0045*	8710*	22,300*
ST-7-3	42.0	0.618	0.252	0.0045*	8710*	22,300*
ST-8	42.0	0.422	0.266	0.0039	5650	25,200
ST-12	41.8	3.00**	0.200**	0.0045	6720	23,100

Wings with Tip Tanks

Model	℄ spar %chord	B_o spar inches	H_o spar inches	ρ_{BA} #/in^3	E_{BA} psi	G_{BA} psi
ST-1a	42.0	2.721	0.171	0.0045*	8710*	22,300*
ST-1c	37.0	2.721	0.171	0.0030	7800	17,400
ST-4a	42.0	4.214	0.160	0.0039*	7880	19,800
ST-4b	42.0	4.214	0.160	0.0039*	7880	19,800
ST-4c,-1	42.0	4.214	0.160	0.0045*	8710*	22,300*
ST-4c-2	42.0	4.214	0.160	0.0045*	8710*	22,300*
ST-4c-3	42.0	4.214	0.160	0.0045*	8710*	22,300*

Wings with Ailerons

Model	℄ spar % chord	B_o spar inches	H_o spar inches	ρ_{BA} #/in^3	E_{BA} psi	G_{BA} psi
ST-1b	41.8	2.721	0.171	0.0045*	8710*	22,300*
ST-1e	42.0	2.721	0.171	0.0032	11,800	20,400
ST-1f	42.0	2.721	0.171	0.0032	11,800	20,400

*Assumed Balsa Properties

**Built-up rectangular spar; 24ST Alloy, skin thickness at root = 0.023"; Balsa Core; all dimensions tapered linearly to tip

TABLE D.2

DESIGN DATA FOR SWEPT WINGS

Bare Wings

Model	℄ spar % chord	B_o spar inches	H_o spar inches	ρ_{BA} #/in^3	E_{BA} psi	G_{BA} psi
SW-2a	35.2	1.355	0.253	0.0160**	988,500**	162,500**
SW-2a-1	35.2	1.355	0.253	0.0160**	988,500**	162,500**
SW-2b	35.2	1.355	0.253	0.0040*	5700*	16,400*
SW-2b-1	35.2	1.355	0.253	0.0040*	5700*	16,400*
SW-2b-2	35.2	1.355	0.253	0.0040	5700	16,400
SW-3	41.9	0.783	0.292	0.0038	6200	20,000
SW-3-1	41.9	0.783	0.292	0.0052	8800	28,900
SW-3c	36.9	0.783	0.292	0.0055	9900	30,300
SW-3d	46.9	0.783	0.292	0.0053	9050	29,750
SW-4	41.8	0.661	0.246	0.0057	14,500	31,500
SW-5	41.7	0.410	0.306	0.0048	9300	24,000
SW-8	41.8	0.668	0.334	0.0060	12,400	34,900
SW-8-1	41.8	0.668	0.334	0.0060*	12,400*	34,900*

Wings with Tip Tanks

Model	℄ spar % chord	B_o spar inches	H_o spar inches	ρ_{BA} #/in^3	E_{BA} psi	G_{BA} psi
SW-3a	41.9	0.783	0.292	0.0056	10,600	32,000
SW-6	41.9	1.118	0.334	0.0058	12,100	33,600
SW-7	41.8	0.896	0.334	0.0041	8,600	20,000
SW-7a	41.8	0.896	0.334	0.0065	15,300	39,400

Wings with Ailerons

Model	℄ spar % chord	B_o spar inches	H_o spar inches	ρ_{BA} #/in^3	E_{BA} psi	G_{BA} psi
SW-3b	41.9	0.783	0.292	0.0057	10,800	32,600

Note: E for wood measured for bending of the elastic axis
G for wood measured for twisting about the elastic axis

*Estimated balsa properties **Estimated pine properties

TABLE D.3

DESIGN DATA FOR DELTA WINGS

Bare Wings

Model	℄ spar %chord	B_o spar inches	H_o spar inches	ρ_{BA} #/in^3	E_{BA} psi	G_{BA} psi
De-1	50.0	5.00	0.0798	0.0048*	730,000*	25,500*
De-1a	50.0	5.00	0.0798	0.0048*	730,000*	25,500*
De-1a-1	50.0	5.00	0.0798	0.0048*	730,000*	25,500*
De-1a-2	50.0	5.00	0.0798	0.0048*	730,000*	25,500*
De-2	40.0	3.00	0.0500	0.0035	530,000*	17,200*
De-2a-1	40.0	3.00	0.0500	0.0030*	460,000*	14,100*
De-2b	40.0	3.00	0.0500	0.0030*	460,000*	14,100*
De-2c	40.0	3.00	0.0500	0.0030*	460,000*	14,100*
De-2d	40.0	3.00	0.0500	0.0030*	460,000*	14,100*
De-2d-1	40.0	3.00	0.0500	0.0030*	460,000*	14,100*
De-2d-2	40.0	3.00	0.0500	0.0030*	460,000*	14,100*
De-3-1	40.0	2.40	0.0500	0.0045*	690,000*	23,500*
De-3a	40.0	2.40	0.0500	0.0046	700,000*	23,600*
De-3b	40.0	2.40	0.0500	0.0032	490,000*	15,500*
De-3c	40.0	2.40	0.0500	0.0027	410,000*	12,200*
De-3d	26.0	2.40	0.0500	0.0030	460,000*	14,100*
De-3e	40.0	2.40	0.0500	0.0027*	410,000*	12,200*
De-3f	40.0	2.40	0.0500	0.0032*	490,000*	15,500*
De-3f-1	40.0	2.40	0.0500	0.0032*	490,000*	15,500*
De-3g	40.0	2.40	0.0500	0.0046*	700,000*	23,600*
De-3h	40.0	2.40	0.0500	0.0045*	690,000*	23,500*
De-3i	40.0	2.40	0.0500	0.0045*	690,000*	23,500*
De-3j	40.0	2.40	0.0500	0.0027*	410,000*	12,200*
De-4	--	--	--	0.0032	490,000*	15,500*
De-4a	--	--	--	0.0032*	490,000*	15,500*
De-4b	--	--	--	0.0032*	490,000*	15,500*
De-4c	--	--	--	0.0032*	490,000*	15,500*
De-4c-1	--	--	--	0.0032*	490,000*	15,500*
De-5	--	--	--	0.0026	2300	11,700
De-6	--	--	--	0.0026*	2300*	11,700*

Wings with Elevons

Model	℄ spar % chord	B_o spar inches	H_o spar inches	ρ_{BA} #/in^3	E_{BA} psi	G_{BA} psi
De-2e	40.0	3.00	0.0500	0.0044	670,000*	23,000*

*Estimated balsa properties

TABLE D.4

MASS AND STIFFNESS DATA FOR STRAIGHT WINGS

Bare Wings

Model	m_o slugs/in	section c.g. % chord	$r^2_{\alpha .42c}$	$(EI)_o$ x 10^{-6} #-in^2	$(GJ)_o$ x 10^{-6} #-in^2	calc. locus of shear centers % chord	measured elastic axis % chord	Remarks
ST-1	0.00406	50.0	0.250	0.0119	0.0249	42.4	44.5	bare wing
ST-1d	0.00464	50.0	0.250	0.0122	0.0226	37.5	39.3	bare wing, spar forward
ST-1d-1	0.00464	50.0	0.250	0.0112	0.0239	37.5	42.8	rebuilt ST-1d
ST-2	0.00378	50.0	0.250	0.0095	0.0165	42.6	48.5	bare wing
ST-3	0.00447	50.0	0.250	0.0067	0.0103	42.9	48.1	bare wing
ST-4	0.00387	50.0	0.250	0.0150	0.0290	42.4	46.5	bare wing
ST-4-1	0.00401	50.0	0.250	0.0159	0.0307	42.4	44.6	rebuilt ST-4
ST-5	0.00457	50.0	0.250	0.0147	0.0297	42.2	43.7	bare wing
ST-5-1	0.00457	50.0	0.250	0.0146	0.0299	42.2	46.2	rebuilt ST-5
ST-6	0.00433	50.0	0.250	0.0109	0.0187	42.3	51.3	bare wing
ST-7	0.00427	50.0	0.250	0.0098	0.0176	42.4	48.0	bare wing
ST-7-1	0.00427	50.0	0.250	0.0090	0.0171	42.7	46.5	rebuilt ST-7
ST-7-2	0.00427	50.0	0.250	0.0088	0.0155	42.7	43.3	rebuilt ST-7-1
ST-7-3	0.00428	50.0	0.250	0.0049	0.0157	42.7	47.8	rebuilt ST-7-2
ST-8	0.00418	50.0	0.250	0.0079	0.0136	42.3	47.5	bare wing
ST-12	0.00229	50.0	0.250	0.0152	0.0289	42.0	--	low-density bare wing

Wings with Tip Tanks

Model	m_o slugs/in	section c.g. % chord	$r^2_{\alpha .42c}$	$(EI)_o$ x 10^{-6} #-in^2	$(GJ)_o$ x 10^{-6} #-in^2	calc. locus of shear centers % chord	measured elastic axis % chord	Remarks
ST-1a	0.00413	50.0	0.250	0.0116	0.0232	42.5	42.8	bare wing same as ST-1
ST-1c	0.00447	50.0	0.250	0.0120	0.0227	37.4	39.1	bare wing same as ST-1d
ST-4a	0.00406	50.0	0.250	0.0150	0.0280	42.2	47.5	bare wing same as ST-4
ST-4b	0.00406	50.0	0.250	0.0150	0.0280	42.2	47.5	bare wing same as ST-4
ST-4c	0.00387	50.0	0.250	0.0147	0.0303	42.4	49.5	bare wing same as ST-4
ST-4c-1	0.00387	50.0	0.250	0.0199	0.0364	42.4	42.4	rebuilt ST-4c
ST-4c-2	0.00387	50.0	0.250	0.0209	0.0352	42.4	39.9	rebuilt ST-4c-1
ST-4c-3	0.00387	50.0	0.250	0.0194	0.0348	42.4	41.0	rebuilt ST-4c-2

Wings with Ailerons

Model	m_o slugs/in	section c.g. % chord	$r^2_{\alpha .42c}$	$(EI)_o$ x 10^{-6} #-in^2	$(GJ)_o$ x 10^{-6} #-in^2	calc. locus of shear centers % chord	measured elastic axis % chord	Remarks
ST-1b	0.00407	50.0	0.250	0.0128	0.0191	42.4	47.0	same as ST-1 but with aileron
ST-1e	0.00388	50.0	0.250	0.0128	0.0220	42.4	48.0	same as ST-1 but with aileron
ST-1f	0.00388	50.0	0.250	0.0123	0.0219	42.4	41.7	same as ST-1 but with aileron

TABLE D.5

MASS AND STIFFNESS DATA FOR SWEPT WINGS

Bare Wings

Model	m_o slugs/in	section c.g. %chord	$r_{\alpha}^2{}_{.42c}$	$(EI)_o$ x 10^{-6} #-in^2	$(GJ)_o$ x 10^{-6} #-in^2	calc. locus of shear centers % chord	measured elastic axis % chord	Remarks
SW-2a	0.00468	50.0	.306	0.0153	0.0328	45.9	54.2	made of pine, grain perpendicular to the ℄ of wing
SW-2a-1	0.00468	50.0	.306	0.0154	0.0305	45.9	50.0	repaired SW-2a
SW-2b	0.00452	50.0	.375	0.0148	0.0227	35.4	41.2	balsa grain perpendicular to center-line of wing
SW-2b-1	0.00452	50.0	.375	0.0144	0.0211	35.4	41.2	repaired SW-2b
SW-2b-2	0.00455	50.0	.375	0.0133	0.0219	35.4	47.0	repaired SW-2b-1
SW-3	0.00401	50.0	.375	0.0135	0.0163	42.0	47.0	bare wing
SW-3-1	0.00413	50.0	.375	0.0133	0.0199	42.0	50.8	rebuilt SW-3
SW-3c	0.00392	50.0	.375	0.0127	0.0173	37.0	47.5	same as SW-3 but elastic axis forward
SW-3d	0.00398	50.0	.375	0.0140	0.0191	47.0	55.1	same as SW-3 but elastic axis aft
SW-4	0.00406	50.0	.375	0.0074	0.0124	42.0	50.0	bare wing
SW-5	0.00391	50.0	.375	0.0078	0.0095	42.0	52.8	bare wing
SW-8	0.00412	50.0	.375	0.0173	0.0199	42.0	46.0	bare wing
SW-8-1	0.00412	50.0	.375	0.0173	0.0199	42.0	46.0	repaired SW-8 wing

Wings with Tip Tanks

Model	m_o slugs/in	section c.g. %chord	$r_{\alpha}^2{}_{.42c}$	$(EI)_o$ x 10^{-6} #-in^2	$(GJ)_o$ x 10^{-6} #-in^2	calc. locus of shear centers % chord	measured elastic axis % chord	Remarks
SW-3a	0.00406	50.0	.375	0.0130	0.0180	42.0	52.8	same as SW-3 but with tip tank
SW-6	0.00409	50.0	.375	0.0274	0.0343	42.0	47.0	cantilever tip-tank wing
SW-7	0.00391	50.0	.375	0.0221	0.0245	42.0	48.8	cantilever tip-tank wing
SW-7a	0.00406	50.0	.375	0.0213	0.0288	42.0	51.4	free to roll, tip-tank wing

Wings with Ailerons

Model	m_o slugs/in	section c.g. %chord	$r_{\alpha}^2{}_{.42c}$	$(EI)_o$ x 10^{-6} #-in^2	$(GJ)_o$ x 10^{-6} #-in^2	calc. locus of shear centers % chord	measured elastic axis % chord	Remarks
SW-3b	0.00426	50.0	.375	0.0140	0.0203	42.0	51.3	wing with aileron

TABLE D.6

MASS AND STIFFNESS DATA FOR DELTA WINGS

Bare Wings

Model	τ	m_o slugs/in	section c.g. % chord	$r^2_{\alpha,42c}$	calc. locus of shear centers % chord	Remarks
De-1	0.060	0.00427	50.0	0.250	50.0	bare wing
De-1a	0.040	0.00398	50.0	0.250	50.0	same as De-1 but with τ reduced
De-1a-1	0.040	0.00409	50.0	0.250	50.0	rebuilt De-1a
De-1a-2	0.040	0.00409	50.0	0.250	50.0	rebuilt De-1a-1
De-2	0.060	0.00462	50.0	0.250	49.9	bare wing
De-2a-1	0.060	0.00459	50.0	0.250	49.9	bare wing
De-2b	0.060	0.00502	--	--	49.9	same as De-2a-1 with lead added
De-2c	0.050	0.00445	50.0	0.250	49.7	same as De-2a-1 but with τ reduced
De-2d	0.040	0.00430	50.0	0.250	49.5	same as De-2a-1 but with τ reduced
De-2d-1	0.040	0.00470	50.0	0.250	49.5	rebuilt De-2d
De-2d-2	0.040	0.00470	50.0	0.250	49.5	rebuilt De-2d-1
De-3-1	0.060	0.00452	50.0	0.250	49.9	bare wing
De-3a	0.060	0.00455	45.0	0.250	49.9	same as De-3-1 but with c. g. forward
De-3b	0.060	0.00469	55.0	0.250	49.9	same as De-3-1 but with c. g. aft
De-3c	0.060	0.00276	50.0	0.250	49.9	same as De-3-1 but less dense
De-3d	0.060	0.00420	50.0	0.250	49.7	same as De-3-1 but with spar forward
De-3e	0.030	0.00234	50.0	0.250	49.0	same as De-3c but with τ reduced
De-3f	0.040	0.00441	55.0	0.250	49.6	same as De-3b but with τ reduced
De-3f-1	0.040	0.00448	55.0	0.250	49.6	rebuilt De-3f
De-3g	0.050	0.00441	45.0	0.250	49.9	same as De-3a but with τ reduced
De-3h	0.060	0.00499	--	--	49.9	same as De-3-1 but with lead added
De-3i	0.045	0.00430	50.0	0.250	49.8	same as De-3-1 but with τ reduced
De-3j	0.040	0.00231	50.0	0.250	49.6	same as De-3c but with τ reduced
De-4	0.060	0.00336	50.0	0.250	50.0	no spar
De-4a	0.060	0.00381	--	--	50.0	no spar, same as De-4 with lead added
De-4b	0.050	0.00321	50.0	0.250	50.0	no spar, same as De-4 but with τ reduced
De-4c	0.040	0.00307	50.0	0.250	50.0	no spar, same as De-4 but with τ reduced
De-4c-1	0.040	0.00302	50.0	0.250	50.0	rebuilt De-4c
De-5	0.030	0.00438	60.0	0.300	50.0	no spar, balsa grain parallel to root
De-6	0.030	0.00583	60.0	0.300	50.0	same as De-5; 0.004 in. brass shim in mid-plane

Wings with Elevons

Model	τ	m_o slugs/in	section c.g. % chord	$r^2_{\alpha,42c}$	calc. locus of shear centers chord	Remarks
De-2e	0.040	0.00413	50.0	0.250	49.7	aileron wing

[redacted]

TABLE D.7

EXPERIMENTAL FLUTTER DATA FOR STRAIGHT WINGS

Bare Wings

Model	M_f	ω_f cps	v_f ft/sec	μ_f	$\frac{v_f}{b_o\omega_f}$	$\frac{v_f}{b_o\omega_{\alpha_1}}$	ω_{α_1} cps	$\frac{\omega_{h_1}}{\omega_{\alpha_1}}$	$\frac{\omega_{h_2}}{\omega_{\alpha_1}}$	Remarks
ST-1	1.52	85.7	1390	62.2	6.20	3.47	153.0	0.308	1.18	legitimate flutter
ST-1d	1.59	82.7	1480	70.9	6.84	4.02	140.5	0.299	1.20	legitimate flutter
ST-1d-1	1.52	86.2	1400	53.2	6.20	3.77	142.0	0.329	1.22	legitimate flutter
ST-2 *	1.71	110.0	1560	77.0	5.42	5.42	110.0	0.345	1.36	injection flutter
ST-3	1.95	--	--	--	--	--	90.0	0.382	1.51	destroyed during injection
ST-4	1.52	93.7	1420	55.6	5.79	3.25	167.0	0.349	1.30	legitimate flutter
ST-4-1	1.30	98.4	1270	47.2	4.93	2.76	176.0	0.338	1.35	legitimate flutter
ST-5	1.44	83.3	1370	64.9	6.28	3.45	151.7	0.332	1.25	legitimate flutter
ST-5-1	1.47	89.5	1360	54.8	5.80	3.44	151.0	0.351	1.30	legitimate flutter
ST-6	1.72	78.3	1530	76.2	7.46	4.15	140.9	0.363	1.28	legitimate flutter
ST-7	1.91	--	--	--	--	--	128.3	0.368	1.26	destroyed by starting shock
ST-7-1*	1.88	76.9	1620	81.7	8.05	5.48	113.0	0.346	1.31	injection flutter
ST-7-2*	1.92	108.0	1630	83.9	5.76	5.61	111.0	0.396	1.35	injection flutter
ST-7-3	1.94	81.5	1650	72.4	7.73	5.12	123.0	0.359	1.34	legitimate flutter
ST-8	1.90	--	--	--	--	--	108.0	0.410	1.40	destroyed during injection
ST-12	1.45	120.8	1360	27.4	4.30	2.28	228.0	0.315	1.19	legitimate flutter

Wings with Tip Tanks

Model	M_f	ω_f cps	v_f ft/sec	μ_f	$\frac{v_f}{b_o\omega_f}$	$\frac{v_f}{b_o\omega_{\alpha_1}}$	ω_{α_1} cps	$\frac{\omega_{h_1}}{\omega_{\alpha_1}}$	$\frac{\omega_{h_2}}{\omega_{\alpha_1}}$	$\frac{\bar{S}_T}{\frac{S_T}{(mb)_{.70}\ell_{span}}}$	Remarks
ST-1a*	1.80	21.4	1630	75.6	29.1	4.07[1]	153.0	0.308[1]	1.18[1]	0.401	cantilever; injection flutter
ST-1c*	1.83	18.1	1600	89.5	33.8	4.43[1]	138.0	0.319[1]	1.25[1]	0.0506	cantilever; injection flutter
ST-4a	1.43	26.3	1360	53.2	19.8	2.93[1]	177.0	0.323[1]	1.19[1]	-0.511	cantilever; legitimate flutter
ST-4b*	1.83	29.4	1590	79.1	20.7	3.43[1]	177.0	0.323[1]	1.19[1]	1.05	cantilever; injection flutter
ST-4c	1.47	--	1390	52.6	--	3.03[1]	175.0	0.343[1]	1.36[1]	-0.517	free-to-roll; against roll stop during flutter
ST-4c-1	1.33	33.9	1290	59.5	14.5	2.82[1]	175.0[2]	0.343[1,2]	1.36[1,2]	-0.517	free-to-roll; legitimate flutter; flutter mode shape changed from primarily torsion to primarily bending and roll at lower Mach number
ST-4c-2	1.32	30.0	1260	57.5	16.0	2.75[1]	175.0[1,2]	0.343[1,2]	1.36[1,2]	-0.517	
ST-4c-3	1.32	32.7	1280	56.8	15.0	2.79[1]	175.0[1]	0.365[1]	1.34[1]	-0.517	

Wings with Ailerons

Model	M_f	ω_f cps	v_f ft/sec	μ_f	$\frac{v_f}{b_o\omega_f}$	$\frac{v_f}{b_o\omega_{\alpha_1}}$	ω_{α_1} cps	$\frac{\omega_{h_1}}{\omega_{\alpha_1}}$	$\frac{\omega_{h_2}}{\omega_{\alpha_1}}$	$\frac{\omega_\beta}{\omega_{\alpha_1}}$	Remarks
ST-1b*	1.80	200.0	1620	84.0	3.09	3.19	194.0	0.253	--	0.691[3]	aileron free; injection flutter
ST-1e	1.72	87.9	1550	69.9	6.74	4.20	141.0	0.373	1.35	1.49[3]	aileron free; legitimate flutter; three degrees of freedom in flutter mode
ST-1f	1.65	87.5	1500	64.7	6.55	3.89	147.2	0.335	1.30	∞[3]	aileron locked; legitimate flutter

* Injection flutter

1 Based on cantilever frequencies of bare wing (see Table D.14 for further Vibration Data)
2 Data for ST-4c used since these are rebuilt wings
3 Coupled aileron frequency

TABLE D.7a

EXPERIMENTAL FLUTTER DATA FOR STRAIGHT WINGS (Cont.)

Model	$\frac{V_f}{b_{0.75}\omega_f}$	$\frac{V_f}{b_{0.75}\omega_{\alpha_1}}$	$\frac{b_{0.75}\omega_{h1}}{a_f}\sqrt{\left(\frac{\mu_f}{\mu_{rf}}\right)_{0.75}}$
Bare Wings			
ST-1	9.92	5.55	0.268
ST-1d	10.94	6.43	0.258
ST-1d-1	9.92	6.03	0.228
ST-2*	8.67	8.67	0.215
ST-4	9.26	5.20	0.271
ST-4-1	7.89	4.42	0.251
ST-5	10.05	5.52	0.261
ST-5-1	9.28	5.50	0.245
ST-6	11.94	6.64	0.281
ST-7-1*	12.88	8.77	0.241
ST-7-2*	9.22	8.98	0.243
ST-7-3	12.37	8.19	0.250
ST-12	6.88	3.65	0.258
Wings with Tip Tanks			
ST-1a*	46.6	6.51(1)	--
ST-1c*	54.1	7.09(1)	--
ST-4a	31.7	4.69(1)	--
ST-4b*	33.1	5.49(1)	--
ST-4c	--	4.85(1)	--
ST-4c-1	23.2	4.51(1)	--
ST-4c-2	25.6	4.40(1)	--
ST-4c-3	24.0	4.46(1)	--
Wings with Ailerons			
ST-1b*	4.94	5.10	--
ST-1e	10.8	6.72	--
ST-1f	10.5	6.22	0.264

* Injection Flutter

TABLE D.8

EXPERIMENTAL FLUTTER DATA FOR SWEPT WINGS

Bare Wings

Model	M_f	ω_f cps	v_f ft/sec	μ_f	$\frac{v_f}{b_o\omega_f}$	$\frac{v_f}{b_o\omega_{\alpha_1}}$	ω_{α_1} cps	$\frac{\omega_{h_1}}{\omega_{\alpha_1}}$	$\frac{\omega_{h_2}}{\omega_{\alpha_1}}$	Remarks
SW-2a	1.84-1.46	--	--	97-63	--	--	225	0.169	0.654	no flutter
SW-2a-1	1.79-1.32	--	--	74-50	--	--	217	0.162	0.608	no flutter
SW-2b	1.75-1.34	--	--	86-56	--	--	140	0.224	0.743	no flutter
SW-2b-1	1.73-1.34	--	--	82-54	--	--	137	0.228	0.796	no flutter
SW-2b-2	1.48-1.28	--	--	76-53	--	--	140	0.222	0.793	no flutter
SW-3	1.41	111	1340	51.9	4.61	3.88	132	0.254	0.902	legitimate flutter
SW-3-1+	1.26	100	1240	53.1	4.74	3.24	146	0.234	0.822	retraction flutter
SW-3c	1.48	110	1390	63.4	4.83	3.93	135	0.255	0.844	legitimate flutter
SW-3d	1.25	116	1230	50.5	4.05	3.43	137	0.258	0.927	legitimate flutter
SW-4*	1.85	90.4	1620	84.3	6.85	5.11	121	0.225	0.807	injection flutter
SW-5*	1.87	77.8	1630	78.2	8.00	5.51	113	0.247	0.870	injection flutter
SW-8	1.62-1.26	--	--	76-53	--	--	150	0.252	0.853	no flutter, first test
SW-8*	1.62	116	1470	58.9	4.84	3.74	150	0.252	0.853	rerun SW-8 at lower μ; injection flutter
SW-8-1	1.42	120	1330	49.5	4.23	3.48	146	0.255	0.856	legitimate flutter

Wings with Tip Tanks

Model	M_f	ω_f cps	v_f ft/sec	μ_f	$\frac{v_f}{b_o\omega_f}$	$\frac{v_f}{b_o\omega_{\alpha_1}}$	ω_{α_1} cps	$\frac{\omega_{h_1}}{\omega_{\alpha_1}}$	$\frac{\omega_{h_2}}{\omega_{\alpha_1}}$	Remarks
SW-3a*	1.92	35.5	1650	87.6	17.8	4.35[1]	145[1]	0.240[1]	0.828[1]	cantilever;injection flutter
SW-6	1.30	31.2	1260	45.0	15.4	2.55[1]	189[1]	0.277[1]	0.799[1]	cantilever;legitimate flutter
SW-7	1.44	30.0	1350	48.6	17.2	3.20[1]	161[1]	0.315[1]	0.845[1]	cantilever;legitimate flutter
SW-7a	1.92	24.4	1630	79.8	25.5	3.64[1]	171[1]	0.295[1]	0.871[1]	free-to-roll;legitimate flutter

Wings with Ailerons

Model	M_f	ω_f cps	v_f ft/sec	μ_f	$\frac{v_f}{b_o\omega_f}$	$\frac{v_f}{b_o\omega_{\alpha_1}}$	ω_{α_1} cps	$\frac{\omega_{h_1}}{\omega_{\alpha_1}}$	$\frac{\omega_{h_2}}{\omega_{\alpha_1}}$	$\frac{\omega_\beta}{\omega_{\alpha_1}}$	Remarks
SW-3b	1.47	114	1370	53.6	4.59	3.55	147.6	0.237	0.885	1.00[2]	aileron frequency taken same as first torsion; legitimate flutter; very little aileron motion in flutter mode

* Injection flutter
\+ Retraction flutter
1 Based on cantilever frequencies of bare wing (see Table D.15 for further vibration data)
2 Coupled aileron frequency

TABLE D.8a

EXPERIMENTAL FLUTTER DATA FOR SWEPT WINGS (Cont.)

Model	$\frac{V_f}{b_{0.75}\omega_f}$	$\frac{V_f}{b_{0.75}\omega_{\alpha_1}}$	$\frac{b_{0.75}\omega_{\alpha_1}}{a_f}\sqrt{\left(\frac{\mu_f}{\mu_{ref}}\right)_{0.75}}$
Bare Wings			
SW-3	8.38	7.05	0.179
SW-3-1+	8.62	5.89	0.193
SW-3c	8.78	7.14	0.204
SW-3d	7.36	6.24	0.177
SW-4*	12.45	9.29	0.227
SW-5*	14.54	10.02	0.205
SW-8*	8.80	6.80	0.227
SW-8-1	7.69	6.33	0.196
Wings with Tip Tanks			
SW-3a*	32.4	7.91	--
SW-6	28.0	4.64	--
SW-7	31.3	5.82	--
SW-7a	46.4	6.62	--
Wings with Ailerons			
SW-3b	8.34	6.45	0.204

* Injection Flutter
\+ Retraction Flutter

TABLE D.9

EXPERIMENTAL FLUTTER DATA FOR DELTA WINGS

Bare Wings

Model	M_f	ω_f cps	v_f ft/sec	μ_f	$\frac{v_f}{b_o\omega_f}$	$\frac{v_f}{b_o\omega_{\alpha_1}}$	ω_{α_1} cps	$\frac{\omega_{h_1}}{\omega_{\alpha_1}}$	$\frac{\omega_{h_2}}{\omega_{\alpha_1}}$	Remarks
De-1	1.72-1.32	--	--	86-72	--	--	361	0.346	--	no flutter
De-1a+	1.26	305	1220	40.9	1.53	1.49	313 Est.	0.307 Est.	0.821 Est.	retraction flutter
De-1a-1*	1.49	345	1400	72.0	1.55	1.71	313	0.345	0.891	injection flutter
De-1a-2*	1.92	260	1630	80.3	2.39	2.10	297	0.316	0.875	injection flutter
De-2	1.72-1.41	--	--	90-67	--	--	320	0.419	1.10	no flutter
De-2a-1	1.80-1.26	--	--	98-57	--	--	310	0.471	1.39	no flutter
De-2b	1.85-1.27	--	--	98-54	--	--	337	0.475	1.25	no flutter
De-2c	1.92-1.26	--	--	98-49	--	--	283	0.477	1.27	no flutter
De-2d	1.34	138	1290	48.7	3.57	2.19	225	0.340	1.22	legitimate flutter
De-2d-1	1.62-1.26	--	--	86-58	--	--	240	0.463	1.23	no flutter
De-2d-2	1.30	190	1260	50.4	2.53	2.04	236	0.445	1.22	same as De-2d-1 but at lower μ; legitimate flutter
De-3-1	1.82-1.28	--	--	93-55	--	--	318	0.712	1.87	no flutter
De-3a	1.86-1.37	--	--	93-57	--	--	320	0.459	1.24	no flutter
De-3b	1.87-1.33	--	--	98-61	--	--	362	0.486	1.29	no flutter
De-3c	1.84-1.43	--	--	55-40	--	--	357	0.448	1.24	no flutter
De-3d	1.79-1.61	--	--	84-68	--	--	302	0.384	1.06	no flutter
De-3e*	1.80	167	1590	47.2	3.64	2.92	208	0.385	1.15	injection flutter
De-3f	1.80	132	1590	80.4	4.60	2.89	210	0.407	1.21	legitimate flutter
De-3f-1*	1.90	172	1620	86.5	3.60	2.60	238	0.399	1.08	injection flutter
De-3g	1.90	--	--	--	--	--	286	0.479	1.22	model destroyed by starting shock
De-3h	1.84-1.26	--	--	100-55	--	--	333	0.411	1.15	no flutter
De-3i	1.92	--	--	--	--	--	280	0.421	1.19	model destroyed by starting shock
De-3j*	1.92	343	1620	45.0	1.80	2.45	253	0.415	1.19	injection flutter
De-4	1.84-1.36	--	--	69-44	--	--	310	0.506	1.25	no flutter
De-4a	1.90-1.26	--	--	94-44	--	--	314	0.458	1.23	no flutter
De-4b	1.90	--	--	--	--	--	275	0.484	1.20	model destroyed by starting shock
De-4c	1.67	225	1510	50.1	2.56	2.50	231	0.437	1.18	legitimate flutter
De-4c-1	1.46	200	1350	42.6	2.58	2.21	233	0.455	1.22	legitimate flutter
De-5*	1.80	163	1590	86.0	3.73	3.23	188	0.247	0.718	injection flutter
De-6*	1.92	784	1630	113.5	7.94	4.83	129	0.355	0.868	injection flutter

Wings with Elevons

Model	M_f	ω_f cps	v_f ft/sec	μ_f	$\frac{v_f}{b_o\omega_f}$	$\frac{v_f}{b_o\omega_{\alpha_1}}$	ω_{α_1} cps	$\frac{\omega_{h_1}}{\omega_{\alpha_1}}$	$\frac{\omega_{h_2}}{\omega_{\alpha_1}}$	$\frac{\omega_\beta}{\omega_{\alpha_1}}$	Remarks
De-2e *	1.92	273	1620	81.1	2.27	2.77	223	0.695	1.12	1.42[1]	aileron buzz throughout run

*Injection flutter
+Retraction flutter
(1) Coupled aileron frequency

TABLE D.9a

EXPERIMENTAL FLUTTER DATA FOR DELTA WINGS (Cont.)

Model	$\frac{v_f}{b_{0.75}\, f}$	$\frac{v_f}{b_{0.75}\, 1}$	$\frac{b_{0.75}\,\omega_\alpha}{a_f}\sqrt{\left(\frac{\mu_t}{\mu_{nt}}\right)_{0.75}}$
Bare Wings			
De-1a+	6.12	5.96	---
De-1a-1*	6.20	6.84	---
De-1a-2*	9.56	8.40	---
De-2d	14.28	8.76	0.132
De-2d-2	10.12	8.16	0.141
De-3e*	14.56	11.68	0.131
De-3f	18.40	11.56	0.172
De-3f-1*	14.40	10.40	0.211
De-3j*	7.20	9.80	0.164
De-4c	10.24	10.00	0.147
De-4c-1	10.32	8.84	0.133
De-5*	14.92	12.92	0.160
De-6*	31.76	19.32	0.132
Wings with Elevons			
De-2e*	9.08	11.08	---

* Injection Flutter

\+ Retraction Flutter

TABLE D.10

TIP-TANK PARAMETERS FOR STRAIGHT WINGS

Model	m_o slugs/in	$\frac{M_T}{M_W}$	$(c.g.)_T$ % wing tip chord	$\frac{(r_{\alpha_{c.g._T}}^2)}{\frac{(I_{c.g.})_T}{M_T(b_T)^2}}$	calc. locus of shear centers % chord	$\frac{\bar{S}_T}{\frac{S_T}{(mb)\ell}}$ .70 span
ST-1a	0.00413	1.40	56.0	0.155	42.5	0.401
ST-1c	0.00447	1.40	39.1	0.149	37.4	0.0506
ST-4a	0.00406	1.40	25.0	0.133	42.2	-0.511
ST-4b	0.00406	1.40	77.5	0.0977	42.2	1.05
ST-4c**	0.00387	1.40	25.0	0.131	42.4	-0.517
ST-4c-1**	0.00387	1.40	25.0	0.131	42.4	-0.517
ST-4c-2**	0.00387	1.40	25.0	0.131	42.4	-0.517
ST-4c-3**	0.00387	1.40	25.0	0.131	42.4	-0.517

*about calc. locus of shear centers

**free-to-roll, $I_S = 0.00150$ slug-ft^2

Geometrical shape - body of revolution obtained from sector of circle

Tip tank symmetrically located at wing tip chord

Fineness ratio = 0.10

$\frac{\text{length tip tank}}{\text{wing tip chord}} = 3$

TABLE D.11

TIP-TANK PARAMETERS FOR SWEPT WINGS

Model	m_o slugs/in	$\frac{M_T}{M_W}$	$(c.g.)_T$ % wing tip chord	$\frac{(r^2_{c.g.})_T}{M_T(b_T)^2}$	calc. locus of shear centers % chord	$\frac{\bar{S}_T}{S_T}$ $(\overline{mb})$ .70 span
SW-3a	0.00406	1.40	25.0	0.116	42.0	-0.51
SW-6	0.00409	1.39	25.0	0.128	42.0	-0.51
SW-7	0.00391	1.45	25.0	0.125	42.0	-0.53
SW-7a*	0.00406	1.40	25.0	0.119	42.0	-0.51

*free-to-roll, I_S = 0.00150 slug-ft^2

Geometrical shape - body of revolution obtained from sector of circle

Tip tank symmetrically located at wing tip chord

Fineness ratio = 0.10

$\frac{\text{length tip tank}}{\text{wing tip chord}}$ = 3

[redacted]

TABLE D.12		
AILERON PARAMETERS FOR STRAIGHT AND SWEPT WINGS		
Model	Half-span aileron (outboard)	
ST-1b ST-1e ST-1f SW-3b	Aileron hinge line	80.0% of wing chord (no aerodynamic balance)
	Ratio of aileron mass per unit span to total wing mass per unit span	0.100
	Aileron center of gravity in per cent of aileron chord	30.0%
	Aileron radius of gyration about aileron hinge line in per cent of aileron chord	45.0%

TABLE D.13		
ELEVON PARAMETERS FOR DELTA WINGS		
Model	Full-span elevon, constant chord, no aerodynamic balance	
De-2e	Elevon hinge line	perpendicular to root, 14.0% of wing root chord
	Ratio of average elevon mass per unit span to average total wing mass per unit span	0.10
	Elevon center of gravity in per cent of elevon chord	33%
	Elevon radius of gyration about elevon hinge line in per cent of elevon chord	45%

[redacted]

TABLE D.14

EXPERIMENTAL VIBRATION DATA FOR STRAIGHT WINGS

MODEL	ST—1	ST—1d	ST—1d—1
FIRST NATURAL FREQUENCY	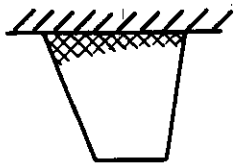 ω = 47.1 g = .006	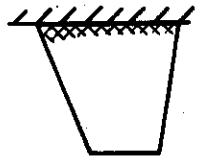 ω = 42.0 g = .008	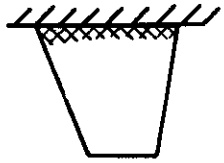 ω = 46.7 g = .031
SECOND NATURAL FREQUENCY	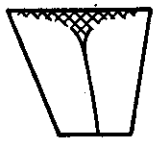 ω = 153 g = .007	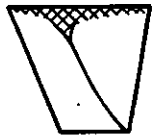 ω = 140.5 g = .007	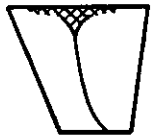 ω = 142 g = .015
THIRD NATURAL FREQUENCY	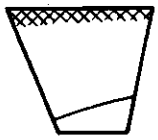 ω = 181 g = .007	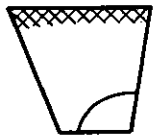 ω = 168 g = .007	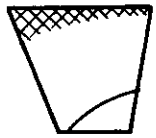 ω = 173 g = .013
FOURTH NATURAL FREQUENCY			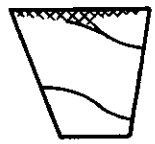 ω = 300 g = .019

▨ NULL AREAS ω = cps.

[redacted]

TABLE D.14 (CONT.)

EXPERIMENTAL VIBRATION DATA FOR STRAIGHT WINGS

MODEL	ST—2	ST—3	ST—4
FIRST NATURAL FREQUENCY	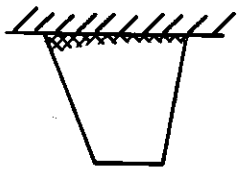 ω = 38.00 g = .015	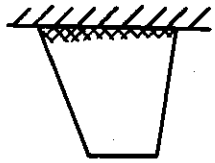 ω = 34.38 g = .018	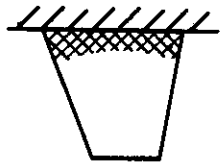 ω = 57.6 g = .011
SECOND NATURAL FREQUENCY	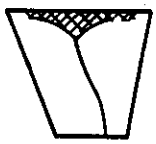 ω = 110 g = .012	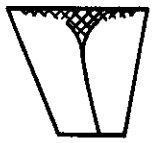 ω = 90.0 g = .010	 ω = 167 g = .008
THIRD NATURAL FREQUENCY	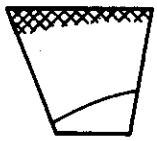 ω = 150 g = .010	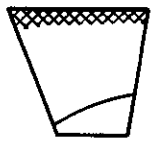 ω = 136 g = .019	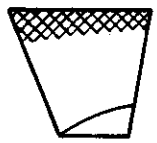 ω = 217 g = .008
FOURTH NATURAL FREQUENCY	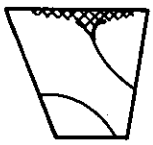 ω = 235 g = .012	NO NODAL LINES AVAILABLE 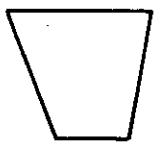 ω = 204 g = .008	

NULL AREAS ω = cps.

TABLE D.14 (CONT.)

EXPERIMENTAL VIBRATION DATA FOR STRAIGHT WINGS

MODEL	ST—4—1	ST—5	ST—5—1
FIRST NATURAL FREQUENCY	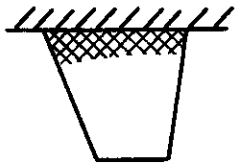 ω = 59.5 g = .018	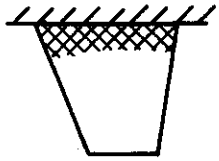 ω = 50.3 g = .012	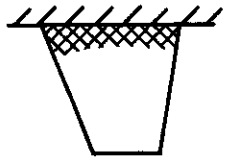 ω = 53.0 g = .010
SECOND NATURAL FREQUENCY	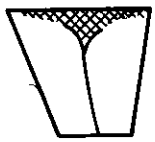 ω = 176 g = .013	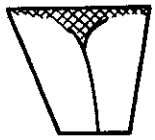 ω = 151.7 g = .009	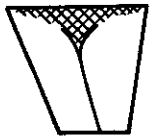 ω = 151 g = .008
THIRD NATURAL FREQUENCY	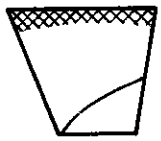 ω = 237 g = .021	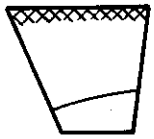 ω = 189 g = .011	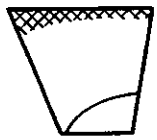 ω = 195 g = .008
FOURTH NATURAL FREQUENCY		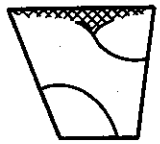 ω = 302 g = .013	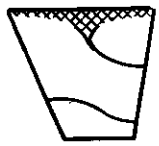 ω = 296 g = .009

▩ NULL AREAS ω = cps.

TABLE D.14 (CONT)

EXPERIMENTAL VIBRATION DATA FOR STRAIGHT WINGS

MODEL	ST—6	ST—7	ST—7—1
FIRST NATURAL FREQUENCY	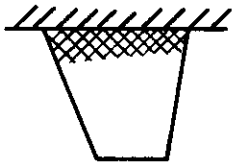 ω = 51.2 g = .027	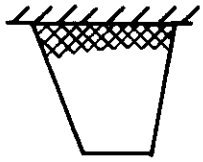 ω = 47.2 g = .044	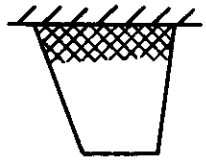 ω = 39.1 g = .036
SECOND NATURAL FREQUENCY	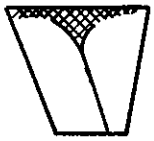 ω = 140.9 g = .011	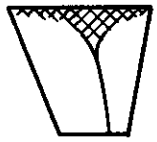 ω = 128.3 g = .014	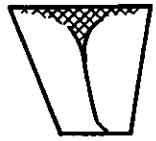 ω = 113 g = .017
THIRD NATURAL FREQUENCY	 ω = 181 g = .015	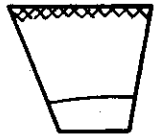 ω = 162 g = .019	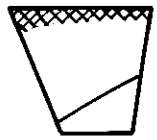 ω = 148 g = .014
FOURTH NATURAL FREQUENCY	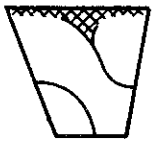 ω = 300 g = .017	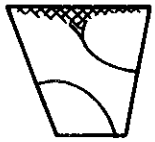 ω = 270 g = .014	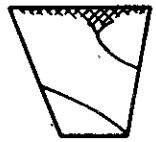 ω = 220 g = .017

NULL AREAS ω = cps.

TABLE D.14 (CONT.)

EXPERIMENTAL VIBRATION DATA FOR STRAIGHT WINGS

MODEL	ST-7-2	ST-7-3	ST-8
FIRST NATURAL FREQUENCY	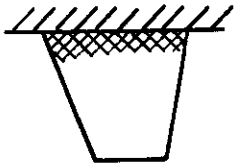 ω = 44.0 g = .056	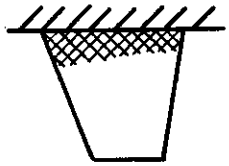 ω = 44.2 g = .018	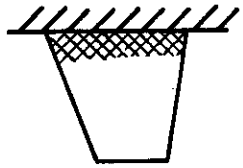 ω = 44.3 g = .055
SECOND NATURAL FREQUENCY	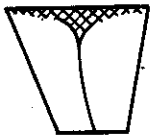 ω = 111 g = .016	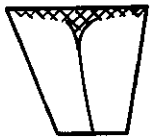 ω = 123 g = .016	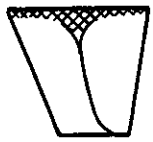 ω = 108 g = .015
THIRD NATURAL FREQUENCY	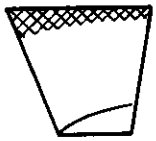 ω = 150 g = .017	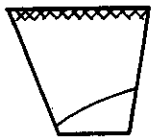 ω = 165 g = .022	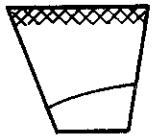 ω = 151.3 g = .012
FOURTH NATURAL FREQUENCY		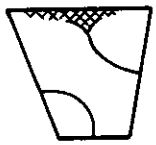 ω = 265 g = .026	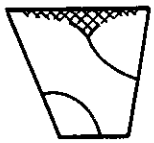 ω = 241 g = .017

▨ NULL AREAS ω = cps.

TABLE D.14 (CONT.)

EXPERIMENTAL VIBRATION DATA FOR STRAIGHT WINGS

MODEL	ST—12	ST—1a CANTILEVER	ST—1a CANTILEVER
FIRST NATURAL FREQUENCY	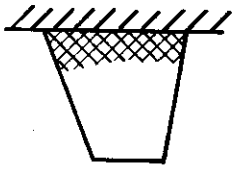 ω = 71.8 g = .024	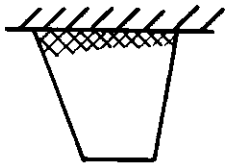 ω = 47.1 g = .006	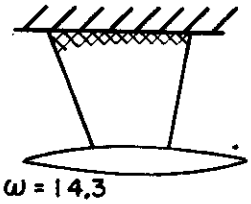 ω = 14.3 g = .009
SECOND NATURAL FREQUENCY	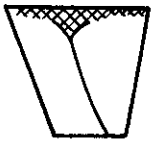 ω = 228 g = .014	 ω = 153 g = .007	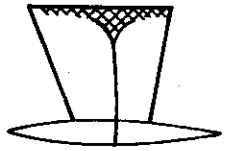 ω = 31.0 g = .017
THIRD NATURAL FREQUENCY	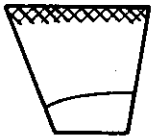 ω = 272 g = .022	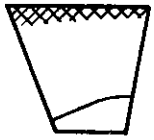 ω = 181 g = .007	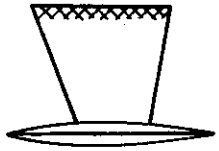 ω = 125 g = .007
FOURTH NATURAL FREQUENCY			NO NODAL LINES AVAILABLE 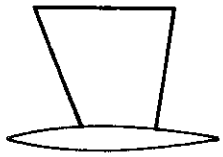 ω = 235 g = .004

▨ NULL AREAS ω = cps.

TABLE D.14 (CONT.)

EXPERIMENTAL VIBRATION DATA FOR STRAIGHT WINGS

MODEL	ST—1c CANTILEVER	ST—1c CANTILEVER	ST—4a CANTILEVER
FIRST NATURAL FREQUENCY	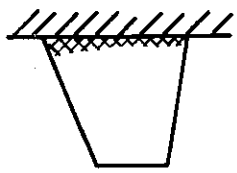 ω = 44.0 g = .012	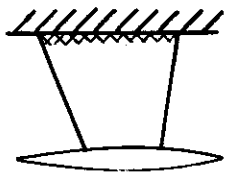 ω = 13.82 g = .012	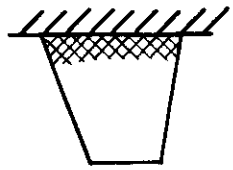 ω = 57.1 g = .017
SECOND NATURAL FREQUENCY	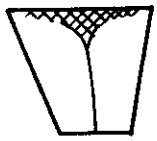 ω = 138 g = .015	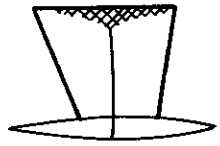 ω = 28.04 g = .014	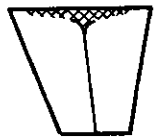 ω = 177 g = .007
THIRD NATURAL FREQUENCY	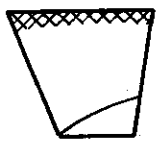 ω = 172 g = .010	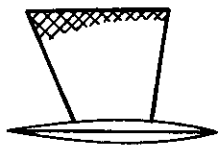 ω = 106.8 g = .012	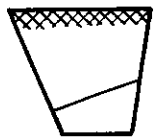 ω = 211 g = .009
FOURTH NATURAL FREQUENCY	NO NODAL LINES AVAILABLE 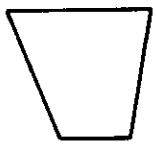 ω = 265 g = .009	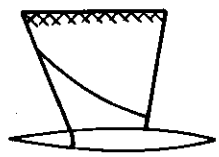 ω = 196 g = .007	

NULL AREAS ω = cps.

TABLE D.14 (CONT.)

EXPERIMENTAL VIBRATION DATA FOR STRAIGHT WINGS

MODEL	ST—4a CANTILEVER	ST—4b CANTILEVER	ST—4b CANTILEVER
FIRST NATURAL FREQUENCY	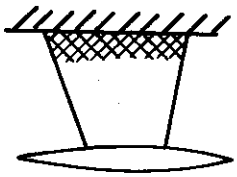 ω = 16.23 g = .006	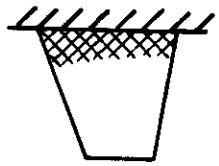 ω = 57.1 g = .017	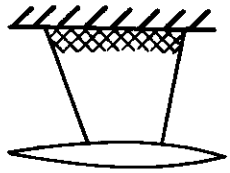 ω = 14.41 g = .012
SECOND NATURAL FREQUENCY	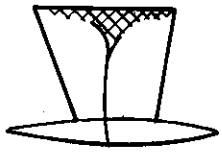 ω = 35.6 g = .006	 ω = 177 g = .007	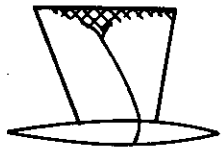 ω = 45.7 g = .014
THIRD NATURAL FREQUENCY	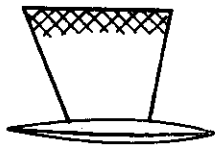 ω = 137.2 g = .006	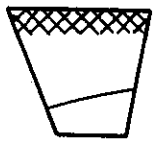 ω = 211 g = .009	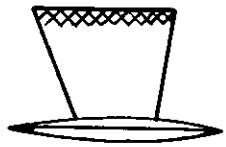 ω = 138 g = .010
FOURTH NATURAL FREQUENCY	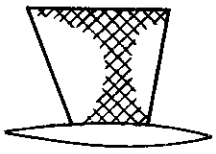 ω = 254 g = .005		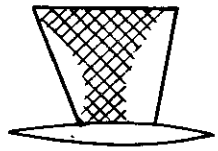 ω = 244 g = .006

▨ NULL AREAS ω = cps.

TABLE D.14 (CONT.)

EXPERIMENTAL VIBRATION DATA FOR STRAIGHT WINGS

MODEL	ST—4c CANTILEVER	ST—4c CANTILEVER	ST—4c FREE TO ROLL
FIRST NATURAL FREQUENCY	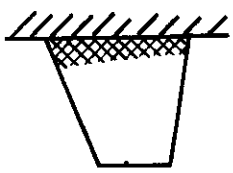 ω = 60.00 g = .007	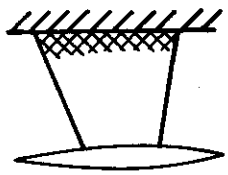 ω = 16.46 g = .013	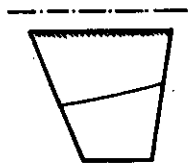 ω = 100 g = .006
SECOND NATURAL FREQUENCY	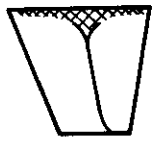 ω = 175 g = .008	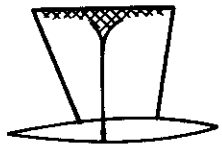 ω = 39.4 g = .014	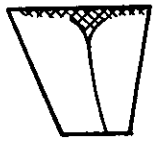 ω = 176 g = .005
THIRD NATURAL FREQUENCY	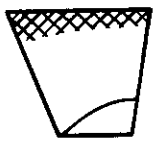 ω = 238 g = .015	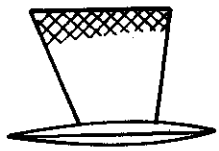 ω = 144 g = .026	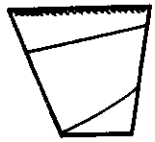 ω = 254 g = .008
FOURTH NATURAL FREQUENCY			

NULL AREAS ω = cps.

TABLE D.14 (CONT.)

EXPERIMENTAL VIBRATION DATA FOR STRAIGHT WINGS

MODEL	ST—4c FREE TO ROLL	ST—4c—1 FREE TO ROLL	ST—4c—1 FREE TO ROLL
FIRST NATURAL FREQUENCY	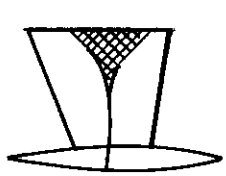 ω = 35.8 g = .009	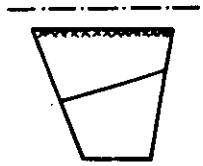 ω = 101 g = .010	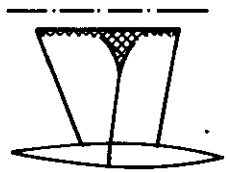 ω = 36.45 g = .012
SECOND NATURAL FREQUENCY	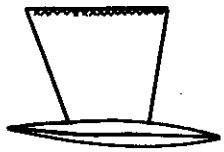 ω = 54.5 g = .008	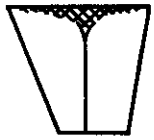 ω = 176 g = .010	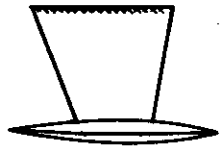 ω = 55.6 g = .011
THIRD NATURAL FREQUENCY	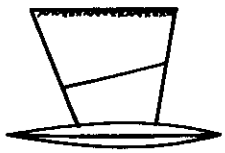 ω = 170 g = .005	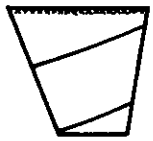 ω = 264 g = .008	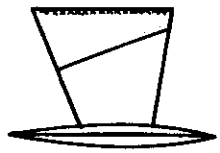 ω = 178 g = .005
FOURTH NATURAL FREQUENCY	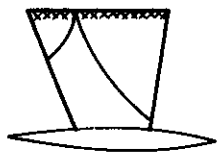 ω = 242 g = .005		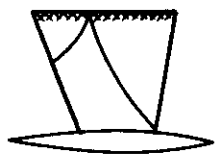 ω = 250 g = .008

▨ NULL AREAS ω = cps.

TABLE D.14 (CONT.)

EXPERIMENTAL VIBRATION DATA FOR STRAIGHT WINGS

MODEL	ST—4c—2 FREE TO ROLL	ST—4c—2. FREE TO ROLL	ST—4c—3 CANTILEVER
FIRST NATURAL FREQUENCY	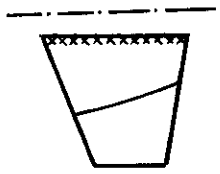 ω = 99.0 g = .010	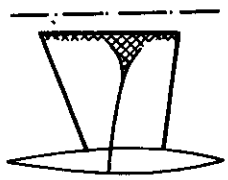 ω = 34.8 g = .018	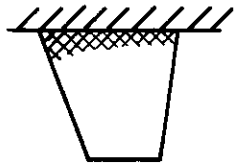 ω = 63.8 g = .026
SECOND NATURAL FREQUENCY	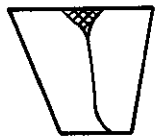 ω = 174 g = .008	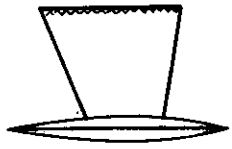 ω = 55.3 g = .015	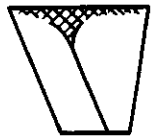 ω = 175 g = .010
THIRD NATURAL FREQUENCY	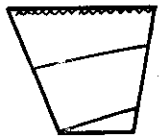 ω = 262 g = .007	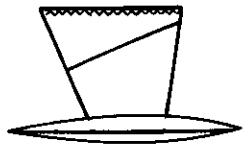 ω = 172 g = .008	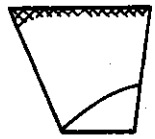 ω = 235 g = .013
FOURTH NATURAL FREQUENCY		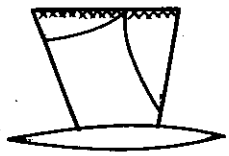 ω = 246 g = .006	 ω = 333 g = .014

NULL AREAS ω = cps.

TABLE D.14 (CONT.)

EXPERIMENTAL VIBRATION DATA FOR STRAIGHT WINGS

MODEL	ST—4c—3 CANTILEVER	ST—4c—3 FREE TO ROLL	ST—4c—3 FREE TO ROLL
FIRST NATURAL FREQUENCY	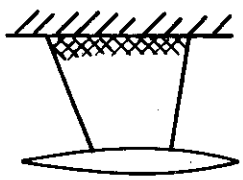 ω = 20.45 g = .003	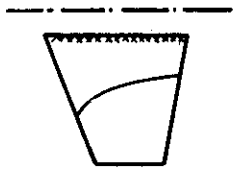 ω = 100.0 g = .014	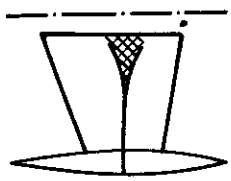 ω = 36.5 g = .012
SECOND NATURAL FREQUENCY	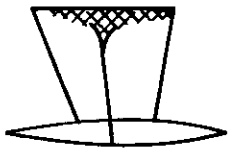 ω = 35.88 g = .014	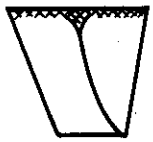 ω = 175 g = .006	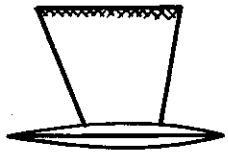 ω = 58.3 g = .010
THIRD NATURAL FREQUENCY	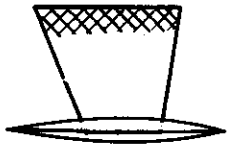 ω = 144 g = .026	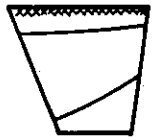 ω = 253 g = .009	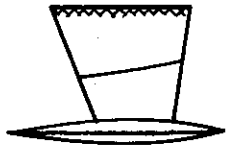 ω = 175. g = .008
FOURTH NATURAL FREQUENCY	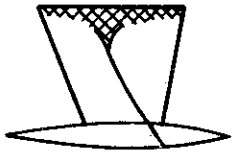 ω = 247 g = .014		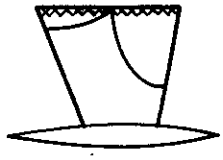 ω = 247 g = — —

▨ NULL AREAS ω = cps.

TABLE D.14 (CONT.)

EXPERIMENTAL VIBRATION DATA FOR STRAIGHT WINGS

MODEL	ST—1b AILERON	ST—1e AILERON	ST—1f AILERON LOCKED
FIRST NATURAL FREQUENCY	WING UNCLAMPED 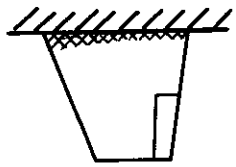 ω = 49.07 g = .010	WING UNCLAMPED 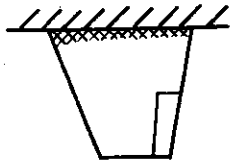 ω = 52.6 g = .029	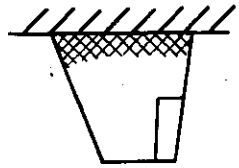 ω = 49.3 g = .016
SECOND NATURAL FREQUENCY	AILERON MODE 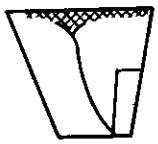 ω = 134 g = .009	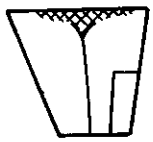 ω = 141 g = .007	 ω = 147.2 g = .013
THIRD NATURAL FREQUENCY	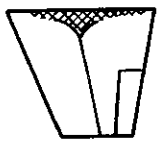 ω = 194 g = .008	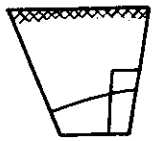 ω = 190 g = .008	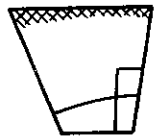 ω = 192 g = .014
FOURTH NATURAL FREQUENCY		AILERON MODE NO NODAL LINES AVAILABLE 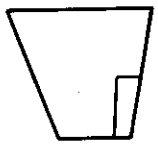 ω = 210 g = — —	

NULL AREAS ω = cps.

[redacted]

TABLE D.15

EXPERIMENTAL VIBRATION DATA FOR SWEPT WINGS

MODEL	SW — 2a	SW — 2a — 1	SW — 2b
FIRST NATURAL FREQUENCY	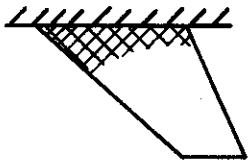 ω = 37.5 g = .015	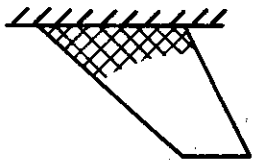 ω = 35.2 g = .016	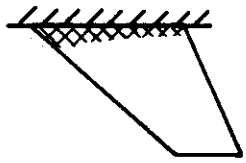 ω = 31.4 g = .013
SECOND NATURAL FREQUENCY	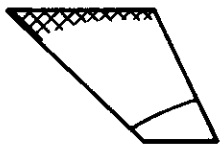 ω = 140.2 g = .004	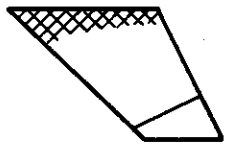 ω = 132 g = .012	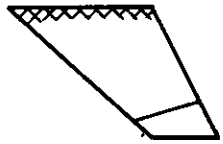 ω = 104 (EST.) g = ---
THIRD NATURAL FREQUENCY	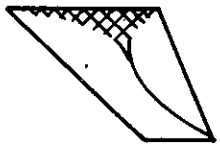 ω = 225 g = .005	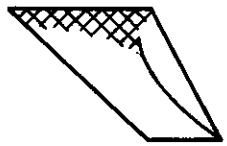 ω = 217 g = .014	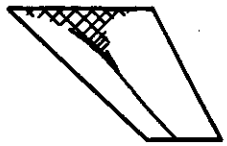 ω = 140 (EST.) g = ---

▩ NULL AREAS ω = cps.

[redacted]

TABLE D.15 (CONT.)

EXPERIMENTAL VIBRATION DATA FOR SWEPT WINGS

MODEL	SW—3—1	SW—3c	SW—3d
FIRST NATURAL FREQUENCY	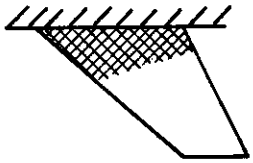 ω = 34.1 g = .042	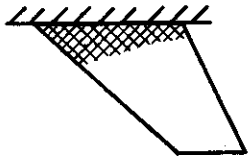 ω = 34.5 g = .044	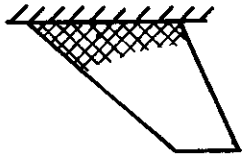 ω = 35.3 g = .034
SECOND NATURAL FREQUENCY	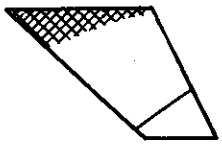 ω = 120 g = .014	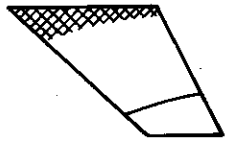 ω = 114 g = .014	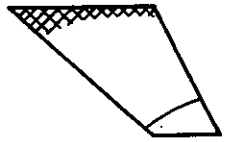 ω = 127 g = .013
THIRD NATURAL FREQUENCY	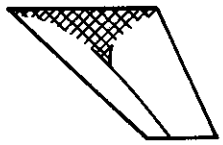 ω = 146 g = .013	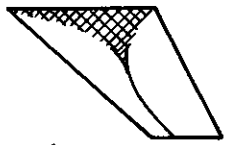 ω = 135 g = .010	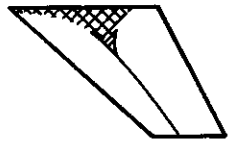 ω = 137 g = .009
FOURTH NATURAL FREQUENCY	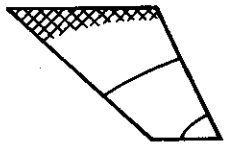 ω = 241 g = .017	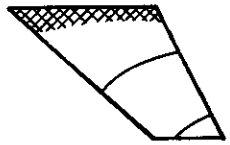 ω = 218 g = .019	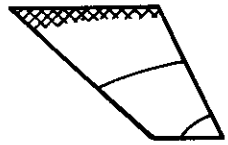 ω = 255 g = .017
FIFTH NATURAL FREQUENCY		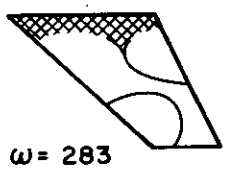 ω = 283 g = .011	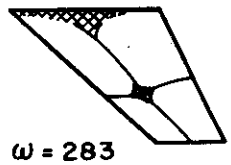 ω = 283 g = .009

NULL AREAS ω = cps.

TABLE D.15 (CONT.)

EXPERIMENTAL VIBRATION DATA FOR SWEPT WINGS

MODEL	SW-2b-1	SW-2b-2	SW-3
FIRST NATURAL FREQUENCY	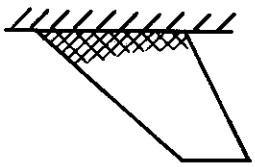 ω = 31.2 g = .007	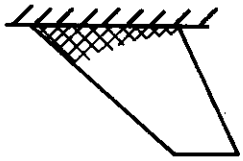 ω = 31.2 g = .015	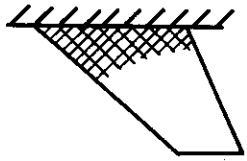 ω = 33.5 g = .020
SECOND NATURAL FREQUENCY	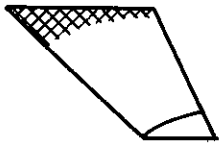 ω = 109 g = .006	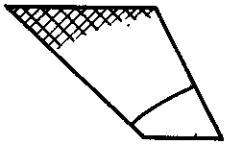 ω = 111 g = ---	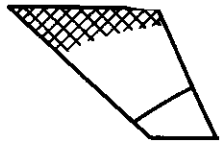 ω = 119 g = .013
THIRD NATURAL FREQUENCY	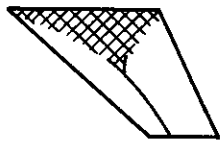 ω = 137 g = .005	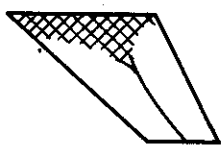 ω = 140 g = ---	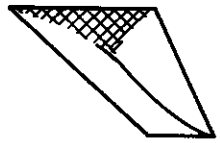 ω = 132 g = .015
FOURTH NATURAL FREQUENCY	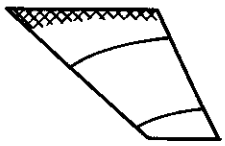 ω = 214 g = .004		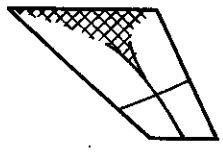 ω = 261 g = .014

NULL AREAS ω = cps.

TABLE D.15 (CONT.)

EXPERIMENTAL VIBRATION DATA FOR SWEPT WINGS

MODEL	SW—4	SW—5	SW—8
FIRST NATURAL FREQUENCY	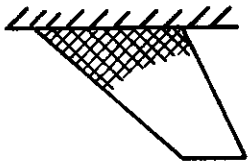 ω = 27.2 g = .024	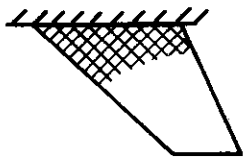 ω = 28.4 g = .024	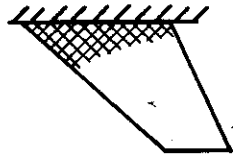 ω = 37.86 g = .013
SECOND NATURAL FREQUENCY	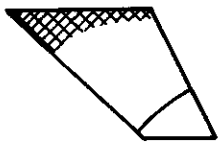 ω = 97.6 g = .022	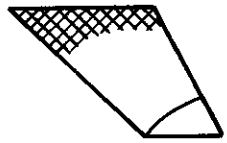 ω = 100.0 g = .018	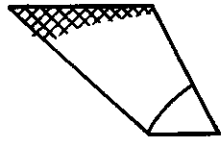 ω = 128 g = .024
THIRD NATURAL FREQUENCY	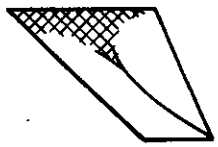 ω = 121 g = .031	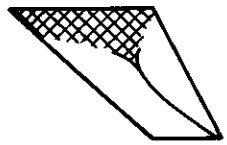 ω = 113 g = .022	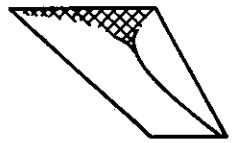 ω = 150 g = .011
FOURTH NATURAL FREQUENCY		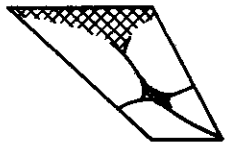 ω = 231 g = .020	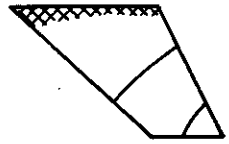 ω = 237 g = .031
FIFTH NATURAL FREQUENCY			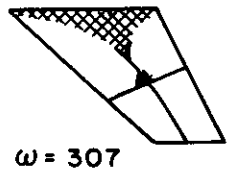 ω = 307 g = .024

NULL AREAS ω = cps.

TABLE D.15 (CONT.)

EXPERIMENTAL VIBRATION DATA FOR SWEPT WINGS

	SW-8-1	SW-3a CANTILEVER	SW-3a CANTILEVER
FIRST NATURAL FREQUENCY	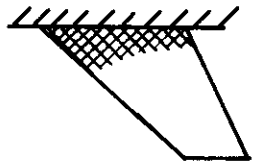 ω = 37.18 g = .015	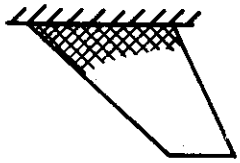 ω = 34.78 g = .025	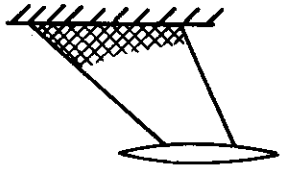 ω = 9.93 g = .010
SECOND NATURAL FREQUENCY	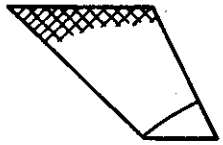 ω = 125 g = .028	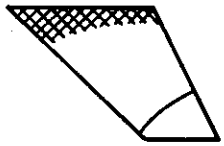 ω = 120 g = .012	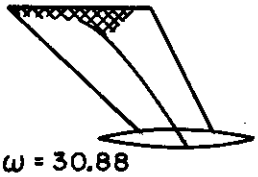 ω = 30.88 g = .010
THIRD NATURAL FREQUENCY	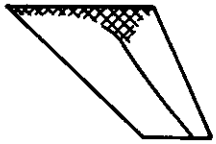 ω = 146 g = .014	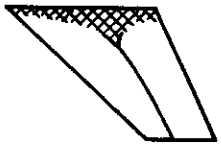 ω = 145 g = .010	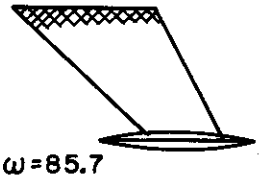 ω = 85.7 g = .013
FOURTH NATURAL FREQUENCY	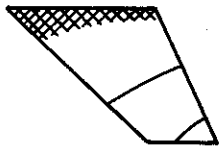 ω = 241 g = .034	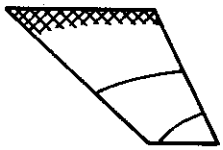 ω = 237 g = .018	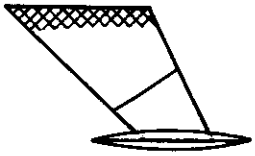 ω = 200 g = .007
FIFTH NATURAL FREQUENCY	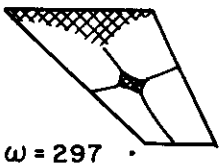 ω = 297 g = .016	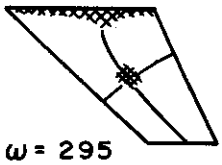 ω = 295 g = .010	

NULL AREAS ω = cps.

[redacted]

TABLE D.15 (CONT)

EXPERIMENTAL VIBRATION DATA FOR SWEPT WINGS

MODEL	SW-6 CANTILEVER	SW-6 CANTILEVER	SW-7 CANTILEVER
FIRST NATURAL FREQUENCY	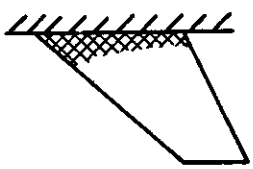 $\omega = 52.4$ $g = .027$	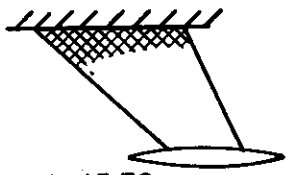 $\omega = 15.79$ $g = .021$	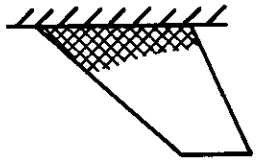 $\omega = 50.7$ $g = .030$
SECOND NATURAL FREQUENCY	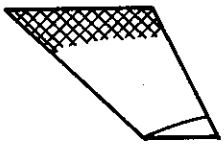 $\omega = 151$ $g = .050$	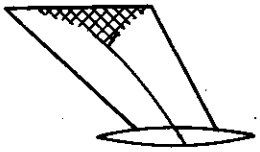 $\omega = 42.1$ $g = .047$	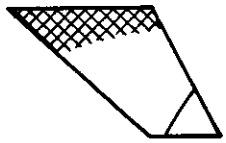 $\omega = 136$ $g = .030$
THIRD NATURAL FREQUENCY	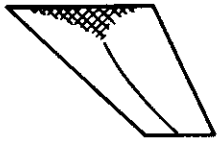 $\omega = 189$ $g = .009$	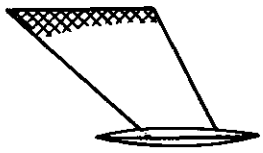 $\omega = 115.2$ $g = .014$	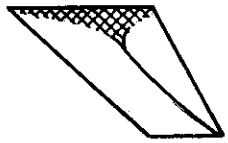 $\omega = 161$ $g = .012$
FOURTH NATURAL FREQUENCY			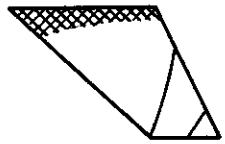 $\omega = 222$ $g = .040$
FIFTH NATURAL FREQUENCY			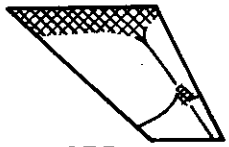 $\omega = 273$ $g = .014$

NULL AREAS ω = cps.

[redacted]

TABLE D.15 (CONT.)

EXPERIMENTAL VIBRATION DATA FOR SWEPT WINGS

MODEL	SW-7 CANTILEVER	SW-7a CANTILEVER	SW-7a CANTILEVER
FIRST NATURAL FREQUENCY	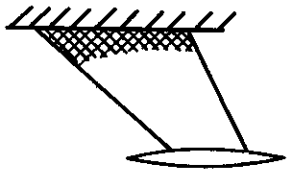 ω = 12.40 g = .012	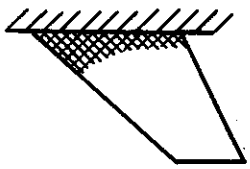 ω = 50.5 g = .027	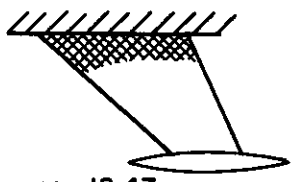 ω = 12.47 g = .013
SECOND NATURAL FREQUENCY	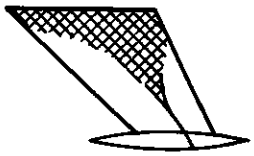 ω = 36.4 g = .026	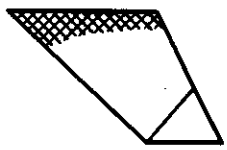 ω = 149 g = .022	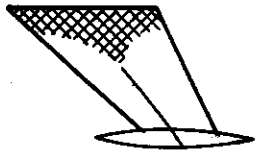 ω = 37.1 g = .015
THIRD NATURAL FREQUENCY	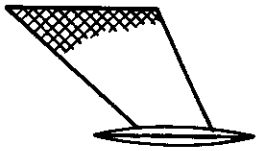 ω = 105 g = .026	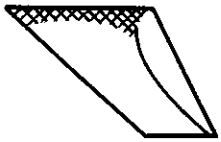 ω = 171 g = .011	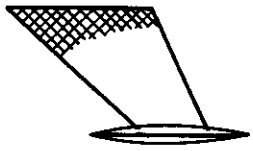 ω = 105 g = .015
FOURTH NATURAL FREQUENCY	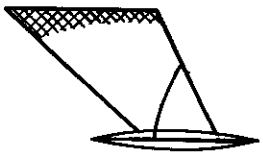 ω = 233 g = .016	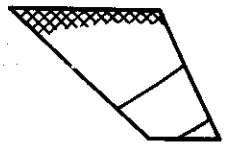 ω = 233 g = .029	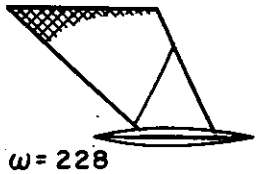 ω = 228 g = .009

NULL AREAS ω = cps.

TABLE D.15 (CONT.)

EXPERIMENTAL VIBRATION DATA FOR SWEPT WINGS

MODEL	SW-7a FREE TO ROLL	SW-7a FREE TO ROLL	SW-3b AILERON
FIRST NATURAL FREQUENCY	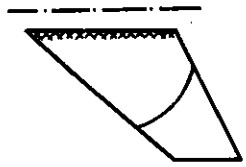 ω = 73.70 g = .011	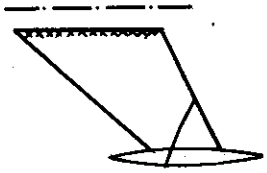 ω = 29.75 g = .011	WING UNCLAMPED 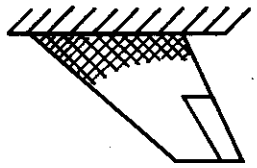 ω = 35.0 g = .021
SECOND NATURAL FREQUENCY	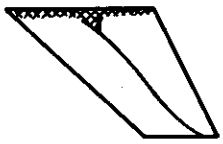 ω = 175 g = .006	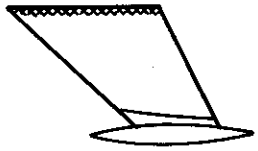 ω = 53.3 g = .011	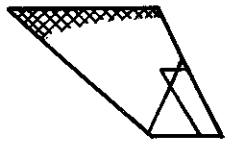 ω = 130.6 g = .014
THIRD NATURAL FREQUENCY	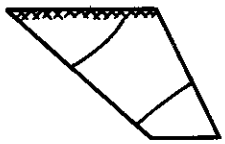 ω = 231 g = .007	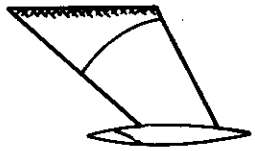 ω = 125 g = .013	AILERON FREQUENCY 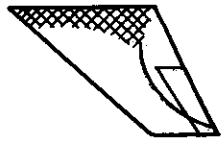 ω = 147.6 g = .015
FOURTH NATURAL FREQUENCY		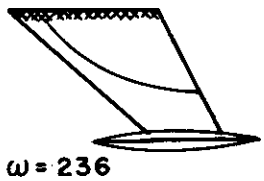 ω = 236 g = .009	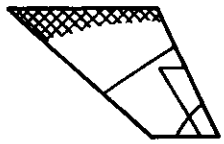 ω = 280 g = .015

▩ NULL AREAS ω = cps.

TABLE D.16

EXPERIMENTAL VIBRATION DATA FOR DELTA WINGS

MODEL	De – 1	De – 1a	De–1a–1
FIRST NATURAL FREQUENCY	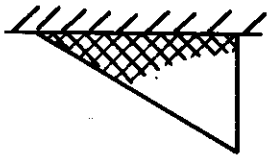 ω=125 g=.017	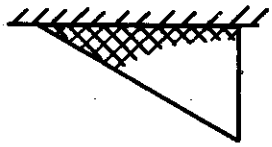 ω=96.2 g=.016	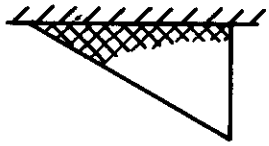 ω=108 g=.018
SECOND NATURAL FREQUENCY	 ω=361 g=.021	 ω=257 g=.016	 ω=279 g=.024
THIRD NATURAL FREQUENCY			 ω=313 g=.018
FOURTH NATURAL FREQUENCY			 ω=508 g=.016

▨ NULL AREAS ω = cps.

TABLE D.16 (CONT.)

EXPERIMENTAL VIBRATION DATA FOR DELTA WINGS

MODEL	De-1a-2	De-2	De-2a-1
FIRST NATURAL FREQUENCY	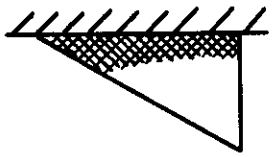 ω = 94 g = .026	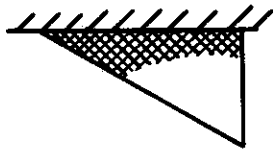 ω = 134 g = – –	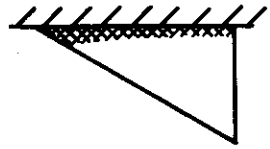 ω = 146.1 g = .032
SECOND NATURAL FREQUENCY	 ω = 260 g = .034	 ω = 320 g = – –	 ω = 310 g = .03
THIRD NATURAL FREQUENCY	 ω = 297 g = .019	 ω = 351 g = – –	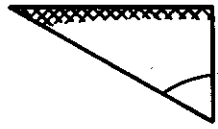 ω = 430 g = .05
FOURTH NATURAL FREQUENCY	 ω = 487 g = .027	 ω = 580 g = – –	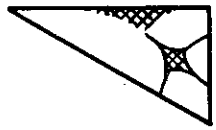 ω = 640 g = .05

▩ NULL AREAS ω = cps.

[redacted]

TABLE D.16 (CONT.)

EXPERIMENTAL VIBRATION DATA FOR DELTA WINGS

MODEL	De – 2b	De – 2c	De – 2d
FIRST NATURAL FREQUENCY	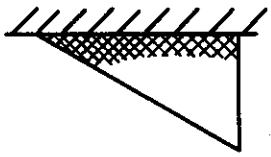 ω = 160 g = .044	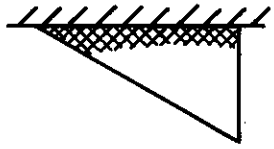 ω = 135 g = .033	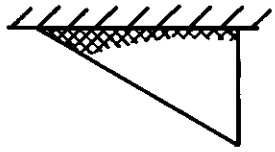 ω = 76.5 g = .041
SECOND NATURAL FREQUENCY	 ω = 337 g = .038	 ω = 283 g = .030	 ω = 225 g = .023
THIRD NATURAL FREQUENCY	 ω = 421 g = .02	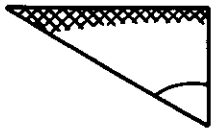 ω = 360 g = .035	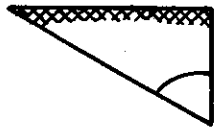 ω = 275 g = .041
FOURTH NATURAL FREQUENCY			

NULL AREAS ω = cps.

[redacted]

TABLE D.16 (CONT.)

EXPERIMENTAL VIBRATION DATA FOR DELTA WINGS

MODEL	De – 2d – 1	De – 2d – 2	De – 3 – 1
FIRST NATURAL FREQUENCY	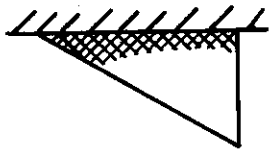 ω = 111 g = .025	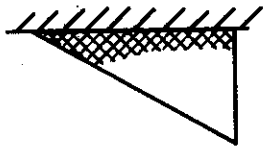 ω = 105 g = .024	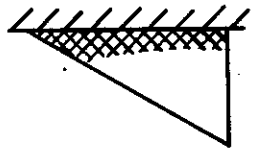 ω = 142 g = .04
SECOND NATURAL FREQUENCY	 ω = 240 g = .026	 ω = 236 g = .024	 ω = 318 (EST.) g = — —
THIRD NATURAL FREQUENCY	 ω = 296 g = .03	 ω = 287 g = .04	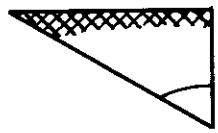 ω = 370 g = .04
FOURTH NATURAL FREQUENCY	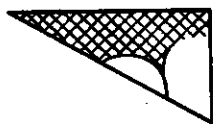 ω = 438 g = .02	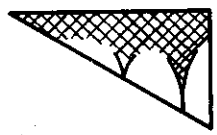 ω = 432 g = .02	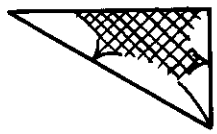 ω = 580 g = .02

NULL AREAS ω = cps.

TABLE D.16 (CONT.)

EXPERIMENTAL VIBRATION DATA FOR DELTA WINGS

MODEL	De — 3a	De — 3b	De — 3c
FIRST NATURAL FREQUENCY	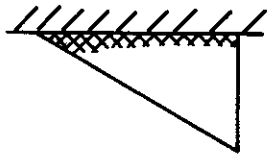 ω = 147 g = .021	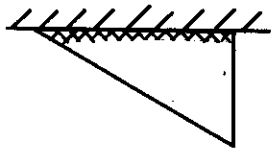 ω = 176 g = .044	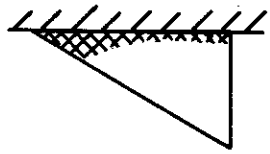 ω = 160 g = .014
SECOND NATURAL FREQUENCY	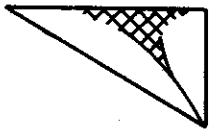 ω = 320 g = .016	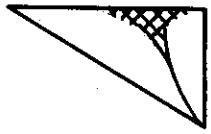 ω = 362 g = .027	 ω = 357 g = .014
THIRD NATURAL FREQUENCY	 ω = 396 g = .030	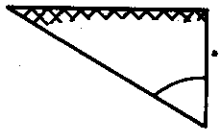 ω = 466 g = .03	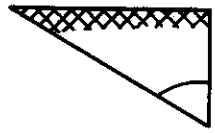 ω = 443 g = .021
FOURTH NATURAL FREQUENCY	 ω = 520 g = .03	 ω = 640 g = .04	 ω = 760 g = .02

NULL AREAS ω = cps.

TABLE D.16 (CONT.)

EXPERIMENTAL VIBRATION DATA FOR DELTA WINGS

MODEL	De – 3d	De – 3e	De – 3f
FIRST NATURAL FREQUENCY	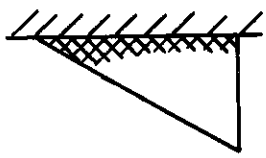 ω = 116 g = .025	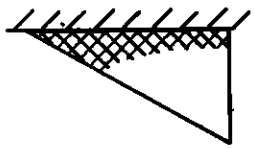 ω = 80 g = .049	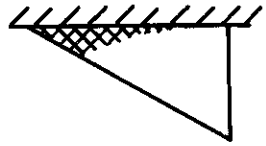 ω = 85.5 g = .022
SECOND NATURAL FREQUENCY	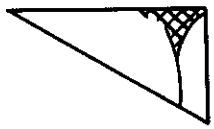 ω = 302 g = .024	 ω = 208 g = .023	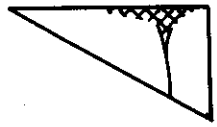 ω = 210 g = .018
THIRD NATURAL FREQUENCY	 ω = 320 g = .04	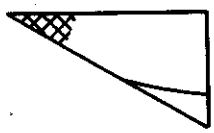 ω = 240 g = .010	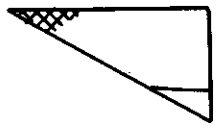 ω = 254 g = .033
FOURTH NATURAL FREQUENCY	 ω = 500 g = .02	 ω = 380 g = .022	 ω = 378 g = .02

NULL AREAS ω = cps.

TABLE D.16 (CONT.)

EXPERIMENTAL VIBRATION DATA FOR DELTA WINGS

MODEL	De-3f-1	De-3g	De-3h
FIRST NATURAL FREQUENCY	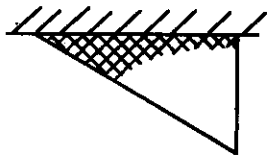 ω = 95 g = .026	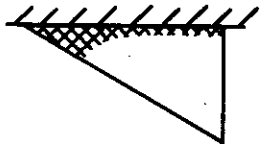 ω = 137 g = .039	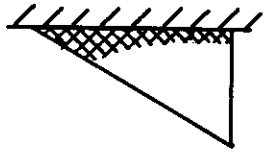 ω = 137 g = .049
SECOND NATURAL FREQUENCY	 ω = 238 g = .037	 ω = 286 g = .012	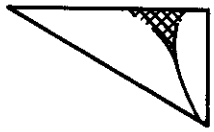 ω = 333 g = .04
THIRD NATURAL FREQUENCY	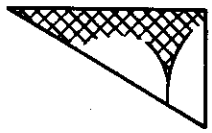 ω = 256 g = .022	 ω = 348 g = .03	 ω = 348 g = .03
FOURTH NATURAL FREQUENCY	 ω = 440 g = .024		

▨ NULL AREAS ω = cps.

TABLE D.16 (CONT.)

EXPERIMENTAL VIBRATION DATA FOR DELTA WINGS

MODEL	De – 3i	De – 3j	De – 4
FIRST NATURAL FREQUENCY	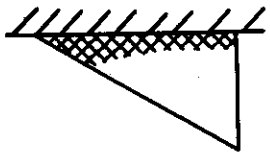 ω = 118 g = .035	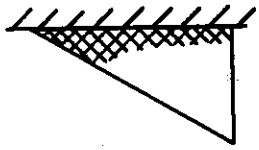 ω = 105 g = .019	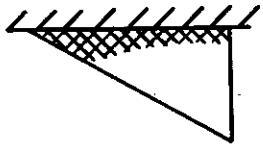 ω = 157 g = .018
SECOND NATURAL FREQUENCY	 ω = 280 g = .023	 ω = 253 g = .021	 ω = 310 g = .024
THIRD NATURAL FREQUENCY	 ω = 333 g = .031	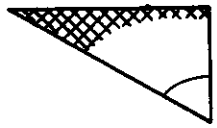 ω = 300 g = .04	
FOURTH NATURAL FREQUENCY		 ω = 467 g = .03	

NULL AREAS ω = cps.

TABLE D.16 (CONT.)

EXPERIMENTAL VIBRATION DATA FOR DELTA WINGS

MODEL	De – 4a	De – 4b	De – 4c
FIRST NATURAL FREQUENCY	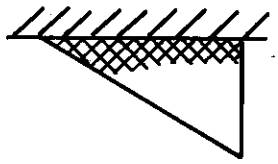 ω = 144 g = .036	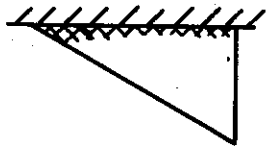 ω = 133 g = .036	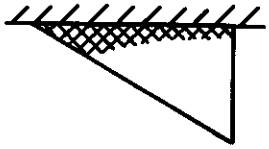 ω = 101 g = — —
SECOND NATURAL FREQUENCY	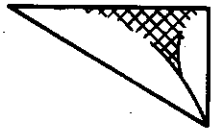 ω = 314 g = .032	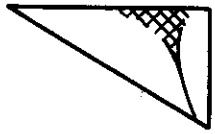 ω = 275 g = .100	 ω = 231 g = — —
THIRD NATURAL FREQUENCY	 ω = 385 g = .026	 ω = 330 g = .034	 ω = 272 g = — —
FOURTH NATURAL FREQUENCY			

 NULL AREAS ω = cps.

TABLE D.16 (CONT.)

EXPERIMENTAL VIBRATION DATA FOR DELTA WINGS

MODEL	De-4c-1	De-5	De-6
FIRST NATURAL FREQUENCY	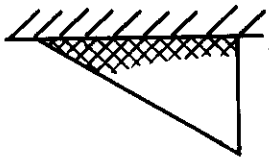 ω=106 g=.025	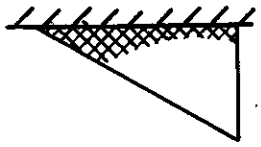 ω = 46.4 g = .071	 ω = 45.8 g=.051
SECOND NATURAL FREQUENCY	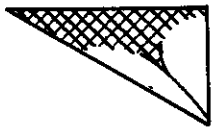 ω = 233 g=.03	 ω = 135 g = .059	 ω = 112 g =.09
THIRD NATURAL FREQUENCY	 ω = 285 g= .033	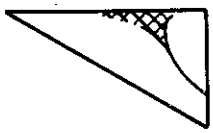 ω = 188 g =.058	 ω = 129 g =.09
FOURTH NATURAL FREQUENCY	 ω = 437 g = .028	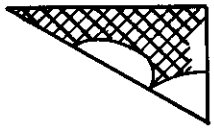 ω = 266 g =.07	

 NULL AREAS ω = cps.

TABLE D.16 (CONT.)

EXPERIMENTAL VIBRATION DATA FOR DELTA WINGS

MODEL	De-2e AILERON	De-2e (CONT.)	
FIRST NATURAL FREQUENCY	WING UNCLAMPED 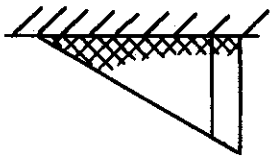 ω = 155 g = .020	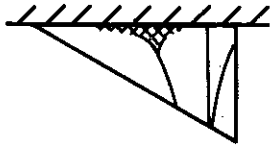 ω = 400 g = .02	
SECOND NATURAL FREQUENCY	 ω = 223 g = .024		
THIRD NATURAL FREQUENCY	 ω = 250 (EST.) g = — —		
FOURTH NATURAL FREQUENCY	AILERON MODE 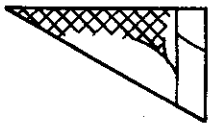 ω = 317 g = .028		

NULL AREAS ω = cps.

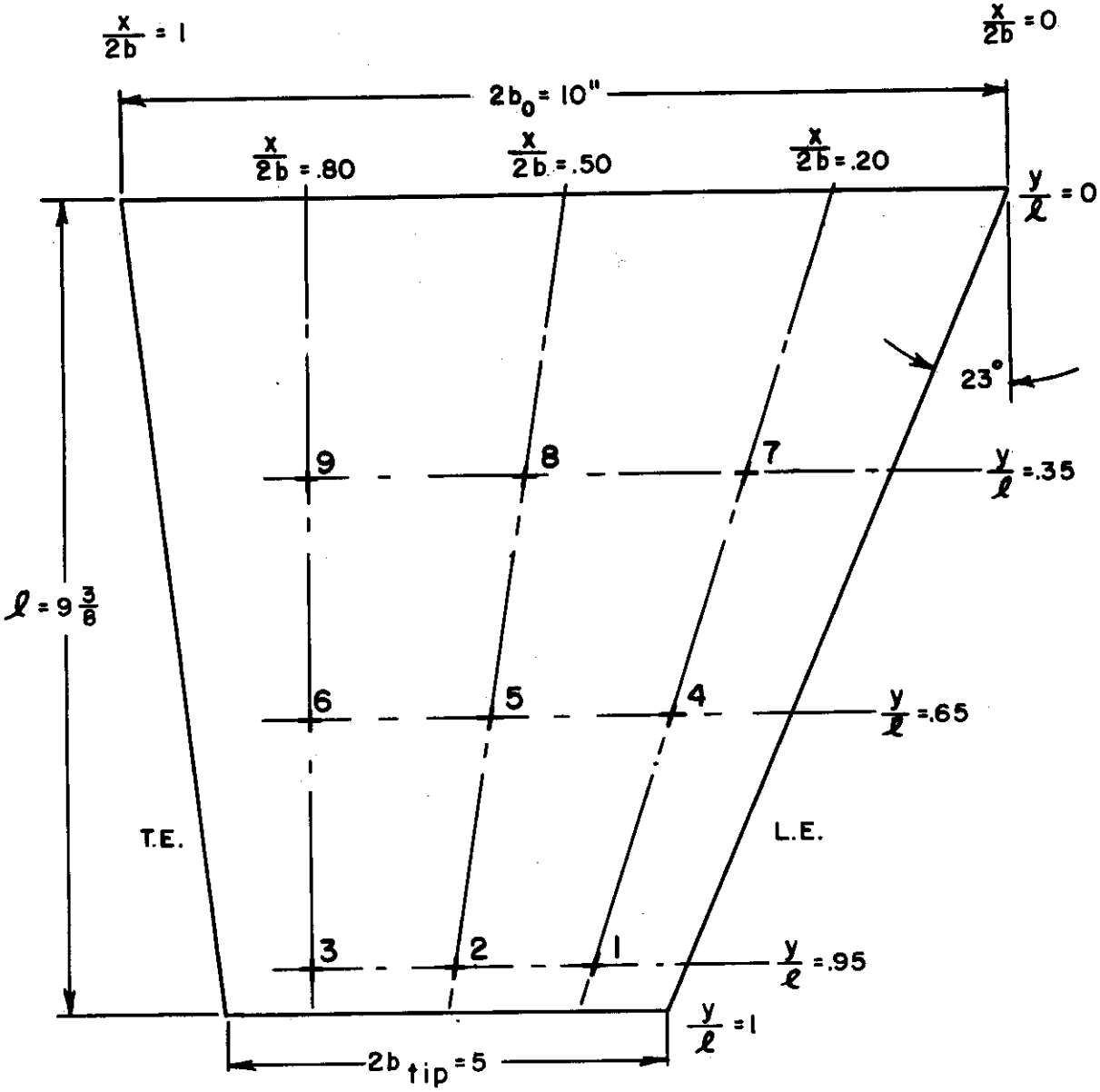

FIGURE D.7 LOCATION OF INFLUENCE-COEFFICIENT POINTS FOR STRAIGHT-WING MODELS

TABLE D.17a

EXPERIMENTALLY DETERMINED FORCE-DEFLECTION INFLUENCE-COEFFICIENT MATRIX FOR MODEL ST-1d-1

	(1)	(2)	(3)	(4)	(5)	(6)	(7)	(8)	(9)
(1)	0.0371	0.0374	0.0384	0.0158	0.0172	0.0182	0.0039	0.0048	0.0053
(2)	0.0379	0.0417	0.0457	0.0160	0.0190	0.0222	0.0037	0.0054	0.0069
(3)	0.0384	0.0457	0.0551	0.0156	0.0208	0.0258	0.0034	0.0058	0.0082
(4)	0.0169	0.0165	0.0161	0.0094	0.0090	0.0088	0.0026	0.0028	0.0028
(5)	0.0180	0.0195	0.0213	0.0091	0.0111	0.0129	0.0024	0.0035	0.0047
(6)	0.0186	0.0222	0.0260	0.0086	0.0127	0.0184	0.0014	0.0041	0.0064
(7)	0.0042	0.0038	0.0035	0.0028	0.0024	0.0019	0.0013	0.0010	0.0006
(8)	0.0053	0.0055	0.0059	0.0030	0.0037	0.0041	0.0008	0.0016	0.0022
(9)	0.0053	0.0065	0.0079	0.0028	0.0045	0.0062	0.0006	0.0021	0.0051

Units are inches/#

TABLE D.17b

EXPERIMENTALLY DETERMINED FORCE-DEFLECTION INFLUENCE-COEFFICIENT MATRIX FOR MODEL ST-4-1

	(1)	(2)	(3)	(4)	(5)	(6)	(7)	(8)	(9)
(1)	0.0276	0.0271	0.0263	0.0120	0.0128	0.0126	0.0030	0.0038	0.0037
(2)	0.0268	0.0291	0.0309	0.0113	0.0135	0.0147	0.0026	0.0038	0.0039
(3)	0.0258	0.0309	0.0383	0.0107	0.0143	0.0171	0.0023	0.0039	0.0049
(4)	0.0119	0.0114	0.0108	0.0072	0.0066	0.0059	0.0020	0.0020	0.0014
(5)	0.0123	0.0132	0.0141	0.0064	0.0076	0.0084	0.0016	0.0024	0.0028
(6)	0.0124	0.0149	0.0174	0.0058	0.0086	0.0124	0.0012	0.0026	0.0036
(7)	0.0030	0.0027	0.0023	0.0021	0.0017	0.0013	0.0012	0.0007	0.0001
(8)	0.0037	0.0039	0.0041	0.0022	0.0025	0.0028	0.0007	0.0010	0.0011
(9)	0.0036	0.0044	0.0052	0.0018	0.0030	0.0040	0.0004	0.0012	0.0029

Units are inches/#

TABLE D.17c

EXPERIMENTALLY DETERMINED FORCE-DEFLECTION INFLUENCE-COEFFICIENT MATRIX FOR MODEL ST-5-1

	(1)	(2)	(3)	(4)	(5)	(6)	(7)	(8)	(9)
(1)	0.0290	0.0285	0.0277	0.0128	0.0129	0.0133	0.0033	0.0033	0.0034
(2)	0.0289	0.0316	0.0339	0.0122	0.0142	0.0164	0.0031	0.0038	0.0047
(3)	0.0281	0.0338	0.0406	0.0113	0.0149	0.0188	0.0027	0.0040	0.0054
(4)	0.0131	0.0125	0.0119	0.0077	0.0068	0.0063	0.0024	0.0020	0.0018
(5)	0.0135	0.0145	0.0153	0.0068	0.0079	0.0092	0.0020	0.0024	0.0030
(6)	0.0135	0.0163	0.0188	0.0061	0.0090	0.0131	0.0015	0.0028	0.0042
(7)	0.0033	0.0028	0.0023	0.0023	0.0017	0.0014	0.0013	0.0008	0.0002
(8)	0.0041	0.0043	0.0045	0.0023	0.0027	0.0030	0.0007	0.0011	0.0015
(9)	0.0042	0.0051	0.0061	0.0020	0.0030	0.0046	0.0003	0.0016	0.0036

Units are inches/#

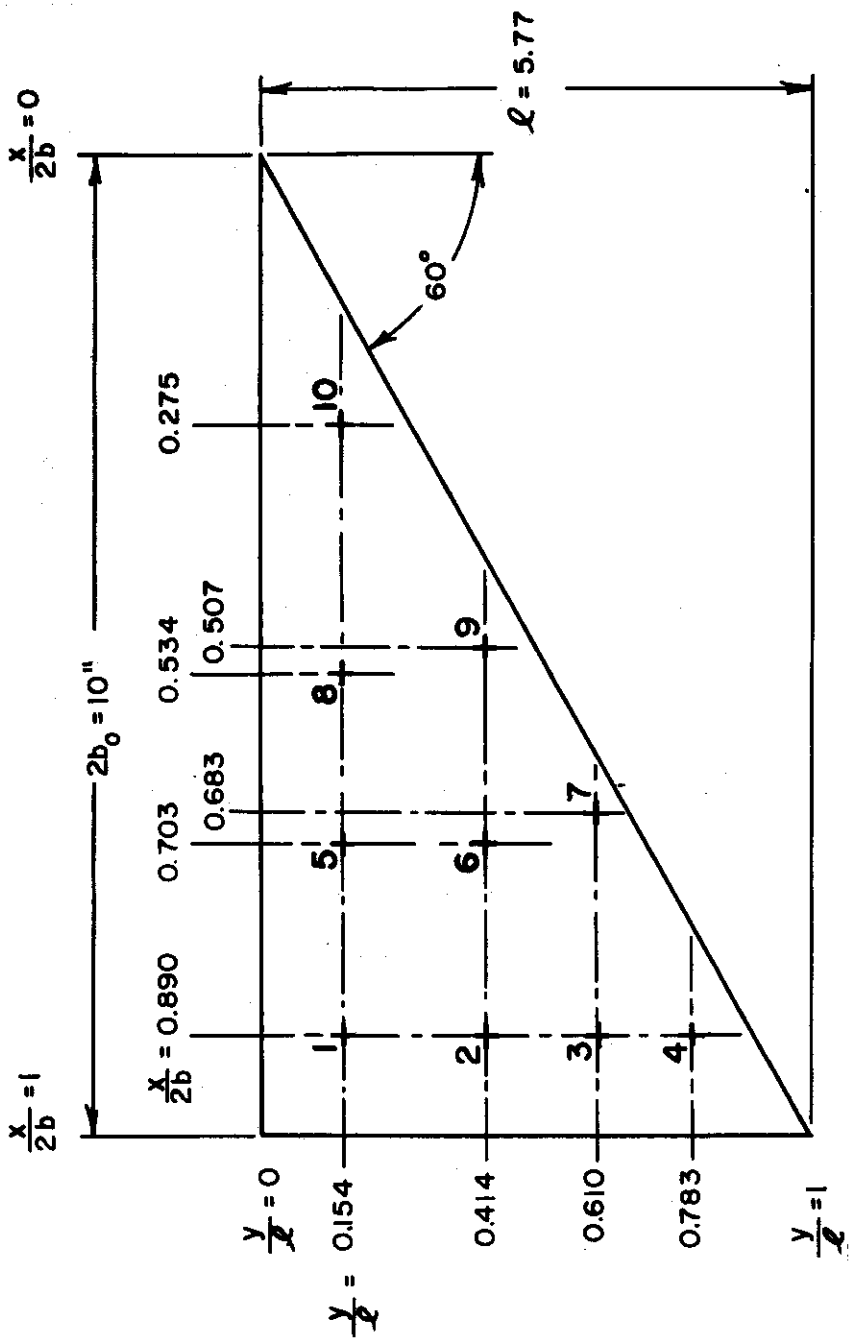

FIGURE D.8a LOCATION OF INFLUENCE-COEFFICIENT POINTS FOR DELTA-WING MODEL WITHOUT ELEVON

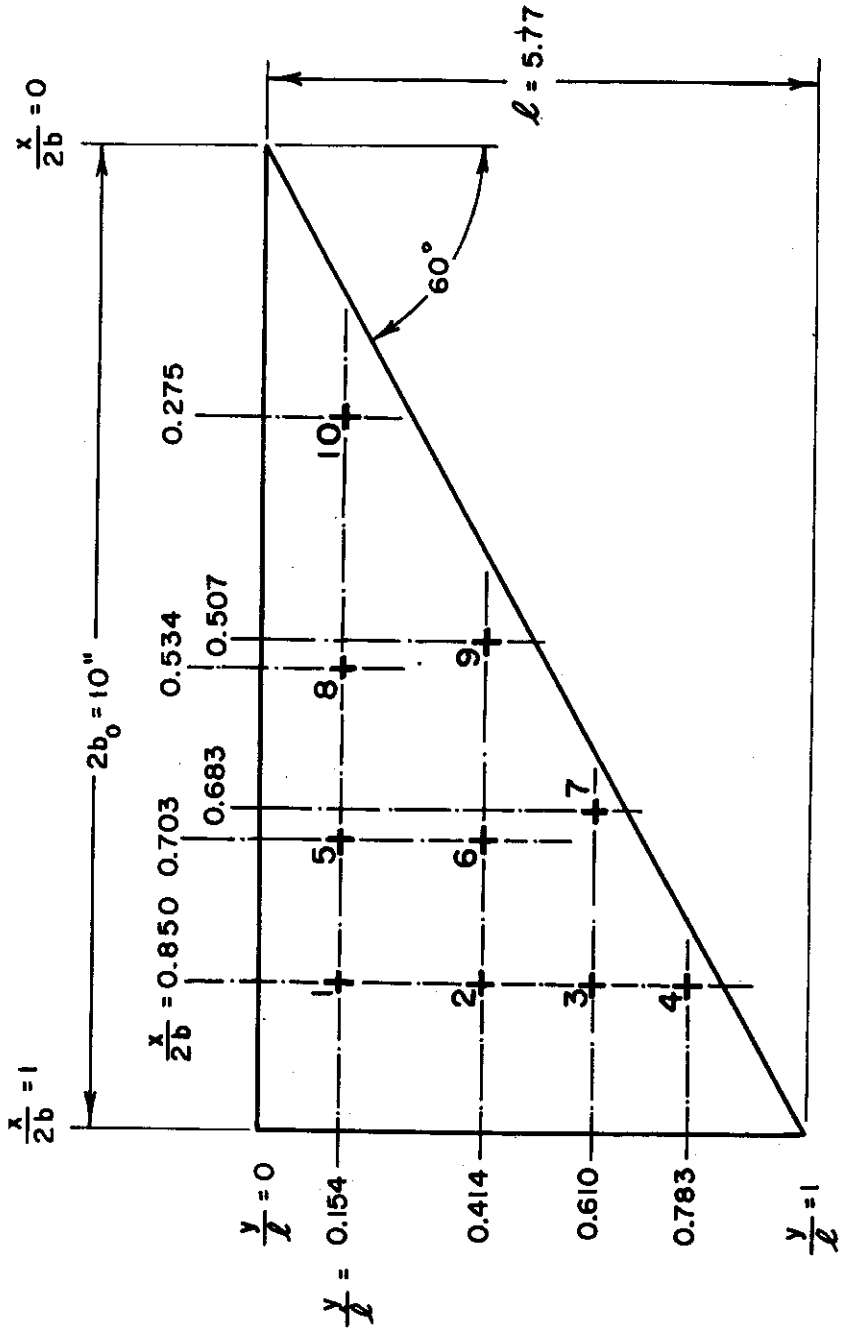

FIGURE D.8b LOCATION OF INFLUENCE-COEFFICIENT POINTS FOR DELTA-WING MODEL WITH ELEVON

TABLE D.18a

EXPERIMENTALLY DETERMINED FORCE-DEFLECTION INFLUENCE-COEFFICIENT MATRIX FOR MODEL De-1a-1

	(1)	(2)	(3)	(4)	(5)	(6)	(7)	(8)	(9)	(10)
(1)	0.0027	0.0024	0.0025	0.0026	0.0003	0.0007	0.0007	0.0000	0.0000	0.0000
(2)	0.0028	0.0097	0.0126	0.0143	0.0007	0.0035	0.0053	0.0001	0.0006	0.0000
(3)	0.0028	0.0132	0.0254	0.0343	0.0011	0.0063	0.0111	0.0004	0.0018	0.0000
(4)	0.0029	0.0156	0.0352	0.0671	0.0012	0.0086	0.0177	0.0006	0.0029	0.0000
(5)	0.0004	0.0008	0.0011	0.0013	0.0003	0.0006	0.0006	0.0002	0.0005	0.0000
(6)	0.0008	0.0033	0.0056	0.0074	0.0007	0.0034	0.0053	0.0004	0.0016	0.0001
(7)	0.0008	0.0053	0.0111	0.0169	0.0008	0.0059	0.0163	0.0005	0.0030	0.0000
(8)	0.0000	0.0001	0.0004	0.0005	0.0001	0.0004	0.0005	0.0002	0.0006	0.0000
(9)	0.0001	0.0007	0.0018	0.0029	0.0003	0.0016	0.0031	0.0006	0.0065	0.0001
(10)	0.0000	0.0000	0.0000	0.0000	0.0000	0.0000	0.0001	0.0000	0.0000	0.0017

Units are inches/#

TABLE D.18b

EXPERIMENTALLY DETERMINED FORCE-DEFLECTION INFLUENCE-COEFFICIENT MATRIX FOR MODEL De-1a-2

	(1)	(2)	(3)	(4)	(5)	(6)	(7)	(8)	(9)	(10)
(1)	0.0049	0.0034	0.0037	0.0032	0.0004	0.0008	0.0009	0.0000	0.0000	0.0000
(2)	0.0035	0.0118	0.0147	0.0167	0.0009	0.0038	0.0057	0.0001	0.0006	0.0000
(3)	0.0037	0.0149	0.0276	0.0387	0.0012	0.0065	0.0119	0.0004	0.0018	0.0000
(4)	0.0037	0.0174	0.0389	0.0714	0.0014	0.0089	0.0174	0.0006	0.0028	0.0000
(5)	0.0004	0.0010	0.0014	0.0016	0.0003	0.0007	0.0009	0.0002	0.0002	0.0000
(6)	0.0008	0.0035	0.0061	0.0081	0.0007	0.0033	0.0051	0.0002	0.0014	0.0000
(7)	0.0009	0.0059	0.0116	0.0170	0.0008	0.0057	0.0144	0.0006	0.0031	0.0000
(8)	0.0000	0.0002	0.0004	0.0006	0.0001	0.0003	0.0006	0.0003	0.0005	0.0000
(9)	0.0001	0.0007	0.0188	0.0029	0.0003	0.0015	0.0032	0.0007	0.0059	0.0001
(10)	0.0000	0.0000	0.0000	0.0000	0.0000	0.0000	0.0000	0.0002	0.0001	0.0012

Units are inches/#

TABLE D.18c

EXPERIMENTALLY DETERMINED FORCE-DEFLECTION INFLUENCE-COEFFICIENT MATRIX FOR MODEL De-2d-2

	(1)	(2)	(3)	(4)	(5)	(6)	(7)	(8)	(9)	(10)
(1)	0.0033	0.0027	0.0023	0.0019	0.0004	0.0007	0.0006	0.0001	0.0001	0.0000
(2)	0.0029	0.0109	0.0121	0.0123	0.0013	0.0037	0.0043	0.0005	0.0011	0.0001
(3)	0.0025	0.0124	0.0237	0.0301	0.0018	0.0075	0.0104	0.0010	0.0026	0.0001
(4)	0.0023	0.0128	0.0306	0.0637	0.0021	0.0108	0.0188	0.0014	0.0047	0.0001
(5)	0.0003	0.0012	0.0016	0.0018	0.0006	0.0010	0.0009	0.0002	0.0002	0.0000
(6)	0.0007	0.0036	0.0069	0.0097	0.0009	0.0044	0.0067	0.0008	0.0025	0.0001
(7)	0.0006	0.0043	0.0105	0.0187	0.0009	0.0072	0.0173	0.0013	0.0058	0.0001
(8)	0.0001	0.0004	0.0009	0.0011	0.0001	0.0011	0.0013	0.0004	0.0009	0.0001
(9)	0.0001	0.0009	0.0026	0.0043	0.0002	0.0026	0.0054	0.0008	0.0057	0.0005
(10)	0.0000	0.0000	0.0001	0.0001	0.0000	0.0002	0.0002	0.0001	0.0004	0.0012

Units are inches/#

TABLE D.18d

EXPERIMENTALLY DETERMINED FORCE-DEFLECTION INFLUENCE-COEFFICIENT MATRIX FOR MODEL De-3f-1

	(1)	(2)	(3)	(4)	(5)	(6)	(7)	(8)	(9)	(10)
(1)	0.0040	0.0032	0.0027	0.0032	0.0004	0.0007	0.0009	0.0000	0.0001	0.0000
(2)	0.0032	0.0132	0.0153	0.0163	0.0014	0.0043	0.0056	0.0003	0.0010	0.0000
(3)	0.0029	0.0162	0.0299	0.0377	0.0019	0.0080	0.0124	0.0006	0.0024	0.0000
(4)	0.0024	0.0176	0.0394	0.0754	0.0022	0.0114	0.0220	0.0009	0.0043	0.0000
(5)	0.0004	0.0014	0.0017	0.0019	0.0007	0.0009	0.0010	0.0001	0.0002	0.0000
(6)	0.0007	0.0044	0.0079	0.0112	0.0009	0.0048	0.0072	0.0006	0.0021	0.0000
(7)	0.0006	0.0060	0.0128	0.0211	0.0010	0.0077	0.0206	0.0011	0.0059	0.0001
(8)	0.0001	0.0004	0.0008	0.0011	0.0002	0.0006	0.0010	0.0003	0.0007	0.0000
(9)	0.0002	0.0012	0.0025	0.0048	0.0003	0.0022	0.0054	0.0007	0.0061	0.0002
(10)	0.0000	0.0000	0.0001	0.0001	0.0000	0.0001	0.0002	0.0000	0.0003	0.0014

Units are inches/#

TABLE D.18e

EXPERIMENTALLY DETERMINED FORCE-DEFLECTION INFLUENCE-COEFFICIENT MATRIX FOR MODEL De-4c

	(1)	(2)	(3)	(4)	(5)	(6)	(7)	(8)	(9)	(10)
(1)	0.0043	0.0032	0.0039	0.0033	0.0006	0.0010	0.0009	0.0001	0.0002	0.0000
(2)	0.0033	0.0148	0.0174	0.0168	0.0019	0.0050	0.0065	0.0006	0.0011	0.0001
(3)	0.0039	0.0166	0.0308	0.0404	0.0023	0.0100	0.0156	0.0012	0.0031	0.0002
(4)	0.0010	0.0140	0.0373	0.0756	0.0022	0.0143	0.0283	0.0018	0.0057	0.0003
(5)	0.0007	0.0012	0.0019	0.0021	0.0007	0.0011	0.0013	0.0003	0.0004	0.0001
(6)	0.0005	0.0043	0.0091	0.0129	0.0012	0.0061	0.0091	0.0010	0.0029	0.0002
(7)	0.0000	0.0043	0.0125	0.0249	0.0011	0.0093	0.0203	0.0016	0.0073	0.0003
(8)	0.0000	0.0013	0.0012	0.0017	0.0002	0.0010	0.0016	0.0005	0.0010	0.0001
(9)	0.0000	0.0000	0.0028	0.0054	0.0002	0.0030	0.0077	0.0012	0.0081	0.0006
(10)	0.0000	0.0000	0.0003	0.0005	0.0000	0.0002	0.0004	0.0002	0.0004	0.0023

Units are inches/# (Note: Early wing - data somewhat inaccurate)

TABLE D.18f

EXPERIMENTALLY DETERMINED FORCE-DEFLECTION INFLUENCE-COEFFICIENT MATRIX FOR MODEL De-2e

	(1)	(2)	(3)	(4)	(5)	(6)	(7)	(8)	(9)	(10)
(1)	0.0012	0.0015	0.0014	0.0015	0.0003	0.0004	0.0003	0.0000	0.0001	0.0000
(2)	0.0015	0.0051	0.0069	0.0072	0.0008	0.0024	0.0028	0.0002	0.0006	0.0000
(3)	0.0012	0.0065	0.0125	0.0156	0.0011	0.0045	0.0061	0.0005	0.0015	0.0001
(4)	0.0009	0.0073	0.0159	0.0320	0.0012	0.0068	0.0121	0.0007	0.0028	0.0000
(5)	0.0003	0.0008	0.0012	0.0013	0.0004	0.0028	0.0006	0.0001	0.0001	0.0000
(6)	0.0003	0.0023	0.0042	0.0063	0.0021	0.0028	0.0041	0.0004	0.0015	0.0000
(7)	0.0002	0.0027	0.0062	0.0115	0.0006	0.0041	0.0125	0.0007	0.0039	0.0000
(8)	0.0000	0.0005	0.0001	0.0003	0.0001	0.0005	0.0008	0.0002	0.0006	0.0000
(9)	0.0000	0.0007	0.0014	0.0026	0.0001	0.0014	0.0038	0.0006	0.0050	0.0003
(10)	0.0000	0.0000	0.0000	0.0004	0.0000	0.0001	0.0001	0.0000	0.0004	0.0010

Units are inches/#

TABLE D.19

SOME EXPERIMENTAL DATA FOR THE XF-92A AIRPLANE

NATURAL FREQUENCIES	
FIRST SYMMETRICAL FREQUENCY	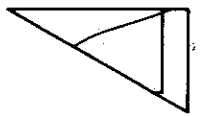 ω = 13.25 cps.
SECOND SYMMETRICAL FREQUENCY	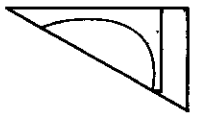 ω = 28.33 cps.
THIRD SYMMETRICAL FREQUENCY	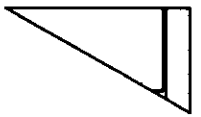 ω = 32.5 cps.
FOURTH SYMMETRICAL FREQUENCY	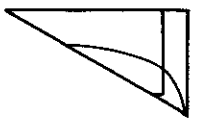 ω = 45.5 cps.

EXPERIMENTALLY DETERMINED FORCE-DEFLECTION

INFLUENCE-COEFFICIENT MATRIX FOR XF-92A DELTA WING

	1	2	3	4	5	6	7	8	9	10
1	0.294	0.417	0.497	0.527	0.120	0.271	0.298	0.031	0.126	-0.019
2	0.417	0.965	1.24	1.43	0.200	0.610	0.804	0.096	0.321	0.005
3	0.497	1.24	1.84	2.30	0.252	0.807	1.21	0.136	0.469	0.035
4	0.527	1.43	2.30	3.19	0.285	0.945	1.52	0.170	0.590	0.046
5	0.120	0.200	0.252	0.285	0.108	0.184	0.212	0.069	0.150	0.025
6	0.271	0.610	0.807	0.945	0.184	0.520	0.654	0.120	0.368	0.052
7	0.298	0.804	1.21	1.52	0.212	0.654	1.19	0.140	0.486	0.063
8	0.031	0.096	0.136	0.170	0.069	0.120	0.140	0.067	0.115	0.019
9	0.126	0.321	0.469	0.590	0.150	0.368	0.486	0.115	0.368	0.076
10	-0.019	0.005	0.035	0.046	0.025	0.052	0.063	0.019	0.076	0.141

Each element of matrix must be multiplied by the factor 10^{-4}

Units are inches/#

Influence coefficients have been averaged so as to obey Maxwell's Reciprocal Theorem for structures

Mass semi-wing = 36.26 slugs

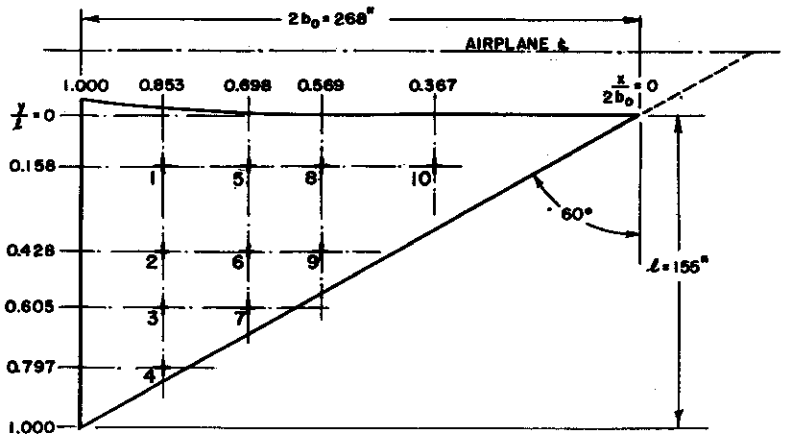

LOCATION OF POINTS FOR INFLUENCE-COEFFICIENT MATRIX